

Electronic Thesis and Dissertation Repository

6-22-2021 9:30 AM

Development of New Bonding Technologies for Powder Coatings

Wei Liu, *The University of Western Ontario*


Supervisor: Jesse Zhu, *The University of Western Ontario*

Joint Supervisor: Hui Zhang, *The University of Western Ontario*

A thesis submitted in partial fulfillment of the requirements for the Doctor of Philosophy degree
in Chemical and Biochemical Engineering

© Wei Liu 2021

Follow this and additional works at: <https://ir.lib.uwo.ca/etd>

 Part of the [Polymer Science Commons](#), and the [Process Control and Systems Commons](#)

Recommended Citation

Liu, Wei, "Development of New Bonding Technologies for Powder Coatings" (2021). *Electronic Thesis and Dissertation Repository*. 7933.

<https://ir.lib.uwo.ca/etd/7933>

This Dissertation/Thesis is brought to you for free and open access by Scholarship@Western. It has been accepted for inclusion in Electronic Thesis and Dissertation Repository by an authorized administrator of Scholarship@Western. For more information, please contact wlsadmin@uwo.ca.

Abstract

The metallic effect powder coatings (MEPC), composed of regular powder coating materials and metallic pigments, share an increasing market because they provide an aesthetic metallic effect and also enhance protection. Mainstream industrial production employs a thermal bonding technology to incorporate and immobilize the metallic pigments to coating particles. However, a series of inherent shortcomings of the thermal technology have affected the promotion and deployment of MEPC, such as mis-bonding, metallic flake deformation, inability for high-temperature bonding, etc. To address these issues, cold, single-component-heating (SCH) and microwave bonding methods have been proposed and tested in this thesis work.

The cold and SCH bonding methods both were shown to have enhanced bonding quality and small Al-content relative difference of less than 5%, but could not compete with the microwave bonding method that has high heating rates and easy real-time control, and is more readily for industrialization. A thorough study on the microwave bonding method from lab to industrial experiments provided a comprehensive understanding of the process and mechanism of microwave bonding including the bonding quality and color stability. Microwaves exhibited significant advancements in heating rate (10-23°C/min), which enabled a much higher production efficiency and a lower energy consumption than the current bonding technology. In the microwave bonding, the temperature of particles is easy to control. Furthermore, the bonding quality increased by 100% and the color is much more stable compared to the current commercial method. Based on solid experiments and reliable results, the microwave bonding devices have been scaled up from lab-scale (0.05 kg/batch) to pilot-scale (10 kg/batch) and finally to industrial-scale (100 kg/batch). The industrial microwave bonding machine successfully overcame the shortcomings of the current commercial bonding machine, and achieved better bonding quality and more stable color with higher productivity and less energy consumption.

In conclusion, the microwave bonding method shows obvious superiority over the current bonding technology, as well as the cold and SCH bonding methods studied here. It avoids the current shortcomings of bonding, provides better bonding quality and color stability, and achieves higher production efficiency. The industrial-scale microwave bonding machines are expected to replace the current bonding machines in the very near future.

Keywords: Microwave bonding, metallic pigment, powder coating, CFD simulation.

Summary for Lay Audience

Powder coating is an environmentally friendly painting process that has 100% solid ingredients of resin, pigment, filler, and additives. The excluding of solvent avoids atmosphere pollution. Metallic effect powder coating (MEPC) provides a finish with high protection and sparkling (metal) effect that has been heavily applied in the fields of domestic appliances, building materials, automobile parts, electronic instrumentation and other industrial products.

The most important production procedure for MEPC is the bonding treatment that aims to bond the coating particle with metallic pigment to ensure the color stability of the final films. The current commercial bonding technology employs high-speed stirring and water/oil jackets to heat and bond the two components. However, there are several inherent shortcomings, such as mis-bonding, bending and grinding of metallic pigments, high-temperature bonding, etc.

In this work, to overcome the above shortcomings and improve bonding quality, several bonding methods have been proposed and tested. Cold bonding is using water-soluble binders to bond the coating particles and metallic pigments at room temperature. In the single-component-heating bonding, the metallic pigments are heated alone and then immediately dispersed into the fluidized coating particles to bond them. At last, the microwave bonding method has been established and developed, which selectively heats the two materials and bonds them. The microwave bonding device has been scaled up from lab-scale (0.05 kg/batch) to pilot-scale (10 kg/batch) and finally to industrial-scale (100 kg/batch).

The bonding quality and color stability of the bonded samples were analyzed by a series of characterizations, such as ash test, gas-volumetric analysis, FTIR, optical microscope, colorimeter, SEM, and EDS. The results show that the microwave bonding method obtains better bonding quality and color stability than the cold, SCH and current commercial bonding methods. More specifically, the bonding rate increased from 35% to 72% and the color difference decreased from 2.9 to 0.3. In addition, microwave bonding device provides higher productivity with lower energy consumption compared to the commercial technology.

In summary, the microwave bonding method gains better bonding quality and higher color stability than the current commercial bonding technology. The industrial microwave bonding machine is expected to replace the current bonding machine and create enormous commercial value in the near future.

Co-Authorship Statement

Dr. Jesse Zhu and Dr. Hui Zhang provided full supervision to this PhD thesis study and over saw all writings of the following publications.

Chapter 2 was co-authored with the Dr. Hui Zhang and Dr. Jesse Zhu who provided technical advice and revised these manuscripts. Specially, I performed the PVA bonding tests, data analysis, data visualization and manuscript writing. The raw data of Section 2.4.2 were from Dr. Jing Fu. All other coauthors provided technical advice and reviewed the manuscript.

Chapter 4 and 5 were coauthored with two professors from Tianjin University. Dr. Yuanyuan Shao and Haiping Zhang revised the manuscript and provided technical advice during my study. I designed and performed all experiments and drafted the manuscript.

Chapter 6 was coauthored with two researchers from Huajinag Powder Technology Co. and two professors from Tianjin University. Xinning Zhu Yufu Wei provided materials and helped me set up the experimental devices. Dr. Yuanyuan Shao and Haiping Zhang revised the manuscript and provided technical advice. The scale-up information was confidential and not discussed in this thesis, which was responsible for Wei Liu, Yufu Wei and Hui Zhang.

Chapter 7 and 10 have been submitted to peer-reviewed journals and were co-authored with Dr. Yuanyuan Shao and Haiping Zhang who provided technical advice.

Chapter 9 was significantly helped by Zhengyuan Deng, especially CFD settings.

Related publications:

1. **Liu, W.**, Fu, J., Zhang, H., Shao, Y., Zhang, H., & Zhu, J. (2018). Cold bonding method for metallic powder coatings. *Materials*, 11(11), 2086.
2. **Liu, W.**, Zhang, H., Shao, Y., Zhu, X., Wei, Y., Zhang, H., & Zhu, J. (2020). Applying microwave energy to fabricate powder coatings with strong and stable metal shine. *Progress in Organic Coatings*, 149, 105929.
3. **Liu, W.**, Zhang, H., Shao, Y., Zhang, H., & Zhu, J. (2020). Preparation of aluminium metallic effect powder coatings with high color stability using a novel method: Microwave bonding. *Progress in Organic Coatings*, 147, 105787.
4. **Liu, W.**, Zhang, H., Shao, Y., Zhang, H., & Zhu, J.(2021). "Produce various powder coated surfaces with stable metal shine via microwave energy." *Progress in Organic Coatings*, 154: 106199.
5. **Liu, W.**, Zhang, H., Shao, Y., Zhang, H., & Zhu, J. (2021). Application of fine powder coatings to plastic substrates via a bifunctional additive. *Progress in Organic Coatings*, submitted.
6. **Liu, W.**, Zhang, H., Shao, Y., Zhang, H., & Zhu, J. (2021). Microwave bonding enables powder-coating finishes with stable and high metal shine. *Chemical Engineering Journal*, submitted.
7. **Liu, W.**, Zhang, H., & Zhu, J, Chinese patent (2019), A microwave bonding device for metallic powder coating, Publication Patent Number: CN 209646365 U.
8. **Liu, W.**, Zhang, H., & Zhu, J, Chinese patent (2021), A method of bonding powder coatings with metallic pigments by microwave, Publication Patent Number: CN 109181400 A.

Acknowledgements

I would first like to express my deep gratitude to my supervisor Dr. Jesse Zhu. The forward-looking guidance and comprehensive support with his expertise encouraged me throughout my entire research over the past 4 years. Dr. Zhu is a professor of broad mind, wide vision, novel ideas. I have always been benefited from his overview guidance of my research work.

The deep appreciation would also be extended to my co-supervisor, Dr. Hui Zhang. He is always very patient and would help and guide me as long as I have problems in the experiment. Dr. Zhang is also a professor with first-class hands-on ability. He always taught us how to solve the problems with some novel and simple ideas and designs.

I would sincerely like to thank the following faculty members for providing me with mentor-ship in various areas during my time at Western: Drs. Sohrab Rohani, Shahzad Barghi, Lars Rehmman, Charles Xu. I would like to thank Natural Sciences and Engineering Research Council of Canada, China Scholarship Council for providing the financial supports to my graduate studies. I would also like to thank Huajiang Powder Coating Co., Ltd. (Guangdong, China) and Donghui powder equipment Co., Ltd. (Shandong, China) for the technical supports.

I would also thank the Profs. Yuanyuan Shao and Haiping Zhang for academic helps when I studied in Tianjin Universit. At the same time, I would like to thank Yufu Wei and Chenze Liu from Huajiang Powder Coatings Co., especially Xinping Zhu for their helps in the pilot-scale and industrial-scale tests. Thanks to Shubo Wang from Donghui Technology for his help in manufacturing the industrial-scale microwave device.

I am also grateful for the fun and support from my labmates including Jinbao Huang, Dannie Bao, Zhengyuan Deng, Marshall Yang, Zeneng Sun, Michael Nelson, and Yuqing Ye, Zehao Jing, Zhijie Fu, and Tian Nan. I would like to thank for the colleagues from our group including Zhi Zhang, professor Ying Ma.

I would also thank my dear parents and brother for their long-term understanding and support. Finally, I would like to thank my lovely wife Yujie Zhang for her understanding and encouragement, standing by my side throughout my graduate studies. I dedicate the work to my family.

Contents

Abstract	ii
Summary for Lay Audience	iii
Co-Authorship Statement	iv
Acknowledgements	v
List of Figures	xii
List of Tables	xxi
List of Appendices	xxiv
List of Abbreviations, Symbols, and Nomenclature	xxv
1 Introduction	1
1.1 General Introduction	1
1.1.1 Thermosetting powder coatings	3
1.1.2 Thermoplastic powder coatings	11
1.1.3 Metallic effect powder coatings	13
1.2 Objectives	16
1.2.1 Specific objectives	16
1.3 Thesis structure	17
2 Cold bonding method for metallic effect powder coating	20
2.1 Abstract	20

2.2	Introduction	21
2.3	Materials and methods	23
2.3.1	Materials and equipment	23
2.3.2	Cold bonding process	24
2.3.3	Analysis of bonding quality	24
2.4	Results and discussion	26
2.4.1	Control samples	26
2.4.2	bonded by PA	28
2.4.3	Bonded by PVA	31
2.5	Conclusions	35
3	Single-component-heating bonding for powder coatings	39
3.1	Abstract	39
3.2	Introduction	40
3.3	Materials and methods	42
3.3.1	Materials and equipment	42
3.3.2	Single-component-heating bonding method	42
3.3.3	Analysis of bonding quality	43
3.4	Results and discussion	44
3.4.1	non-bonded samples	44
3.4.2	SCHB bonded samples	45
3.4.3	Comparisons of SCHB and industrial bonding Methods	48
3.5	Conclusions	49
4	Primary study on microwave bonding method	51
4.1	Abstract	51
4.2	Introduction	52
4.3	Materials and methods	55
4.3.1	Materials and equipment	55
4.3.2	Microwave-heating bonding device	55
4.3.3	Preparation of samples	56

4.3.4	Characterization of powders and final films	56
4.4	Results and discussion	57
4.4.1	Non-bonded samples	57
4.4.2	Microwave-bonded samples	60
4.5	Conclusions	67
5	Lab-scale study on microwave bonding method for powder coatings	72
5.1	Abstract	72
5.2	Introduction	73
5.3	Materials and methods	76
5.3.1	Materials and equipment	76
5.3.2	Microwave bonding device	76
5.3.3	Preparation of samples	77
5.3.4	Characterization of powders	78
5.3.5	Characterization of films	79
5.4	Results and discussion	79
5.4.1	Epoxy-polyester hybrid powder coating system	79
5.4.2	Polyester powder coating system	86
5.4.3	PVDF powder coating system	89
5.4.4	Performance	92
5.5	Conclusions	93
6	Pilot-scale microwave bonding machine based on rotating	99
6.1	Abstract	99
6.2	Introduction	100
6.3	Materials and methods	103
6.3.1	Materials and equipment	103
6.3.2	Microwave bonding machine	103
6.3.3	Preparation of samples	104
6.3.4	Characterizations of powders and films	105
6.4	Results and discussion	107

6.4.1	Microwave-bonded samples with low Al addition	107
6.4.2	Microwave-bonded samples with high Al addition	115
6.5	Conclusions	120
7	Pilot-scale microwave bonding machine based on stirring	125
7.1	Abstract	125
7.2	Introduction	126
7.3	Materials and methods	129
7.3.1	Materials and equipment	129
7.3.2	Microwave bonding machine	129
7.3.3	Preparation of samples	130
7.3.4	Characterization of powders	131
7.3.5	Characterization of films	132
7.4	Results and discussion	133
7.4.1	Low addition of Al flakes	133
7.4.2	High addition of Al flakes	142
7.4.3	Performances of films	146
7.5	Conclusions	147
8	The industrial-scale microwave bonding machine	152
8.1	Abstract	152
8.2	Introduction	153
8.3	Materials and methods	155
8.3.1	Materials and equipment	155
8.3.2	Industrial microwave bonding machine	156
8.4	Results and discussion	158
8.4.1	Heating test	158
8.4.2	Bonding test	161
8.5	Conclusions	167
9	The optimization of impeller blade by CFD simulation	169

9.1	Abstract	169
9.2	Introduction	170
9.3	Numerical simulation	171
9.3.1	Geometry and mesh	171
9.3.2	CFD model	171
9.3.3	Boundary conditions and solver	174
9.4	Results and discussion	174
9.4.1	Volume fraction of particle	174
9.4.2	Average velocity	177
9.4.3	Radial velocity	181
9.4.4	Axial velocity	182
9.5	Conclusions	187
10	Applying fine powder coatings to plastic substrates	189
10.1	Abstract	189
10.2	Introduction	190
10.3	Materials and methods	191
10.3.1	Preparation of bifunctional additive and powder-coating surfaces	192
10.3.2	Characterizations of powder samples	192
10.3.3	Characterizations of films.	193
10.4	Results and discussion	194
10.4.1	Characterizations of the bifunctional additive	194
10.4.2	Epoxy powder coating	195
10.4.3	Epoxy-polyester powder coating	201
10.4.4	Properties and performances of films	206
10.5	Conclusions	207
11	Conclusions	211
11.1	Conclusions	211
11.2	Contributions	212
11.3	Future Work	213

Appendix A Original data for the figures in each chapter	214
A.1 Chapter 2	214
A.2 Chapter 3	214
A.3 Chapter 4	215
A.4 Chapter 5	216
A.5 Chapter 6	217
A.6 Chapter 7	218
A.7 Chapter 8	220
A.8 Chapter 10	221
 Appendix B The settings of CFD simulation	 223
 Curriculum Vitae	 230

List of Figures

1.1	The production process of powder coating [6].	2
1.2	The spraying process of powder coating.	3
1.3	The structural formula of polyester resin for powder coating.	4
1.4	The cross-linking reaction of TGIC polyester powder coating.	4
1.5	The structural formula of HAA.	5
1.6	The cross-linking reaction of HAA polyester powder coating.	5
1.7	The structural formula of epoxy resin.	6
1.8	The cross-linking reaction of dicyandiamide and epoxy resin.	6
1.9	The cross-linking reaction between DADH and epoxy resin.	7
1.10	The cross-linking reaction of epoxy-polyester powder coating.	7
1.11	The cross-linking reaction of polyurethane powder coating.	8
1.12	The structural formula of acrylic resin.	9
1.13	The cross-linking reaction of glycidyl acrylic resin.	10
1.14	The cross-linking reaction of FEVE fluorocarbon powder coating.	11
1.15	The structural formula of polyethylene resin.	11
1.16	The structural formula of polyvinyl chloride resin.	11
1.17	The structural formula of polyamide resin.	12
1.18	(a) PTFE; (b) PTFCE; (c) PVDF	13
1.19	The diagram (a) and picture (b) of the commercial bonding machine.	14
1.20	Images of aluminum pigment.	14
2.1	The process of cold bonding method.	24
2.2	Sampling process for the ash test.	25
2.3	Size distribution of the non-bonded sample.	27

2.4	Scanning electron microscope (SEM) and energy-dispersive X-ray spectroscopy (EDS) images of control samples. A, B) SEM images of non-bonded sample; C) EDS scanning of aluminum element; D) EDS spectrum of the rectangle area in B.	28
2.5	The relationship between $\Delta\omega$ and the dosage of water and polyacrylic acid (PA)	30
2.6	Size distribution of PA bonded sample.	31
2.7	SEM and EDS images of PA bonded samples. A, B) SEM images of cold bonded sample by PA; C) EDS scanning of aluminum element; D) EDS spectrum of the rectangle area in B	32
2.8	The relationship between $\Delta\omega$ and the dosage of water and PVA	33
2.9	Particle size distribution of PVA bonded sample.	34
2.10	SEM and EDS images of PVA-bonded samples. A, B) SEM images of cold bonded sample by PVA; C) EDS scanning of aluminum element; D) EDS spectrum of the rectangle area in B.	35
2.11	Surface comparisons between final films from various samples. (A) Clear coat, (B) Non-bonded sample, (C) Bonded sample.	36
3.1	Schematic diagram of the SCHB device. 1. Temperature sensor; 2. PTFE cylinder; 3. Ceramic heating tube; 4. Vibrator; 5. Al flakes; 6. Ultrasonic sieve; 7. fluidized bed; 8.Coating powder.	43
3.2	The particle size distribution of the non-bonded powder	44
3.3	A) Comparisons between Al contents in the original and deposited powders; B) relative differences of the Al contents in the original and deposited powders.	46
3.4	The characterizations of bonded powder prepared at 75°C. A-C) SEM images; D) EDX spectroscopy; E) particle size distribution. All the scale bars are 50 μm	47
3.5	The surface comparisons of final films, A,D) clear coat; B,E) non-bonded film; C,F) bonded film. All the scale bars are 30 μm	47
3.6	Visual and optical images of thermal and SCHB bonded samples. A, C, E) thermal-bonded film; B, D, F) SCHB-bonded film. All the scale bars are 20 μm	48

4.1	The difference between non-bonded and bonded metallic effect powder coatings when sprayed by an electrostatic system. The green patterns represent coating particles; the gold plates represent metallic pigments. A) Non-bonded powders; B) Effectively bonded powders.	53
4.2	Schematic diagram of the microwave bonding device. 1. Shell; 2. Drum; 3. baffles; 4. Microwave transmitters; 5. Power; 6. Discharger; 7. Thermocouple; 8. Rotating shaft. .	56
4.3	SEM images and size distribution of non-bonded sample. A) Low-magnification SEM image; B) Zoomed-in SEM image; C) Size distribution; D) EDS spectrum of the black site in B.	58
4.4	The deposited Al contents (A) and relative difference (B) at various mass and spray voltages	59
4.5	Mechanism of the spray process of non-bonded sample. The golden flakes represent Al flakes; the black round dots stand for clear coating particles.	61
4.6	The relative differences of Al contents of bonded samples made at different rotating speeds.	62
4.7	The relative differences of Al contents of bonded powders prepared at various temperatures.	64
4.8	SEM, EDS and size distribution of bonded sample. A) Low-magnification SEM image of microwave-bonded sample; B) High-magnification SEM image; C) EDS scanning of the element of Al and C; D) EDS spectrum of the black site in B; E) Size distribution.	66
4.9	Optical images of the surfaces of final films that cured from the non-bonded (A) and optimal samples (B), and the spray voltages separately are: 1) 30kV; 2) 60kV; 3) 90kV. The scale bars are 50μm.	67
5.1	The behaviors of metallic pigment of non-bonded (a) and bonded (b) powders during the electrostatic spraying. The green flakes and gray spheres stand for metallic pigments and coating particles, respectively.	74
5.2	The diagram of the microwave bonding device (a) and the picture of the drum (b). 1) Microwave transmitter; 2) Motor for vertical rotation; 3) Drive belt; 4) Baffles; 5) Thermocouple; 6) Drum; 7) Motor for horizontal rotation; 8) Door.	77

5.3	The $\Delta\omega$ of hybrid samples at various bonding temperatures and microwave powers.	81
5.4	FTIR spectra of non-bonded and microwave-bonded hybrid powder samples.	83
5.5	The SEM and EDS images of non-bonded and microwave-bonded hybrid samples. a,b) Non-bonded sample; c,d) bonded sample; e) EDS scanning of d, the green and blue spots represent aluminum and titanium, respectively; f) EDS spectroscopy of the white point in d. All the scale bars are 10 μ m.	84
5.6	The optical images of top surfaces (a, b) and cross-sections (c, d) of the non-bonded and microwave-bonded films.	85
5.7	The $\Delta\omega$ of polyester samples at various bonding temperatures.	87
5.8	FTIR spectra of non-bonded and microwave-bonded polyester powder samples.	88
5.9	The SEM and EDS images of non-bonded and microwave-bonded polyester samples. a,b) Non-bonded sample; c,d) Bonded sample; e) EDS scanning of d, the green and blue spots represent aluminum and titanium, respectively; f) EDS spectroscopy of the white point in d. All the scale bars are 10 μ m.	89
5.10	The optical images of top surfaces (a, b) and cross-sections (c, d) of the non-bonded and microwave-bonded polyester films (prepared at 68°C).	89
5.11	The $\Delta\omega$ of polyester samples at various bonding temperatures.	90
5.12	FTIR spectra of non-bonded and microwave-bonded PVDF powder samples.	91
5.13	The SEM and EDS images of non-bonded and microwave-bonded PVDF samples. a,b) Non-bonded sample; c,d) bonded sample; e) EDS scanning of d, the green and blue spots represent aluminum and titanium, respectively; f) EDS spectroscopy of the white point in d. The scale bars are 10 μ m.	92
5.14	The optical images of top surfaces (a, b) and cross-sections (c, d) of the non-bonded and microwave-bonded PVDF films.	93
6.1	The difference of non-bonded and bonded metallic powder paints sprayed by an elec- trostatic system. The black spheres stand for coating particles; the gold flakes represent metallic pigments. A) Non-bonded powder; B) Effectively bonded powder.	101

6.2	The schematic diagram (A) and picture (B) of the microwave bonding machine. 1. Digital display of nitrogen content; 2. Flowmeter of nitrogen; 3. Control panel; 4. Door; 5. Shell; 6. Microwave transmitters; 7. PTFE cylinder; 8. Temperature sensor; 9. Loaded materials; 10. Power system.	104
6.3	The bonding rates of samples bonded at different temperatures.	109
6.4	Color differences of final films prepared from the samples bonded at different temperatures.	112
6.5	Bonding rates and color differences of bonded samples at various rotating speeds. . . .	113
6.6	SEM, EDS and size distribution of the non-bonded, thermal-bonded and microwave-bonded powders. A,B) non-bonded; C,D) thermal-bonded; E,F) microwave-bonded; G) EDS scanning of F; H) EDS spectroscopy of the white point in F; I) Size distribution of the sample prepared at 59.5°C and 40rpm.	114
6.7	Optical images of top surface and cross-section of the final films obtained from non-bonded and bonded samples. A,D) Non-bonded powder; B,E) Thermal-bonded powder; C,F) Microwave-bonded powder prepared at 59.5°C and 40rpm.	116
6.8	Bonding rates and color differences of the bonded samples prepared at various temperatures.	118
6.9	SEM, EDS and size distribution of the non-bonded, thermal-bonded and microwave-bonded powders. A,B) non-bonded; C,D) thermal-bonded; E,F) microwave-bonded; G) EDS scanning; H) EDS spectroscopy of the white point in F; I) Size distribution. . .	119
6.10	Optical images of top surface and cross-section of the final films obtained from non-bonded and bonded samples. A,D) Non-bonded sample; B,E) Thermal-bonded sample; C,F) Microwave-bonded sample prepared at 61°C and 40rpm.	119
7.1	The diagram of the difference between non-bonded and bonded metallic effect powder coatings when sprayed by an electrostatic system. The grey spheres and gold plates represent coating particles and flaky metallic pigments, respectively.	127

7.2	The schematic diagram (A) and picture (B) of the microwave bonding machine. 1. Digital display board of nitrogen content; 2. The flowmeter of nitrogen; 3. Control panel; 4. Door; 5. Shells; 6. Microwave transmitters; 7. PTFE cylinder; 8. Temperature sensors; 9. Three-layer impeller; 10. Coating particles and Al flakes; 11. Protective system of cold air of microwave transmitters; 12. Power system.	130
7.3	The sieve residue rates and pictures of microwave-bonded samples prepared at different temperatures. The scale bars are 10cm.	134
7.4	The bonding rates of microwave-bonded samples made at various temperatures. . . .	136
7.5	SEM, EDS and size distribution of the powder samples with low Al addition. A,B,C) SEM images of the non-bonded, thermal-bonded, and microwave-bonded powders, respectively; D) EDS scanning; E) EDS spectrum of the white point in C2 ; F) Size distribution.	137
7.6	TIR spectra of non-bonded and microwave-bonded hybrid powder samples. . .	140
7.7	The color difference of the final films cured from different samples.	141
7.8	Optical images of the top surface (1) and cross-section (2) of the final films heat-cured from different powders. A) Non-bonded powder; B) Thermal-bonded powder; C) Microwave-bonded powder prepared at 59.5°C and 800rpm.	141
7.9	The bonding rates of microwave-bonded samples prepared at various temperatures. . .	143
7.10	SEM, EDS and size distribution of the powder samples with high Al addition. A,B,C) SEM images of the non-bonded, thermal-bonded, and microwave-bonded powders, respectively; D) EDS scanning; E) EDS spectrum of the white point in C2 ; F) Size distribution.	144
7.11	The color difference of the films prepared from various samples.	145
7.12	Optical images of top surfaces (1) and cross-sections (2) of the final films cured from different powders. A) Non-bonded powder; B) Thermal-bonded powder; C) Microwave-bonded powder prepared at 60°C and 800rpm.	146
8.1	The selective heating of microwave bonding method.	154
8.2	The tested area of the films prepared at 1 and 3 bar.	156
8.3	The picture of the industrial microwave bonding machine.	157

8.4	The four-layer agitator inside the bonding tank.	157
8.5	The control panel of the industrial microwave bonding machine.	158
8.6	The relationship between power and heating rate of the machine.	160
8.7	The real-time temperature in commercial and microwave bonding machines along with process time.	163
8.8	The particle size distribution of non-bonded and bonded samples. A) non-bonded; B) commercial-bonded; C) microwave-bonded.	165
8.9	The images of films prepared at 1 and 3 bar from different powders. A) non-bonded; B) commercial bonded; C) microwave bonded.	166
9.1	Six impellers: 10d-0) inclination angle is 10°; 10d-33) inclination angle is 10°, reverse-angling ratio is 1/3; 10d-66) inclination angle is 10°, reverse-angling ratio is 2/3; 20d-0) inclination angle is 20°; 20d-33) inclination angle is 20°, reverse-angling ratio is 1/3; 20d-66) inclination angle is 20°, reverse-angling ratio is 2/3.	172
9.2	Three rotational regions (a) and five marked lines (b).	172
9.3	The images of the meshes of tank (a,b) and rotational regions (c)	173
9.4	The volume fraction change along with time in the case of 10d-0.	176
9.5	The volume fractions of different cases at 3.9 seconds.	177
9.6	The volume fractions at the five lines in different cases. a) line 1; c) line 2; d) line 3; e) line 4; f) line 5.	178
9.7	The average velocities of the six cases with respect to time.	179
9.8	The average velocity distributions of the six cases at 3.9 seconds.	179
9.9	The average velocities at the five lines of the six cases (3.9 seconds). a) line 1; c) line 2; d) line 3; e) line 4; f) line 5.	180
9.10	The radial velocities of the six cases along with time.	181
9.11	The radial velocity distributions of the six cases at 3.9 seconds.	182
9.12	The radial velocities at the five lines of the six cases (3.9 seconds). a) line 1; c) line 2; d) line 3; e) line 4; f) line 5.	183
9.13	The axial velocities of the six cases along with time.	184
9.14	The axial velocity distributions of the six cases at 3.9 seconds.	185

9.15	The axial velocities at the five lines of the six cases (3.9 seconds). a) line 1; c) line 2; d) line 3; e) line 4; f) line 5.	186
10.1	XRD patterns of as prepared bifunctional additive (a) along with the stick patterns for the JCPDS files No. 50-741 (b) and 71-1123 (c). d) FTIR spectrum of the bifunctional additive.	195
10.2	SEM and EDS characterizations of different powders, (a, b) the bifunctional additive; (c, d) the epoxy coating powder; (e, f) the epoxy coating powder added the additive. . .	196
10.3	SEM images and size distributions of the coarse (a,c) and fine (b,d) epoxy powder coatings.	197
10.4	The flowability of the fine epoxy powder coatings with various contents of the bifunctional additive (wt%).	197
10.5	The DSC analyses of coarse and fine epoxy powders. a) Dynamic scanning of heat flow; b) Isothermal scanning for determining the degree of cure.	199
10.6	The top and cross-sectional surfaces of qualified epoxy films. a, c, e) Coarse powder coating (160°C / 0wt%); b, d, f) fine powder coating (140°C / 0.5wt%).	201
10.7	The surface roughness of the coarse and fine epoxy powder-coating films, a) coarse film; b) fine film; c) the profile of AC line in a; d) the profile of AC line in b.	202
10.8	The flowability of the fine hybrid powder coatings with various contents of the bifunctional additive.	202
10.9	The DSC analyses of coarse and fine hybrid powders. a) Dynamic scanning of heat flow; b) Isothermal scanning for determining the degree of cure.	204
10.10	The top and cross-sectional surfaces of qualified hybrid films. a, c, e) Coarse powder coating (150°C / 0wt%); b, d, f) fine powder coating (130°C / 0.3wt%).	205
10.11	The surface roughness of the coarse and fine hybrid powder-coating films, a) coarse film; b) fine film; c) the profile of AC line in a; d) the profile of AC line in b.	206
B.1	The turbulence model	223
B.2	Cell zone conditions of rotor areas.	223
B.3	Cell zone conditions of static area.	224
B.4	Boundary conditions of rotor areas.	224

B.5	Boundary conditions of the surface close to the rotor area.	224
B.6	Boundary conditions of the surface close to the static area.	225
B.7	Boundary conditions of the tank wall.	225
B.8	Properties of the particle phase.	226
B.9	Parts of the residuals.	227
B.10	Parts of the residuals.	228
B.11	Parts of the residuals.	229

List of Tables

2.1	Al content comparisons of non-bonded powder (30 kV).	28
2.2	Al contents (wt.%) of the samples before and after spraying tests (30 kV).	29
2.3	Al contents (wt.%) of the samples before and after spraying tests (30 kV).	32
3.1	The original and deposited Al contents of non-bonded samples	45
4.1	The deposited Al contents (wt%) of the samples prepared at different rotating speeds. .	62
4.2	The deposited Al contents (wt%) of bonded powders prepared at various temperatures.	63
5.1	The deposited Al contents (wt%) of hybrid powders obtained at different bonding temperatures and microwave powers.	80
5.2	The original (ω_{ori} / wt%) and deposited (ω_{dep} / wt%) Al contents as well as the relative difference ($\Delta\omega$ / %) of hybrid powders with low Al addition.	86
5.3	The original (ω_{ori} / wt%) and deposited (ω_{dep} / wt%) Al content as well as the relative difference ($\Delta\omega$ / %) of hybrid powders with high Al addition.	86
5.4	The deposited Al contents (ω_{dep} / wt%) of polyester powders prepared at different temperatures.	87
5.5	The deposited Al contents (ω_{dep} / wt%) of PVDF powders bonded at different temperatures.	90
5.6	The performances of hybrid, polyester and PVDF films sprayed at 90kV.	93
6.1	Deposited Al contents (/wt%) of microwave-bonded powders with low Al addition. . .	108
6.2	Deposited Al contents (/wt%) of bonded powders prepared at various rotating speeds. .	113
6.3	Deposited Al contents (/wt%) of bonded powders prepared at different temperatures. .	116

7.1	Deposited Al contents (wt%) of non-, thermal- (TM), and microwave-bonded samples with low Al addition.	134
7.2	Deposited Al contents (wt%) of non-, thermal- (TM), and microwave-bonded powders with high Al addition.	142
7.3	The performances of non-bonded and bonded films with low and high Al additions.	146
8.1	The heating data of PVDF metallic effect powder coating.	159
8.2	The heating data of polyester powder coating.	161
8.3	Some basic parameter comparisons between the commercial and microwave bonding machines.	162
8.4	Comparisons of bonding parameters between commercial and microwave machines. . .	162
8.5	Parameters of heating, holding and cooling.	164
8.6	The color difference between films prepared at 1 and 3 bar.	166
9.1	Computational model parameters	175
9.2	The summary of average, radial and axial velocity	185
10.1	The double rubs of epoxy films prepared at different curing temperatures and additive contents.	198
10.2	The double rubs of hybrid films prepared at different curing temperatures and additive contents.	203
10.3	The comparisons of hardness, adhesion and water absorption of films.	207
A.1	The original data for Fig. 2.5	214
A.2	The original data for Fig. 2.8	214
A.3	The original data for Fig. 3.3	214
A.4	The original data for Fig. 4.4A	215
A.5	The original data for Fig. 4.4B	215
A.6	The original data for Fig. 4.6	215
A.7	The original data for Fig. 4.7	215
A.8	The original data for Fig. 5.7	216

A.9	The original data for Fig. 5.3	216
A.10	The original data for Fig. 5.11	216
A.11	The original data for Fig. 6.3	217
A.12	The original data for Fig. 6.4	217
A.13	The original data for Fig. 6.5A	217
A.14	The original data for Fig. 6.5B	218
A.15	The original data for Fig. 6.8A	218
A.16	The original data for Fig. 6.8B	218
A.17	The original data for Fig. 7.3	218
A.18	The original data for Fig. 7.4	219
A.19	The original data for Fig. 7.7	219
A.20	The original data for Fig. 7.9	219
A.21	The original data for Fig. 7.11	220
A.22	The original data for Fig. 8.6	220
A.23	The original data for the red curve in Fig. 8.7	220
A.24	The original data for the blue curve in Fig. 8.7	221
A.25	The original data for Fig. 10.4	221
A.26	The original data for Fig. 10.8	222

List of Appendices

Appendix A	214
Appendix B	223

List of Abbreviations and Symbols

Abbreviations:

FTIR	Fourier transform infrared
DSC	Differential scanning calorimetry
TM	Thermal
SCHB	Single-component-heating bonding
MW	Microwave
CFD	Computational Fluid Dynamics
PA	Polyacrylic acid
PVA	Polyvinyl alcohol
T _g	Glass transition temperature
RFI	Radio frequency interference
PVDF	Polyvinylidene fluoride
PTFE	Polytetrafluoroethylene

Symbols:

D_{10}	The size of 10% of particles is lower than this value	μm
D_{50}	The size of 50% of particles is lower than this value	μm
D_{90}	The size of 90% of particles is lower than this value	μm
M_w	Absorbed water mass	g
M_0	Original mass of substrate and film	g
AOR	Angle of repose	°
ω	Al content	wt%
$M_{residual}$	Mass of residual	g
M_0	Mass of powder before ash test	g
$\Delta\omega$	Relative difference of Al content	%
ω_{ori}	Al content of original powder	wt%
ω_{dep}	Al content of deposited powder	wt%
Q_{max}	Electrons captured by a particle passing an electric field	C
r	Equivalent sphere radius	m
ϵ_0	Dielectric constant of vacuum	-
E	Electric intensity	N/C
ϵ_r	Relative permittivity	-
n_{max}	Maximum speed for a powder to be not compacted	rpm
g	Gravitational acceleration	m^2/s
r	drum radius	m
P	Microwave power absorbed by unit volume of material	W/m^3

f	Microwave frequency	Hz
ϵ''_{eff}	Effective dissipation factor of materials	-
$\epsilon''_{dipolar}$	Effective dissipation factor of dipolar polarization	-
ϵ''_{MW}	Effective dissipation factor of interface polarization	-
ϵ'	The real part of the complex permittivity of materials	-
$\tan\delta$	Tangent of dielectric loss angle	-
v	Volume fraction of conductive materials	-
f_{max}	Maximum loss frequency	Hz
δ	Conductivity	S/m
τ	Relaxation time constant	-
V_{H_2}	Volume of hydrogen	m ³
M_{Al}	Atomic mass of aluminum	g/mol
V_m	Molar volumes of gases at 1 atm and 25 °C	m ³ /mol
M_{sample}	Mass of powder sample	g
γ	Bonding rate	%
ω_{add}	Al additon	wt%
ω_{dep}^B	Deposited Al content of bonded samples	wt%
ω_{dep}^N	Deposited Al content of non-bonded samples	wt%
ΔE	Total color difference	-
I_{sample}	Reflected light intensity of sample	cd
$I_{reference}$	Reflected light intensity of reference	cd
V_{total}	Total heating rate of microwave bonding device	°C/min
Gloss 20°	Gloss at 20°	-
Gloss 60°	Gloos at 60°	-
DOI	Distinctness of Image	-
E_{stir}	Energy consumption of stirring motor	kWh/t
E_{MW}	Energy consumption of microwave	kWh/t
P	Energy consumption of single microwave transmitter	kW

1 Introduction

1.1 General Introduction

Coating is applied to the surface of an object by different coating processes to form a solid covering with strong adhesion, continuity, and sufficient strength. The covering formed in this way is generally called film that mainly provides protection and decoration with the substrate.

Coatings are mainly composed of resins, solvents, pigments, fillers, and additives. There is no agreement on the origin of coatings so far in academic circles. From 2003 to 2004, archaeologists in South Africa discovered a 100000-year-old mixture of artificial ochre in the Blombos Cave, which can be used as a pigment [1]. In 2011, further excavation in the same cave led to the discovery of the complete tool for grinding pigments and the material for manufacturing the original pigments [2]. About 40000 years ago, some cave murals were painted with primitive pigments (red or yellow ochre, hematite, manganese oxide, and charcoal) [3]. About 7000 BC, China began to use natural resins as film-forming materials called Daqi. This kind of paint film is rare now due to produce a pungent and harmful odor. In the middle of the 18th century, steam engine equipment began to be used to grind paint pigments, and people found an approach to replace lead-based pigments in white zinc oxide derivatives. In the 19th century, interior painting became increasingly popular because it could not only decorate the indoor environment but also prevent the walls from rotting due to moisture. At this time, linseed oil was increasingly used as a cheap solvent. Man-made resins or alcohols were invented to work as a solvent because World War II affected the supply of linseed oil and caused a shortage of linseed oil. Because of the low price, easy fabrication, abundant colors, and good durability, these man-made solvents were quickly promoted to the market.

It was only in the middle of the 19th century that fast-drying coatings were made by dissolving solid natural resins with solvents. Among them, the most simple waterborne coating is a lime emulsion. About one hundred years ago, some people added emulsified linseed oil to modify the lime emulsion, which is probably the earliest latex paint. Since the 1970s, due to the establishment of environmental protection law, lots of countries have restricted the emission of organic solvents and harmful substances, thus limiting the use of paint [4]. In addition,

75% of the paint manufacturing raw materials come from the petrochemical industry. Due to the economic crisis in western industrial countries and the adjustment of oil prices in the Third World countries, more countries generally require energy and resource conservation, which further limits the use of traditional organic paint.

Based on the above reasons, Gustin et al invented the powder coating in the 1960s [5]. It is a 100%-solid powder coating composed of four components, solid resin, pigments, fillers, and additives. Different from the traditional solvent-based coatings and waterborne coatings, its dispersion medium is not solvent or water, but air. Hence, powder coating has no solvent pollution, 100% film formation, low energy consumption, and is a very eco-friendly coating. Powder coatings are fabricated by the steps shown in Fig. 1.1:

1. premix the four components and transfer them into an extruder;
2. extrude the powdered components into chips at a certain temperature;
3. grind the chips into powder with expected size;
4. obtain final products after sieving the powder.

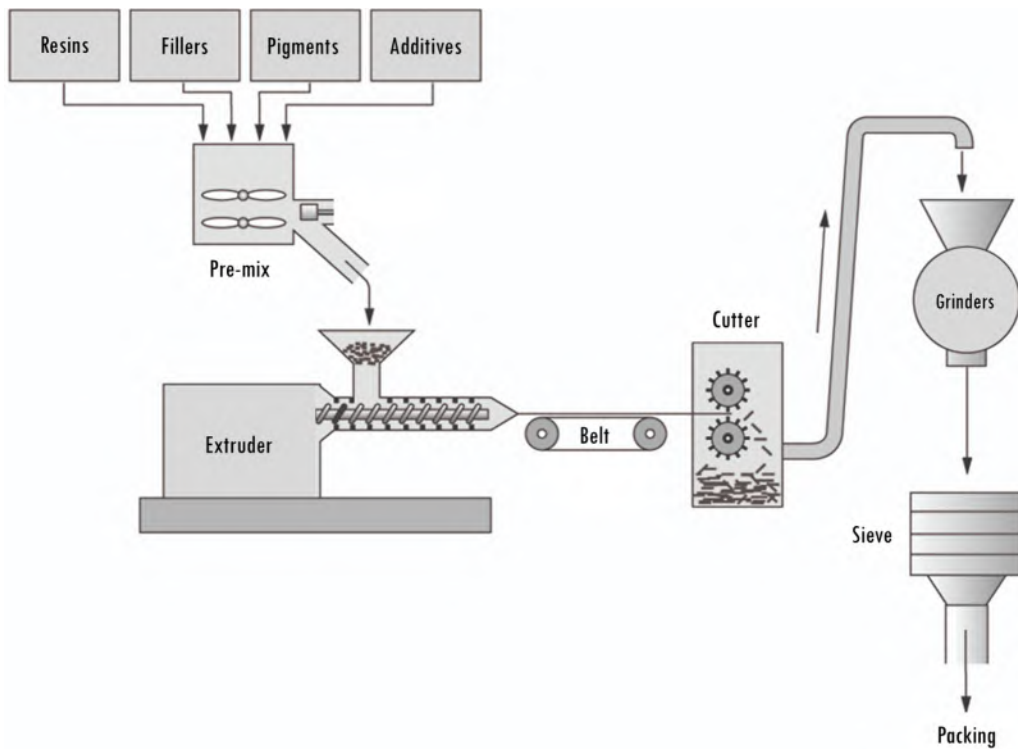


Figure 1.1: The production process of powder coating [6].

The spraying process of powder coating also differs from the liquid paints, which usually employs an electrostatic system. A most general spraying process is given in Fig. 1.2. The powder coating is first fluidized by the air and pneumatically transported to a electrostatic gun. The coating particles capture electrons and ions when passing the nozzle and deposit onto grounded substrates. The Most important advantage of this process is that the usage of powder coating can reach almost 100% by reclaiming and re-spraying the over-sprayed particles.

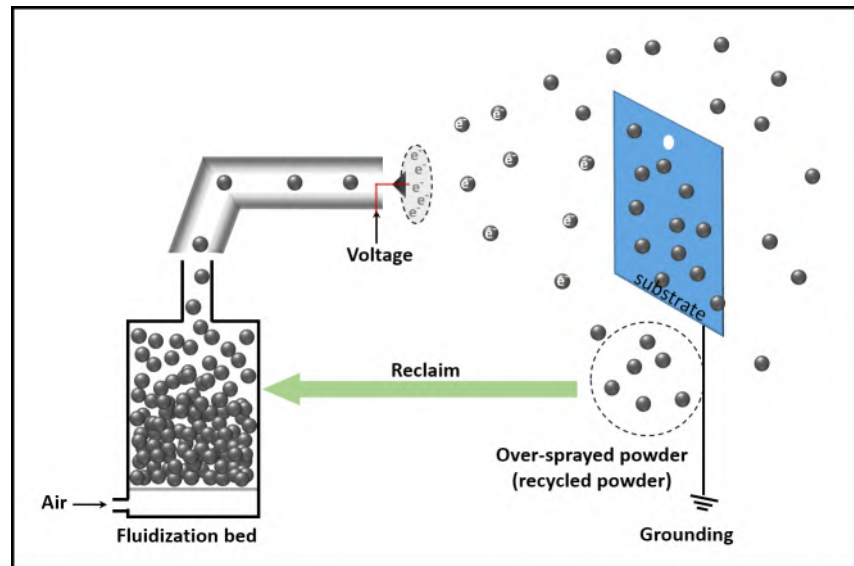


Figure 1.2: The spraying process of powder coating.

According to the report of Global Market Forecast to 2025 [7], the market size for powder coatings is projected to grow from USD 11.6 billion (2020) to USD 14.9 billion (2025). Strong growth can be found in the powder coatings market in China, India, and South-East Asian countries. Since the pigment, filler, and additives are similar to the traditional paint, this chapter will introduce the powder coatings by resin types. In addition, some attentions will be put on metallic effect powder coatings which is the main research object of this thesis.

1.1.1 Thermosetting powder coatings

At present, the main varieties of thermosetting powder coatings on the market are: polyester powder coatings, epoxy powder coatings, epoxy-polyester powder coatings, polyurethane powder coatings, acrylic powder coatings, fluoro-resin powder coatings, etc.

Polyester powder coatings

Polyester powder coating is the most widely used weatherable powder coating on the market, applied on many substrates, such as aluminum materials for doors and windows, road marker posts, accessories or hubs of bicycle body, automobile and motorcycle, air conditioner shell, handrail and fence, and agricultural equipment [8]. The polyester resin structural formula is shown in Fig. 1.3:

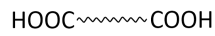


Figure 1.3: The structural formula of polyester resin for powder coating.

The common curing agents of polyester powder coatings are TGIC (triglyceride isocyanurate) and HAA (hydroxyalkyl amide) [9]. The curing reaction of TGIC and polyester resin is shown in Fig. 1.4, which is an addition reaction between epoxy and carboxyl groups.

The advantages of TGIC polyester powder coatings are listed as below:

1. The film has strong weather resistance.
2. No byproducts such as water or ethanol in the curing reaction, so there are usually no pinholes and pockmarks in the coating.
3. Polyester resin has a good heat resistance and is not easy to yellow when curing.
4. The adhesion between polyester resin and substrate is generally strong, so primer is not necessary.
5. Good chemical resistance.

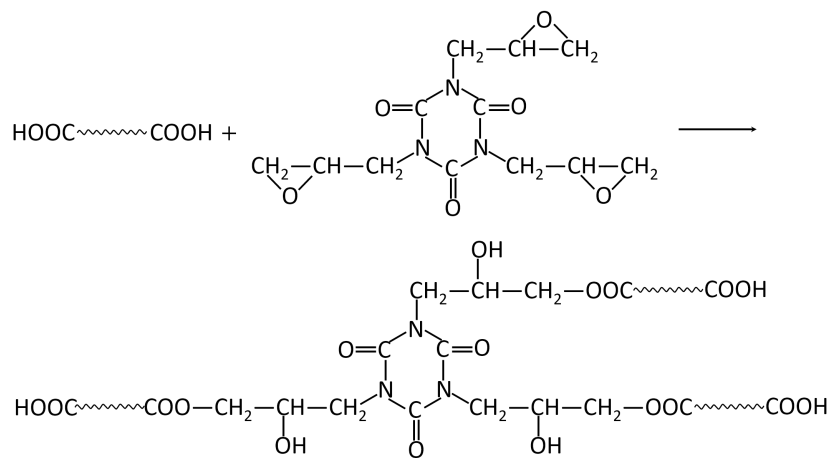


Figure 1.4: The cross-linking reaction of TGIC polyester powder coating.

TGIC powder coatings also have some disadvantages:

1. The alkali resistance is slightly poor due to the carboxyl groups.
2. TGIC has a degree of irritation and will slowly absorb water in the air, so the powder coating also has a little irritation and need to be stored drily.

Another commonly used curing agent, HAA [10], contains four hydroxyl groups, and its structural formula is given in Fig. 1.5. The curing reaction is presented in Fig. 1.6. The hydroxyl and carboxyl groups condense and release water molecules during the curing. The advantage of HAA polyester powder coating is that it has no irritating smell and is not harmful to the skin. But the disadvantage is that the heat resistance is not as good as the TGIC type, and pinholes tend to form in the film due to the byproduct of water, especially when the film is thick.

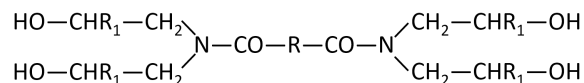


Figure 1.5: The structural formula of HAA.

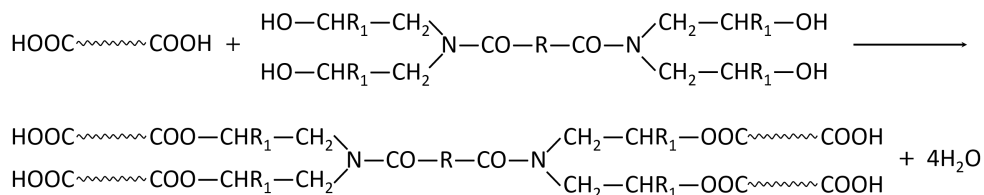


Figure 1.6: The cross-linking reaction of HAA polyester powder coating.

Epoxy powder coatings

Epoxy powder coating is the earliest thermosetting powder coating on the market, which has a wide range of uses and a large number of varieties. It is mainly used in inner and outer walls of pipes, agricultural machinery, kitchen supplies, marine equipment, building materials, interior decoration, and electrical insulation coating [11]. The structural formula of epoxy resin is exhibited in Fig. 1.7:

The main advantages of epoxy powder coatings:

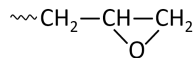


Figure 1.7: The structural formula of epoxy resin.

1. The film has good leveling property due to the low melt viscosity of the epoxy resin and there are no small-molecule compounds generated during curing, so the coating is generally smooth and even without pinholes and other problems.
2. The film has good adhesion to the substrate due to the existence of hydroxyl, thus primer is not necessary generally.
3. The film has high scratch resistance as well as good chemical and corrosion resistance.
4. There are many kinds of curing agents for epoxy powder coating, enabling it is adaptable for many fields.

The curing agents commonly used for epoxy powder coatings are dicyandiamide and its derivatives. The curing reaction between them is shown in Fig. 1.8. The curing temperature of dicyandiamide is as high as 200°C and its compatibility with the resin is not good enough. Thus, additional curing accelerators are necessary to help the curing, such as imidazole, guanidine, hydrazine, and guanidine [12]. One of the derivatives, substituted dicyandiamide, was obtained by the following two steps: a) add ammonia to dicyandiamide; b) replace the alkyl with aromatic organic compounds. This modified dicyandiamide has better compatibility with epoxy resin and lower curing temperature.

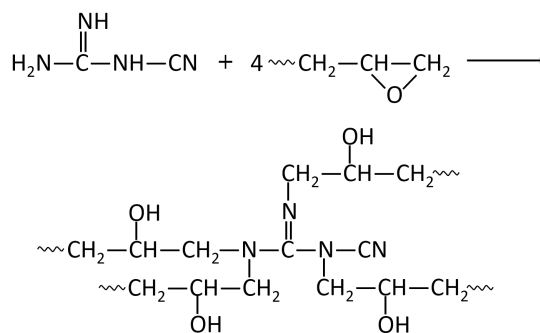


Figure 1.8: The cross-linking reaction of dicyandiamide and epoxy resin.

Another mostly used curing agent is dicarboxylic acid diacid hydrazine (DADH), and its curing reaction is shown in Fig. 1.9. Group R could be alkane or aromatic hydrocarbon. Since DADH is a long-chain aliphatic organic compound, the flexibility of this kind of paint film is excellent. In addition, some curing agents, such as imidazole, phenolic resin, anhydride, etc, are also frequently used in epoxy powder coatings.

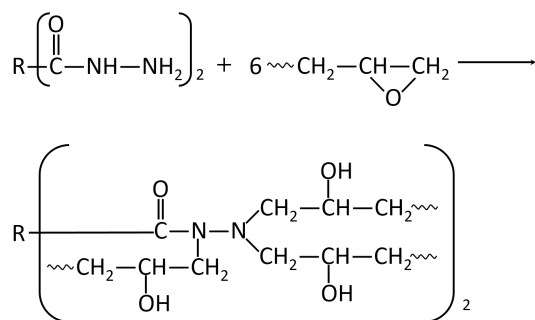


Figure 1.9: The cross-linking reaction between DADH and epoxy resin.

Epoxy-polyester powder coatings

Epoxy-polyester resin is a mixture of polyester and epoxy resin, which are curing agents for each other. The polyester resin used here is different from that of pure polyester powder coating, for instance, substituent group and chain length. It was first popularized and used in Europe as interior paint, and now it is also the most widely used powder coating with the largest output in China. It is mainly used for the surfaces of the automobile, household appliances, metal furniture, indoor fitness equipment, instrumentation, radiator, etc [13]. The curing is an addition reaction between the carboxyl and epoxy groups, as shown in Fig. 1.10.

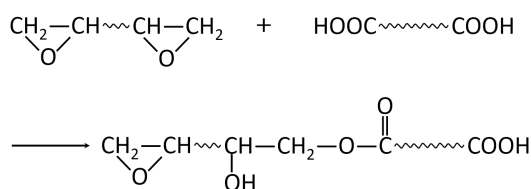


Figure 1.10: The cross-linking reaction of epoxy-polyester powder coating.

The advantages of epoxy-polyester powder coating:

1. The film has fewer pinholes and other defects due to no byproduct during curing reaction.

2. It has a variety of characteristics due to the variety of epoxy and polyester resins.
3. Films are smooth and even due to the low melt viscosity of resins.
4. The film has good adhesion to the substrate, good mechanical properties, and does not need a primer.
5. The alkali resistance is slightly poor, and the resistance to other chemicals is close to that of epoxy powder coatings.
6. The film has super decoration performance, good resistance to over baking, and excellent appearance fullness.

However, epoxy-polyester powder coating has an obvious disadvantage, bad weather resistance, so it is usually used indoors. Although reducing the content of epoxy resin can improve the weather resistance, it is still not as good as pure polyester powder coating.

Polyurethane powder coatings

Polyurethane powder coating is mainly composed of hydroxyl polyester resin, blocked isocyanate resin, pigment, filler, and additives. It is known as one of the main weatherable powder coatings, widely used in bicycles, motorcycles, street lamps, air conditioners, refrigerators, doors and windows, washing machines and other household appliances, high-end furniture, and automobile industries [14]. The reaction between hydroxyl polyester and blocked isocyanate resin is shown in Fig. 1.11.

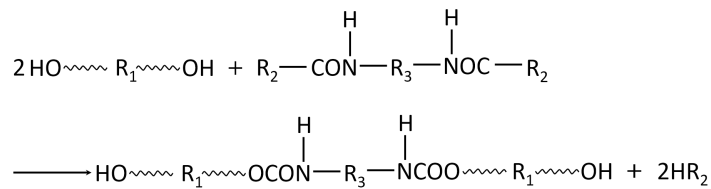


Figure 1.11: The cross-linking reaction of polyurethane powder coating.

The advantages of polyurethane powder coating:

1. The film has excellent leveling property because the sealant will not react with the polyurethane resin before unsealing, which allows it has enough leveling time.

2. Good adhesion to substrates and no primer is needed.
3. The film has good physical and mechanical properties and chemical resistance.
4. The formula range is wide, so the film with different performance requirements and curing speed can achieve.

The biggest disadvantage of polyurethane powder coating is that air pollution due to the release of the sealant during the curing. This is also easy to cause pinholes or bubbles, especially when the film is thick. Therefore, it is necessary to reduce the amount of sealants as much as possible and consider the use of non-toxic sealants. At present, a new internal sealant (urea diketone) was synthesized that will not release gases, which significantly avoids air pollution and reduces the pinholes.

Acrylic powder coatings

Acrylic powder coating is also one type of weather-resistant powder coating, usually applied in the fields of automobile, high-end furniture, electronics, etc [15]. The main resin and curing agent systems are as follows:

1. Glycidyl acrylic resin, polycarboxylic acid curing agent;
2. Hydroxyl acrylic resin, blocked isocyanate or amino resin curing agent;
3. Carboxylic acrylic resin, TGIC curing agent;
4. Acrylamide self-crosslinking system;
5. Acrylic resin, epoxy, or polyester resin curing agent.

The resin of acrylic powder coating is polymerized acrylic acid, whose structural formula is shown in Fig. 1.12.

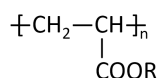


Figure 1.12: The structural formula of acrylic resin.

Here, the first system is taken as an example. The curing agents of glycidyl acrylic resin include polycarboxylic acid, polyanhydride, and polyphenol. Aliphatic dicarboxylic acid is one of the most commonly used curing agents, and the curing reaction is illustrated in Fig. 1.13.

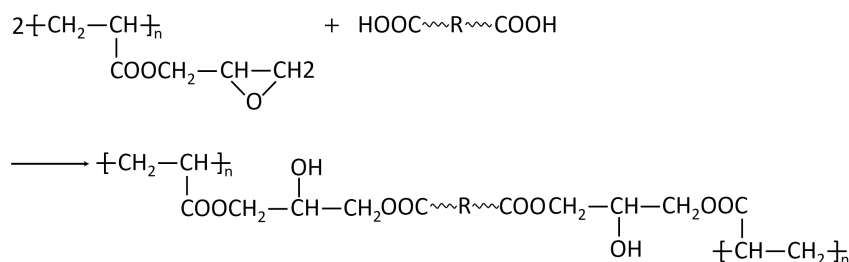


Figure 1.13: The cross-linking reaction of glycidyl acrylic resin.

The main advantages of acrylic powder coatings:

1. Excellent mechanical properties and good chemical resistance.
2. The exposure, stain, and weather resistance of the film are better than other thermosetting powder coatings, so it is most suitable for outdoor high decorative coating.

However, acrylic powder coating also has several distinct disadvantages, such as high cost, high melt viscosity, and poor film leveling.

Fluororesin powder coatings

Thermosetting FEVE fluorocarbon powder coating is a kind of heavy-duty anticorrosion coating, which has superior protection performance in heavy pollution and strong corrosion [16]. It is broadly applied in the chemical industry, construction, machinery, household products and other fields. FEVE fluorocarbon resin is a copolymer of fluoroolefins and alkyl vinyl ethers/esters, whose fluorine content can reach 20-35%. The curing process is the reaction between the hydroxyl group from FEVE fluorocarbon resin and the blocked isocyanate resin as shown in Fig. 1.14.

FEVE fluorocarbon powder coating has excellent weather, chemical, corrosion and pollution resistance, but poor surface gloss, high curing temperature and high cost.

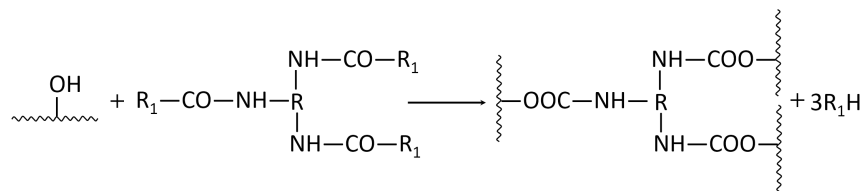


Figure 1.14: The cross-linking reaction of FEVE fluorocarbon powder coating.

1.1.2 Thermoplastic powder coatings

Currently, the frequently used thermoplastic powder coatings are polyethylene, polyvinyl chloride, polyamide, fluoro-resin powder coatings, etc.

Polyethylene (PE) powder coatings

The structural formula of PE resin is shown in Fig. 1.15. PE powder coating has excellent corrosion resistance and electrical insulation, good chemical and ultraviolet radiation resistance. However, the film shows bad mechanical strength and poor adhesion to the substrate. It can be used for impeller, chemical tank, pump, the inner wall of a pipe, inner net plates of a refrigerator, metal plate, automobile parts, etc [17].

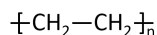


Figure 1.15: The structural formula of polyethylene resin.

Polyvinyl chloride (PVC) powder coatings

Fig. 1.16 presents the structural formula of PVC resin. PVC powder is one of the cheapest polymers for industrial mass production. PVC film has excellent solvent resistance, impact resistance, salt spray resistance, good corrosion resistance to water and acid, and has the ability to prevent food pollution. Hence, PVC powder coatings are mainly used for painting steel furniture, metal mesh, chemical equipment, etc [18].

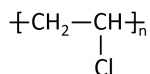


Figure 1.16: The structural formula of polyvinyl chloride resin.

Polyamide powder coatings

It is also known as nylon powder coating. The structural formula of polyamide resin is shown in Fig. 1.17. The melting point of polyamide resin is generally high, mainly because the N atom of the amino group in the resin molecule is easy to form hydrogen bonds with an adjacent hydrogen atom. Nylon has the advantages of high impact resistance, mechanical strength, wear resistance, low hardness and friction coefficient, and low dust absorption, which can be used for spraying parts with special requirements, such as pump impeller, marine propeller, textile machinery parts, motorcycle bracket, automobile wheels, etc. In addition, since nylon would not be eroded by mold or promotes bacterial growth, and has excellent saltwater resistance, it is very suitable for spraying objects immersed in or in contact with sea water [19]. At the same time, because nylon powder coating is nontoxic, tasteless, and inert to mold and bacteria, it is also heavily used in the food industry, such as drinking water pipes and food packaging.

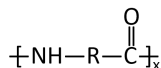


Figure 1.17: The structural formula of polyamide resin.

Fluororesin powder coatings

Some structural formulas of fluororesins are shown in Fig. 1.18. Many kinds of fluoropolymers can be used as powder coatings, such as polytetrafluoroethylene (PTFE), Polychlorotrifluoroethylene (PTFCE), polyvinylidene fluoride (PVDF), etc [20]. The melting point of PTFE is 327 °C, and it is able to work for a long time in the range of -160 to 260 °C. It has excellent corrosion resistance and does not dissolve even in aqua regia. It also has excellent dielectric properties, a very low friction coefficient and self-lubrication. Although the price is high, it has been widely applied in petroleum, sealing, chemical anticorrosion coating, electronic materials, ship launching guide rail and non-stick pot coating. PTFCE is cheaper than PTFE, and the production temperature is also much lower. The coating is very stable when works below 130°C. Its resistance to alkali and hydrogen fluoride is better than enamel, and the resistance to sulfuric acid and chlorine is better than stainless steel. It can be applied on many fields, such as anticorrosion equipment or reactors for chemical factories, pesticide plants, pharmaceutical manufactures. The main advantages of PVDF powder coatings are excellent weather

resistance, dust resistance and lasting luster when used outdoors.

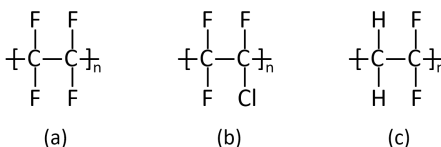


Figure 1.18: (a) PTFE; (b) PTFCE; (c) PVDF

1.1.3 Metallic effect powder coatings

Metallic effect powder coating, the main research object in this thesis, is a type of paint that mainly consists of general powder coating and metallic pigments. The most important production procedure for this type of coating is the bonding process, aiming to bond the two materials to ensure the color stability of final films [21]. The bonding process starts with making the surfaces of coating particles sticky by heating them to glass transition temperature (T_g). The metallic pigments then adhere to the sticky surfaces and bonded particles will be formed finally. Fig. 1.19 shows the diagram and picture of a commercial bonding machine, which uses high-speed stirring and water/oil jacket as heating sources. Due to the heating modes, there are many inherent drawbacks, such as low heating rate, bending or grinding of metallic pigments, high-temperature bonding, mis-bonding, etc.

For powder coating that has been introduced in the above sections, metallic pigments will be focused here. In industry, Aluminum, Copper, Zinc, Mica, and Pearlescent pigments are frequently used in powder coatings.

Aluminum pigment

Aluminum pigment, also known as “silver pigment”, is in the shape of a flake with a diameter of 5-70 μm as shown in Fig. 1.20. Al pigment is the most widely used metallic pigment in powder coating because of its low price, wide use, and large demand. The Al pigment is generally manufactured by ball milling the aluminum foil with the protection of inert gas or petroleum solvent. Sometimes, for better protection or other purposes, the surfaces of Al pigment are covered by specific materials, such as acrylic resin, silica, stearic acid, alumina and oleic acid. Al pigmented powder coating has heavy applications in the fields of high-end

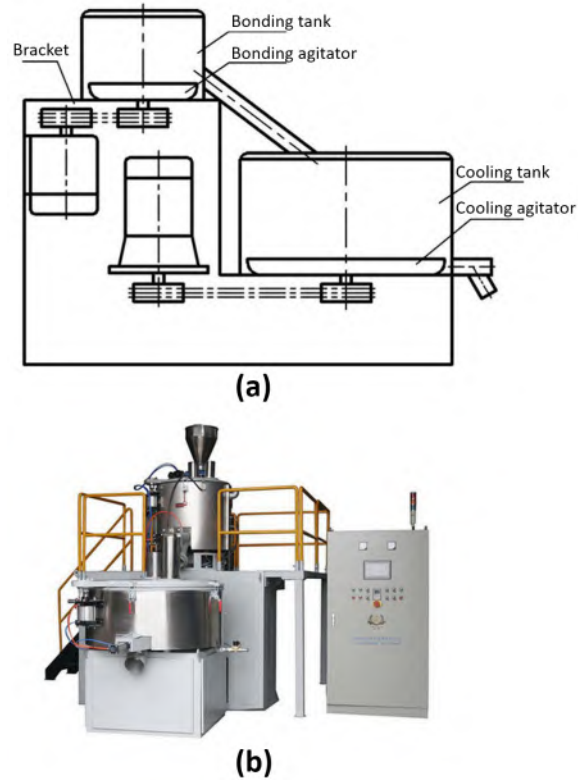


Figure 1.19: The diagram (a) and picture (b) of the commercial bonding machine.

furniture, domestic appliances, automobile parts, bike parts, electronics, etc [22]. The characteristics of Al pigment are listed below.

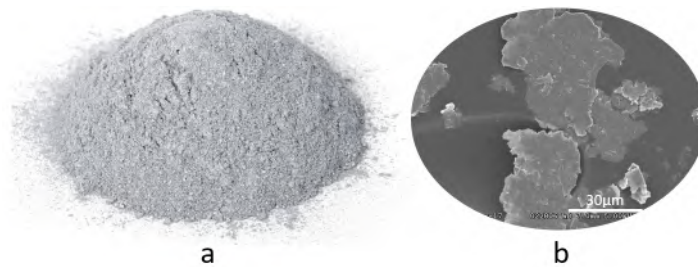


Figure 1.20: Images of aluminum pigment.

a. Covering

As stated that Al pigment is flake-like, and the ratio of the diameter and thickness of the flake is in the range 40:1 to 100:1. Al pigments in powder coating tend to parallel with the substrate during the curing. Many Al pigments connect with each other to form a continuous metal film, covering the substrate and reflecting the light. The covering property of Al pig-

ment largely depends on the value of the superficial area. The greater the ratio of diameter to thickness, the better the covering property.

b. Shielding

As mentioned, Al pigments form continuous metal films inside the coating, which cut off the capillary pores of the coating and impede water and gas to reach the bottom through these pores. This is the physical shielding property of Al pigment in coatings.

c. Optical properties

The surface of Al pigment is smooth and bright, which has the ability to reflect 60% - 90% of visible, ultraviolet and infrared lights. This property provides a film with a sparkle and shiny appearance.

Copper pigment

The copper pigment is usually used to mimic gold color in powder coatings. It is produced by ball milling the coarse copper powder and stearic acid or its esters into small and bright flakes. The pigment made by copper-zinc alloy powder provides red- or green-light gold color, and copper-tin alloy powder presents the color ranging from bronze to gold bronze.

Zinc pigment

At present, zinc pigment is mainly used in anticorrosion powder coating that is also called zinc-rich powder coating. The zinc pigment concentration of this coating can be as high as 80 wt%. It is manufactured by evaporating zinc into vapor under nitrogen protection, followed by rapid condensation to form spherical zinc particles. The faster the condensation rate, the smaller the particle size. The oxygen content in the condenser should be strictly controlled to ensure the purity of the product and the zinc oxide content should be controlled below 6 wt%.

Mica and pearlescent pigment

Mica powder is a kind of silicate with a layered structure, which mainly consists of three layers. The top and bottom layers are silicon oxide tetrahedron and the middle layer are usually aluminum oxide octahedron. The mica pigment is prepared by splitting the mica powder into a very thin sheet, and the sheet thickness can be less than 1 μm . The pearlescent pigment is

a layered composite, which is composed of a substrate and covering layer. The substrate is usually natural muscovite, silica, aluminum, or mica, and the covering is titanium dioxide, iron oxide, ferrocyanide, or carmine, etc. Compared to metallic luster, the mica and pearlescent pigments both have a Flip-Flop or two-tone effect, which results from the alteration of the luminance sensation during modification of the viewing angle. This mainly because these layer structures of the two pigments enable them to have a multipath reflection of light.

1.2 Objectives

The overall objective of this research is to achieve high bonding quality and color stability for the metallic effect powder coating. Some new bonding methods have been also established and developed to avoid the drawbacks of the current commercial bonding technology. The final goal of this work is to replace the existing commercial bonding machine by our self-designed bonding device with better bonding quality.

1.2.1 Specific objectives

1. Establishments of the new bonding methods
 - (a) Cold bonding method by using adhesive polymers;
 - (b) Single-component-heating bonding method via heating the metallic pigment alone;
 - (c) Microwave bonding method based on the selective microwave heating.
2. Optimization of bonding parameters in different bonding methods
 - (a) Optimizing the usages of water and PVA/PA in cold bonding method;
 - (b) Adjusting the bonding temperature in the single-component-heating bonding method;
 - (c) Optimizing the motion mode, microwave power, stirring speed, rotating speed, and bonding temperature of microwave bonding method;
 - (d) Applying microwave bonding to polyester, epoxy, PVDF powder coatings.
3. Industrialization of the microwave-bonding device
 - (a) Setting up a lab-scale microwave-bonding device with a two-directional rotating drum;
 - (b) Design and construction of a pilot-scale device with a rotating drum;
 - (c) Modification of the pilot-scale device from the mode of rotation to agitation;
 - (d) Construction of an industrial-scale microwave bonding device with the mode of agitation.

1.3 Thesis structure

- Chapter 1** The introductory chapter overviews the research background and specific objectives of the thesis.
- Chapter 2** In this chapter, the cold bonding method was established, which applies PVA/PA to bond the coating particles and metallic pigments at room temperature.
- Chapter 3** To avoid mis-bonding, this chapter develops a new bonding method (single-component-heating bonding method) which heating metallic pigments alone to bond metallic effect powder coatings.
- Chapter 4** The chapter includes the construction of a lab-scale microwave bonding device and the preliminary exploration of using this device to bond a polyester clear powder coating and aluminum pigments.
- Chapter 5** This chapter reports on the expansion of the microwave bonding method to bond other commercial powder coatings, such as polyester, epoxy, epoxy-polyester, and PVDF powder coatings.
- Chapter 6** In this chapter, the lab microwave bonding device (0.05 kg/batch) was scaled up to pilot-scale one (10 kg/batch). This chapter summarizes the optimizations of bonding conditions of the pilot-scale bonding device.
- Chapter 7** To increase the bonding quality, the rotation of the pilot-scale microwave bonding device was modified to agitation. The bonding conditions were optimized and the bonding quality of samples was compared.
- Chapter 8** The pilot-scale microwave bonding device (10 kg/batch) was scaled up to industrial-scale one (100 kg/batch). The heating and bonding experiments were conducted by this device.
- Chapter 9** The agitator blade for the microwave bonding device was optimized by CFD simulation to improve the uniformity of the stirring.
- Chapter 10** To improve the flowability of fine powders and lower the curing temperature of coatings, a bifunctional additive was prepared and then tested in epoxy and epoxy-polyester powder coatings.
- Chapter 11** This chapter summarizes the results from this research, and it provides possible avenues for future work.

Bibliography

- [1] Hillary Mayell. Is bead find proof modern thought began in Africa. *Retrieved February, 25:2006, 2004.*
- [2] Stephanie Pappa. Oldest human paint-making studio discovered in cave. *Live Science. Retrieved October, 14:2011, 2011.*
- [3] Thomas J. Craughwell. 30,000 years of inventions: Breakthroughs, discoveries, and accidents that changed human history. *Black Dog & Leventhal Pub, 2012.*
- [4] Vasilios A Sakkas, Ioannis K Konstantinou, Dimitra A Lambropoulou, and Triantafyllos A Albanis. Survey for the occurrence of antifouling paint booster biocides in the aquatic environment of greece. *Environmental Science and Pollution Research, 9(5):327–332, 2002.*
- [5] Daniel S Gustin and Albert W Wainio. Electrostatic coating method and apparatus, January 16 1951. US Patent 2,538,562.
- [6] Jing Fu. Characterization of fine powders and development of processes for powder coatings, 2014. 2026.
- [7] MarketsandMarkets INC. Powder coatings market - global market forecast to 2025. 2020.
- [8] Daniel Maetens. Weathering degradation mechanism in polyester powder coatings. *Progress in organic coatings, 58(2-3):172–179, 2007.*
- [9] Zhongyan Du, Shaoguo Wen, Jihu Wang, Changle Yin, Dayang Yu, and Jian Luo. The review of powder coatings. *Journal of Materials Science and Chemical Engineering, 4(3):54–59, 2016.*
- [10] Anuradha C Abhyankar, Neil R Edmonds, and Allan J Eastal. Composite manufacture from waste powder coatings: a step toward industrial ecology. *Centre for Advanced Composite Materials, The University of Auckland, Auckland, 2007.*
- [11] Kimmo Peltonen. Gas chromatographic-mass spectrometric determination of phenols and heterocyclic nitrogen compounds in the thermal degradation products of epoxy powder paint. *Journal of analytical and applied pyrolysis, 10(1):51–57, 1986.*
- [12] SJ Garcia, A Serra, and J Suay. New powder coatings with low curing temperature and enhanced mechanical properties obtained from dgeba epoxy resins and meldrum acid using erbium triflate as curing agent. *Journal of Polymer Science Part A: Polymer Chemistry, 45(11):2316–2327, 2007.*
- [13] Ivan Stojanović, Vinko Šimunović, Vesna Alar, and Frankica Kapor. Experimental evaluation of polyester and epoxy–polyester powder coatings in aggressive media. *Coatings, 8(3):98, 2018.*
- [14] Fred W Light Jr, James D Hood, and Yeong-Ho Chang. Polyurethane powder coating compositions, August 22 1989. US Patent 4,859,760.

- [15] DC Andrei, JL Keddie, JN Hay, SG Yeates, BJ Briscoe, and D Parsonage. Nano-mechanical properties and topography of thermosetting acrylic powder coatings. *Journal of Coatings Technology*, 73(912):65–73, 2001.
- [16] Yong-zhong Gong, Hai-feng Zhang, and Lei Wang. Study on performances of thermosetting fluorocarbon powder resins and coatings therefrom. *Xiandai Tuliao Yu Tuzhuang*, 10(10):22, 2007.
- [17] Ya-kang Liu, Gu-fan Zhao, Jian-min Lu, et al. Study on modification of polyethylene powder coatings. *Paint & Coatings Industry*, 3, 2003.
- [18] Subadhra Janardhanan, Irina Zvonkina, and Mark D Soucek. Powder coating technology. *Kirk-Othmer Encyclopedia of Chemical Technology*, pages 1–16, 2000.
- [19] Maria Fernández-Álvarez, Francisco Velasco, Asuncion Bautista, Flavia Cristina M Lobo, Emanuel M Fernandes, and Rui L Reis. Manufacturing and characterization of coatings from polyamide powders functionalized with nanosilica. *Polymers*, 12(10):2298, 2020.
- [20] Zhuyqhg Qiang. Progress of high performance polymer powder coatings. *Materials Review*, 6, 2005.
- [21] Jostein Mrdalen, John Erik Lein, Helene Bolm, Merete Hallenstvet, and Volker Rekowski. Time and cost effective methods for testing chemical resistance of aluminium metallic pigmented powder coatings. *Progress in Organic Coatings*, 63(1):49–54, 2008.
- [22] S González, F Cáceres, V Fox, and RM Souto. Resistance of metallic substrates protected by an organic coating containing aluminum powder. *Progress in organic coatings*, 46(4):317–323, 2003.

2 Cold bonding method for metallic effect powder coating

2.1 Abstract

An efficient and simple method for preparing bonded metallic effect powder coating is in high demand in the paint manufacturing and application industries. The bonding purpose is to keep the content of metallic pigment consistent between the original and recycled coating powder, which aims at solving the problem of recyclability. One possible method capable of realizing this goal is using the binder to cohere metallic pigment with base particles through a cold bonding method. Through this approach, the pre-curing and high-reject-rate problems generally present in thermal bonding can be completely eliminated. In this paper, polyacrylic acid (PA) and polyvinyl alcohol (PVA) are applied as binders for the bonding process. At various dosages of liquid binder and D.I. water, bonded samples with different bonding effects were prepared. Finally, a good bonding quality with the lowest relative difference between the contents of Al flakes in the original powder (before spray) and deposited powder (after spray) 2.94% with PA as a binder and 0.46% with PVA as a binder was achieved. These results manifest that the cold bonding method is a green and simple approach for preparing the metallic effect powder coating.¹

Keywords: Powder coating; Metallic flakes; Bonding.

¹With minor editorial changes to fulfill formatting requirements, this chapter is substantially as it appears in the “Cold Bonding Method for metallic effect powder coatings.” *Materials* 11, no. 11 (2018): 2086, Wei Liu, Jing Fu, Haiping Zhang, Yuanyuan Shao, Hui Zhang, and Jesse Zhu.

2.2 Introduction

Metallic effect powder coating, which is a powder coating incorporated with metallic pigment(s), has been gaining increased market share in recent years [1, 2, 3]. Powder coatings are dry paints formulated with resins, pigments, and additives, which are similar to the solvent-borne paints with the exception of no solvent present; while metallic pigments, such as aluminum, copper, nickel and zinc, are introduced for providing better aesthetic appearance and protection. Metallic effect powder coatings are usually applied on premium products, for instance, automotive, computer and high-end appliance parts etc. [4, 5, 6]. Their final films exhibit extra shine and deepness to the color by introducing a metallic effect.

Initially, all metallic effect powder coatings were non-bonded, which means that a powder base coat was prepared and then metal flakes were dry-blended into the powder to create a metallic effect [7, 8, 9]. There is no adhesion between metallic flakes and base particles. This method is simple, but the product is unstable, due to the poor recyclability caused by non-bonding between the two. Recyclability means that over-sprayed powders (about 10 to 40%), which failed to deposit onto a substrate at first spray, can be re-sprayed after being recycled by a powder collecting system [10, 11]. This is one of the biggest advantages of powder coating [10]. The sharp distinctions between base particle and metallic flake, such as shape, surface conductivity, volume and mass, result in a difference in the concentrations of the metallic pigment in the final film and the original coating powder when using the electrostatic spraying process, which is the main spraying method in the powder coating industry due to its ability to realize full-automatic painting with thick films (50–300 μm) on a large scale [12, 13, 14]. This difference of course leads to the inconsistency of the metallic pigment concentrations between the over-sprayed powder (the part that fails to deposit onto the workpiece) and the original coating powder, making the over-sprayed non-recyclable. Additionally, the electrostatic spraying makes the metal flakes “bunch” together due to electrostatic force, and therefore causes a non-uniform shininess over the final coating film. In addition, there are some other drawbacks with the non-bonded product, such as metallic flakes accumulating on the head of the spray gun, which has a high risk of discharging and burning [15]. On the contrary, a fully bonded product can overcome all of these problems.

Melt-extrusion and thermal bonding are the two methods used to produce bonded metallic effect powder coating in current industries [16, 17]. The first approach follows the same production process as the conventional plain powder, except that the pigments contain strip-shaped metallic flakes with special surface treatment. All these ingredients (pigments, resins, additives, and fillers) are well-mixed, melt-extruded, and then ground into powders, which are the final bonded product. Apparently, metallic flakes and base particles have been well bonded with each other after the melting process, which makes this kind of bonded product with excellent operation stability. However, the mixing and shearing in the extruder at a high temperature are more likely to change the pigment particle size and ruin the metal surface effect [18, 19]. Therefore, the melt-extrusion method did not find wide application in the powder coating industry for the main-stream sheet-shaped metallic pigments.

In the thermal bonding method, metallic flakes and coating powders are heated in a chamber by high-speed stirring until the temperature precisely reaches the softening point (glass transition temperature) of the coating powder [20]. Then, the sticky surface of the base particles glue up the metallic flakes. This approach not only solves the problems in the non-bonding and melt-extrusion methods but also gives the product a shiny and uniform final appearance. With this method, the temperature control of the blending process is critical [20, 21]. If it is under the softening temperature, there will be no bonding between metallic flakes and base particles. Once it exceeds this point by a couple of degrees, particles of the powder are easily bonded with each other (mis-bonding) and may even cause pre-curing. This requires bonding machines that are competent for precisely controlling the inner temperature. Moreover, in industrial applications, the temperature is generally set a little higher than the softening point to ensure well-bonding, which would increase the possibility of mis-bonding base particles and pre-curing of coating powders [22]. Therefore, in order to ensure the quality of metallic effect powder coating, post-treatments (such as grinding and sieving) are necessary. These issues make the bonding process complicated, expensive, and low-efficient, which limits the application level and field of the metallic effect powder coatings.

Thus, seeking an efficient, simple-operation and cost-saving bonding method is the objective of this paper, which is highly demanded expanding metallic effect powder coating to wider applications, such as coatings for bikes, regular appliances, and decorative building materials.

To achieve this objective, a novel cold bonding method through polymers by high-speed stirring is proposed. If a polymer is water-soluble, adhesive as well as compatible with resin (i.e., polyester in this paper), it can be the candidate binder. Based on previous work [23, 24], two types of candidate binder polymers were used to bond aluminum flake and a base coating particle at room temperature. In addition, Al flake was used as a metallic pigment in all experiments, because more than 90% of metallic pigments in this field are Al flakes. These binders work like glues between the Al flakes and coating particles and bind them by adhesive and cohesive forces. After a detailed investigation on the dependence of bonding quality on different binder-water formulas, the optimal formula was determined, and a simple and economic cold bonding method was developed.

2.3 Materials and methods

2.3.1 Materials and equipment

The following materials were employed in this study: Aluminum flakes (SILBERCOTE PC 3101X, with inorganically treated surfaces) from Silberline Manufacturing Co., Inc. (Tamaqua, PA, USA) was used as metallic pigments; Water-soluble polyacrylic acid (PA, A-725) from Macklin Biochemical Co., Ltd. (Shanghai, China) and polyvinyl alcohol (PVA, 1788) from Sanwei Co., Inc. (Shanxi, China) was chosen as two binders; High gloss polyester clear powder coating ($D_{50} = 44 \mu\text{m}$, with 7 wt.% triglycidyl trimeric isocyanate as crossing linking catalyst, 9910-01289) from TCI powder coating Co. (Ellaville, GA, USA) worked as base powder coating; Al panel (A-2-3.5) from Q-Lab Co. (Westlake, OH, USA) and contrast panels (T12G, 76 mm \times 132mm) from Leneta Co. (Mahwah, NJ, USA) were utilized as substrates.

Mixer (CBG100SC) from Applica Consumer Products, Inc. (Miramar, FL, USA) was performed in Step 3 of the bonding process; Electrostatic powder coating system (Surecoat Manual) from Nordson Co., Ltd. (Westlake, OH, USA) was used for the coating substrate. A laser particle size analyzer (BT-2000B) from Bettersize Instruments Ltd. (Liaoning, China) was utilized to analyze the size distributions of the powder samples. A Scanning Electron Microscope (SEM) (S-4800) from Hitachi Limited (Tokyo, Japan) was employed to observe the bonding situation between Al flake and coating particle. The thickness of the final films was measured by a thickness meter (Positector 6000) from Defeisko Co. (Ogdensburg, NY, USA)

and the final surfaces were characterized by an optical microscope (OT4975) from Mitutoyo Inc. (Kawasaki, Japan).

2.3.2 Cold bonding process

The flow chart of the proposed cold bonding method for the metallic effect powder coating is shown in Fig. 2.1. It started with the dissolving of the liquid binder (PA or PVA) by D.I. water. Afterward, a mixing process of the Al flakes and the binder solution proceeded, as depicted in step 1. After mechanically stirring (60 rpm) this mixture for 30 min, 15 g polyester clear coat (which does not contain fillers and pigments) was added and the mixture was stirred for another 30 min (step 2). In step 3, the half-wetted mixture was fed into a grinder. It was ground in the chamber through high-speed stirring for 20 s and dried up in the air for 24 h; the final product was then collected.

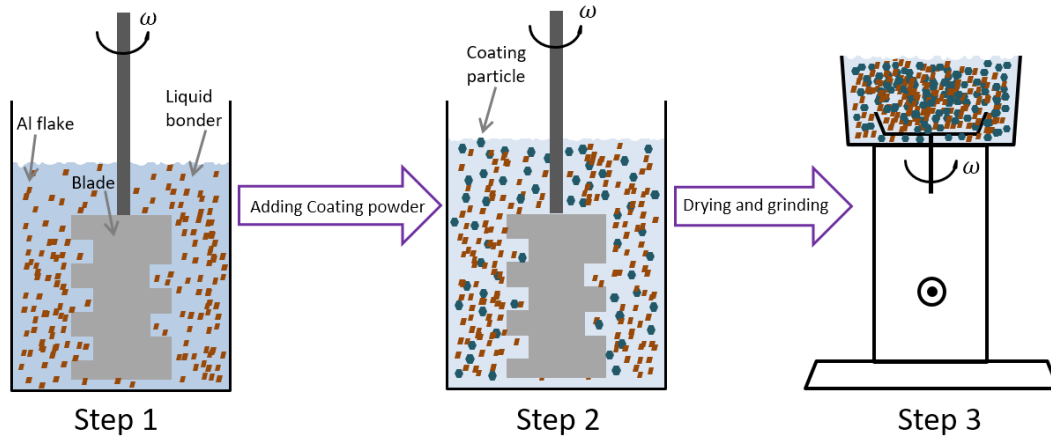


Figure 2.1: The process of cold bonding method.

2.3.3 Analysis of bonding quality

At first, the non-bonded or obtained bonded coating powders were sprayed onto one side of the Al panels (2 inch \times 5 inch) by an electrostatic coating powder system at 30 kV and 30 μ A. The spraying distance is 30 cm and the powder flow rate is approximately 50 g/min.

The bonded samples prepared by the cold bonding method were first analyzed by an ash test [25], which aims at revealing the contents of Al flakes in the original powder (before spray) and deposited powder (after spray). The sampling process of the ash test is shown in Fig. 2.2.

Specifically, the original powder (bonded or non-bonded) was first sprayed onto a metal panel through the electrostatic spraying system at different spray voltages (step 1). Then, the deposited powder on the surface of the substrate was scraped off into a crucible, which was labeled as “sample 2”; as illustrated in step 2. After weighing this sample, another sample with almost the same mass as that of the “sample 2”; was directly taken out of the original powder (step 3), and named “sample 1”. All powders and final films were treated by gold-sputtering before SEM canning.

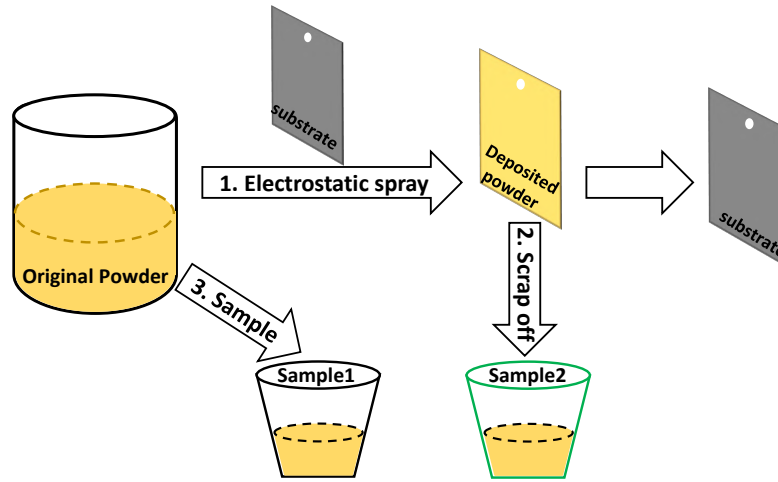


Figure 2.2: Sampling process for the ash test.

The ash test in this work is that burning samples at a high temperature (530°C) for 1.5 hours. The polyester clear powder coating (which only contains polyester resin) in samples will be burned into CO₂, H₂O, other gases and a trace amount of ash residual (0.02 wt%). However, Al flakes are not affected by the high temperature except forming a micron-scale oxide film, whose mass increase is negligible (0.04 wt%), on its surface. The equation for calculating the content of Al flake in metallic effect powder coating is:

$$\omega = \frac{M_{residual}}{M_0} \times 100\% \quad (2.1)$$

where, ω is the Al content, $M_{residual}$ is the residual mass after the burning process. M_0 is the mass of the sample before burning. As a result, the Al content in the original powder (before spray, ω_{ori}) and deposited powder (after spray, ω_{dep}) can be calculated by Equation 2.1. Obviously, a lower difference between ω_{ori} and ω_{dep} means a better bonding.

In order to have a better understanding on the results, the relative difference ($\Delta\omega$) between ω_{ori} and ω_{dep} is defined by the following equation:

$$\Delta\omega = \frac{\omega_{ori} - \omega_{dep}}{\omega_{ori}} \times 100\% \quad (2.2)$$

where, ω_{ori} and ω_{dep} are the contents of Al flake in the powder coatings before and after spraying, respectively. It is clear that lower $\Delta\omega$ represents a better bonding effect. To characterize the influence of the dosages of liquid binder (m_b) and water (m_w) on the relative difference between ω_{ori} and ω_{dep} , different combinations of m_b and m_w were tested.

Based on the ash test, the best ones of these original powder samples were first gold coated and then characterized by SEM equipped with an energy-dispersive X-ray spectroscopy (EDS) analyzer. SEM images can directly display the bonding situation between base particles and Al flakes. Lastly, these samples were measured by a size analyzer, which provides the size change information before and after the cold bonding process.

Non-bonded powder coating samples were prepared, sprayed and analyzed as a control group before the cold bonding experiments. The non-bonded (around 2 wt.% of Al flakes in 98 wt.% base powder) were made using a simple dry blending with no binder and water. The final films were obtained from curing deposited powder and substrate at 180°C for 15 minutes, and the powder on the substrate was turned into a film after cross-linking reactions.

2.4 Results and discussion

2.4.1 Control samples

The particle size distribution of the non-bonded samples is shown in figure 2.3. The black line is cumulative distribution (cumu%), which refers to the number or volume percentage of particles larger or smaller than a certain diameter in unit volume; the dark gray area is differential distribution (diff%), which is the number or volume percentage of particles in a certain diameter range. The results show that the values of D_{10} , D_{50} and D_{90} of the non-bonded powders are 14.75, 39.16 and 95.91 μm , respectively. D_{10} , D_{50} , and D_{90} is the diameter value of abscissa corresponding to the cumulative distribution of ordinate at 10%, 50% and 90%, respectively. D_{50} is also known as the median size or the median particle size, which is often

used to represent the average particle size of the powder. The physical meaning of D_{50} is that particles larger than this size account for 50% and particles smaller than it also account for 50%.

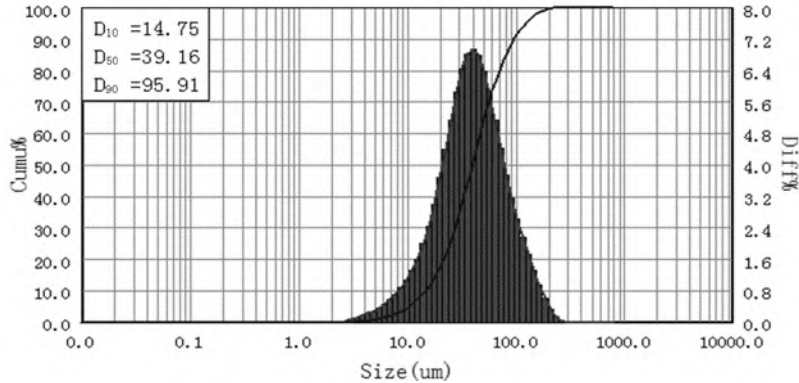


Figure 2.3: Size distribution of the non-bonded sample.

Fig. 2.4 displays some of the Al flakes dispersed in the base particles, but no distinct bonding is observed between these flakes and particles. An Al flake without any particle on its surface is clearly seen at high magnification in Fig. 2.4B. This indicates there is no bonding between the flake and particle. The aluminum scanning result (Fig. 2.4C) from EDS illustrates the plate in Fig. 2.4B is an Al flake and those particles around the plate are coating powder. The energy-dispersive spectrum observed in Fig. 2.4D further proves the flake is pure aluminum.

Table 2.1 presents the results of the ash test of Al content before and after spraying these samples, where each experiment was repeated three times. It can be seen that the contents of Al flakes in the original non-bonded coating powders were 2.15 ± 0.02 wt.% (before spray), but the Al contents in the deposited powders increased to 5.08 ± 0.03 wt.% (after spray). The increase indicates that more Al flakes than needed were deposited onto the panel surface. In other words, the content of the Al flake in the over-sprayed coating powder was less than desired. The main reason for this result is that the Al flake can capture more electrons than base powder in a low electric field when spraying at 30 kV due to the lower dielectric constant of base particles.

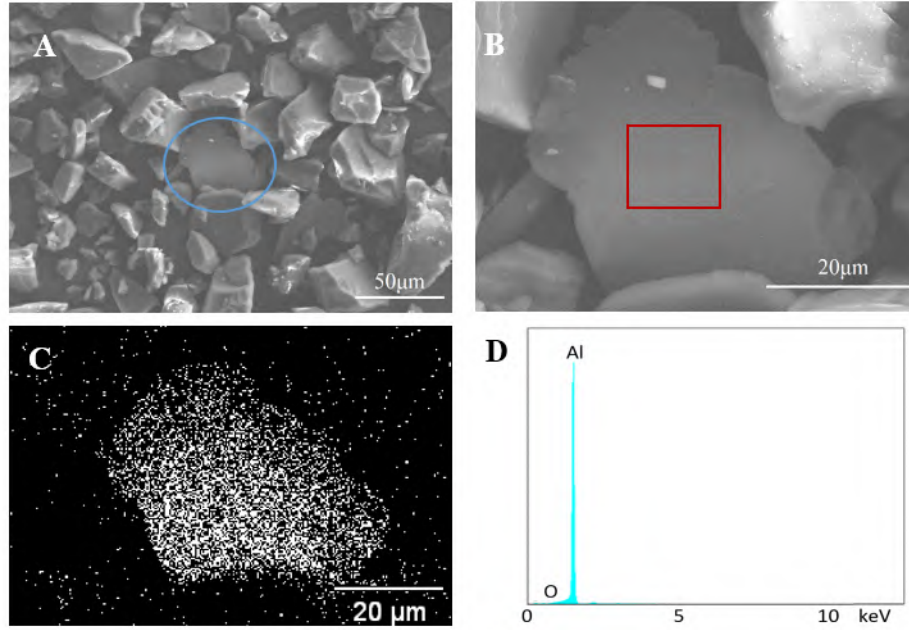


Figure 2.4: Scanning electron microscope (SEM) and energy-dispersive X-ray spectroscopy (EDS) images of control samples. A, B) SEM images of non-bonded sample; C) EDS scanning of aluminum element; D) EDS spectrum of the rectangle area in B.

Table 2.1: Al content comparisons of non-bonded powder (30 kV).

#	$\omega_{ori}/wt\%$				$\omega_{dep}/wt\%$			
	1	2	3	Ave.	1	2	3	Ave.
Al%	2.14	2.17	2.15	2.15 ± 0.02	5.05	5.10	5.08	5.08 ± 0.03

2.4.2 bonded by PA

It was expected that both the dosages of binder and water would affect the bonding quality. In order to study the effects of binder and water dosages on bonding quality, different mass amounts of water and PA resin were tested for the same mass of powder coating (15 g, contains 2.0 wt.% Al flakes). The results of the ash test are presented in Table 2.2. All the values of ω_{ori} fluctuate around 2 wt.%, rather than remaining at 2 wt.% (the Al content before cold bonding). The fluctuation is likely caused by the mass loss of Al flakes or base particles during the process of cold bonding. Because a high amount of binder may cause surface with orange peel (rough surface) or lower gloss and too much water will reduce the bonding effect, the dosages of binder and water were set to less than 0.060 g and 0.50 g, respectively. According to the control tests, the Al content in the deposited powders is 5.08 ± 0.03 wt.%. After being

bonded by 0.01 g PA, ω_{dep} becomes even higher than in the control test, which implies that no effective bonding was formed and side effects may be generated during the bonding process. A possible reason for this result is that a dilute and thin PA solution layer on Al flakes is not able to glue the base particle. But this layer increases the total electrons carried by the Al flake, which makes more Al flakes deposit onto the substrate. When the mass of PA increases to 0.03 g, the Al contents in the deposited powder (ω_{dep}) get closer to those of their corresponding virgin powders, except the one using 0.5g water. After using 0.06g PA, the values of ω_{dep} (2.25–2.10 wt.%) and ω_{ori} (2.23–2.04 wt.%) are highly similar while the water dosage is less than 0.30 g. This indicates that the cold bonding method is able to gain a good bonding effect for the metallic effect powder coatings.

Table 2.2: Al contents (wt.%) of the samples before and after spraying tests (30 kV).

		$\omega_{ori}/wt\%$			$\omega_{dep}/wt\%$		
		0.01	0.03	0.06	0.01	0.03	0.06
H_2O/g	PA/g						
	0.10	2.19	2.19	2.23	7.60	2.96	2.25
	0.20	2.10	2.18	2.04	7.20	3.23	2.10
	0.30	1.99	1.98	2.22	6.96	3.84	2.60
	0.50	2.06	2.19	2.14	8.09	6.14	3.38

According to Mistry's work, they used Gloss 20° and 60° to indirectly judge the bonding effect of the microwave bonding method [29]. In this work, the relative difference between ω_{ori} and ω_{dep} ($\Delta\omega$) was taken as a direct and quantitative judgment of bonding efficiency. Fig. 2.5 demonstrates the three series of mass content divisions before and after spray, $\Delta\omega$, which is plotted with respect to the water content. The samples with 0.01 g PA have the highest $\Delta\omega$, exhibiting the worst bonding performance overall. As the amount of PA increases, the $\Delta\omega$ drastically decreases. The lowest $\Delta\omega$ is obtained when the amount of PA is 0.06 g. This is mainly because the bonding force increases with the dosage of the binder (PA). In addition, the three curves also reveal that $\Delta\omega$ can also be reduced by decreasing water content, which is due to the fact that the over-diluted binder tends to be removed from the Al flakes as a result of abrasion from the base particles. It is evident that in the tested PA and water dosage ranges, a higher amount of PA or lower amount of water is preferable for obtaining a lower $\Delta\omega$, namely a better bonding effect. In addition, the three curves display that the impact of

PA is greater than water on bonding. As to the optimum formula, the water dosage should not be kept too low, otherwise, it can cause poor dispersion of the metallic pigment in the powder coating. Furthermore, too high a binder amount will have side effects on the final appearance. Therefore, the dosage of 0.06 g PA with 0.2 g H₂O is selected as the optimal formulation, whose $\Delta\omega$ is 2.94%. In summary, almost equal Al contents before and after spraying were obtained using the cold bonding method with proper PA and water dosages, reflecting its great potential to achieve a desirable bonding performance.

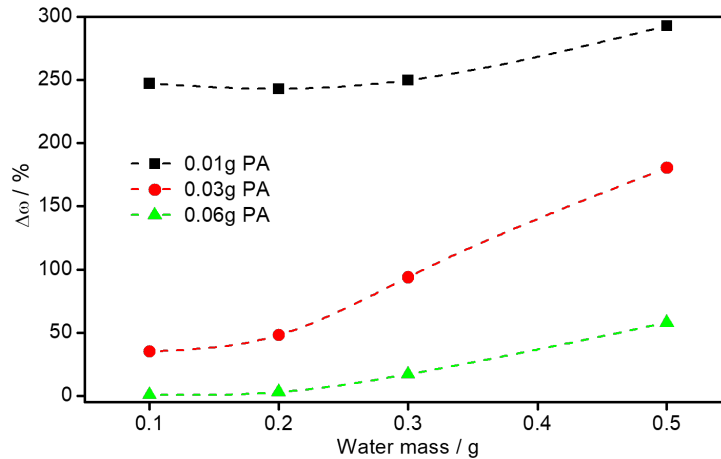


Figure 2.5: The relationship between $\Delta\omega$ and the dosage of water and polyacrylic acid (PA)

The sample prepared by 0.06 g PA and 0.2 g H₂O was further characterized. As shown in Fig. 2.6, the D_{10} , D_{50} , and D_{90} of this sample are 16.11, 41.42, and 99.43 μm , respectively. Compared to the non-bonded one, both D_{10} and D_{50} increase by about 2 μm and D_{90} by 4 μm , which is reasonable because the base powder particles are bonded to Al flakes and formed larger particles.

From the SEM images of Fig. 2.7, it can be seen that many small (<20 μm) and medium-size particles (20 μm) were stuck on the surface of Al flakes, as exhibited in the circled area. This is because small or medium size particles have less mass so, the bond between the flake and particle is able to survive during mixing in the mixer. Gunde and co-authors also took SEM images as their judgment basis for thermal bonding [30], however, they had some mis-bonding between Al flakes, which is not found in this work. Additionally, there are some small particles bonded on the surface of the big particles as exhibited, which may also lead to a size increase. This result also matches the conclusion of size distribution analysis. The EDS scanning for

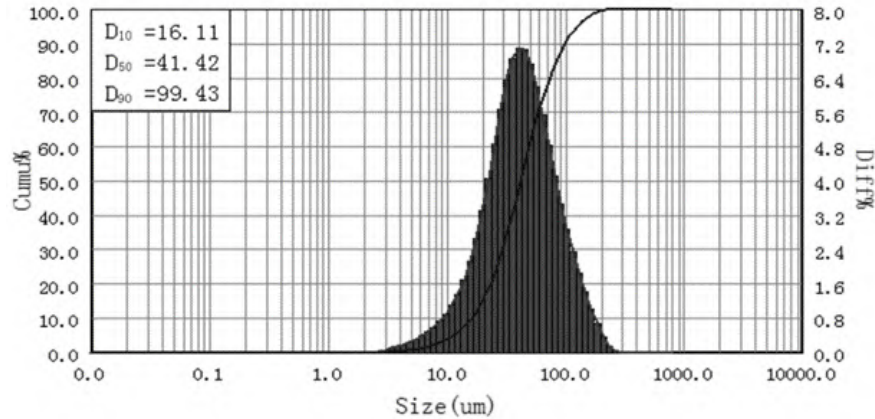


Figure 2.6: Size distribution of PA bonded sample.

aluminum reveals that there are some dark areas (blockage of aluminum scanning) on the Al flake (Fig. 2.7C), which coincide with the locations of the small particles seen in Fig. 2.7B. This proves that the bonding of small particles on the Al flake surfaces occurs. In addition, the energy-dispersive spectra (Fig. 2.7D) of the rectangular area in Fig. 2.7B confirms that this flake is comprised of aluminum. Small peaks of the elements of C and O are mainly caused by PA. Above all, these images and element analysis verifies the ash test result that bonding is indeed formed between Al flake and base particle.

2.4.3 Bonded by PVA

The previous results of PA have proved the potential of the cold bonding method for metallic effect powder coating. To verify the universality of the cold bonding method, another liquid binder, PVA, was investigated. Furthermore, the stickiness of the PVA solution is a little higher than PA when at the same concentrations (0.5–5 wt.%) [26, 27], so a lower amount of PVA was employed in this study. The dosages of binder and water are less than 0.016 g and 0.60 g, respectively.

Here, various combinations of PVA (0.008 to 0.016 g) and water (0.4 to 0.6 g) were studied, and the results are presented in Table 3. Table 3 shows the Al contents of PVA bonded samples before (ω_{ori}) and after (ω_{dep}) spraying. All the values of ω_{ori} are around 2 wt.%. When the mass of PVA and water are 0.016 g and 0.4 g, respectively, The ω_{dep} is at its highest at 2.80 wt.%. After increasing the mass of water to 0.6 g, the Al content slightly decreases to 2.55 wt.%. This

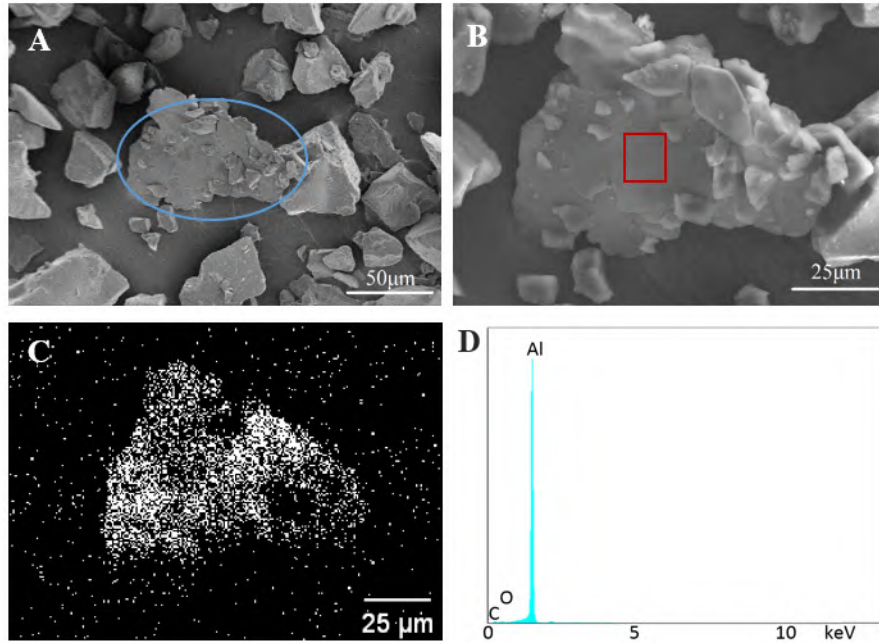


Figure 2.7: SEM and EDS images of PA bonded samples. A, B) SEM images of cold bonded sample by PA; C) EDS scanning of aluminum element; D) EDS spectrum of the rectangle area in B

result implies that a high PVA dosage cannot produce the ideal bonding performance. When reducing the dosage of PVA solution to 0.008 g, the Al contents after spraying are lower than 2.29 wt.%, indicating that manifesting a lower amount of PVA (0.008 g) is better for providing a stronger bonding effect between the Al flakes and base particles. Overall, these data illustrate that PVA is also an efficient binder candidate for the cold bonding process of metallic effect powder coating.

Table 2.3: Al contents (wt.%) of the samples before and after spraying tests (30 kV).

		$\omega_{ori}/wt\%$			$\omega_{dep}/wt\%$		
		0.008	0.012	0.016	0.008	0.012	0.016
H_2O/g	PVA/g						
	0.40	2.12	1.91	2.28	2.11	2.20	2.80
	0.50	2.17	2.08	2.07	2.18	2.34	2.62
	0.60	2.17	1.83	2.11	2.29	1.91	2.55

For further comprehending the relationship between ω_{dep} and the dosages of PVA and water, the results were calculated by Equation (2), as illustrated in Fig. 2.8. When bonded by 0.016 g PVA, all the relative differences are a little higher than 20%, which are much higher

than other PVA dosages. This is mainly because the bonding force supported by 0.016 g PVA and 0.4 g water is too strong and causes mis-bonding between Al flakes in Step 1, which of course will hinder the bonding between Al flakes and base particles. When the amount of PVA is reduced to 0.012 g, the relative difference shows a decline during the increasing dosage of water (0.4 to 0.6 g). This means a better bonding effect was obtained after the diluting of PVA, which also implies that the mis-bonding between Al flakes in Step 1 was reduced. However, when bonded by 0.008 g PVA, the relative difference increases from 0.56 to 5.62% with the increased amount of water from 0.4 to 0.6 g. This shows diluting by water will reduce the bonding effect, which is mainly due to the fact the low dosage of PVA (0.008 g) will not cause mis-bonding in Step 1, but the dilution will reduce the bonding between Al flakes and base particles in Step 2. In these samples, the lowest relative difference is 0.46%, which is gained by 0.008 g PVA and 0.5 g water.

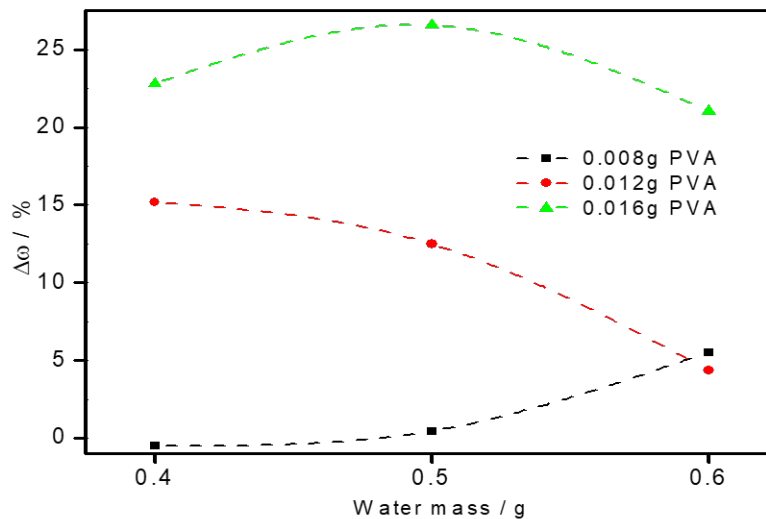


Figure 2.8: The relationship between $\Delta\omega$ and the dosage of water and PVA

In summary, the optimum formula (when $\Delta\omega$ is 0.46%) in the PVA work is using 0.008 g PVA and 0.5 g water respectively. Compared to the optimal condition in the PA section (when $\Delta\omega$ is 2.94%), the lowest $\Delta\omega$ of PVA is a little lower than the one from PA. Overall, it is true that PVA is also a strong liquid binder for the cold bonding method.

From the $\Delta\omega$ analysis, the optimal sample is made by 0.008 g PVA and 0.5 g water. SEM

and a size analyzer were applied to observe the bonding status of this bonded sample. The results are shown in Fig. 2.9. The particle size of this sample is a little larger than that of the control, which reveals that a few small particles were glued on the surface of the larger ones.

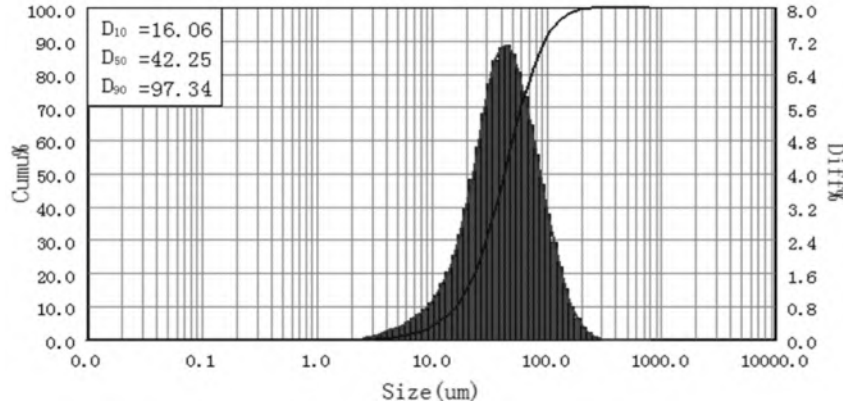


Figure 2.9: Particle size distribution of PVA bonded sample.

Small particles bonding with large ones is also proved by the SEM images in Fig. 2.10A. Although the particle size distribution of the bonded metallic coating powder has changed a little compared to the non-bonded sample, the influence on the final appearance is slight. There are several Al flakes bonded with base particles as exhibited in the circled area in Fig. 2.10A. This area was magnified in Fig. 2.10B, which clearly shows that both sides of Al flakes were well-bonded with base particles. In addition, the EDS scanning result shown in Fig. 2.10C also reveals there are some base particles bonded on its surface. Fig. 2.10D proves that the flake in Fig. 2.10B is aluminum. The small peak in Fig. 2.10D around 2 keV was caused by gold coating.

In order to visually prove the bonding effect, some final films were prepared. Because the base coating powder is a polyester clear coat, which is transparent after curing, special metal substrates (contrast panels, Leneta Company) with half black and half white surfaces were employed to create a better comparison after coating. After adding Al flakes as pigments, the colors of the substrate will be partially covered. It is understandable that more Al flakes in the final film means less original color of substrate will be shown. Based on the above results, the relative difference of Al content of the PVA sample (0.46%) is a little lower than PA (2.94%), even with less dosage comparing to PA. Therefore, a final film, as shown in Fig. 2.11C (thickness is $77.8 \pm 6.1 \mu\text{m}$), was obtained from a PVA bonded sample by spraying

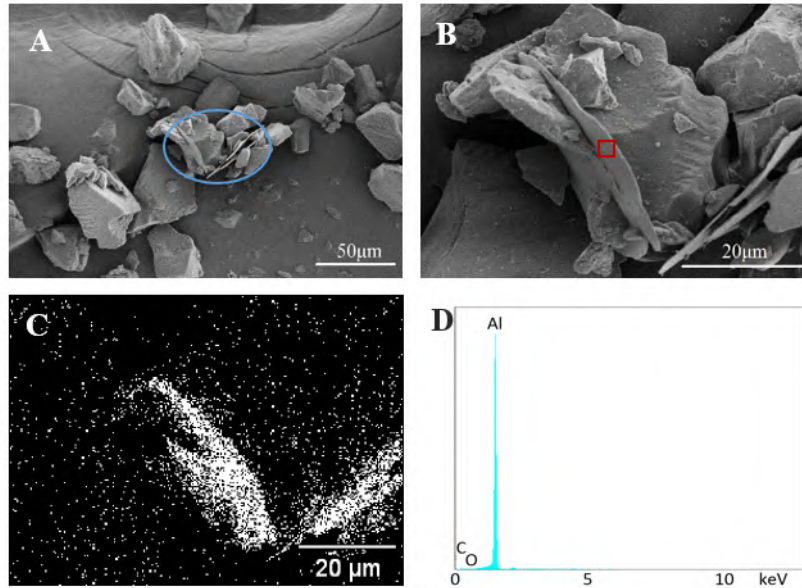


Figure 2.10: SEM and EDS images of PVA-bonded samples. A, B) SEM images of cold bonded sample by PVA; C) EDS scanning of aluminum element; D) EDS spectrum of the rectangle area in B.

(at 30 kV) onto a metal substrate and then curing at 180 °C for 20 min. When without Al flake, the final film from the polyester clear coat is transparent as presented in Fig. 2.11A ($75.5 \pm 6.7 \mu\text{m}$). The final film from non-bonded samples with 2 wt.% Al flakes is shown in Fig. 2.11B ($81.0 \pm 5.6 \mu\text{m}$). It can be seen that the original color of the substrate in Fig. 2.11B is less exhibited than in Fig. 2.11C, that is to say, the Al content in the final film from the non-bonded sample (Panel B) is higher than the PVA bonded sample (Panel C). An optic microscope was used to observe these final films as shown in the top-right insert images found in Fig. 2.11. These microscopic pictures further confirm the visual observation. This conclusion is also in agreement with the ash test results, which show the Al contents in deposited coatings from the non-bonding and PVA bonded samples are 5.08 and 2.18 wt.%, respectively. In addition, the Gloss and haze of panel C are 82.50 ± 0.76 and 21.6 ± 0.99 respectively, which are close to that of commercial one (83.03 ± 0.87 and 22.6 ± 1.02).

2.5 Conclusions

A cold bonding method using a water soluble resin binder for fabricating metallic effect powder coating is proposed and tested. The results of the investigation suggest that: a) the metallic effect powder coating can be well bonded by this cold method; b) the bonding effect

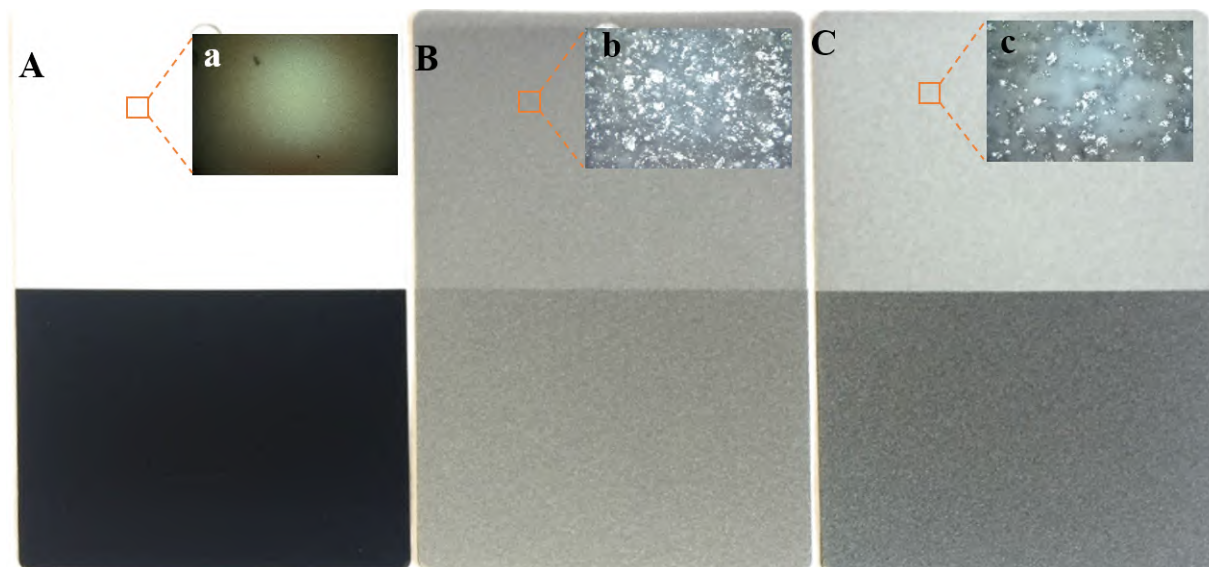


Figure 2.11: Surface comparisons between final films from various samples. (A) Clear coat, (B) Non-bonded sample, (C) Bonded sample.

is highly dependent on the dosages of binders (PA and PVA) and D.I. water; and c) the proposed ash test method performs well in quantitatively characterizing the bonding effect of the bonded powder samples, while qualitative characterizing methods such as SEM and optical microscope observations, EDS scan, and visual observation can be used for further confirmation. By comparing the Al contents in the original coating powder and deposited powder, the optimal formula in the tested ranges for PA (the lowest $\Delta\omega$ is 2.94%) is 0.3 g Al flakes with 0.060 g PA and 0.20 g water, and for PVA (the lowest $\Delta\omega$ is 0.46%) is 0.3 g Al flakes with 0.008 g PVA and 0.5 g water. In addition, the surface comparison suggests the bonded sample from this cold bonding method is able to have a similar surface quality with the one from a commercially bonded product. Therefore, cold bonding is an effective method to solve the bonding problems in the metallic effect powder coating. Further studies are expected to find other possible binders and establish a new approach for bonding the metallic effect powder coating.

Bibliography

- [1] Mohammad Diab, Xin Pang, and Hamid Jahed. The effect of pure aluminum cold spray coating on corrosion and corrosion fatigue of magnesium (3% Al-1% Zn) extrusion. *Surface and Coatings Technology*, 309:423–435, 2017.
- [2] Md J Nine, Shervin Kabiri, Tran Thanh Tung, Diana NH Tran, and Dusan Losic. Electrostatic powder coatings of pristine graphene: A new approach for coating of granular and fibril substrates. *Applied Surface Science*, 441:187–193, 2018.
- [3] Hongxia Wan, Dongdong Song, Xiaogang Li, Dawei Zhang, Jin Gao, and Cuiwei Du. Effect of zinc phosphate on the corrosion behavior of waterborne acrylic coating/metal interface. *Materials*, 10(6):654, 2017.
- [4] Behzad Shirkavand Hadavand, Maryam Ataefard, and Hamed Fakharizadeh Bafghi. Preparation of modified nano ZnO/polyester/TGIC powder coating nanocomposite and evaluation of its antibacterial activity. *Composites Part B: Engineering*, 82:190–195, 2015.
- [5] Sijia Sun, Hao Ding, and Xifeng Hou. Preparation of CaCO₃-TiO₂ composite particles and their pigment properties. *Materials*, 11(7):1131, 2018.
- [6] Wanting Chen, Yu Liang, Xifeng Hou, Jing Zhang, Hao Ding, Sijia Sun, and Hu Cao. Mechanical grinding preparation and characterization of TiO₂-coated wollastonite composite pigments. *Materials*, 11(4):593, 2018.
- [7] Stuart C Porter and Edward J Woznicki. Dry edible film coating composition, method and coating form, September 24 1985. US Patent 4,543,370.
- [8] H Honda, M Kimura, F Honda, T Matsuno, and M Koishi. Preparation of monolayer particle coated powder by the dry impact blending process utilizing mechanochemical treatment. *Colloid. Surface. A*, 82(2):117–128, 1994.
- [9] Glenn Roy Himes. Dry blending and molding process, October 12 1976. US Patent 3,985,702.
- [10] RA Sims, MK Mazumder, Xiaohong Liu, W Chok, JR Mountain, DL Wankum, P Pettit, and T Chasser. Electrostatic effects on first pass transfer efficiency in the application of powder coatings. *IEEE Transactions on industry applications*, 37(6):1610–1617, 2001.
- [11] Jing Fu, Matthew Krantz, Hui Zhang, Jesse Zhu, Harry Kuo, Yar Ming Wang, and Karen Lis. Investigation of the recyclability of powder coatings. *Powder Technology*, 211(1):38–45, 2011.
- [12] Qiaoyan Ye and Joachim Domnick. On the simulation of space charge in electrostatic powder coating with a corona spray gun. *Powder Technology*, 135:250–260, 2003.
- [13] Nicholas P Liberto. Understanding powder coating equipment and application. *Metal Finish*, 109:27–32, 2011.

- [14] Q Ye, T Steigleder, A Scheibe, and J Domnick. Numerical simulation of the electrostatic powder coating process with a corona spray gun. *J. Electrostat.*, 54(2):189–205, 2002.
- [15] NAN Ren-zhi, NAN Yan, and LIU Zheng-tang. Preliminary discussion on powder coatings containing aluminum powder. *Modern Paint & Finishing*, 8, 2006.
- [16] J Bailey, D Worden, E Breton, and J Wolf. Coating metallic substrate with powdered filler and molten metal, July 3 1973. US Patent 3,743,556.
- [17] Ernest J Breton, John M Handzel, and Otis K Tennant. Process for making wear-resistant coatings, November 18 2003. US Patent 6,649,682.
- [18] S González, F Cáceres, V Fox, and RM Souto. Resistance of metallic substrates protected by an organic coating containing aluminum powder. *Progress in organic coatings*, 46(4):317–323, 2003.
- [19] TH Van Steenkiste, JR Smith, and RE Teets. Aluminum coatings via kinetic spray with relatively large powder particles. *Surface and Coatings Technology*, 154(2-3):237–252, 2002.
- [20] Douglas S Richart and Andrew T Daly. Thermosetting resin-based coating powders containing metal flakes, February 16 1993. US Patent 5,187,220.
- [21] Wei-Hsing Tuan, HH Wu, and TJ Yang. The preparation of $\text{Al}_2\text{O}_3/\text{Ni}$ composites by a powder coating technique. *J. Mater. Sci.*, 30(4):855–859, 1995.
- [22] Tosko Aleksandar Misev. *Powder coatings: chemistry and technology*. John Wiley & Sons Inc, 1991.
- [23] GW Beckermann and Kim L Pickering. Engineering and evaluation of hemp fibre reinforced polypropylene composites: fibre treatment and matrix modification. *Composites Part A: Applied Science and Manufacturing*, 39(6):979–988, 2008.
- [24] AH De Boer, GK Bolhuis, and CF Lerk. Bonding characteristics by scanning electron microscopy of powders mixed with magnesium stearate. *Powder Technology*, 20(1):75–82, 1978.
- [25] Standard test method for ash content in plastics (D5630-13). *ASTM Standard*, 8:1–5, 2013.
- [26] Riaz Hussain, Sobia Tabassum, Mazhar Amjad Gilani, Ejaz Ahmed, Ahsan Sharif, Faisal Manzoor, Asma Tufail Shah, Anila Asif, Faiza Sharif, Farasat Iqbal, et al. In situ synthesis of mesoporous polyvinyl alcohol/hydroxyapatite composites for better biomedical coating adhesion. *Applied Surface Science*, 364:117–123, 2016.
- [27] Riccardo Po. Water-absorbent polymers: a patent survey. *Journal of Macromolecular Science, Part C: Polymer Reviews*, 34(4):607–662, 1994.

3 Single-component-heating bonding for powder coatings with metallic pigments

3.1 Abstract

With the increasing public focus on environmental protection and high-quality life, there is a corresponding interest in metallic effect powder coating, owing to its zero VOC emission, sparkling aesthetic appearance, and high protective property. Metallic effect powder coatings are composed of two non-compatible ingredients: base powder coating(s) and metallic pigment(s). In this work, a direct and quantitative characterization method, ash test, was first used to analyze the powder utilization of the two components. Through this test, a comprehensive investigation on dry-blending samples was performed at first, which aims at quantitatively revealing the influence of non-compatibility on the utilization of metallic pigment. Furthermore, to avoid production problems of the current industrial method (thermal bonding method), such as pre-curing and metallic flake deformation, a novel bonding method—single-component-heating bonding (SCHB)—was developed and assessed. The ash test shows these samples were well-bonded when the heating temperature ranging from 75 to 150°C. At last, a series of surface comparisons suggest that the SCHB film has a similar surface quality to the commercial one. This work investigated the utilization of metallic effect powder coating and demonstrated SCHB has great potential in producing metallic effect powder coating, resulting in exploitation of the powder paint industry.²

Keywords: Powder coating; Aluminum flakes; Bonding.

²With minor editorial changes to fulfill formatting requirements, this chapter is to be submitted to *Coatings*, ISSN 2079-641, Wei Liu, Hui Zhang and Jesse Zhu.

3.2 Introduction

Metallic effect powder coatings—powder coatings cooperated with metallic pigments—have an increasing share of the powder paint market in the last few years, due to shiny metal-effect surface and excellent protective performance [1]. Powder coatings have a similar formula to traditional solvent-borne paints except for no solvents [2]. Metallic pigments are mostly aluminum or copper flake for silver- or gold-color, respectively. Thus, metallic effect powder coatings have the advantages of powder coatings and metallic coatings: no VOC emission and aesthetic surface.

However, there is an inevitable problem in the production process that is the non-compatibility between the two ingredients: coating particles and metallic pigments. This non-compatibility comes from their huge distinctions in some physical properties, such as shape, resistance, density, and dielectric constant. This problem leads to different contents of metallic pigment in original, deposited and over-sprayed powders, which will impede the recyclability of over-sprayed powders when spraying by an electrostatic spraying system [3]. Recyclability of metallic effect powder coatings is that over-sprayed powders (usually 10-40 wt% of the total powder), which failed to deposit to a substrate at first spray, can be re-sprayed after recycled by a collecting system. As a result of non-compatibility, the over-sprayed powder cannot be re-sprayed, which contributes to high cost and material waste [2].

Although manufacturers and researchers know the non-compatibility is an annoying problem, there are few reports about how much impact this issue has on the content of metallic pigment. Most manufacturers prefer to apply gloss and metallic travel angles to judge the utilizations of metallic pigment [4], while these methods are indirect and inaccurate. Some researchers also use SEM to make a direct observation [5], which is of course a direct approach, but not quantitative. In this work, an ash test was carried out to have a direct and quantitative characterization of the contents of metallic pigment.

Nowadays, there are two main production methods of metallic effect powder coatings. The first one is dry-blending (small batch production): simply dry blending metallic pigments with base powder coatings [6]. This process does not consider the influence of non-compatibility, so the weight percentage of metallic pigments in the original and deposited powders would

be different. In industry, workers usually evaluate the color difference by observation and experience. Here, a new characterization method based on an ash test was established to quantitatively analyze the bonding quality. The precise analyses give some suggestions about the application of dry-blending metallic effect powder coatings and also show a better understanding of how the non-compatibility affects the utilization of metallic pigment.

The second one is the current commercial bonding method (thermal bonding technology), which was invented to tackle the problem of non-compatibility by bonding coating particle and metallic pigment [7]. In this approach, metallic pigments and coating powders are heated in a chamber by high-speed stirring till the temperature exactly reaches the glass transition temperature (T_g) of the coating powder [8, 9, 10]. Then the metallic pigments adhere to the sticky surfaces of coating particles. After bonding, the bonded particles (metallic pigments + base coating particles) will have similar physical properties (dielectric constant, density, and resistance) with base coating particles. When spraying by an electrostatic gun, bonded and base particles will carry a close number of electrons due to these similar properties [11], so the content of the metallic pigment in the deposited powder would equal that in the original powder. However, the temperature control of the blending process is critical within this method [5]. If it was under the T_g , there will be no bonding between them. Once it exceeds this point by a couple of degrees, coating particles are easily bonded with each other (mis-bonding) and may even cause pre-curing. Moreover, the temperature is generally set slightly higher than the T_g to ensure well bonding in industrial applications, which correspondingly increases the possibility of mis-bonding and pre-curing of coating powders. These issues presenting in the thermal bonding process limit the application level and field of the metallic effect powder coatings.

Therefore, in this paper, SCHB method was established to bond metallic pigments and coating particles. This method is just heating metallic pigments alone to bond rather than heating coating powders and metallic pigments at the same time as mentioned in the thermal bonding method. SCHB method avoids those disadvantages which exist in the current industrial bonding method, such as mis-bonding between coating particles and metallic flake deformation. At last, to assess the bonding quality from the SCHB method, a series of final surface comparisons between SCHB and thermally bonded samples were proceeded.

3.3 Materials and methods

3.3.1 Materials and equipment

The following materials were employed in this study: Aluminum flakes (SILBERCOTE PC 3101X, with inorganically treated surface) from Silberline Manufacturing Co., Inc. (Tamaqua, PA, USA) was used as metallic pigments. High gloss polyester clear powder coating ($D_{50} = 44 \mu\text{m}$, with 7 wt% triglycidyl trimeric isocyanates as crossing linking catalyst, 9910-01289) from TCI powder coating Co. (Ellaville, GA, USA) worked as base powder coating. Al panels (A-2-3.5) from Q-Lab Co. (Westlake, OH, USA) were utilized as substrates. Commercial metallic effect powder coating (HS-0460-S) from Prism Powder Coatings Ltd. (Concord, ON, Canada) was used as thermal-bonded samples.

Ceramic electric heating sleeve (length: 129mm; internal diameter: 13mm; external diameter: 17mm) from Yangling automation technology Co., Ltd (Shandong, China) performed as a heater in the SCHB method. Electrostatic powder coating system (Surecoat Manual) from Nordson Co., Ltd. (Westlake, OH, USA) was used for coating substrates. A laser particle size analyzer (BT-2000B) from Bettersize Instruments Ltd. (Liaoning, China) was utilized to analyze the size distributions of the powder samples. A Scanning Electron Microscope (SEM) (S-4800) with Energy dispersive X-ray (EDX) from Hitachi Limited (Tokyo, Japan) was employed to observe the bonding situation between Al flake and coating particle. The thickness of the final films was measured by a thickness meter (Positector 6000) from Defeisko Co. (NY, USA). The final surfaces were characterized by an optical microscope (OT4975) from Mitutoyo Inc. (Kawasaki, Japan) and a 408 triple angle gloss & DOI meter from Elcometer Inc. (Michigan, USA).

3.3.2 Single-component-heating bonding method

The device diagram of the SCHB method is shown in Fig. 3.1. Al flakes ($\sim 1.0\text{g}$) were first heated to a certain temperature in a ceramic electric heater under the protection of nitrogen. When the temperature was stable, the ultrasonic vibration for the sieve (140 mesh) was turned on to help metallic pigments gradually disperse into the coating particles ($\sim 49.0\text{g}$) which were minimum fluidized in an air-bed (internal diameter=8cm; height=25cm) [12, 13]. Stopping the

flows of air and nitrogen after the metallic pigments are fed up, followed by the collection of SCHB bonded samples from the fluidized bed.

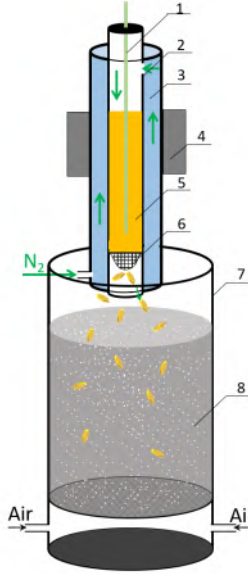


Figure 3.1: Schematic diagram of the SCHB device. 1. Temperature sensor; 2. PTFE cylinder; 3. Ceramic heating tube; 4. Vibrator; 5. Al flakes; 6. Ultrasonic sieve; 7. fluidized bed; 8. Coating powder.

3.3.3 Analysis of bonding quality

The bonding quality was analyzed by determining the Al content in original and deposited powders via ash tests. The Al content in the original powder and deposited powder were calculated by Eq. 3.1:

$$\omega = \frac{M_{residual}}{M_0} \times 100\% \quad (3.1)$$

where, ω is the Al content, $M_{residual}$ is the residual mass after the burning process, and M_0 is the mass of the sample before burning. The Al contents of original and deposited powders are named ω_{ori} and ω_{dep} , respectively. Obviously, a lower difference between ω_{ori} and ω_{dep} means a better bonding.

In order to have a better understanding on the results, the relative difference ($\Delta\omega$) between ω_{ori} and ω_{dep} is defined by the following equation:

$$\Delta\omega = \frac{\omega_{ori} - \omega_{dep}}{\omega_{ori}} \times 100\% \quad (3.2)$$

It is clear that lower $\Delta\omega$ represents a better bonding effect. The selected powder samples based on the ash test results were further characterized by SEM and EDS. These images can directly show the bonding situation between Al flakes and coating particles. Secondly, the non-bonded and bonded samples were tested by a laser particle size analyzer. After curing at 180°C for 15min, the deposited powders on the substrate were turned into films. These films were measured by a triple-angle gloss & DOI meter to show their surface quality and then observed by SEM (after gold-sputtering) and an optical microscope to analyze their microstructures.

3.4 Results and discussion

3.4.1 non-bonded samples

Film thickness is quite significant in the coating industry. It is directly proportional to the mass of the deposited powder. When the mass of powder is 5.3 mg/cm² and 11.6 mg/cm², the thicknesses are 39.5μm and 82.4μm, respectively. Generally, the thickness is between 60 to 80μm in the industrial application when the medium diameter of coating powder is around 40μm. The particle size distribution of the non-bonded powder is shown in Fig. 3.2, and the medium diameter is 39.28 μm. To keep the film thickness around 60μm, the deposition mass is kept at around 8.9 mg/cm² during all these spraying processes.

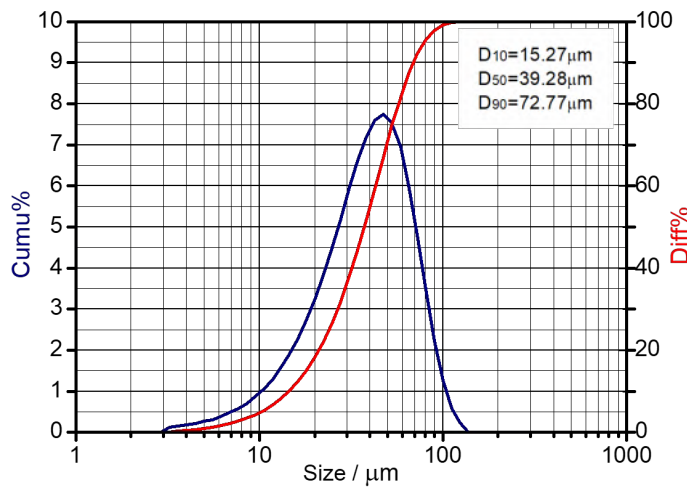


Figure 3.2: The particle size distribution of the non-bonded powder

At first, the non-bonded powder was sprayed at 90 kV and the Al contents were compared in Table 3.1. The original Al content was 2.13%, but the deposited Al content largely reduces to 1.03%. This means that the metallic effect was much less than it should be. As mentioned in Chapter 2, the deposited Al content was about 5% when sprayed at 30 kV. The mechanism for this difference will be discussed in Chapter 4.

Table 3.1: The original and deposited Al contents of non-bonded samples

#	$\omega_{ori}/wt\%$				$\omega_{dep}/wt\%$			
	1	2	3	Ave.	1	2	3	Ave.
Al%	2.10	2.15	2.14	2.13±0.03	1.02	1.05	1.04	1.03±0.02

3.4.2 SCHB bonded samples

Bonded samples were prepared by the self-designed bonding device shown in Fig. 3.1. To find an optimal temperature to bond Al flakes and coating particles, various temperatures were tested in this work. Based on former results on film thickness and spraying process, deposited mass and spray voltage were kept unchanged at 60kV and 0.4g, respectively. The non-bonded sample was obtained from the bonding device while there was no heating. The data in Fig. 3.3A presents this sample contained 2.23 wt% of Al flake before spraying, but the Al content in the deposited powder decreased to 1.08 wt%. The relative difference, depicted in Fig. 3.3B, is as high as -51.57% calculated from Eq. (2). This means high content of Al flake added but less metal effect was gained. Almost the same result was obtained when heating at 50°C, which means the coating particle is not softened or sticky at this temperature. While rising the temperature to 75°C, the ω_{ori} and ω_{dep} are 2.25±0.01% and 2.26±0.08%, respectively. Precisely, the relative difference ($\Delta\omega$) is only around 0.38% from the results exhibited in Fig. 3.3B. It implicates that the temperature at 75°C is high enough to soften the surface of clear coating particles (soften point is around 50°C). After bonding temperature further increases from 75 to 150°C, all the differences between ω_{ori} and ω_{dep} are less than 0.16% (Fig. 3.3A) and the values of $\Delta\omega$ are lower than 15% (Fig. 3.3B), which are considered better when comparing to the non-bonded samples. These results indicate that when the supplied heat is sufficient to soften the clear coating particles, the SCHB method can gain good product. Meanwhile, this approach is of no necessity for precise temperature control compared to the traditional thermal

bonding method. No higher temperatures were tested given the higher cost and the protection of Al flakes.

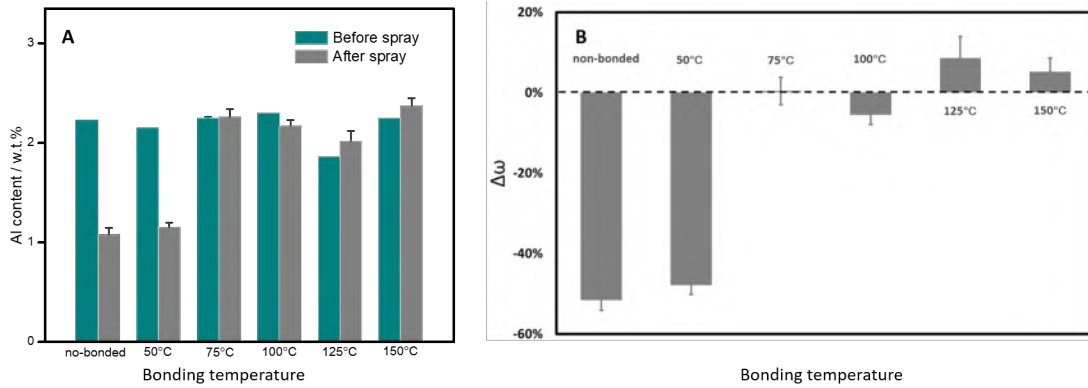


Figure 3.3: A) Comparisons between Al contents in the original and deposited powders; B) relative differences of the Al contents in the original and deposited powders.

From previous results, the optimal bonded sample was obtained when bonding at 75°C. To directly observe the bonding effect in this sample, SEM and EDS were applied. The low-resolution image in Fig. 3.4A shows some flakes disperse among plenty of coating particles. And some obvious bonding can be found between flakes and particles, such as circled areas. Meanwhile, much less separated Al flakes were found (dash circles). The blue and black dots stand for the elements of Al and C, respectively. Fig. 3.4B and C present that about ten Al flakes adhere to the surface of a big coating particle. The red spot in Fig. 3.4B was analyzed by EDX, and it also shows the plate is almost totally composed of aluminum. The medium diameter of the bonded powder, shown in Fig. 3.4E, is 39.47 μm , which is very close to that of the non bonded sample (39.28 μm), indicating that the SCHB method will not significantly increase the particle size. This benefits from the main advantage of the SCHB method—only Al flakes are heated, but the coating particles are not at all. As a result, the formations of large particles (a coating particle bonds other coating particles) will almost completely avoid. In one word, effective bondings between Al flakes and coating particles were observed after SCHB.

Fig. 3.5 shows the visual and optical microscope images of different final films sprayed at 90 kV. The final film is clear and only the color of the substrate can be seen when there is no Al flake (Fig. 3.5A and D). In the visual images of the films from the non-bonded and bonded powders (name them as non-bonded and bonded films), it is obvious that bonded film

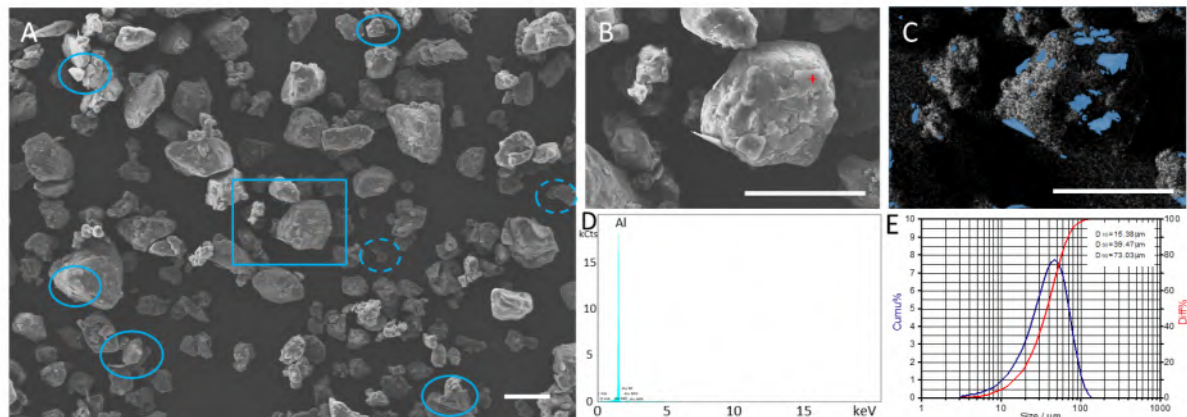


Figure 3.4: The characterizations of bonded powder prepared at 75°C. A-C) SEM images; D) EDX spectroscopy; E) particle size distribution. All the scale bars are 50 μm

(Fig. 3.5C) is shinier than the non-bonded one (Fig. 3.5B). In addition, the optical magnified images represent that the bonded film (Fig. 3.5F) contains more aluminum than the non-bound film (Fig. 3.5E). The above comparisons prove that the bonding effect of SCHB method is significant.

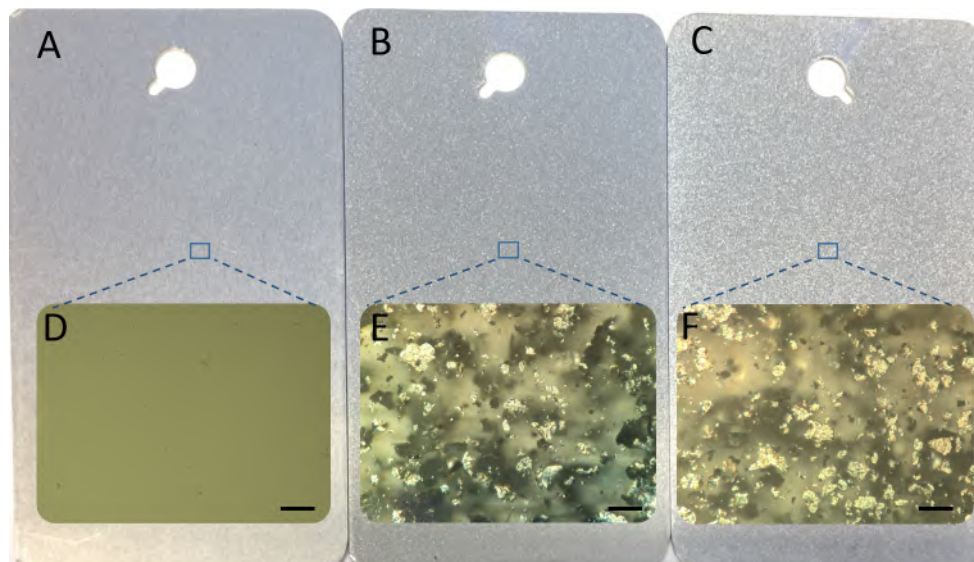


Figure 3.5: The surface comparisons of final films, A,D) clear coat; B,E) non-bonded film; C,F) bonded film. All the scale bars are 30 μm .

3.4.3 Comparisons of SCHB and industrial bonding Methods

The above results suggest that the SCHB method is effective in clear powder coating. To compare with the current industrial bonding method, a non-bonded sample was separately bonded by the thermal bonding method in a company and SCHB method in our laboratory. The visual and optical images of the thermal-bonded and SCHB-bonded films are compared in Fig. 3.6. The visual appearances of the two films were shown in Fig. 3.6A and B, which presents that both films are shiny and even. The shiny areas in Fig. 3.6C-F are the result of Al flakes, which reflect light under optical observation. The sizes of the Al flakes in Fig. 3.6C are slightly larger than that in figure Fig. 3.6E. In the magnified images (Fig. 3.6D and F), more small Al flakes were found in thermal-bonded samples than that in SCHB one. This is mainly due to the high-speed stirring in the process of the industrial bonding method. On the contrary, SCHB does not use stirring, but fluidization, so the Al flakes maintain their original size.

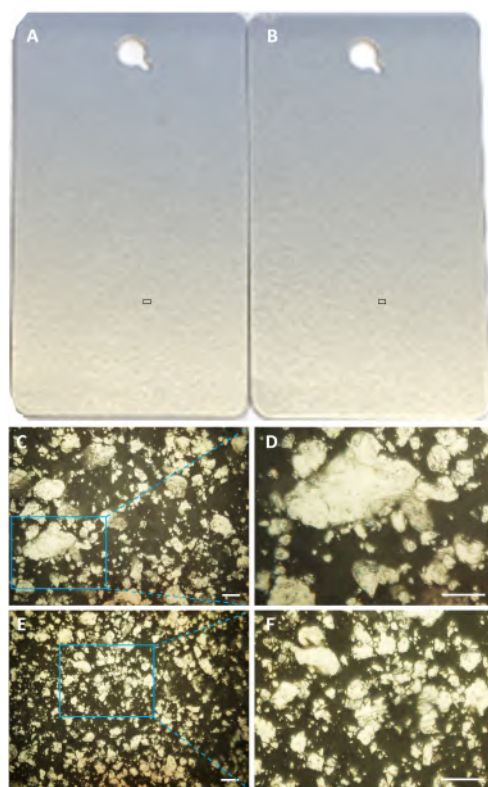


Figure 3.6: Visual and optical images of thermal and SCHB bonded samples. A, C, E) thermal-bonded film; B, D, F) SCHB-bonded film. All the scale bars are 20 μm .

3.5 Conclusions

The SCHB is an effective method for producing metallic effect powder coatings. The heating temperature range of the SCHB method is much wider than that of the industrial bonding method. High bonding quality can be obtained when heating from 75 to 150 °C, and the lowest relative difference is 0.38%. The bondings between coating particles and Al flakes were observed by SEM. The particle size of the Al flake in the SCHB film is larger than that in the thermal-bonded one. The SCHB method is a simple and feasible preparation method for metallic effect powder coatings, and the product quality is as good as the thermal-bonded one.

Bibliography

- [1] María Fernández-Álvarez, Francisco Velasco, and Asunción Bautista. Epoxy powder coatings hot mixed with nanoparticles to improve their abrasive wear. *Wear*, 448:203211, 2020.
- [2] Wei Liu, Haiping Zhang, Yuanyuan Shao, Hui Zhang, and Jesse Zhu. Preparation of aluminium metallic pigmented powder coatings with high color stability using a novel method: Microwave bonding. *Progress in Organic Coatings*, 147:105787, 2020.
- [3] Bing Han, Yang Yu Liu, and Tian Yu Mao. Evaluation of adhesion of steel pipe fusion bonded epoxy powder coating by pull-off test. *Total Corrosion Control*, 2019.
- [4] Jigar K Mistry, Jan Peter Frick, and James Petersen. Microwave bonding for coating compositions, July 6 2017. US Patent 15/463,131.
- [5] Marta Klanjšek Gunde, Matjaž Kunaver, Anton Hrovat, and Uroš Cvelbar. Bonding process efficiency and Al-flake orientation during the curing of powder coatings. *Progress in Organic Coatings*, 54(2):113–119, 2005.
- [6] H Honda, M Kimura, F Honda, T Matsuno, and M Koishi. Preparation of monolayer particle coated powder by the dry impact blending process utilizing mechanochemical treatment. *Colloid. Surface. A*, 82(2):117–128, 1994.
- [7] Douglas S Richart and Andrew T Daly. Thermosetting resin-based coating powders containing metal flakes, February 16 1993. US Patent 5,187,220.
- [8] JA Forrest, K Dalnoki-Veress, and JR Dutcher. Interface and chain confinement effects on the glass transition temperature of thin polymer films. *Physical Review E*, 56(5):5705, 1997.
- [9] JA Forrest, K Dalnoki-Veress, JR Stevens, and JR Dutcher. Effect of free surfaces on the glass transition temperature of thin polymer films. *Phys. Rev. Lett.*, 77(10):2002, 1996.
- [10] H Stutz, K-H Illers, and J Mertes. A generalized theory for the glass transition temperature of crosslinked and uncrosslinked polymers. *Journal of Polymer Science Part B: Polymer Physics*, 28(9):1483–1498, 1990.
- [11] P Haring Bolivar, Martin Brucherseifer, J Gómez Rivas, Ramón Gonzalo, Iñigo Ederra, Andrew L Reynolds, M Holker, and Peter de Maagt. Measurement of the dielectric constant and loss tangent of high dielectric-constant materials at terahertz frequencies. *IEEE T Microw. Theory.*, 51(4):1062–1066, 2003.
- [12] Chunbao Xu and Jesse Zhu. Parametric study of fine particle fluidization under mechanical vibration. *Powder Technology*, 161(2):135–144, 2006.
- [13] Chunbao Xu, Yi Cheng, and Jesse Zhu. Fluidization of fine particles in a sound field and identification of group C/A particles using acoustic waves. *Powder technology*, 161(3):227–234, 2006.

4 Primary study on microwave bonding method for metallic-effect clear powder coating

4.1 Abstract

This paper focuses on the preparation of metallic effect powder coatings with high color stability via a self-designed microwave bonding device. With the increasing environmental regulation on the use of traditional metallic paint, there has been a corresponding interest in metallic effect powder coating, owing to its zero VOCs emission, high protective property as well as sparkling aesthetic appearance. Metallic effect powder coatings are mainly composed of two non-compatible ingredients: base powder coating(s) and metallic pigment(s). Bonding the two kinds of materials together is an effective approach to eliminate their non-compatibility problem and ensure color stability. Here, a self-designed bonding device based on microwave heating was invented to bond metallic effect powder coatings. Furthermore, a direct and quantitative characterization method, ash test, was first used to reveal the bonding quality by analyzing the content of metallic pigment in the powders. A comprehensive investigation on non-bonded powder was performed as a control test. The microwave-bonded samples were prepared with the device at various temperatures and rotating speeds followed by evaluation with ash test. After microwave treatment, reliable bonding of base powder coating and metallic pigment were proved via a series of characterizations, such as ash test, SEM, EDS, optical observation and size analysis. Therefore, the microwave bonding method is trusted to be a feasible and effective production method of metallic effect powder coatings.³

Keywords: Microwave bonding; Metallic pigment, Powder coating; Interface polarization.

³With minor editorial changes to fulfill formatting requirements, this chapter is substantially as it appears in the “Preparation of aluminium metallic effect powder coatings with high color stability using a novel method: Microwave bonding.” *Progress in Organic Coatings* 147 (2020): 105787. Wei Liu, Haiping Zhang, Yuanyuan Shao, Hui Zhang, and Jesse Zhu.

4.2 Introduction

Metallic effect powder coatings — powder coatings incorporated with metallic pigments — have been widely applied in building materials, domestic appliances, automobile hubs, electronic instrumentation and other industries [1, 2, 3]. As an upgraded product of metallic solvent paint, they are able to provide excellent protection and metal-effect surfaces, like the solvent one. More significantly, they emit few volatile organic compounds (VOCs) during the film-forming, unlike the solvent one [4, 5]. The first component, base powder coating (30 to 45 μm), has a similar formula to traditional solvent-borne paints with the exception of no solvents [6, 7]. The second component, metallic pigments (4 to 70 μm), are mostly aluminum or copper flakes for producing silver- or gold-colored films, respectively. As a result of these advantages, metallic effect powder coatings have a rising share of the paint market in the past few years.

However, there are a few applications of metallic effect powder coating on high-end products, such as cellphones, automobiles, and laptops, because these products require extremely high color stability and appearance quality [8, 9, 10]. When an electrostatic spraying system is applied to spray metallic powder paint, ensuring the color stability of the final film is challenging, due to the poor compatibility of the two ingredients [11, 12]. This compatibility problem mainly comes from their sharp distinction in some physical properties, such as density, electric resistance, dielectric constant. As given in Fig. 4.1A, the contents of metallic pigment in the deposited, over-sprayed, and original powders are inconsistent as a result of the problem [13]. Given that the over-sprayed powder is recycled without considering inconsistencies, the final films will have apparent color differences, meaning that the product has inferior color consistency and often leads to rejects. Or worse, discarding the over-sprayed powder will cause high costs and material waste.

Thermal bonding was invented by Richart and coauthors in 1993 to improve the color stability of metallic effect powder coatings [14]. As presented in Fig. 4.1B, because the bonded particles have similar electric properties to the base coating particles, especially in electric resistance and the dielectric constant, the content of metallic pigment in the over-sprayed and original powders would be equal. As a consequence, the over-sprayed powder can be readily

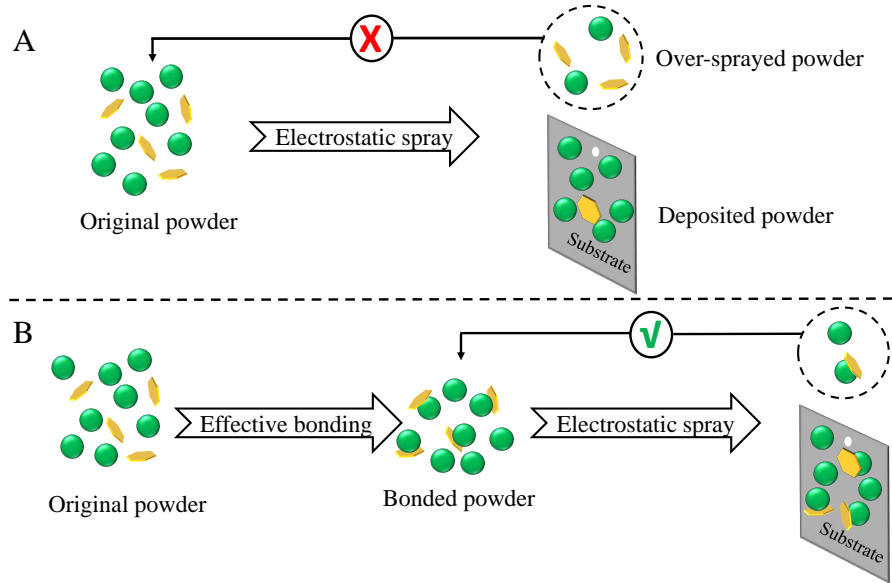


Figure 4.1: The difference between non-bonded and bonded metallic effect powder coatings when sprayed by an electrostatic system. The green patterns represent coating particles; the gold plates represent metallic pigments. A) Non-bonded powders; B) Effectively bonded powders.

recycled without a visual color difference. At the beginning of this bonding approach, metallic pigments and coating powders are heated in a chamber by high-speed stirring and/or oil/water-jacket until the temperature exactly reaches the glass transition temperature (T_g) of the base coating powder [15, 16, 17]. Then, the resin part of coating particles becomes sticky and glues metallic pigments on its surface. Lastly, bonded particles are prepared after rapid cooling. However, the bonding quality of this method is highly sensitive to the bonding temperature [14, 18]; if it is under the glass transition temperature, there will be no bonding between them. Once it exceeds this point by a couple of degrees, the base coating particles are easily bonded with each other (mis-bonding) and may even cause pre-curing. Moreover, the temperature is generally set slightly higher than the T_g to guarantee good bonding in industrial applications, but at the same time increasing the possibility of mis-bonding and pre-curing of coating powders [19]. Also, high-speed stirring tends to bend and even tear up the metal flakes that will significantly reduce the metal effect. More importantly, the metallic effect powder coating prepared by this method is not a product that completely meets the requirements of high-end products. These issues being present in the thermal bonding process limit the application scope of the metallic effect powder coatings.

The powder coating industry highly demands an improved method for bonding metallic effect powder coatings. There have been several attempts to improve bonding quality by using some adhesive materials or pre-treatment on the basis of the thermal bonding, such as surface pre-treatment of aluminum [20], primer [21, 22], and metal nanoparticles [23]. However, these methods have limitations in many ways, for example, cost, industrialization, and pollution. Microwave has been widely used over many fields, such as cooking, sterilization, drying materials, medical treatments and so on [24, 25, 26]. Mistry and coauthors reported that metallic powder paints could be bonded by a variable frequency microwave oven via microwave radiation in C-bands (5.8 to 7GHz) and X-bands (7.3 to 8.7GHz) [27], which are not in the Industrial Scientific Medical (ISM) bands that are defined by the International Telecommunications Union-Radio communications (ITU-R) in 5.138, 5.150, and 5.280 of the Radio Regulations [28]. Therefore, this technology has not ever been applied in industrial production because of the inevitable radio frequency interference (RFI) and high cost. Microwave has many advantages as a heating source, such as clean, pollution-free, efficient, safe and controllable. More importantly, Metaxas and coauthors reported a heat-selectivity phenomenon at the metal/non-metal boundaries possibly attributable to a greater interfacial microwave absorption. [29, 30]. This finding implies that a higher temperature will occur at the interface of metal and nonmetal. Metallic effect powder coatings just consist of a nonmetal (base coating particle) and metal (metal pigment), so a higher temperature is expected at the metal-to-nonmetal contact area, which the bonding process exactly desires. This should be greatly helpful to reduce the mis-bonding and enhance the color stability.

In this paper, an originally self-made microwave-heating device with a fixed center frequency in 2.45GHz was built up at an economical cost and without RFI. Furthermore, a novel bonding method was systematically established on the basis of the microwave as a heating source instead of current-state-of-the-art, such as friction of high-speed stirring and hot jacket. In addition, tumbling, a much more moderate motion, was employed to prevent metallic pigment from breaking and bending. The present work aims at optimizing the operation conditions and characterizing the bonding quality and color stability.

4.3 Materials and methods

4.3.1 Materials and equipment

The following materials were employed in this study: Aluminum flakes (SILBERCOTE PC 3101X, with inorganically treated surface) from Silberline Manufacturing Co., Inc. (Tamaqua, PA, USA) were used as a metallic pigment; High gloss polyester clear powder coating ($D_{50} = 43 \mu\text{m}$, with 7 wt% 1,3,5-Triglycidyl Isocyanurate as cross-linking catalyst, 9910-01289) from TCI powder coating Co. (Ellaville, GA, USA) worked as base powder coating; Al panels (A-2-3.5) from Q-Lab Co. (Westlake, OH, USA) were utilized as substrates.

An Electrostatic powder coating system (Surecoat Manual) and a corona spray gun from Nordson Co., Ltd. (Westlake, OH, USA) were used for coating substrates. A laser particle size analyzer (BT-2000B) from Bettersize Instruments Ltd. (Niaoning, China) was utilized to analyze the size distributions of powdered samples. A Scanning Electron Microscope (SEM) (S-4800) with energy dispersive spectrometer (EDS) from Hitachi Limited (Tokyo, Japan) was employed to observe the bonding situation between Al flakes and coating particles. The thickness of the final films was measured by a thickness meter (Positector 6000) from Defeisko Co. (Ogdensburg, NY, USA). The final surfaces were characterized by an optical microscope (OT4975) from Mitutoyo Inc. (Kawasaki, Japan) and a 408 triple angle gloss & DOI meter from Elcometer Inc. (Michigan, USA).

4.3.2 Microwave-heating bonding device

The diagram of the microwave bonding device is shown in Fig. 4.2. A self-made device (50cm in length; 45cm in width; 40cm in height) with microwave radiation in the frequency of $2.45 \pm 0.05 \text{GHz}$ was used as a heating source. A drum (14cm in inner diameter; 1cm in thickness; 5cm in width) made by polytetrafluoroethylene (PTFE) and glass worked as a container for powders. Because PTFE and glass both have extremely low microwave-absorption capacity, microwave is able to heat the loaded powder freely. Coating powders and aluminum flakes were loaded inside the drum whose rotation was driven by a motor-reducer system outside the shell through a shaft. The two powdered components could be well mixed and heated in this rotary drum without bending or grinding. The tumbling motion of the powdered mix-

ture keeps the metal flakes from agglomerating. A thermocouple inside the drum bearing was used to detect the real-time temperature of powders. Once a set temperature was reached, microwave radiation was shut down to stop heating, while rotation was maintained to cool the powders to room temperature. At last, the microwave-bonded metallic effect powder coating was discharged and collected from the drum.

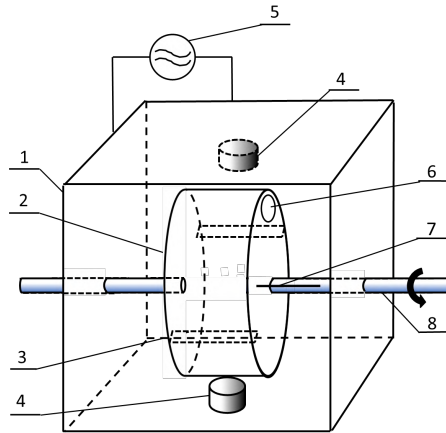


Figure 4.2: Schematic diagram of the microwave bonding device. 1. Shell; 2. Drum; 3. baffles; 4. Microwave transmitters; 5. Power; 6. Discharger; 7. Thermocouple; 8. Rotating shaft.

4.3.3 Preparation of samples

Non-bonded samples were prepared by dry blending 2000g of base powder coating and 45g of Al flakes. Microwave-bonded samples were made by the self-designed bonding device under different temperatures (45-50°C) and rotating speeds (30-60rpm). The sampling process of the ash test is shown in Fig. 2.2.

4.3.4 Characterization of powders and final films

As discussed before, the better the bonding quality, the higher the color stability. The change between the aluminum contents of the original and deposited powders, separately named as original and deposited Al content for short, was used to evaluate the bonding quality of metallic effect powder coating [31]. In this work, the ash test was applied to reveal the content of Al flake in the powders. In this test, samples were burned at a high temperature (530°C) for 1.5 hours. The polyester clear powder coating (which contains no fillers or pigments) in samples would be burned into CO₂, H₂O, other gases and a trace amount of ash residual (0.02

wt%). Meanwhile, Al flakes were not affected by the high temperature except forming a thin oxide film on its surface, whose mass increase was negligible (0.04 wt%). Through this test, the content of aluminum can be calculated by the equation:

$$\omega = \frac{M_r}{M_o} \times 100\% \quad (4.1)$$

Here, ω is the content of Al flake, M_r is the remaining mass after the burning process, and M_o is the mass of original non-bonded or bonded powder. As a result, the original (ω_{ori}) or deposited (ω_{dep}) Al content can be calculated by Eq. 4.1. As such, a lower difference between ω_{ori} and ω_{dep} means a better bonding quality. For a clearer comparison, the relative difference ($\Delta\omega$) between ω_{ori} and ω_{dep} was calculated:

$$\Delta\omega = \frac{\omega_{ori} - \omega_{dep}}{\omega_{ori}} \times 100\% \quad (4.2)$$

Integrating the previous discussion, a lower absolute value of $\Delta\omega$ represents a better bonding quality and color stability. In term of the ash test results, some of the samples with high bonding qualities were characterized by SEM, EDS. The sizes of non-bounded and bonded powders were detected by a laser particle size analyzer.

To examine the color stability of a sample, the following steps have been performed: a) the sample was sprayed onto substrates at three different voltages (30, 60 and 90kV); b) the deposited powders were cured into films; c) the numbers of Al flakes on the surfaces of these films were compared by an optical microscope. The smaller the number change, the better the color stability.

4.4 Results and discussion

4.4.1 Non-bonded samples

Film thickness is one of the most significant concerns in the coating industry, so the relationship between the thickness of the final film and the mass of deposited powder was first calibrated by using the non-bonded powder. The results show the thickness of the final film is proportional to the mass of deposited powder when sprayed at 30kV. For the Al panels used in

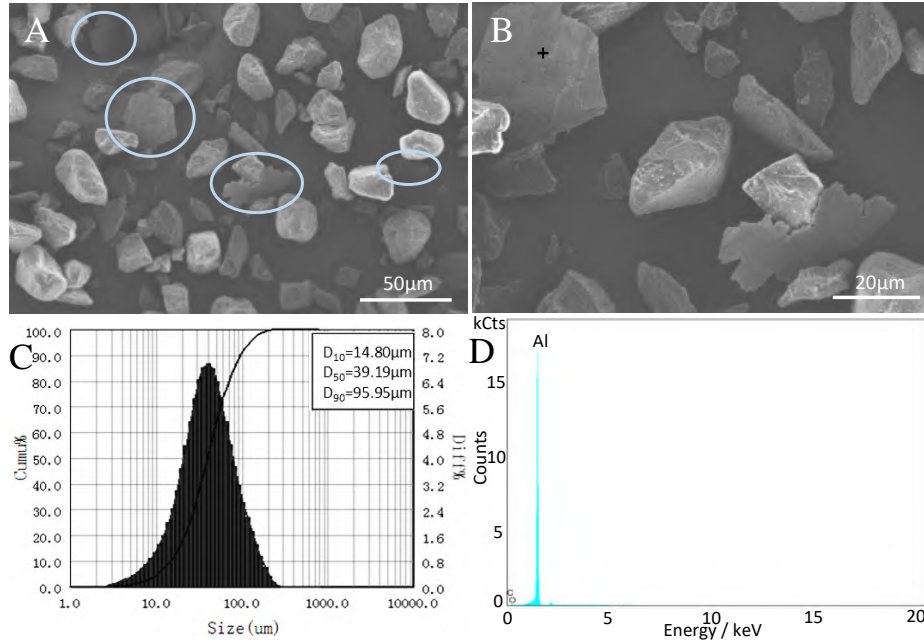


Figure 4.3: SEM images and size distribution of non-bonded sample. A) Low-magnification SEM image; B) Zoomed-in SEM image; C) Size distribution; D) EDS spectrum of the black site in B.

this study, when the powder mass was 0.34g and 0.52g, the thickness was 62.5 μm and 82.4 μm, respectively. Generally, the thickness is between 60 to 80 μm in the industrial application when the diameter of coating powder is around 40 μm[32]; therefore, the deposited mass was controlled in the range of 0.3 to 0.5g.

SEM was employed to observe the situation between Al flakes and coating particles, as shown in Fig. 4.3. Two flakes lean on particles and the other two lie down alone as viewed in these circle areas in Fig. 4.3A. Furthermore, a zoomed-in image (Fig. 4.3B) shows the surfaces of the two flakes are clean and smooth, which indicates there are no smaller coating particles bonded on these flakes. Thus, even though they are in touch with coating particles, it is deemed that there is no bonding between them. Also, Energy dispersive spectroscopy of the black site in Fig.4.3B confirms that the flake is almost entirely composed of aluminum, so the flakes in these images are trusted to be the Al flakes. Additionally, the size analysis in Fig. 4.3C indicates the medium size of this non-bonded sample is 39.19 μm.

Based on previous knowledge, deposited mass and spray voltage are considered two vital influencing factors on the deposited Al content [21]. In industry, the spray voltage is no more than 90kV [33]. Accordingly, various deposited mass and voltages were studied as observed

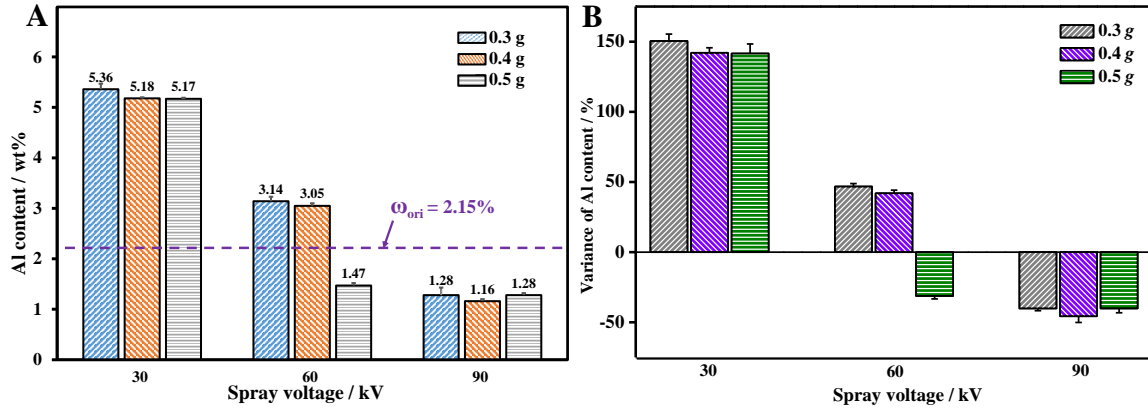


Figure 4.4: The deposited Al contents (A) and relative difference (B) at various mass and spray voltages

in Fig. 4.4. The non-bonded sample with Al flake addition of 2.2 wt% was prepared at the beginning. Its accurate aluminum content turned out to be 2.15 wt% by ash test, as revealed by the dashed line in Fig. 4.4. However, the deposited Al contents go over 5 wt% when the non-bonded sample was sprayed at 30kV. The relative difference of Al content is as high as 150 % as shown in Fig. 4.4B. On the contrary, under a very high spray voltage of 90kV, all of the deposited Al contents, around 1.2 wt%, are much lower than the original Al content. Fig. 4.4B shows that the relative differences of Al content are around -40% .

At the medium spray voltage of 60kV, the deposited Al contents are higher than the original one when the masses are 0.3 and 0.4g; however, it is a bit lower than the original one, as the deposited mass increased to 0.5g. Also, the relative difference changes from a positive value to a negative one as viewed in Fig. 4.4B. This means there is a possible spray condition, which allows the deposited Al content to be equal to the original one. This possibility only occurs under a narrow operation condition, which may be helpful for industrial applications. These results prove that the deposited Al content dramatically fluctuates when the spray voltage and deposited mass change. This certainly leads to final films with different metal effects and colors, meaning that the paint is not a stable and qualified product. Of course, the over-sprayed powder of non-bonded powder can not be recycled due to the distinct Al contents.

From previous results, the deposited mass and spray voltage shows great influence on the deposited Al content. The main reason for these results is the difference between the two materials in dielectric constant and equivalent spherical radius. According to Pauthenier equation

[34]:

$$Q_{max} = 4 \pi r^2 \epsilon_0 E \frac{3\epsilon_r}{\epsilon_r + 2} \quad (4.3)$$

where Q_{max} is the maximum charge accumulated by a particle passing through an electric field; r is the equivalent spherical radius; ϵ_0 is permittivity of vacuum; E is the electric field strength; ϵ_r is the relative dielectric constant. The dielectric constant of Al flake (covered by alumina on the skin) is around $7 F/m$ [35, 36], which is higher than that of the coating particle ($\sim 1.6 F/m$) [37, 38]. The equivalent spherical radius of Al flake and coating particle are $\sim 8\mu m$ and $\sim 40\mu m$, respectively. Calculating with Eq. 4.3, the maximum charge of coating particle exceeds 10 times of that of Al flake. When moving in an electric field, a higher charge implies a stronger driving force and more deposition.

At the low voltage of 30kV, Al flakes almost get the maximum charge while coating particles are less charged, which leads to a higher Al content (Fig. 4.5A). However, at the high voltage of 90kV, coating particles carry much more electrons/anions than Al flakes and results in a higher content of coating particles. In other words, the lower content of Al flake will be found in the final film (Fig. 4.5C). At the medium voltage of 60kV, the two components are supposed to have a similar driving force. However, the electrostatic repulsion between deposited particles and charged particles is growing higher when the deposition becomes thicker. In addition, a coating particle has a great opportunity to get a heterogeneous distribution of surface charges due to its high electric resistance, while an Al flake has a uniform charge distribution [39]. Thus, charged coating particles receive less repulsive force due to the fact that they can be re-orientated when moving into the range adjacent to the already deposited powder layer, which probably is the primary reason for the decline of Al content while the deposited mass increased from 0.4 to 0.5g.

4.4.2 Microwave-bonded samples

The rotating speed of the drum and the heating temperature of the loaded powder are considered as two main factors in the microwave bonding process. The maximum rotating speed (n_{max}) that allows powders to stay clear from compaction in a drum can be estimated through

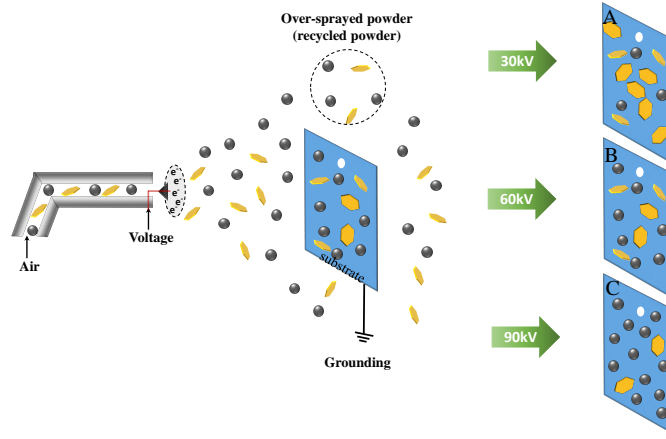


Figure 4.5: Mechanism of the spray process of non-bonded sample. The golden flakes represent Al flakes; the black round dots stand for clear coating particles.

the following equation:

$$n_{max} = \frac{30}{\pi} \sqrt{\frac{g}{r}} \quad (4.4)$$

where, r is the radius of the drum; g is the acceleration of gravity (m/s^2). Theoretically, the highest rotating speed calculated by Eq. 4.4 is $113rpm$ when the drum radius is $7cm$. According to Huang's study, with the increasing rotating speed, the motion of powder in a drum will go through five stages: slipping regime, avalanching-sliding regime, aerated regime, fluidization regime, and re-compacted regime [40]. For the purpose of better bonding, the loaded powders must stay in the fluidization regime to ensure uniform heating. Huang also suggested that installing baffles inside the drum could greatly help the loaded powder fluidizing at a slower speed [40] and thus three rotating speeds, 30 , 45 , and $60rpm$, were applied while the temperature was kept at $47^\circ C$.

After mixing and bonding, the original Al content of each bonded sample turned out to be around 2.2% . A small deviation from that of non-bonded samples (2.15%) is found because the losses of the coating particle and Al flakes are different in every bonding process. Each sample was sprayed at different voltages of 30 , 60 , and $90kV$ to a substrate with the same deposited mass of $0.4g$, aiming at examining its color stability. Table 4.1 summarizes the deposited Al contents of non- and microwave-bonded samples. The three bonded samples have a smaller change (1.55 to 3.78%) in the deposited Al contents than the non-bonded sample (1.16 to 5.18%). We know that the smaller the change the better the bonding quality. Thus, it can

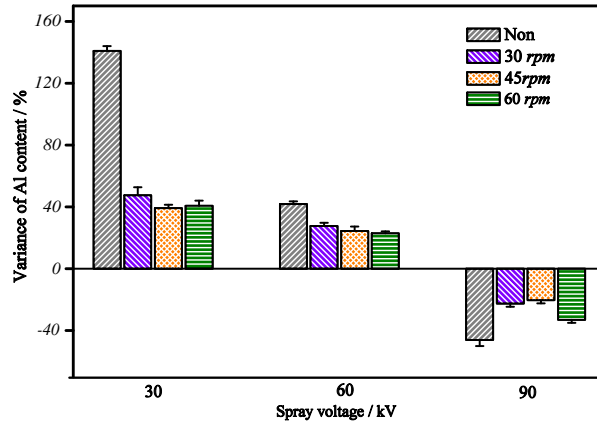


Figure 4.6: The relative differences of Al contents of bonded samples made at different rotating speeds.

be held that effective bonding between coating particles and Al flakes is truly formed after microwave heating treatment.

Table 4.1: The deposited Al contents (wt%) of the samples prepared at different rotating speeds.

	30kV	60kV	90kV	Original
35 rpm	3.14 ± 0.10	2.72 ± 0.03	1.65 ± 0.02	2.13 ± 0.02
45 rpm	3.02 ± 0.06	2.70 ± 0.05	1.73 ± 0.05	2.17 ± 0.03
60 rpm	3.17 ± 0.07	2.77 ± 0.02	1.51 ± 0.04	2.25 ± 0.01
Non-bonded	5.18 ± 0.09	3.05 ± 0.03	1.16 ± 0.05	2.15 ± 0.02

For a more distinct comparison, the relative difference of Al content was calculated by Eq. 4.2 and plotted in Fig. 4.6. It is found that bonded samples have lower relative differences than the non-bonded samples at all voltages, especially at 30kV. When comparing these bonded samples, it is found that although they have a close relative difference at the same voltage, the sample prepared at 45rpm has a slightly lower one at 30 and 90kV. So, the speed of 45rpm is considered to be the best among these three tests. From the experimental observation, the loaded powders remained in the fluidization regime at all of these speeds. The reason for the better bonding quality at the speed of 45rpm is that the slower speed can not provide a swift motion for the loaded powder to receive uniform heating while high speed leads to an excessive shear force which makes the bonding harder.

The optimal rotating speed in the tested samples is found to be 45rpm at the current drum radius, and then the second factor that is also the most important one, heating temperature, was

studied in this section. Here, five different heating temperatures were tested under this rotating speed. Table 4.2 displays the original and deposited Al contents of these bonded samples. A similar finding is that the deposited Al content decreases with the increase of spray voltage. Besides, the largest decline is found at 50°C, because this high temperature tends to make the coating particle not only bond with Al flakes but also other coating particles. Moreover, a few amount of small chunks of particles were formed at this condition. On the contrary, bonding at 48°C has the smallest change in the deposited Al content.

Table 4.2: The deposited Al contents (wt%) of bonded powders prepared at various temperatures.

	30kV	60kV	90kV	Original
45 °C	3.19 ± 0.18	2.41 ± 0.08	1.35 ± 0.06	2.18 ± 0.02
47 °C	3.02 ± 0.06	2.70 ± 0.05	1.73 ± 0.05	2.17 ± 0.03
48 °C	2.71 ± 0.05	2.18 ± 0.03	1.61 ± 0.02	2.12 ± 0.02
49 °C	3.32 ± 0.10	2.09 ± 0.11	1.75 ± 0.03	2.23 ± 0.01
50 °C	3.90 ± 0.09	3.18 ± 0.06	1.60 ± 0.14	2.30 ± 0.02

In Fig. 4.7, the relative differences of non-bonded samples are always higher than that of bonded samples, indicating that bonding at all of the five temperatures is helpful to get a stable color. Among these bonded samples, the relative difference at 48°C is apparently smaller than that of the other four temperatures at 30 and 60kV. In particular, the relative difference at 48°C is very close to zero when the voltage is 60kV. Even though the relative difference at 48°C is slightly higher than that of 47 and 49°C, it is considerably lower than that of 45 and 50°C. In short, it can be concluded that 48°C is the best temperature for bonding coating particles and Al flakes in the tested points. The lowest relative differences of Al contents were found to be 27.8%, 2.83%, and -24.0% when the spray voltages were 30, 60, and 90kV, respectively. These values are much lower than that of the non-bonded sample (142.0%, 41.9%, and -45.8%), indicating that a much higher color stability is obtained.

It is remarkable that the heating temperature (48°C) of the microwave bonding method is much lower than the T_g (52°C) of the coating particle. This low bonding temperature is mainly due to the heating-selectivity of microwave. In the analysis that follows, the radio frequency power absorbed by materials per unit volume is given as below [41]:

$$P = 2\pi f \epsilon_0 E^2 \epsilon''_{eff} \quad (4.5)$$

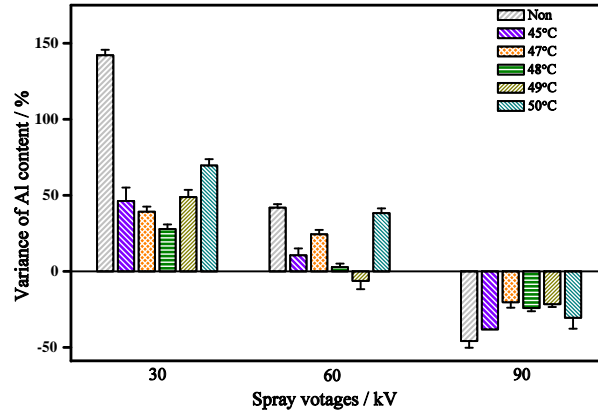


Figure 4.7: The relative differences of Al contents of bonded powders prepared at various temperatures.

where, P is the microwave absorbing power per unit volume (W/m^3); f is the frequency of microwave (Hz); E is the electric field intensity (V/m); ϵ_0 is the permittivity of vacuum; ϵ''_{eff} is the effective dissipation factor of materials.

All the samples in this work are the mixtures of organic powders (base coating powders) and conductive metal plates (Al flakes). In this situation, the main microwave absorption is due to two distinct mechanisms: dipolar polarization of base particles and Maxwell-Wagner polarization (interfacial relaxation) between the interface of coating particles and Al flakes [29]. In order to figure out which one is the dominant mechanism, the same mass of base coating powder and non-bonded powder were separately heated by microwave in the same condition.

First, the base coating powder with no Al flakes was heated by microwave. The major microwave absorption is believed to be dipolar polarization in this process. The effective dissipation factor of dipolar polarization ($\epsilon''_{dipolar}$) can be estimated by Eq. 4.6:

$$\epsilon''_{dipolar} = \epsilon' \tan\delta \quad (4.6)$$

where, ϵ' is the dielectric constant of particle; $\tan\delta$ is the loss tangent of particle. The calculated $\epsilon'_{dipolar}$ is about 0.017 by applying the data from some reported studies [42, 43]. The experimental results show the heating rate of microwave at this condition is $\sim 5^\circ C/min$.

Second, when the non-bonded powder (mixture of base coating powders and Al flakes) was heated by microwave, the effective dissipation factor of Maxwell-Wagner polarization (ϵ''_{MW}) can be evaluated by Eq. 4.7 [30, 29] and 4.8 [44]:

$$\epsilon''_{MW} = \frac{9 v \epsilon'_1 f_{max}}{1.8 \times 10^{10} \delta_2} \frac{2\pi f \tau}{1 + (2\pi f \tau)^2} \quad (4.7)$$

$$\tau = \epsilon_0 \frac{\epsilon'_1 + \epsilon'_2}{\delta_1 + \delta_2} \quad (4.8)$$

where, v is the volume fraction of conductive material; f_{max} in Hz is the frequency of maximum losses; δ is the conductivity in $S m^{-1}$; τ is the relaxation time constant; the subscripts 1 and 2 refer to non-conductive and conductive phase, respectively. After collecting data from published articles [27, 43, 45, 46], ϵ''_{MW} turned out to be around 0.07 which is about four times greater than that of dipolar polarization. Experimentally, a much faster heating rate, $\sim 18^\circ C/min$, of non-bonded powder was observed when comparing to that of base coating powders ($\sim 5^\circ C/min$). These results prove that the interfacial polarization is the main absorption mechanism that allows the interface to have a higher temperature than that of the non-touched surface and interior of each particle. By taking this advantage, the heating temperature of the microwave bonding method is not as sensitive as the thermal one. In addition, the heating rate of the current industrial thermo-bonding machine generally ranges from 3 to $6^\circ C/min$. Above all, bonding metallic effect powder coating by microwave radiation is a rather fast and effective method.

The sample bonded at $48^\circ C$ and $45rpm$ (named as optimal sample for short) was further analyzed by SEM, EDS and particle size analyzer as given in Fig. 4.8. In Fig. 4.8A, several bondings between coating particles and flakes were observed (areas with solid line). Fig. 4.8B magnified from the square area in 4.8A presents several coating particles that stick on both sides of a flake. A further element distribution of Al (white spots) and C (black spots) on the observed area of 4.8B was analyzed by EDS as viewed in Fig. 4.8C. The element analysis proves that the plate-like particle is an Al flake and these particles on its surface are coating particles. The EDS spectroscopy also indicates that the flake is made of aluminum. In addition, 4.8E shows the medium size of this bonded sample ($D_{50} = 43.44\mu m$) is slightly higher than that of the non-bonded sample ($D_{50} = 39.19\mu m$). The primary reason for this size increment

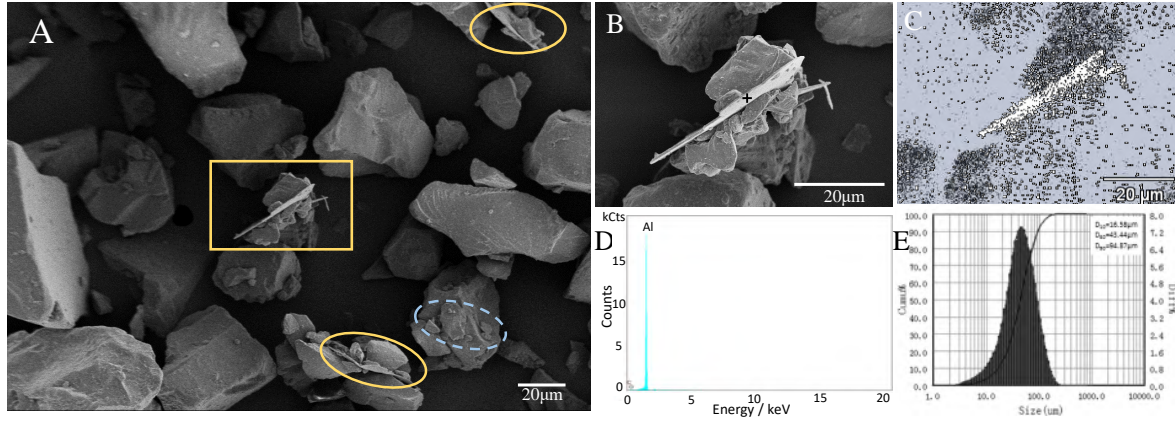


Figure 4.8: SEM, EDS and size distribution of bonded sample. A) Low-magnification SEM image of microwave-bonded sample; B) High-magnification SEM image; C) EDS scanning of the element of Al and C; D) EDS spectrum of the black site in B; E) Size distribution.

is that some small coating particles bonded onto the surface of Al flakes as well as big coating particles, as shown in the circle areas 4.8A. Above all, these results verified that effective bonding between Al flakes and coating particles was achieved by microwave bonding.

The color stability of the final films were qualitatively compared by an optical microscope, as shown in Fig. 4.9. It is hard to have an accurate analysis on the color change, such as color difference and gloss because some areas of the film without Al flake are transparent. Thus, the difference of the number of metallic pigments (Al flakes) on the final surfaces that prepared at three voltages (30, 60, 90kV) is applied to imply the color stability in this work. These shiny plates in Fig. 4.9 are believed to be Al flakes that reflect lights under the observation of the optical microscope. The number of Al flakes fairly decreases in the non-bonded films with the increase of spray voltage. Conversely, it is much more stable in the films prepared from the optimal sample although there is still a slight decline. As presented in Table 4.1 and 4.2, the deposited Al content of the non-bonded sample sprayed at the three voltages are 5.18%, 3.05%, and 1.16% separately as well as that of the optimal sample are 2.71%, 2.18%, and 1.61% respectively. The trends of amount change of Al flakes coincides with these previous analysis. These images of final surfaces provide evidence to confirm that microwave bonding method is able to reach a high color stability. Hence, the samples made by microwave bonding method are trusted to have a smaller color change.

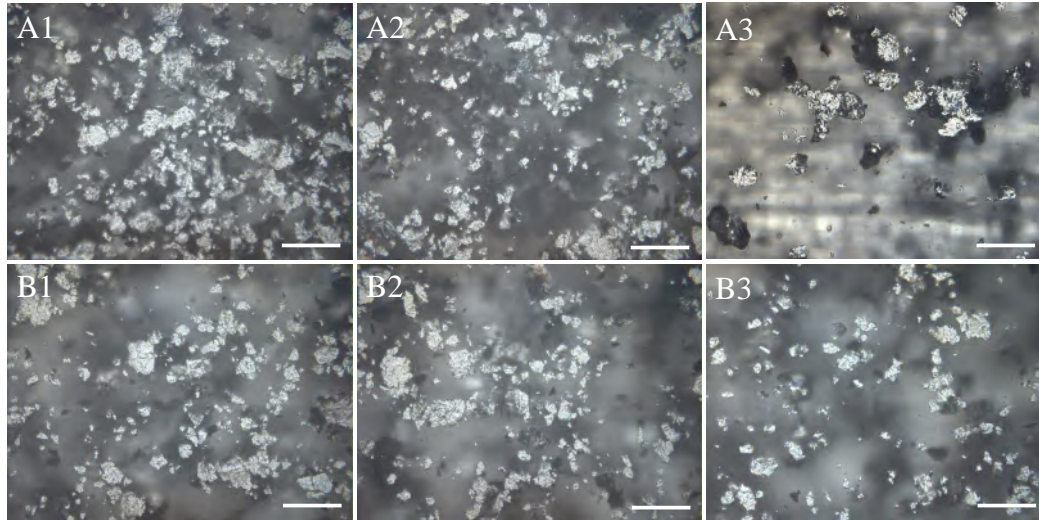


Figure 4.9: Optical images of the surfaces of final films that cured from the non-bonded (A) and optimal samples (B), and the spray voltages separately are: 1) 30kV; 2) 60kV; 3) 90kV. The scale bars are 50 μ m.

4.5 Conclusions

To accomplish high bonding quality and color stability of metallic effect powder coatings, the microwave bonding method (with the center frequency of 2.45GHz) was performed and tested. A completely self-designed microwave bonding device was set up for this study. The best speed and temperature in the tested samples were proved to separately be 60rpm and 48°C. The microwave-bonded samples with the lowest relative differences in Al contents were found to be 27.8%, 2.83%, and -24.0% when the spray voltages were 30, 60, and 90kV, respectively.

The coating particles and Al flakes were well-bonded according to SEM and EDS images. With comparisons to the thermal bonding method, microwave bonding had a much higher heating speed ($\sim 18^{\circ}\text{C}/\text{min}$), a lower bonding temperature (48°C) and a high color stability. The microwave bonding approach had a great possibility to overcome most of the problems associated with the thermal bonding method, such as mis-bonding, pre-curing, and metallic flake bending, without reducing bonding effectiveness. The microwave bonding method is projected to be a promising technology to improve the color stability and bonding efficiency in metallic effect powder coating manufacturing.

Bibliography

- [1] Jostein Mrdalen, John Erik Lein, Helene Bolm, Merete Hallenstvet, and Volker Rekowski. Time and cost effective methods for testing chemical resistance of aluminium metallic pigmented powder coatings. *Progress in Organic Coatings*, 63(1):49 – 54, 2008.
- [2] V Sreenivasulu and M Manikandan. Hot corrosion studies of HVOF sprayed carbide and metallic powder coatings on alloy 80A at 900C. *Mater. Res. Express*, 6(3):036519, 2018.
- [3] Jixing Cui, Rezwana Yeasmin, Yuanyuan Shao, haiping zhang, Hui Zhang, and Jesse Zhu. Fabrication of Ag^+ , Cu^{2+} , Zn^{2+} ternary ion-exchanged zeolite as an antimicrobial agent in powder coating. *Ind. Eng. Chem. Res.*, 59(2):751–762, 2020.
- [4] Fandi Meng, Li Liu, Yu Cui, and Fuhui Wang. Evaluation of coating resistivity for pigmented/unpigmented epoxy coatings under marine alternating hydrostatic pressure. *J Mater. Sci. Tech.*, 2019.
- [5] María Fernández-Álvarez, Francisco Velasco, Asunción Bautista, and Beatriz Galiana. Functionalizing organic powder coatings with nanoparticles through ball milling for wear applications. *Applied Surface Science*, page 145834, 2020.
- [6] Márcio D Lima, Shaoli Fang, Xavier Lepró, Chihye Lewis, Raquel Ovalle-Robles, Javier Carretero-González, Elizabeth Castillo-Martínez, Mikhail E Kozlov, Jiyoun Oh, Neema Rawat, et al. Biscrolling nanotube sheets and functional guests into yarns. *Science*, 331(6013):51–55, 2011.
- [7] Aurélie Dupuis, Thu Huong Ho, Ahmad Fahs, Aurore Lafabrier, Guy Louarn, Jalal Bacharouche, Aissam Airoudj, Emmanuel Aragon, and Jean-François Chailan. Improving adhesion of powder coating on peek composite: Influence of atmospheric plasma parameters. *Applied Surface Science*, 357:1196–1204, 2015.
- [8] SM Mahajan, A Varade Mayur, N Mahajan Pratiksha, and V Patil Sneha. Review on automotive body coating process. *Int. J. Eng. Manage. Res.*, 9(2):103–106, 2019.
- [9] Abdel Salam Hamdy Makhlouf and Yashwanth Gajarla. Advances in smart coatings for magnesium alloys and their applications in industry. In *Advances in Smart Coatings and Thin Films for Future Industrial and Biomedical Engineering Applications*, pages 245–261. Elsevier, 2020.
- [10] Junren Lin, Casey Orgon, Dante Battocchi, and Gordon P Bierwagen. (Mg rich primer-powder topcoat) coating system for the corrosion protection of al alloys. *Progress in Organic Coatings*, 102:138–143, 2017.
- [11] Rezwana Yeasmin, Hui Zhang, Jingxu Zhu, and Peter Cadieux. Fabrication and analysis of antimicrobial additives for powder coated surface. *Progress in Organic Coatings*, 127:308–318, 2019.

- [12] C Gioia, M Vannini, P Marchese, A Minesso, R Cavalieri, M Colonna, and A Celli. Sustainable polyesters for powder coating applications from recycled pet, isosorbide and succinic acid. *Green Chem.*, 16(4):1807–1815, 2014.
- [13] Jing Fu, Matthew Krantz, Hui Zhang, Jesse Zhu, Harry Kuo, Yar Ming Wang, and Karen Lis. Investigation of the recyclability of powder coatings. *Powder Technology*, 211(1):38–45, 2011.
- [14] Douglas S Richart and Andrew T Daly. Thermosetting resin-based coating powders containing metal flakes, February 16 1993. US Patent 5,187,220.
- [15] Kyoko Miyauchi, Yuka Takita, Hidetoshi Yamabe, and Makoto Yuasa. A study of adhesion on stainless steel in an epoxy/dicyandiamide coating system: Influence of glass transition temperature on wet adhesion. *Progress in Organic Coatings*, 99:302 – 307, 2016.
- [16] Md D Hossain, Derong Lu, Zhongfan Jia, and Michael J Monteiro. Glass transition temperature of cyclic stars. *ACS Macro Lett.*, 3(12):1254–1257, 2014.
- [17] M. Szociński and K. Darowicki. Local properties of organic coatings close to glass transition temperature. *Progress in Organic Coatings*, 77(12, Part A):2007 – 2011, 2014.
- [18] TH Van Steenkiste, JR Smith, and RE Teets. Aluminum coatings via kinetic spray with relatively large powder particles. *Surface and Coatings Technology*, 154(2-3):237–252, 2002.
- [19] Wei-Hsing Tuan, HH Wu, and TJ Yang. The preparation of Al₂O₃/Ni composites by a powder coating technique. *J. Mater. Sci.*, 30(4):855–859, 1995.
- [20] Chang-Yeol Yoo and Kong Byung-Seok. Surface treatment method of aluminum for bonding different materials, May 2 2019. US Patent App. 16/156,699.
- [21] Wei Liu, Jing Fu, Haiping Zhang, Yuanyuan Shao, Hui Zhang, and Jesse Zhu. Cold bonding method for metallic powder coatings. *Materials*, 11(11):2086, 2018.
- [22] Liam O’neill, Frederic Gubbels, Stuart Leadley, and Nick Shephard. Bonding an adherent to a substrate via a primer, October 14 2014. US Patent 8,859,056.
- [23] Keiichi Endoh, Aiko Nagahara, Yutaka Hisaeda, and Toshihiko Ueyama. Bonding material using metal nanoparticles coated with c6-c8 fatty acids, and bonding method, October 14 2014. US Patent 8,858,700.
- [24] Yuan-Yuan Pu and Da-Wen Sun. Combined hot-air and microwave-vacuum drying for improving drying uniformity of mango slices based on hyperspectral imaging visualisation of moisture content distribution. *Biosyst. Eng.*, 156:108–119, 2017.
- [25] Yuanyuan Pan, Da-Wen Sun, Jun-Hu Cheng, and Zhong Han. Non-destructive detection and screening of non-uniformity in microwave sterilization using hyperspectral imaging analysis. *Food Anal. Method.*, 11(6):1568–1580, 2018.

- [26] Alexandros Ch Stratakos, Gonzalo Delgado-Pando, Mark Linton, Margaret F Patterson, and Anastasios Koidis. Industrial scale microwave processing of tomato juice using a novel continuous microwave system. *Food Chem.*, 190:622–628, 2016.
- [27] Jigar K Mistry, Jan Peter Frick, and James Petersen. Microwave bonding for coating compositions, July 6 2017. US Patent 15/463,131.
- [28] Hossam Mahmoud Ahmad Fahmy. Wireless sensor networks essentials. In *Wireless Sensor Networks*, pages 3–39. Springer, 2020.
- [29] AC Metaxas and Roger J Meredith. *Industrial microwave heating*. Number 4. IET, 1983.
- [30] T Prodromakis and C Papavassiliou. Engineering the maxwell–wagner polarization effect. *Applied Surface Science*, 255(15):6989–6994, 2009.
- [31] Standard test method for ash content in plastics (D5630-13). *ASTM Standard*, 8:1–5, 2013.
- [32] TA vd Misev and R Van der Linde. Powder coatings technology: new developments at the turn of the century. *Progress in Organic Coatings*, 34(1-4):160–168, 1998.
- [33] K. Dastoori, B. Makin, and J. Telford. Measurements of thickness and adhesive properties of electrostatic powder coatings for standard and modified powder coating guns. *J. Electrostat.*, 51(1):545–551, 2001.
- [34] Daniel Goldwater, Benjamin Stickler, Lukas Martinetz, Tracy E Northup, Klaus Hornberger, and James Millen. Levitated electromechanics: all-electrical cooling of charged nano-and micro-particles. *Quantum Sci. Technol.*, 4, 2019.
- [35] Zhi-Min Dang, Tao Zhou, Sheng-Hong Yao, Jin-Kai Yuan, Jun-Wei Zha, Hong-Tao Song, Jian-Ying Li, Qiang Chen, Wan-Tai Yang, and Jinbo Bai. Advanced calcium copper titanate/polyimide functional hybrid films with high dielectric permittivity. *Adv. Mater.*, 21(20):2077–2082, 2009.
- [36] EMS Sanchez, CAC Zavaglia, and MI Felisberti. Unsaturated polyester resins: influence of the styrene concentration on the miscibility and mechanical properties. *Polymer*, 41(2):765–769, 2000.
- [37] DJ Suh, Ook Park, and KH Yoon. The properties of unsaturated polyester based on the glycolyzed poly (ethylene terephthalate) with various glycol compositions. *Polymer*, 41(2):461–466, 2000.
- [38] James D Christie and William C Howard. Bonded metal hydroxide-organic composite polymer films on particulate substrates, June 12 2001. US Patent 6,245,323.
- [39] Xiahui Gui, Yaowen Xing, Guoqiang Rong, Yijun Cao, and Jiongtian Liu. Interaction forces between coal and kaolinite particles measured by atomic force microscopy. *Powder Technology*, 301:349–355, 2016.

- [40] Qing Huang, Hui Zhang, and Jesse Zhu. Experimental study on fluidization of fine powders in rotating drums with various wall friction and baffled rotating drums. *Chem. Eng. Sci.*, 64(9):2234–2244, 2009.
- [41] Tetsuya Hanai. Dielectric theory on the interfacial polarization for two-phase mixtures. *Bull. Inst. Chem. Res., Kyoto University*, 39(6):341–367, 1962.
- [42] Kwong Siong Kiew, Sinin Hamdan, and Md Rezaur Rahman. Comparative study of dielectric properties of chicken feather/kenaf fiber reinforced unsaturated polyester composites. *BioResources*, 8(2):1591–1603, 2013.
- [43] Hyoung Geun Kim et al. Dielectric cure monitoring for glass/polyester prepreg composites. *Composite Structures*, 57(1-4):91–99, 2002.
- [44] RW Sillars. The properties of a dielectric containing semiconducting particles of various shapes. *J. Inst. Electr. Eng.*, 80(484):378–394, 1937.
- [45] Motohiko Yoshizumi. Electroconductive powder and process for production thereof, June 5 1984. US Patent 4,452,830.
- [46] DW Peters, Lester Feinstein, and Christian Peltzer. On the high-temperature electrical conductivity of alumina. *J Chem. Phys.*, 42(7):2345–2346, 1965.

5 Lab-scale study on microwave bonding method for powder coatings

5.1 Abstract

Metallic effect powder coating, composed of metallic pigments and coating particles, provides coatings with metal shine and functional protection, while causes much less emission of organic solvents, unlike the traditional paint. The greatest challenge of the manufacturing step is binding the two incompatible ingredients together. However, the present industrial binding method, thermal bonding, has some inherent issues, such as pre-curing, pigment bending and high-temperature bonding. Hence, in the present work, a novel approach, microwave bonding, was studied and tested to address these shortcomings. Aluminum flakes were bonded with three types of powder coatings: polyester, hybrid, and polyvinylidene fluoride (PVDF). Microwave bonding shows a more stable metal shine over the non-bonding, obtains a lower bonding temperature than the glass transition temperature, and has a much higher heating rate ($\sim 17^{\circ}\text{C}/\text{min}$) over the thermal bonding method. Therefore, microwave bonding is trusted to have great potential to produce coatings with highly stable metal shine efficiently.⁴

Keywords: Microwave; Bonding; Metallic pigment; Powder coating; Metal shine.

⁴With minor editorial changes to fulfill formatting requirements, this chapter is substantially as it appears in "Produce various powder coated surfaces with stable metal shine via microwave energy". *Progress in Organic Coatings*. 2021 May 1;154:106199, Wei Liu, Haiping Zhang, Yuanyuan Shao, Hui Zhang, and Jesse Zhu.

5.2 Introduction

Metallic effect coating is an established technology that uses metallic pigments in a coating matrix to increase exclusivity and attractiveness. By mimicking a metal surface, it improves the functional protection and toughens the coating [1, 2]. This coating has been heavily used in a broad range of industrial fields, such as automobile and bicycle parts, construction materials, domestic appliances, electronic instrumentation and so on [3, 4, 5]. Metallic effect coating is usually made of two ingredients: metallic pigment and base paint. The first component is commonly in flake form and is composed of metals or metal-like materials for adding various metal shines and functional protection to the finish, for example, aluminum for silver color and copper for gold color [6, 7]. The second component is mostly traditional solvent paint or powder coating. It is known that the emission of volatile organic compounds (VOC) during the film-forming process of the solvent paint has done incalculable damage to the atmospheric environment [8, 9]. Therefore, some authorities put increasing environmental pressure on the solvent paint and even prohibit traditional solvent-borne paint. For environmental sustainability, powder coatings containing 100% free flow solid particles have been invented and developed [10, 11]. Nowadays, powder coating has gradually become the primary base paint for producing metallic effect coating [12].

Nevertheless, a challenge that arises in the production process of the metallic effect powder coating (made by metallic pigment and powder coating) is the color deviation that occurs during electrostatic spraying [13]. As illustrated in Fig. 5.1a, the content of metallic pigment will be different among the non-bonded, over-sprayed, and deposited powders. This problem is mainly caused by the non-compatibility between the two components due to their distinct physical natures, such as density, conductivity, shape, dielectric constant, etc. Bonding the two incompatible ingredients together is an effective method to reduce the color deviation of the powder coating. As shown in Fig. 5.1b, the content of metallic pigment among the three powders will be equal if the two materials are well bonded. Thus, the thermal bonding method, the current industrial bonding approach, was invented in 1993 by Richart and coauthors [14]. This method starts with heating the two components in a tank by high-speed stirring with or without the assistance of a water or oil heating jacket. When the temperature reaches or slightly ex-

ceeds the glass transition point (T_g) of coating particle, its surface will become soft and sticky, allowing metallic pigment to adhere [15, 16]. Continuing to heat at this temperature for 2-3 minutes, then following up with a rapid cooling down of the mixture will allow the bonded metallic effect powder coating to be obtained after screening. However, the thermal bonding

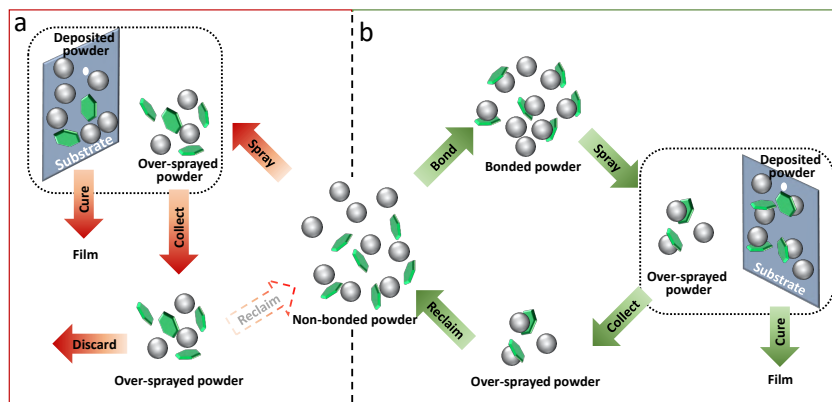


Figure 5.1: The behaviors of metallic pigment of non-bonded (a) and bonded (b) powders during the electrostatic spraying. The green flakes and gray spheres stand for metallic pigments and coating particles, respectively.

method has several intrinsic drawbacks [17, 18]. First, pre-curing tends to happen when the temperature is higher than the T_g . Second, flaky metallic pigments have to face the high risk of bending and damage under high-speed stirring. Third, it is not easy to reach a high bonding temperature, such as 110°C , due to the involved heating mode(s). Finally and most importantly, the thermal-bonded product does not completely meet the requirements of high-end products, such as cell phones, laptops, and automobile body coats, because the bonding quality is not good enough especially when the content of metallic pigment is high. Therefore, an improved bonding method that overcomes the drawbacks mentioned above is highly demanded by manufacturers and engineers.

In recent years, many studies have been conducted to improve the bonding quality. Gunde et al. reported that tuning the bonding time and temperature helps to improve the bonding quality when using a thermal bonding machine [17]. Based on the present bonding method, some researchers have proved that the surface modification of metallic pigment by adhesive materials is also a practical approach, such as acrylic acid [19], polyethylene wax [20], C6-C8 fatty acids [21]. Simultaneously, these modifiers increase the cost of metallic pigment and might affect its metal effect. It is reported that the solutions of polyacrylic acid and polyvinyl alcohol

are able to bond metallic pigment and coating particles at room temperature [22]. However, this method is also restricted in many aspects, for instance, industrialization. Recently, Mistry and coauthors employed a variable frequency microwave oven, which used radio radiation in C-bands (5.8 to 7GHz) and X-bands (7.3 to 8.7GHz), to bind metallic pigments and coating particles [18]. Unfortunately, these frequencies tend to cause radio frequency interference (RFI) according to the 5.138, 5.150, and 5.280 of the Radio Regulation [23]. Therefore, no development and commercialization of this technique has ever been reported, likely due to the high cost of the oven and the RFI of the involved bands. Microwave, serving as a heat source, has a series of advantages over the friction and jacket heating, such as the fact that it is easy to control, safe, clean, efficient, and pollution-free [24, 25, 26]. Also, Metaxas and Meredith pointed out that the interface between the nonmetal and metal particles could have a stronger microwave absorption than other areas due to the selective heating of the microwave [27]. This theory suggests that the contact area between the coating particle (nonmetal) and metallic pigment (metal) particle is expected to obtain a higher temperature, which will be highly beneficial to the reduction of mis-bonding and the improvement of bonding quality. However, the temperatures of coating particles and metal flakes during the traditional bonding process are theoretically the same, which correspondingly increases mis-bonding and pre-curing risks.

In the present work, a fixed center frequency microwave band (2.45GHz) and a drum with two-direction rotations were adopted to bond metallic pigments and coating particles. The fixed band completely avoids the RFI and vastly reduces cost, and the motion of rotations provide the loaded particles with good fluidization and uniform microwave absorption. Our previous results have shown that the microwave bonding method is capable of bonding a clear powder coating (pure organics, without fillers or pigments) and Al flake [28]. However, mostly powder coatings applied in the paint industry contain inorganic filler (barium sulfate, calcium carbonate, etc.) and pigments (titanium dioxide, carbon black, organic pigments, etc.). The inclusion of a large amount of inorganic material in the coating system may impact the bonding effect. Therefore, in this work, to meet the demand of the market and study the effect of filler and pigments, microwave bonding was expanded to bind another three common powder coatings, epoxy-polyester hybrid (indoor paint with normal Tg), polyester (outdoor paint with normal Tg), and PVDF (weather-durable paint with high Tg) powder coatings.

5.3 Materials and methods

5.3.1 Materials and equipment

Hybrid powder coating (white, HS-0460-S) from Prism Powder Coatings Ltd. (ON, Canada), Polyester powder coating (avalanche white, PT922-9003) from Liffey Customer Coatings Inc. (ON, Canada), and PVDF powder coating (grey, PF019051) from Huajiang Powder Coating Co. (Guangdong, China) worked as base powder coatings. Aluminum flakes (PCR 501, $D_{50}=19\mu\text{m}$, with a SiO_2 treated surface) from ECKART America Corporation (KY, USA) were used as metallic pigments. Al panels (A-2-3.5) from Q-Lab Co. (Westlake, OH, USA) were utilized as substrates. Sodium hydroxide from Fisher scientific Co. (Massachusetts, USA) served as a reacting agent for gas-volumetric analysis.

An electrostatic powder coating system (Surecoat manual, corona spray gun system) from Nordson Co., Ltd. (OH, USA) was used to spray powders. A Scanning Electron Microscope (SEM) (SU3500) with an energy dispersive spectrometer (EDS) from Hitachi Limited (Tokyo, Japan) was employed to observe the bonding situation between Al flake and coating particle. The final surfaces were characterized by an optical microscope (Keyence VHX-6000) from Keyence Corporation of America (Itasca, USA).

5.3.2 Microwave bonding device

Fig. 5.2 presents a diagram (a) and a side view (b) of the self-designed microwave bonding device, 60cm in length, 45cm in width, and 40cm in height. 1) One microwave transmitter works as the heat source and the frequency and power rating is $2.45\text{GHz}\pm 50\text{Hz}$ and 700W, respectively. 2,7) Two variable-speed motors separately provide motive power for the vertical and horizontal rotations of the drum. Their shafts are on the same line that is vertical to the horizontal plane, allowing the drum to rotate at the vertical and horizontal directions at the same time. 3) A drive belt is for the transmission of the vertical rotation. 4) Three baffles are evenly distributed on the inner chambered surface of the drum to help the loaded powder have more uniform movements. 5) A thermocouple is installed to monitor the temperature of loaded materials. 6) A drum made by Polymethyl methacrylate (PMMA) serves as the container of powders. 8) A door is used for sample discharging. This microwave bonding device has a

processing capacity of about 50g at a time.

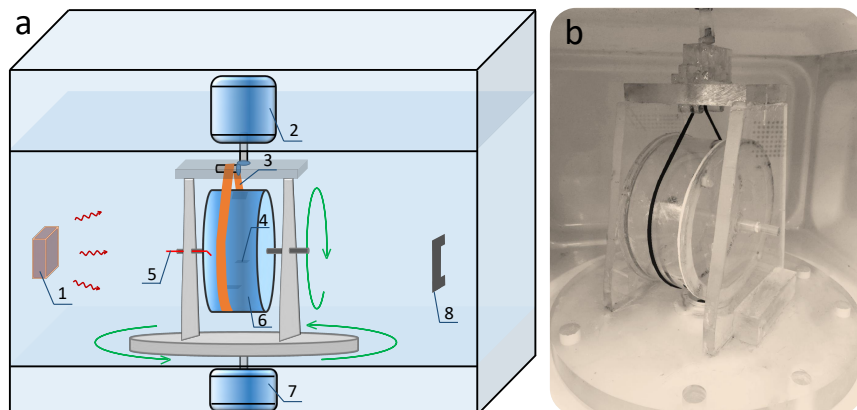


Figure 5.2: The diagram of the microwave bonding device (a) and the picture of the drum (b). 1) Microwave transmitter; 2) Motor for vertical rotation; 3) Drive belt; 4) Baffles; 5) Thermocouple; 6) Drum; 7) Motor for horizontal rotation; 8) Door.

5.3.3 Preparation of samples

The non-bonded powders were prepared by dry blending the Al flakes and the three types of powder coatings, respectively. The following steps fabricated the microwave-bonded powder samples: a) loading the above non-bonded powder (50g) into the drum; b) turning on the two motors and heating the loaded powder through the microwave with various powers (50%, 70%, and 100%) to different bonding temperatures (48-105°C). Based on our previous results [28], the vertical and horizontal rotations were set to 45rpm and 3rpm; c) turning off the microwave transmitter while maintaining the rotating for cooling the loaded powder down; d) collecting the bonded mixture from the drum and then sieving it by a 120 mesh screen. The microwave bonding process was optimized by microwave power and bonding temperatures.

The deposited powder was obtained by the following steps: a) spraying the above non-bonded or bonded powders onto one side of a substrate at a specific spray voltage; b) directly scraping off the deposited powder to a weighing paper. Each powder was sprayed at three voltages, 30, 60, and 90kV, to test its color stability, and these steps were repeated two more times to secure the accuracy of measurement data. The spray current and distance respectively remain unchanged at 30μA and 20cm. The final film was prepared via the following steps: a) spraying a powder to a substrate at a certain spray voltage; b) heating the deposited powder and the substrate in an oven at 180°C for 15 minutes; c) cooling them down to room temperature in

the open air. All of the specimens observed by the optical microscope were cut from the final films that sprayed at 90kV.

5.3.4 Characterization of powders

The bonding quality of powders was characterized by analyzing the Al flake content of powders. As stated in Introduction, the closer the Al content of deposited powder (shortly named “deposited Al content”) to the original Al addition, the better the bonding quality. However, a quantitative analytical method for analyzing the content of the metallic pigment in the field of powder paint has not been established so far. In the present study, since Al flakes were used as metallic pigments, the gas-volumetric method was performed to analyze the Al content accurately [29]. This analysis is dependent on the following chemical reaction:



The Al content of a powdered sample could be deduced from Eq. 5.1:

$$\omega = \frac{2 V_{H_2} M_{Al}}{3 V_m M_{sample}} \times 100\% \quad (5.2)$$

where ω is the Al content; V_{H_2} is the volume of hydrogen; M_{Al} is the relative atomic mass of aluminum; V_m is the molar volume of hydrogen at 25°C and 1atm; M_{sample} is the total mass of the powdered sample.

The deposited Al content was labeled as ω_{dep} and the original Al addition was written as ω_{ori} . Of course, the best bonding quality exists when the two contents are equal. The following equation defined the relative difference of Al content (shortly named “relative difference”, $\Delta\omega$) for a direct understanding:

$$\Delta\omega = \frac{\omega_{dep} - \omega_{ori}}{\omega_{ori}} \times 100\% \quad (5.3)$$

When the $\Delta\omega$ is closer to 0, the sample has a better bonding quality. In detail, $\Delta\omega < 0$ means that the final film has a lower metal effect than it should be. $\Delta\omega = 0$ indicates that the powder has the best bonding quality and the final film will have no color deviation. $\Delta\omega > 0$ hints that the final film has an enhanced metal shine, but the over-sprayed powder has less Al flakes and

probably results in an unacceptable color deviation.

In addition, the chemical composition of three non-bonded and three optimal bonded powders were characterized by X fourier transform infrared spectroscopy (Perkim-Elmer TGA-FTIR coupled system, MA, USA). These six powder samples were also gold-sputtered for 1.5min followed by SEM characterization. The three optimal microwave-bonded samples were also analyzed by EDS under the modes of site and map scanning.

5.3.5 Characterization of films

The non-bonded and optimal bonded films were observed by an optical microscope for analyzing the distribution of Al flakes. The top view of a film is able to reveal the intensity of the metal effect directly. The cross-sectional view of a film could tell the approximate number of Al flakes inside the film. The hardness of the non-bonded and bonded films was measured by a 501 pencil hardness tester (Elcometer Inc., MI, USA) on a 6B to 6H scale based on ASTM D3363. The lowest hardness value of the pencil, which marks the coating, determines the hardness grade. The adhesion of the films was evaluated by an Elcometer 107 cross hatch cutter (Elcometer Inc., MI, USA) on the basis of ASTM D3359. According to the percent of removed area after cross cutting, adhesion is assessed through the following five grades: 0B (>65%), 1B (35-65%), 2B (35-65%), 3B (35-65%), 4B (<5%), and 5B (0%). The reverse impact of the non-bonded and optimal microwave-bonded films were determined by an Elcometer 1615 variable impact tester (Elcometer Inc., MI, USA) based on ASTM D2794-19.

5.4 Results and discussion

5.4.1 Epoxy-polyester hybrid powder coating system

At first, the influence of bonding temperature and microwave power on the bonding quality of hybrid powder coating was studied. A common addition of Al flake, 2.03 ± 0.03 wt%, was investigated considering that the addition is usually below 2.5 wt% in industry. Table 1 summarizes the deposited Al contents of the non-bonded and microwave-bonded samples that were prepared at different bonding temperatures (48 and 50°C) and microwave powers (700W \times 50%, 70%, and 100%). It is found that the deposited Al content decreases with the increase of spray voltage. The deposited Al content of the non-bonded sample ranges from 1.53% to

80 5. LAB-SCALE STUDY ON MICROWAVE BONDING METHOD FOR POWDER COATINGS

2.66% when the spray voltage decreases from 90 to 30kV, denoting a noticeable metal shine change and poor color stability.

Table 5.1: The deposited Al contents (wt%) of hybrid powders obtained at different bonding temperatures and microwave powers.

	Non-bonded	48°C-50%	48°C-70%	48°C-100%	50°C-50%	50°C-70%	50°C-100%
30kV	2.66±0.07	2.69±0.08	2.64±0.02	2.60±0.05	2.27±0.06	2.26±0.01	2.46±0.04
60kV	2.18±0.03	2.51±0.00	2.31±0.01	2.21±0.03	2.21±0.01	2.07±0.05	2.12±0.00
90kV	1.53±0.02	1.67±0.03	1.68±0.08	1.71±0.02	1.71±0.05	1.72±0.03	1.80±0.02

This decline is mainly caused by a difference in charge capacity between Al flake and coating particle. According to the following equation [30]:

$$Q_{max} = 4 \pi r^2 \epsilon_0 E \frac{3\epsilon_r}{\epsilon_r + 2} \quad (5.4)$$

where Q_{max} is the maximum charge accumulated by a particle passing through an electric field; r is the equivalent spherical radius; ϵ_0 is the permittivity of vacuum; E is the electric field strength; ϵ_r is the relative dielectric constant. The dielectric constant of Al flake (covered by a thin layer of alumina) is around $7 F/m$ [31, 32], which is higher than that of the coating particle ($\sim 1.6 F/m$) [33, 34]. The equivalent spherical radius of Al flake and coating particle are $\sim 7\mu m$ and $\sim 40\mu m$, respectively. Calculating with Eq. 5.4, the maximum charge of coating particle is almost twenty times over that of Al flakes. Al flakes almost reach the maximum charge even at a low spray voltage of 30kV, while coating particles capture more electrons and/or ions when the voltage increases. Hence, the deposited content of coating particles will increase with the increase of spray voltage.

The relative differences were plotted for a clearer sense of bonding quality, shown in Fig. 5.3. As previously mentioned, the closer the relative difference to zero, the better the bonding quality. Mistry and coauthors determined the bonding quality by the gloss 20° and 60° and found that the lower the gloss, the better the bonding quality. However, the relationship between gloss and bonding quality is indirect and qualitative [18], so relative difference was performed to reveal the bonding quality. It is evident that bonding quality at $50^\circ C$ is higher than that at $48^\circ C$ when comparing at the same microwave power. This is mainly because the surfaces of coating particles are not soft or sticky enough at $48^\circ C$ to adhere to Al flakes. Exper-

imental results also show that even higher temperatures, such as 52°C, leads to small chunks, which will cause material waste. When bonding at the same temperature, a higher power tends to help obtain a better bonding quality. The probable reason for this is that high power results in a higher heating rate and stronger selective-heating effect. Considering that the most used spray voltage range in the industry is 55kV to 90kV and the relative differences of 60kV and 90 at 50°C-100% separately are 4.6% and -15%, 50°C-100% is considered as the best condition in the present work.

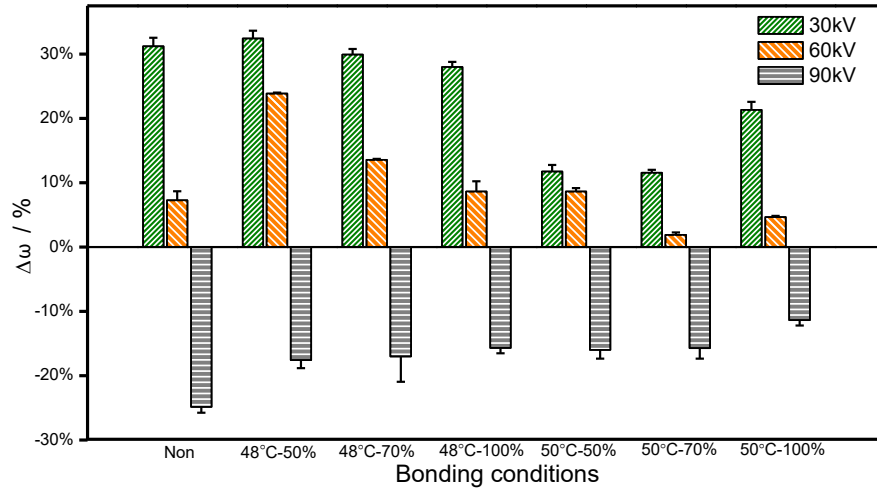


Figure 5.3: The $\Delta\omega$ of hybrid samples at various bonding temperatures and microwave powers.

Another interesting finding is that the bonding temperature (50°C) is lower than the T_g (52°C) of the hybrid coating particle, which is considered to be a result of the microwave heating selectivity, as stated in Introduction. Microwave power absorbed by materials per unit volume is given as follows [35]:

$$P = 2\pi f \epsilon_0 E^2 \epsilon_{eff}'' \quad (5.5)$$

where, P is the microwave absorbing power per unit volume (W/m^3); f is the frequency of microwave (Hz); E is the electric field intensity (V/m); ϵ_0 is the permittivity of vacuum; ϵ_{eff}'' is the effective dissipation factor of material. In our work, f and E stay consistent, so a higher ϵ_{eff}'' means a higher microwave absorption and temperature.

In the present study, metallic effect powder coatings are just composed of nonmetal (coating particles) and metal (Al flakes). According to Wagner's study [36], the primary microwave absorption of metallic effect powder coating is due to two distinct mechanisms: 1) dipolar

polarization of coating particles; 2) interface polarization (Maxwell-Wagner polarization) between coating particle and Al flake. It is worth noting that the interface polarization takes responsibility for the microwave heating selectivity instead of dipolar polarization. To determine which mechanism dominates, theoretical calculations and two comparative experiments were both carried out.

First, the hybrid coating particles (without Al flakes) were heated alone by the microwave bonding device. The major microwave absorption is the dipolar polarization in this trial, and the corresponding effective dissipation factor ($\epsilon''_{dipolar}$) can be calculated by the following equation [37]:

$$\epsilon''_{dipolar} = \epsilon' \tan\delta \quad (5.6)$$

where ϵ' is the real part of dielectric constant of material; $\tan\delta$ is the loss tangent of material. The calculated $\epsilon''_{dipolar}$ is about 0.016 in the use of the data from some published studies [38, 39, 40]. It is found that the heating rate of base coating particles is $\sim 2^\circ\text{C}/\text{min}$.

Second, the non-bonded powder, containing hybrid coating particles and Al flakes, was heated by the same device. Wagner suggested that for the simplest model featuring this type of polarization, consisting of conductive spheres distributed throughout a non-conductive medium, the effective dissipation factor is given by Eq. 5.7 [41, 27, 36], and Sillars pointed out that the τ in Eq. 5.7 can be estimated through Eq. 5.8 by using a double layer arrangement model [42]:

$$\epsilon''_{MW} = \frac{9\nu\epsilon'_1 f_{max}}{1.8 \times 10^{10} \delta_2} \frac{2\pi f \tau}{1 + (2\pi f \tau)^2} \quad (5.7)$$

$$\tau = \epsilon_0 \frac{\epsilon'_1 + \epsilon'_2}{\delta_1 + \delta_2} \quad (5.8)$$

where, ν is the volume fraction of conductive material; f_{max} in Hz is the frequency of maximum losses; δ is the conductivity in S m^{-1} of the conductive phase; τ is the relaxation time constant; the subscripts 1 and 2 refer to the non-conductive and conductive phase, respectively. Applying parameters from published articles [18, 39, 43], the approximate value of ϵ''_{MW} turned out to be 0.06, which is relatively higher than that of the dipolar polarization. In addition, a much faster heating rate, $\sim 17^\circ\text{C}/\text{min}$, was found when heating the non-bonded powder by the microwave.

In summary, comparing the two effective dissipation factors and heating rates, the interface polarization is trusted to be the dominant absorption mechanism and the heating selectivity of the microwave indeed occurs during the bonding process. The heating rate of a present thermal bonding machine generally ranges from 3 to 6°C/min. Obviously, the rather high heating rate of microwave bonding significantly improves bonding efficiency and reduces energy consumption. Above all, microwave bonding is a considerably time-saving and effective method for bonding metallic effect powder coating.

The crosslinking reaction (pre-curing) of resinous components often occurs during the traditional bonding process due to the high heating temperature [44]. In this work, FTIR spectra of non-bonded and microwave-bonded samples were analyzed to judge whether the pre-curing occurred during the microwave bonding, as shown in Fig 5.4. The profiles of the two spectra are almost the same, which proves that the microwave bonding process does not cause pre-curing. Meanwhile, the stretching of C–O and C–O–C of oxirane group are separately found at 934 and 824 cm^{-1} . The stretching of C=O and sutured C–H groups are observed at 1718 and 2969 cm^{-1} , respectively. The stretching of C–N is seen at 1224 cm^{-1} . In conclusion, the FTIR analysis shows no pre-curing in the microwave-bonded hybrid sample.

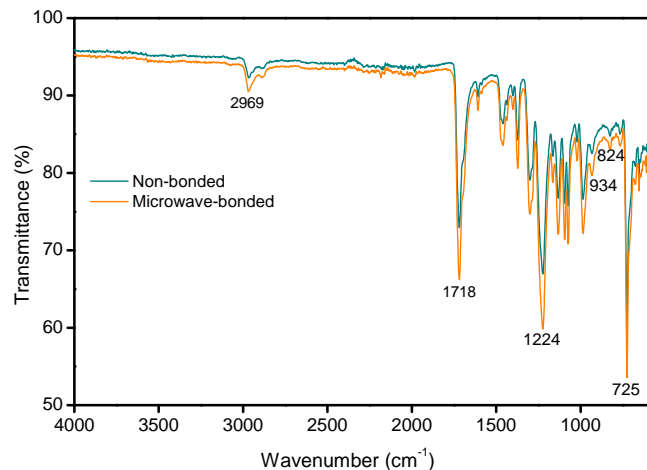


Figure 5.4: FTIR spectra of non-bonded and microwave-bonded hybrid powder samples.

The non-bonded and microwave-bonded (prepared at 50°C-100%) samples were further characterized by SEM and EDS, as presented in Fig. 5.5. For the non-bonded sample, there are several Al flakes with clean and smooth surfaces in Fig. 5.5a and the zoomed-in image

84 5. LAB-SCALE STUDY ON MICROWAVE BONDING METHOD FOR POWDER COATINGS

(Fig. 5.5b) shows an Al flake stands straight with clean sides, indicating there are no binds between coating particles and Al flakes. However, some bonded particles are found in these areas in circles in Fig. 5.5c after microwave bonding. The magnified image (Fig. 5.5d) exhibits that three flakes stick on the top, side, and back of a coating particle. These bonded particles are similar to the results of Gunde and coauthors' work, but they found stacked Al flakes while we did not [17]. The green and blue spots in Fig. 5.5 (the EDS scanning result of Fig. 5.5d) represent aluminum and titanium, respectively. The element of titanium, resulting from the titania that works as white pigments, is employed to represent the place of coating particle. It is clear that these bonds are formed between a coating particle and three Al flakes. The EDS spectroscopy of the white point in Fig. 5.5d also verifies the flake is mainly composed of aluminum.

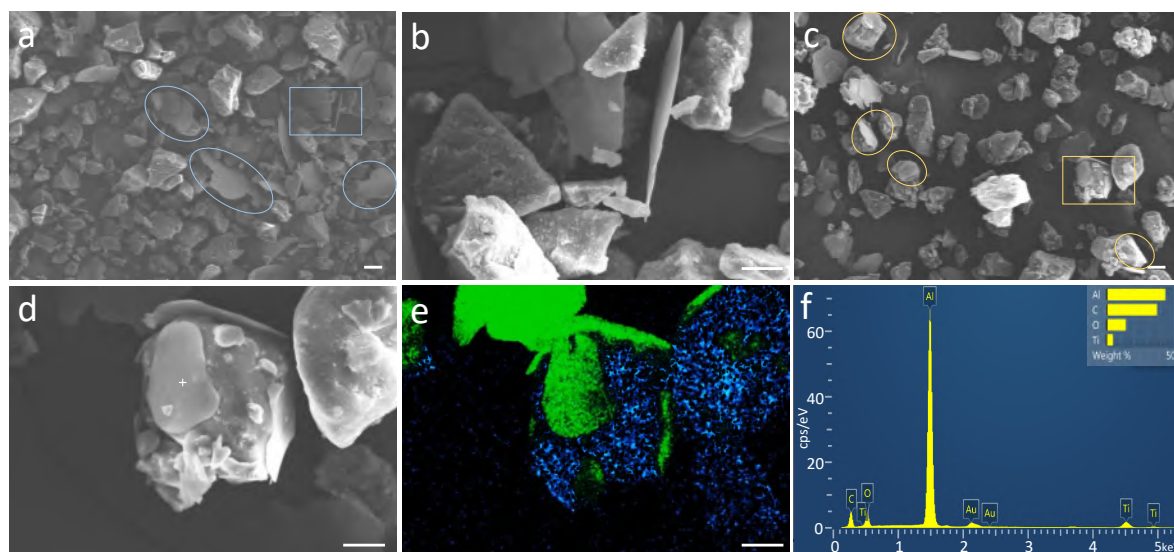


Figure 5.5: The SEM and EDS images of non-bonded and microwave-bonded hybrid samples. **a,b**) Non-bonded sample; **c,d**) bonded sample; **e**) EDS scanning of **d**, the green and blue spots represent aluminum and titanium, respectively; **f**) EDS spectroscopy of the white point in **d**. All the scale bars are 10 μ m.

The optical images of the final films, which prepared from the non-bonded and microwave-bonded (50°C-100%) powders (simply named as “non-bonded film” and “microwave-bonded film”), were gained to reveal the distribution of Al flakes in the top surface and coating, as viewed in Fig. 5.6. The white areas in these images are Al flakes that reflect lights under optical observation. Image J (a software) was utilized to analyze “Al area”, defined as the percentage

of the white area to the observed area. The Al areas of the non-bonded and microwave-bonded films are 9.82% and 11.01%, entailing that microwave-bonded film does have a stronger metal shine compared to the non-bonded one when sprayed at 90kV. This conclusion is in line with the result of the deposited Al contents as given in Table 5.1. The cross-sections imply that the approximate numbers, per square millimeter, of Al flakes of the two films separately are 301 and 323, which also matches well with Al area results. These comparisons demonstrate that microwave bonding obtains a more substantial metal shine over the non-bonding at 90kV.

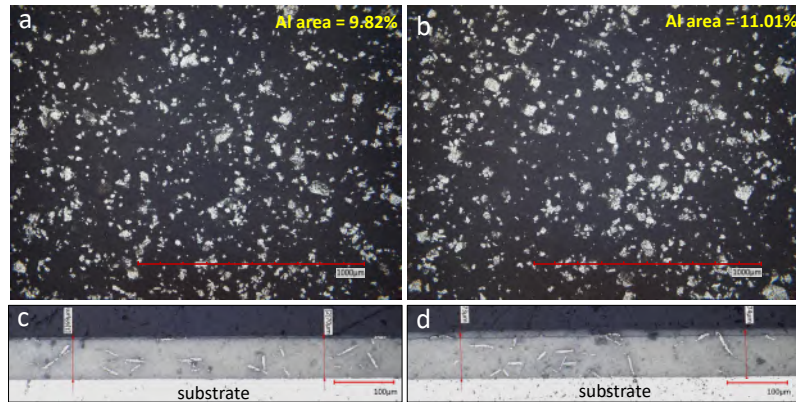


Figure 5.6: The optical images of top surfaces (**a**, **b**) and cross-sections (**c**, **d**) of the non-bonded and microwave-bonded films.

To examine the applicability of the microwave bonding method, two more Al additions were tested. First, hybrid powder coating with a rather low (0.31 ± 0.02 wt%) Al addition was bonded at 50°C -100% and sprayed at the three voltages. Table 5.2 presents that deposited Al contents (ω_{dep}) and relative difference ($\Delta\omega$) between non-bonded and microwave-bonded samples have a reasonably small difference at the same voltage, meaning that microwave bonding has very limited color stability enhancement. Clearly, the relatively low Al addition is expected to lead to a small color deviation even without bonding, so a slight improvement is also significant and reasonable.

Second, an extremely high Al addition (6.2 ± 0.08 wt%) was tested and analyzed. Table 5.3 shows the range of the deposited Al contents is 5.54~9.02% when there is no bonding, while this range shrinks to 5.70~7.24% after microwave bonding. Also, the comparison of the relative differences proves that microwave bonding gets better color stability when sprayed at the same voltage, in particular at 30kV. In addition, compared to the samples with low Al content

Table 5.2: The original (ω_{ori} / wt%) and deposited (ω_{dep} / wt%) Al contents as well as the relative difference ($\Delta\omega$ / %) of hybrid powders with low Al addition.

	ω_{ori}	ω_{dep} -Non	ω_{dep} -Bonded	$\Delta\omega$ -Non	$\Delta\omega$ -Bonded
30kV		0.41±0.02	0.40±0.02	30.5±1.3	27.9±0.6
60kV	0.31±0.02	0.40±0.01	0.36±0.02	26.8±1.1	17.1±0.7
90kV		0.28±0.00	0.29±0.01	-11.5±0.9	-9.1±1.1

(~17°C/min), an even higher heating rate, ~23°C/min, was found when heating the powder with 6.28% Al flake, which could be explained by Eq. 5.5 and 5.7. A higher volume fraction of Al flake (v) leads to a greater ϵ''_{MW} as well as a larger microwave absorption (P). Therefore, the loaded materials absorb more energy per unit of time and gain a higher heating rate. According to the above comparisons, it can be deduced that a higher Al addition is helpful to reduce the processing time of bonding. Conversely, when the Al addition is high, the processing time of thermal bonding might be a bit extended to secure a high bonding quality. Above all, microwave bonding has shown its ability to effectively bind metallic effect powder coating with an extensive range of Al additions.

Table 5.3: The original (ω_{ori} / wt%) and deposited (ω_{dep} / wt%) Al content as well as the relative difference ($\Delta\omega$ / %) of hybrid powders with high Al addition.

	ω_{ori}	ω_{dep} -Non	ω_{dep} -Bonded	$\Delta\omega$ -Non	$\Delta\omega$ -Bonded
30kV		9.02±0.15	7.24±0.11	43.5±2.1	15.3±1.5
60kV	6.28±0.08	7.17±0.20	6.81±0.14	14.1±2.3	8.5±0.9
90kV		5.54±0.11	5.70±0.13	-11.8±0.7	-9.2±0.6

5.4.2 Polyester powder coating system

It has been proved that microwave energy bonds Al flakes with hybrid powder coating well. To expand its generality and adaptability, a polyester powder coating was also tested by the microwave bonding method. The original Al content of this non-bonded sample turned out to be 1.97±0.06 wt% via three paralleled gas-volumetric tests. At first, the deposited Al contents of polyester powders prepared at different bonding temperatures were analyzed as shown in Table 5.4. The non-bonded sample has the biggest range (1.50~3.10%), meaning poor metallic color stability. However, the range becomes narrower while the bonding temperature increases,

indicating that microwave bonding greatly improves color stability.

Table 5.4: The deposited Al contents (ω_{dep} / wt%) of polyester powders prepared at different temperatures.

	Non	62°C	65°C	68°C
30kV	3.10±0.11	3.21±0.08	3.10±0.07	2.70±0.06
60kV	3.07±0.12	2.99±0.13	2.89±0.04	2.58±0.03
90kV	1.50±0.06	1.69±0.04	1.82±0.08	1.86±0.04

Fig. 5.7 shows a decline of the relative difference at 30 and 60kV with the increase of bonding temperature. The lowest relative differences at 30 and 60kV in the tested range separately are 37% and 31%, which respectively reduce by 20% and 25% compared to that of the non-bonded sample. When spraying at 90kV, the relative difference apparently shrinks from -24% to -5% with the increase of bonding temperature. In addition, similar to the Hybrid section, the bonding temperature is lower than the Tg (72°C) of the polyester powder coating and the heating rate is as high as ~16°C/min. These results suggest that microwave bonding is also able to efficiently provide high bonding quality and stable metal shine with the polyester powder coating.

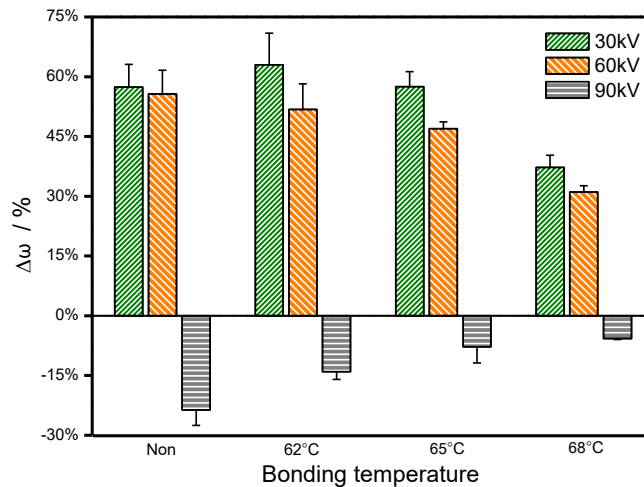


Figure 5.7: The $\Delta\omega$ of polyester samples at various bonding temperatures.

The FTIR results of the non-bonded and microwave-bonded (68°C) polyester samples are presented in Fig. 5.8. Their spectra are almost identical, suggesting that there is hardly any pre-curing after the microwave bonding. In addition, several characteristic peaks of polyester

88 5. LAB-SCALE STUDY ON MICROWAVE BONDING METHOD FOR POWDER COATINGS

are observed, such as the stretching frequencies of -OH and C=O at around 3455 and 1717 cm^{-1} separately, the rocking frequency of $\text{-CH}_2\text{-}$ at 1244 cm^{-1} , the stretching frequencies of saturated C-H and C-C at 2969 and 1099 cm^{-1} , respectively.

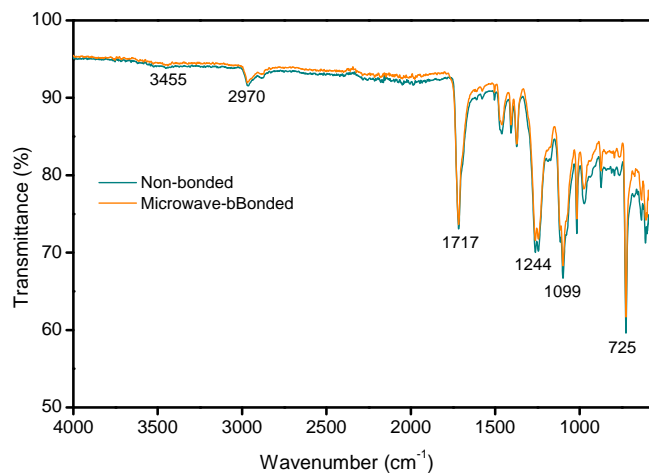


Figure 5.8: FTIR spectra of non-bonded and microwave-bonded polyester powder samples.

Fig. 5.9 displays the SEM and EDS images of the non-bonded and bonded polyester samples (prepared at 68°C). These flakes in Fig. 5.9a and b are believed to separate from the coating particles, like the non-bonded sample in the Hybrid section. Some bonds are viewed in these marked areas in Fig. 5.9c after microwave bonding at 68°C . The zoomed-in image of Fig. 5.9c shows that three flakes adhere to three particles, separately. In addition, EDS results shown in Fig. 5.9e and 5.9f prove that these bonds are well formed between Al flakes and coating particles.

The distribution of Al flakes in the surface and cross-sections (from the sample bonded at 68°C) that sprayed at 90kV are shown in Fig 5.10. The Al areas of non-bonded and bonded films are 9.7% and 11.5% , respectively. The approximate numbers, per millimeter, of Al flakes of the two cross-sections separately are 290 and 359. As stated in Table 5.4, the deposited Al content of the two films respectively are 1.50% and 1.86% . It is clear that the above results match well with each other. In summary, microwave bonding is competent to bind polyester powder coating and Al flakes effectively.

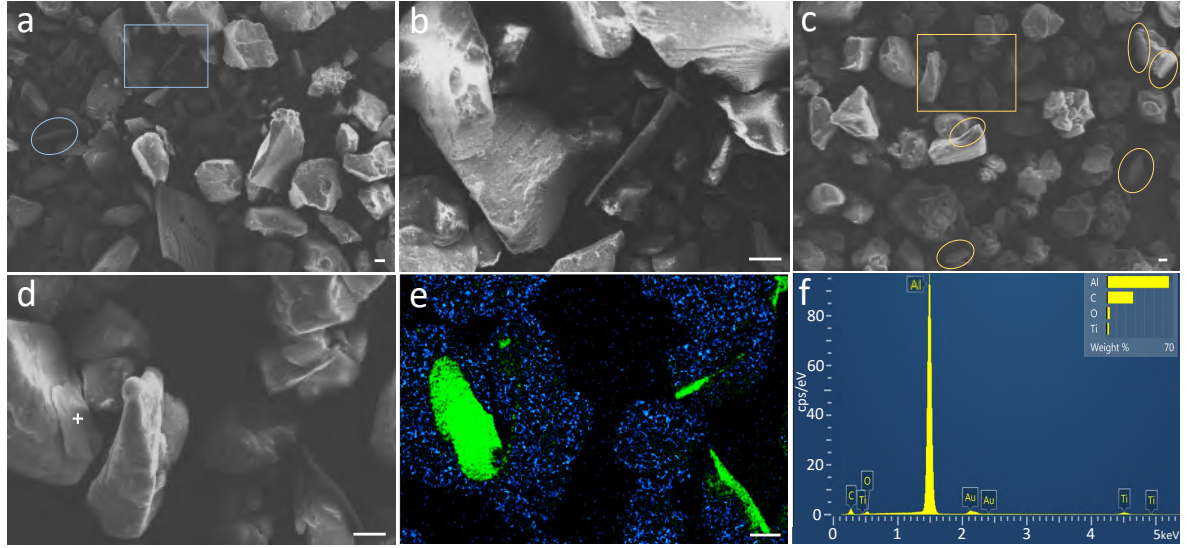


Figure 5.9: The SEM and EDS images of non-bonded and microwave-bonded polyester samples. **a,b)** Non-bonded sample; **c,d)** Bonded sample; **e)** EDS scanning of **d**, the green and blue spots represent aluminum and titanium, respectively; **f)** EDS spectroscopy of the white point in **d**. All the scale bars are 10 μ m.

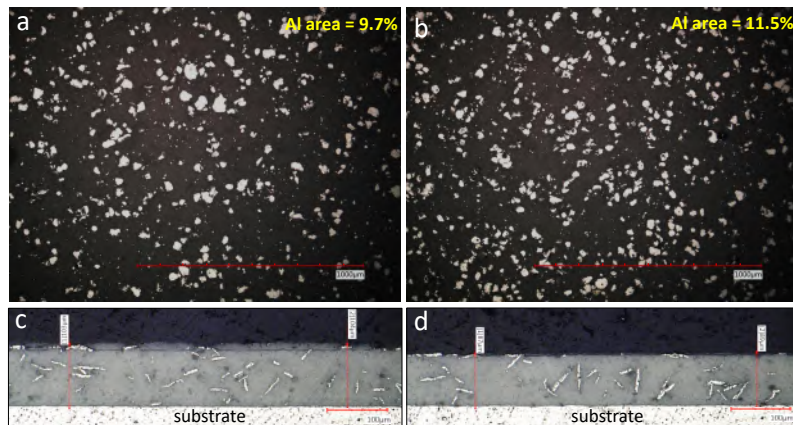


Figure 5.10: The optical images of top surfaces (**a, b**) and cross-sections (**c, d**) of the non-bonded and microwave-bonded polyester films (prepared at 68°C).

5.4.3 PVDF powder coating system

To examine the binding quality of the microwave bonding method at high temperatures, PVDF powder coating was bonded with Al flakes by microwave. It has a fairly high T_g of 114°C and is mostly used as a weather-durable coating. The original Al content is determined to be 1.84 \pm 0.05 wt% by the gas-volumetric method. Similar to the results of polyester, the range of the Al contents shrinks with the increase of bonding temperature, as shown in Ta-

90 5. LAB-SCALE STUDY ON MICROWAVE BONDING METHOD FOR POWDER COATINGS

ble 5.5. The smallest range is 1.78~2.65%, which is much less than that of the non-bonded sample (1.56~3.75%), implying that the microwave-bonded sample has better color stability than the non-bonded one.

Table 5.5: The deposited Al contents (ω_{dep} / wt%) of PVDF powders bonded at different temperatures.

	Non	95°C	100°C	105°C
30kV	3.75±0.13	3.71±0.07	3.10±0.09	2.65±0.05
60kV	2.08±0.06	2.26±0.08	1.90±0.06	2.07±0.06
90kV	1.56±0.01	1.68±0.04	1.73±0.01	1.78±0.04

The analysis of the relative difference illustrated in Fig. 5.11 shows the non-bonded sample has an extremely large value, 104%, at 30kV. The PVDF powder was found to have a low deposited rate of 5% (deposited rate = mass of deposited powder/mass of sprayed powder), meaning it is challenging to capture electrons and (or) ions at this low voltage. Thus, the deposited content of the PVDF coating particles will be much less than its addition. In other words, the deposited Al content will be much more than the Al addition. This possibly is the reason for the dramatically large relative difference at 30kV. However, the relative difference at 30kV goes down to 44% after microwave bonding at 105°C. The lowest relative difference at 90kV, -3.3%, also occurs at 105°C, so this temperature is thought as the best bonding temperature in the tested trials even though the relative difference is a little higher than that of 100°C at 60kV.

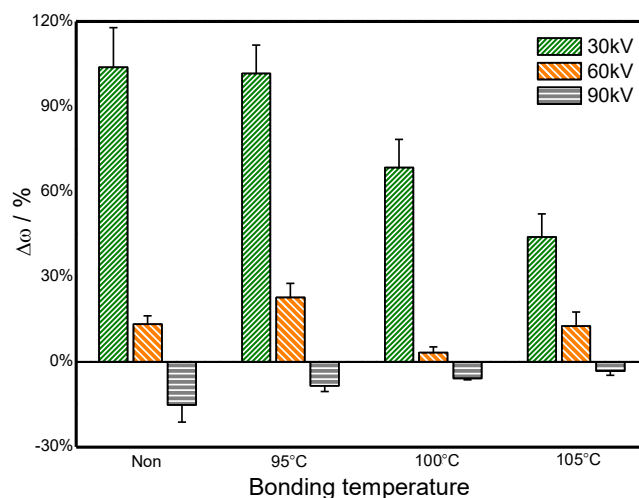


Figure 5.11: The $\Delta\omega$ of polyester samples at various bonding temperatures.

Fig. 5.12 displays the FTIR spectra of the non-bonded and microwave-bonded (105°C) PVDF samples. The almost identical spectra illustrate that the microwave bonding process rarely impacts the composition of PVDF powder. Some characteristic frequencies are found, for example, the deformation bands frequency of $-\text{CH}_2-$ that bonded with $-\text{CF}_2$ at 1401 cm^{-1} , and the stretching frequency of $-\text{CF}_2$ at 1180 cm^{-1} .

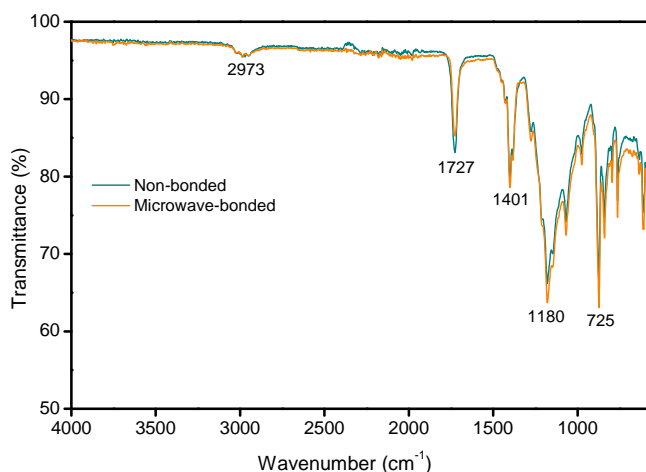


Figure 5.12: FTIR spectra of non-bonded and microwave-bonded PVDF powder samples.

The morphologies of the non-bonded and microwave-bonded PVDF samples are described in Fig. 5.13. These surfaces of the Al flakes in the non-bonded sample (Fig. 5.13a) are clean and smooth, which indicates that there are no binds between them. In addition, the surfaces of PVDF coating particles are shown to be rough and uneven because PVDF is a type of thermoplastic resin that is difficult to be ground. After microwave bonding at 105°C, some bonded particles were observed in Fig. 5.13c (areas in circles). Fig. 5.13d clearly shows one large and one small flake stuck to the top and right side of a coating particle, respectively. Unlike the Hybrid and Polyester counterparts, the fluorine element (the red spots in Fig. 5.13e) was employed to reveal the positions of PVDF coating particles. Both the EDS scanning and spectroscopy provide evidence for the bonding formation between Al flakes and PVDF coating particles.

Fig. 5.14 exhibits the optical images of the top surfaces and cross-sections of non-bonded and bonded (prepared at 105°C and sprayed at 90kV) PVDF films. The Al areas seem to be considerably higher over those of the Hybrid and Polyester sections, mainly because the used

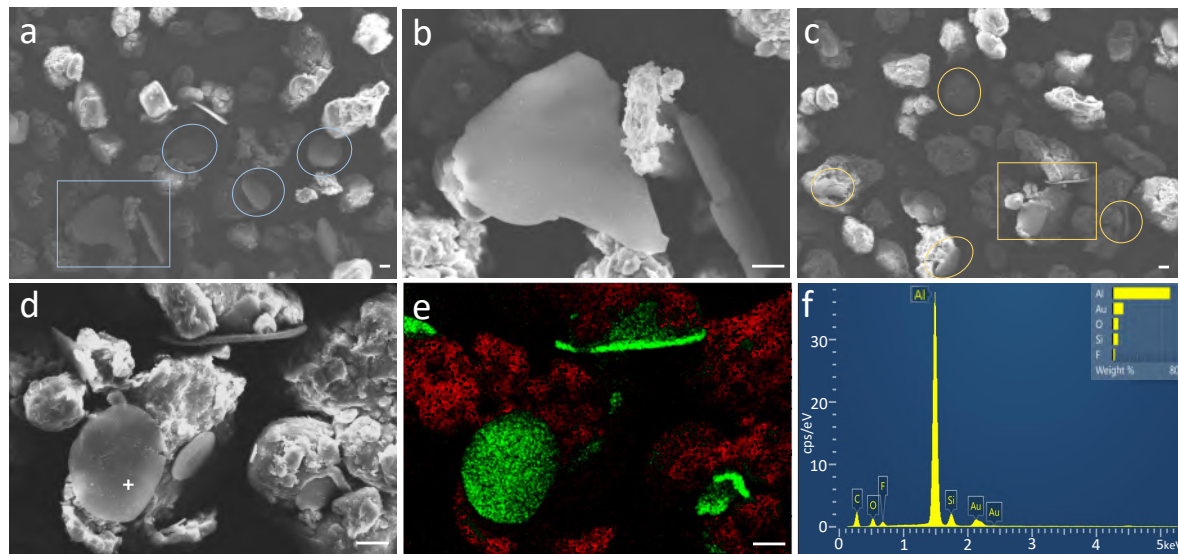


Figure 5.13: The SEM and EDS images of non-bonded and microwave-bonded PVDF samples. **a,b)** Non-bonded sample; **c,d)** bonded sample; **e)** EDS scanning of **d**, the green and blue spots represent aluminum and titanium, respectively; **f)** EDS spectroscopy of the white point in **d**. The scale bars are $10\mu\text{m}$.

PVDF powder coating is a type of half translucent paint that allows the inside Al flakes to reflect lights. After microwave bonding, the Al area increases from 13.4% to 14.4% and the approximate numbers (per millimeter) increase from 312 to 347. As mentioned in Table 5.5, the deposited Al content increases from 1.56% to 1.78% after microwave bonding. Apparently, these increments are consistent with each other. Above all, these optical images prove that microwave bonding is able to improve the stability of metal shine even at an extremely high bonding temperature.

5.4.4 Performance

The hardness, adhesion and impact resistance of non-bonded and bonded films were determined and compared in Table 5.6. The microwave-bonded films have the same hardness and adhesion grades as the non-bonded ones, implying that the microwave bonding process shows very little influence on hardness and adhesion. However, the bonded films appear to have inferior impact resistance. The main reason behind this is that the bonded films have higher contents of Al flakes according to former results (Table 5.1, 5.4 and 5.5). In general, Al flakes contained in films reduce the flexibility of the resinous matrix because they block

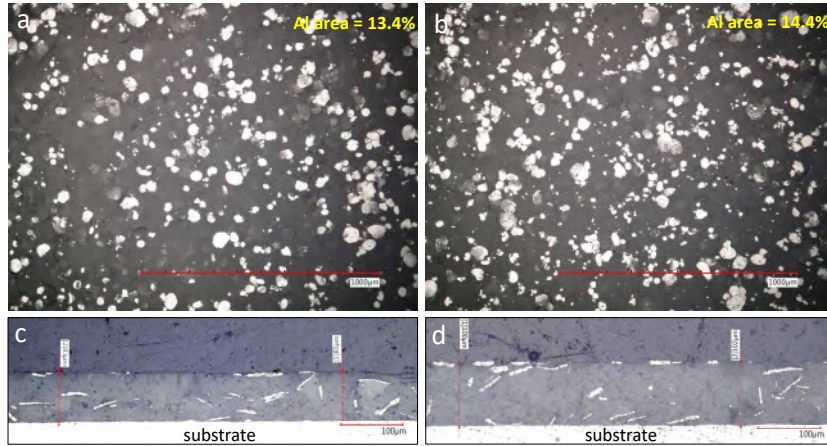


Figure 5.14: The optical images of top surfaces (a, b) and cross-sections (c, d) of the non-bonded and microwave-bonded PVDF films.

the interpenetrating network of the film. The more the Al flakes in films, the lower the impact resistance. Overall, the microwave bonding process does influence the impact resistance but rarely affect hardness and adhesion.

Table 5.6: The performances of hybrid, polyester and PVDF films sprayed at 90kV.

		Hardness	Adhesion	Reverse Impact
Hybrid	Non-bonded	H	5B	411 N·cm
	Bonded	H	5B	392 N·cm
Polyester	Non-bonded	HB	4B	176 N·cm
	Bonded	HB	4B	147 N·cm
PVDF	Non-bonded	F	5B	245 N·cm
	Bonded	F	5B	186 N·cm

5.5 Conclusions

Metallic pigments and three types of powder coatings were effectively bonded by microwave energy via a self-designed bonding device that includes a two-directional rotating drum. The Al content analysis indicates that bonded powders have a significantly smaller change in deposited Al content than the non-bonded ones. The SEM and EDS images show that a large number of bonds are formed between Al flakes and base coating particles. The optical images testify that the bonded films have higher metal shine over the non-bonded ones at the spray voltage of 90kV. To sum up, microwave bonding has the ability to fabricate metallic effect powder coating with highly stable metal shine.

94 5. LAB-SCALE STUDY ON MICROWAVE BONDING METHOD FOR POWDER COATINGS

The heating selectivity of the microwave plays a vital role in the bonding process. Two positive effects were found: 1) The bonding temperature of the microwave bonding method is lower than the T_g of coating particle; 2) The heating rate of microwave bonding is drastically high, from ~16°C/min (low Al addition) to ~23°C/min (high Al addition). All in all, the microwave bonding method has great potential to produce various types of powder coatings with highly stable metal shine.

Bibliography

- [1] Karine Anselme and Maxence Bigerelle. Effect of a gold–palladium coating on the long-term adhesion of human osteoblasts on biocompatible metallic materials. *Surface and Coatings Technology*, 200(22-23):6325–6330, 2006.
- [2] ZB Zheng, YG Zheng, WH Sun, and JQ Wang. Effect of applied potential on passivation and erosion–corrosion of a fe-based amorphous metallic coating under slurry impingement. *Corrosion Science*, 82:115–124, 2014.
- [3] Ali Parsapour, Saied Nouri Khorasani, and Mohammad Hossein Fathi. Effect of surface treatment and metallic coating on corrosion behavior and biocompatibility of surgical 316l stainless steel implant. *Journal of Materials Science & Technology*, 28(2):125–131, 2012.
- [4] S Amookht, S Gorji Kandi, and M Mahdavian. Quantification of perceptual coarseness of metallic coatings containing aluminum flakes using texture analysis and visual assessment methods. *Progress in Organic Coatings*, 137:105375, 2019.
- [5] Gui-Ming Song and Willem G Sloof. Effect of alloying element segregation on the work of adhesion of metallic coating on metallic substrate: Application to zinc coatings on steel substrates. *Surface and Coatings Technology*, 205(19):4632–4639, 2011.
- [6] Yingchao Zhang, Hongqi Ye, Hui Liu, and Kai Han. Preparation and characterisation of aluminium pigments coated with silica for corrosion protection. *Corrosion Science*, 53(5):1694–1699, 2011.
- [7] Hongwei Zhu, Zhenxing Chen, Yong Sheng, and Thu Thuy Luong Thi. Flaky poly-acrylic acid/aluminium composite particles prepared using in-situ polymerization. *Dyes Pigments*, 86(2):155–160, 2010.
- [8] Zhishi Guo, John CS Chang, Leslie E Sparks, and Roy C Fortmann. Estimation of the rate of voc emissions from solvent-based indoor coating materials based on product formulation. *Atmos. Environ.*, 33(8):1205–1215, 1999.
- [9] Mari de Meijer. Review on the durability of exterior wood coatings with reduced voc-content. *Progress in Organic Coatings*, 43(4):217–225, 2001.
- [10] C Klaren. Powder coating composition, October 15 1974. US Patent 3,842,035.
- [11] Memiş Akkus, Turgay Akbulut, and Zeki Candan. Application of electrostatic powder coating on wood composite panels using a cooling method. part 1: Investigation of water intake, abrasion, scratch resistance, and adhesion strength. *BioResources*, 14(4):9557–9574, 2019.
- [12] Jostein Mrdalen, John Erik Lein, Helene Bolm, Merete Hallenstvet, and Volker Rekowski. Time and cost effective methods for testing chemical resistance of aluminium metallic pigmented powder coatings. *Progress in Organic Coatings*, 63(1):49–54, 2008.

96 5. LAB-SCALE STUDY ON MICROWAVE BONDING METHOD FOR POWDER COATINGS

- [13] Qiaoyan Ye and Joachim Domnick. On the simulation of space charge in electrostatic powder coating with a corona spray gun. *Powder Technology*, 135:250–260, 2003.
- [14] Douglas S Richart and Andrew T Daly. Thermosetting resin-based coating powders containing metal flakes, February 16 1993. US Patent 5,187,220.
- [15] Zhangli Huang, Sihai Chen, Yi Chen, Ying Huang, Wen Fu, and Jianjun Lai. Low transition-temperature characteristic in vox films grown on Si₃N₄/glass substrates. *Surface and Coatings Technology*, 207:130–134, 2012.
- [16] E Cañas, V Sanz, MJ Orts, and E Sánchez. Post-deposition heat treatment effect on microstructure of suspension plasma sprayed bioactive glass coatings. *Surface and Coatings Technology*, 371:136–142, 2019.
- [17] Marta Klanjšek Gunde, Matjaž Kunaver, Anton Hrovat, and Uroš Cvelbar. Bonding process efficiency and Al-flake orientation during the curing of powder coatings. *Progress in Organic Coatings*, 54(2):113–119, 2005.
- [18] Jigar K Mistry, Jan Peter Frick, and James Petersen. Microwave bonding for coating compositions, July 6 2017. US Patent 15/463,131.
- [19] Yasushi Takano. Metallic pigment and coating material containing the same, April 3 2008. US Patent App. 11/792,861.
- [20] Guangwen Wu and Demei Yu. Preparation and characterization of a new low infrared-emissivity coating based on modified aluminum. *Progress in Organic Coatings*, 76(1):107–112, 2013.
- [21] Keiichi Endoh, Aiko Nagahara, Yutaka Hisaeda, and Toshihiko Ueyama. Bonding material using metal nanoparticles coated with c6-c8 fatty acids, and bonding method, October 14 2014. US Patent 8,858,700.
- [22] Wei Liu, Jing Fu, Haiping Zhang, Yuanyuan Shao, Hui Zhang, and Jesse Zhu. Cold bonding method for metallic powder coatings. *Materials*, 11(11):2086, 2018.
- [23] Hossam Mahmoud Ahmad Fahmy. Wireless sensor networks essentials. In *Wireless Sensor Networks*, pages 3–39. Springer, 2020.
- [24] Abhishek Babu, HS Arora, Sailesh N Behera, Mukesh Sharma, and HS Grewal. Towards highly durable bimodal composite claddings using microwave processing. *Surface and Coatings Technology*, 349:655–666, 2018.
- [25] Ricardo Marqués, Ferran Martin, and Mario Sorolla. *Metamaterials with negative parameters: theory, design, and microwave applications*, volume 183. John Wiley & Sons, 2011.
- [26] C Pakpum and D Boonyawan. Redeposition-free of silicon etching by CF₄ microwave plasma in a medium vacuum process regime. *Surface and Coatings Technology*, page 126018, 2020.

- [27] AC Metaxas and Roger J Meredith. *Industrial microwave heating*. Number 4. IET, 1983.
- [28] Wei Liu, Haiping Zhang, Yuanyuan Shao, Hui Zhang, and Jesse Zhu. Preparation of aluminium metallic pigmented powder coatings with high color stability using a novel method: Microwave bonding. *Progress in Organic Coatings*, 147:105787, 2020.
- [29] Bing Lei, Man Li, Zhongxing Zhao, Lu Wang, Ying Li, and Fuhui Wang. Corrosion mechanism of an Al–BN abradable seal coating system in chloride solution. *Corrosion Science*, 79:198–205, 2014.
- [30] Daniel Goldwater, Benjamin Stickler, Lukas Martinetz, Tracy E Northup, Klaus Hornberger, and James Millen. Levitated electromechanics: all-electrical cooling of charged nano-and micro-particles. *Quantum Sci. Technol.*, 4, 2019.
- [31] Zhi-Min Dang, Tao Zhou, Sheng-Hong Yao, Jin-Kai Yuan, Jun-Wei Zha, Hong-Tao Song, Jian-Ying Li, Qiang Chen, Wan-Tai Yang, and Jinbo Bai. Advanced calcium copper titanate/polyimide functional hybrid films with high dielectric permittivity. *Adv. Mater.*, 21(20):2077–2082, 2009.
- [32] EMS Sanchez, CAC Zavaglia, and MI Felisberti. Unsaturated polyester resins: influence of the styrene concentration on the miscibility and mechanical properties. *Polymer*, 41(2):765–769, 2000.
- [33] DJ Suh, Ook Park, and KH Yoon. The properties of unsaturated polyester based on the glycolized poly (ethylene terephthalate) with various glycol compositions. *Polymer*, 41(2):461–466, 2000.
- [34] James D Christie and William C Howard. Bonded metal hydroxide-organic composite polymer films on particulate substrates, June 12 2001. US Patent 6,245,323.
- [35] Tetsuya Hanai. Dielectric theory on the interfacial polarization for two-phase mixtures. *Bull. Inst. Chem. Res., Kyoto University*, 39(6):341–367, 1962.
- [36] K Wagner. Explanation of dielectric polarization processes on the basis of maxwellian concepts. *Arch Electrotech.*, 2:371–87, 1914.
- [37] P Debye. reprinted 1954 in collected papers of peter jw debye interscience, new york. *Ver. Deut. Phys. Gesell*, 15:777, 1913.
- [38] Kwong Siong Kiew, Sinin Hamdan, and Md Rezaur Rahman. Comparative study of dielectric properties of chicken feather/kenaf fiber reinforced unsaturated polyester composites. *BioResources*, 8(2):1591–1603, 2013.
- [39] Hyoung Geun Kim et al. Dielectric cure monitoring for glass/polyester prepreg composites. *Composite Structures*, 57(1-4):91–99, 2002.
- [40] Wei Liu, Haiping Zhang, Yuanyuan Shao, Xinping Zhu, Yufu Wei, Hui Zhang, and Jesse Zhu. Applying microwave energy to fabricate powder coatings with strong and stable metal shine. *Progress in Organic Coatings*, 149:105929, 2020.

98 5. LAB-SCALE STUDY ON MICROWAVE BONDING METHOD FOR POWDER COATINGS

- [41] T Prodromakis and C Papavassiliou. Engineering the maxwell–wagner polarization effect. *Applied Surface Science*, 255(15):6989–6994, 2009.
- [42] RW Sillars. The properties of a dielectric containing semiconducting particles of various shapes. *J. Inst. Electr. Eng.*, 80(484):378–394, 1937.
- [43] Motohiko Yoshizumi. Electroconductive powder and process for production thereof, June 5 1984. US Patent 4,452,830.
- [44] María González González, Juan Carlos Cabanelas, and Juan Baselga. Applications of ftir on epoxy resins-identification, monitoring the curing process, phase separation and water uptake. *Infrared Spectroscopy-Materials Science, Engineering and Technology*, 2:261–284, 2012.

6 Pilot-scale microwave bonding machine based on rotating

6.1 Abstract

Metallic effect powder coating, as a unique methodology for coating powders and metallic pigments, has been drawing more attention and occupying more market share with more stringent environmental pressure on traditional metallic solvent paint. To overcome the shortcomings of the thermal bonding method that aims at bonding the two non-compatible ingredients, a self-designed microwave bonding machine was first developed and tested in the present work. Taking advantage of the heating-selectivity of the microwave, a lower bonding temperature was obtained when compared to the thermal bonding method. Also, through the analysis of bonding rate and color difference, a higher bonding quality and enhanced color stability were found. More bondings between coating particles and Al flakes were clearly observed by SEM and EDS in the microwave-bonded samples. The microwave bonding is proved to be a feasible and efficient method and thus the bonding machine has great potential to replace the present bonding machine.⁵

Keywords: Microwave bonding; Metallic effect powder coating; Metallic pigment; Interface polarization.

⁵With minor editorial changes to fulfill formatting requirements, this chapter is substantially appears as in the “Applying microwave energy to fabricate powder coatings with strong and stable metal shine.” Progress in Organic Coatings 149 (2020):105929, Wei Liu, Haiping Zhang, Yuanyuan Shao, Xiping Zhu, Yufu Wei, Hui Zhang, and Jesse Zhu.

6.2 Introduction

Metallic effect powder coating, as an upgraded product of metallic solvent paint, is not only sparkling and highly protective but much more environmentally-benign and solvent-saving. It has been heavily applied in the fields of domestic appliances, building materials, automobile rims, electronic instrumentation and other industrial products [1, 2]. Metallic effect powder coating is mainly manufactured from two non-compatible materials in the industry. The first is the base powder coating ($D_{50} = 30$ to $45\mu\text{m}$) usually composed of resin, regular pigment, filler, and additives. The second is metallic pigments ($D_{50} = 4$ to $70\mu\text{m}$) such as aluminum or copper flakes with a thickness of 1 to $2\mu\text{m}$ to achieve silver- or gold-color metal shine, respectively[3]. The elimination of solvent is another major advance in the reduction of air pollution. In brief, metallic effect powder coating is capable of providing excellent aesthetic appearance and more durable protection, while generating far less VOCs emission during the film formation.

However, there is a rare application of metallic effect powder coating on high-end products, such as cellphones, automobile bodies, and laptops, because these products require coatings to have extremely high color stability and metal shine that metallic effect powder coating could not completely accomplish up to date [4, 5]. The spray process of metallic effect powder coating always involves a powder recovery system to recycle the over-sprayed powder and an electrostatic spray system to employ charged particles to more efficiently paint a workpiece[6, 7]. A challenge in the spraying process of metallic powder paint is the color change, which mostly results from the poor compatibility of the two ingredients coming from their sharp differences in some physical properties, such as shape, resistance, density, and dielectric constant. During the spraying, the poor compatibility leads to different contents of metallic pigment among the over-sprayed, deposited, and virgin powders (Fig. 6.1A). If this over-sprayed powders are reclaimed for re-spraying, the final films will have significantly different colors owing to distinct contents of metallic pigment. Or worse, discarding these over-sprayed powders will lead to high cost and material waste.

The thermal bonding process, which is mainly employed in present industries, was invented in 1993 to eliminate the non-compatible problem of the two ingredients [8]. The term "thermal" refers to the traditional heating modes, such as friction and jacket heating. The bonded

particles (coating particles + metallic pigments) could have similar physical properties with the coating particles, especially dielectric constant and electric resistance. It is universally known that the similarity of electrical property is the prerequisite of the similarity of electrical behavior[9]. As presented in Fig. 6.1B, the contents of metallic pigment in the over-sprayed, deposited and virgin powders are supposed to be equal when all metallic pigments are well bonded with coating particles. Consequently, the over-sprayed powders retain the consistent color to be successfully re-sprayed. This process starts with heating metallic pigments and coating particles in a chamber with high-speed stirring and/or oil/water-jacket, till the temperature exactly reaches or slightly exceeds the glass transition temperature (T_g) of the coating particles [10, 11, 12]. Then the resinous parts of coating particles become soft and adhesive, which allows coating particles to cohere with metallic pigments, followed by a rapid cooling. Lastly, bonded products are collected from the chamber.

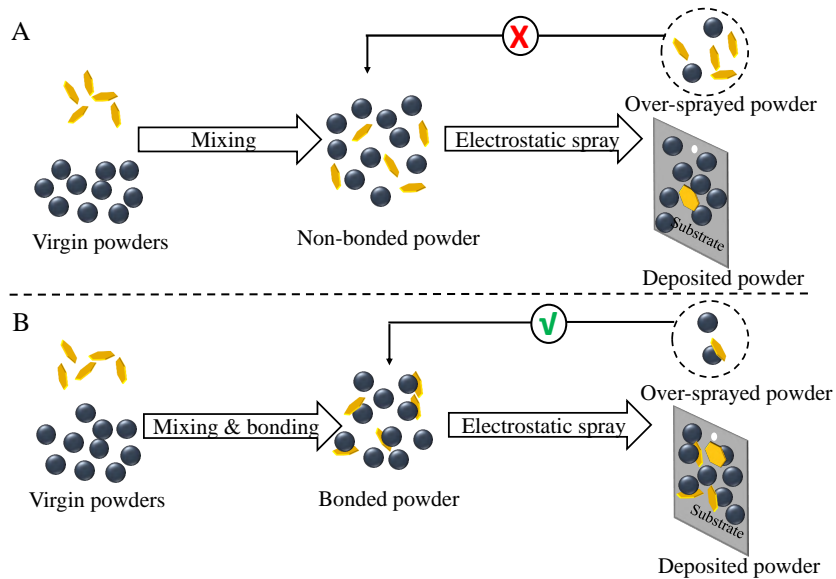


Figure 6.1: The difference of non-bonded and bonded metallic powder paints sprayed by an electrostatic system. The black spheres stand for coating particles; the gold flakes represent metallic pigments. A) Non-bonded powder; B) Effectively bonded powder.

However, there are some inherent issues in the thermal bonding process[13, 14, 15, 16]. The first one is mis-bonding, that a sticky coating particle bonds with another coating particle instead of a metallic pigment. Secondly, the high-speed stirring tends to bend and grind metallic pigments that the resultant films have a reduced metal shine. Thirdly, it is hard to reach high

bonding temperatures such as 120°C owing to its heating modes. The last and most important one is that metallic effect powder coating manufactured by this process is not a product that completely meets the requirement of high-end goods. The color stability with a high addition of metallic pigments, for example, 4 wt%, for a strong metal shine is still unsatisfactory. These issues being present in the thermal bonding process limit the applicable scope of the metallic effect powder coatings. Hence, solving these problems of the thermal bonding approach is highly necessary for manufacturers and engineers nowadays.

There have been some attempts to solve these issues of thermal bonding method by adding some adhesive materials or applying pretreatment on the basis of the thermal bonding, such as surface treatment of aluminum[17], primers[3, 18], and metal nanoparticles[19]. However, these methods have limitations in various aspects, for instance, pollution, cost, and industrialization. Since Percy Spencer found microwave (MW) had heating capacity in 1945[20], this property has been widely utilized over considerable fields, such as cooking, sterilization, drying materials, medical treatments and so on[21, 22, 23, 24]. Mistry and coauthors pointed out that metallic powder paints could be bonded by a variable frequency microwave oven via using radio radiation in C-bands (5.8 to 7GHz) and X-bands (7.3 to 8.7GHz)[16], which are not in the Industrial Scientific Medical (ISM) bands, defined by the International Telecommunications Union-Radio communications (ITU-R), in 5.138, 5.150, and 5.280 of the Radio Regulation [25]. Therefore, this technology has not ever been commercialized because of a huge amount of cost and the inevitable radio frequency interference (RFI). As a heating source, microwave has many advantages, such as clean, efficient, safe, pollution-free, and easy to control. More significantly, Metaxas and Meredith reported that the interface between the metal and non-metallic materials has greater microwave absorption than other areas due to the heating-selectivity of the microwave. [26, 27]. This theory suggests that the interface between metal and nonmetal has a higher temperature than other areas. Metallic effect powder coatings are just made by nonmetal (base coating particle) and metal (metallic pigment), so a higher temperature is expected at the metal-to-nonmetal contact area, which is exactly desired in the bonding process. This should be a great benefit to the reduction of mis-bonding and enhancement of color stability.

In this work, a unique self-designed microwave-heating machine was first invented with

a fixed center frequency of 2.45GHz to greatly reduce the cost and avoid RFI. Moreover, a novel bonding approach was correspondingly established on the dependence of microwave as a heating source instead of current-state-of-the-art such as hot jacket or friction of high-speed stirring. In addition, tumbling motion, instead of high-speed stirring, was utilized to avoid the breaking and bending of metallic pigment. In terms of our previous laboratory experiments, microwave bonding was proved to be a feasible and effective method. Therefore, an advanced microwave bonding machine was designed and constructed for a deeper investigation and industrialization.

6.3 Materials and methods

6.3.1 Materials and equipment

Aluminum flakes (ZPC 330, with stearic acid treated surface) from Zuxing New Material Co., Ltd. (Changsha, China) was used as the metallic pigment; Polyester powder paint (HS136419, Matte grey) from Huajiang Powder Coating Co. (Guangdong, China) served as base powder coating; Al panels (15cm in length, 7.6cm in width) from Q-Lab Co. (OHe, USA) were utilized as substrates; Sodium hydroxide from Xilong Chemical Co., Ltd. (Guangdong, China) worked as a react agent for gas-volumetric analysis.

An electrostatic automatic spraying system with a corona spray gun from Gema Switzerland GmbH (St.Gallen, Switzerland) was applied to spray powders. A thermal bonding machine (SHTBD10) from Sun-hitech Technology Co., Ltd. (Xiamen, China) was used to produce thermal-bonded samples. A laser particle size analyzer (LS-POP6) from Omec Instruments Ltd. (Zhuhai, China) was utilized to analyze the size distributions of powdered samples. A Scanning Electron Microscope (SEM) (SU3500) with energy dispersive spectrometer (EDS) from Hitachi Limited (Tokyo, Japan) was employed to observe the bonding situation between Al flake and coating particle. A colorimeter (CI62) from X-rite Inc. (Michigan, USA) was used to evaluate the color difference of final films.

6.3.2 Microwave bonding machine

The self-designed microwave bonding machine that is 130cm in length, 100cm in width, and 170cm in height is shown in Fig. 6.2. Eight microwave transmitters of $2.45\text{GHz}\pm 50\text{Hz}$ (the

power of each one is 1kW) work as the heating source. The cylinder (38cm in inner diameter; 40cm in inner height) is made of polytetrafluoroethylene (PTFE) working as container for coating powders and aluminum flakes. The rotation of the cylinder was driven by a motor system outside the shell through a shaft. The two components to be bonded could be well mixed by the motion and heated by the microwave.

For safety, a nitrogen atmosphere in the cylinder is required during the bonding process, and a flowmeter was installed to control the flow rate of nitrogen and an oxygen concentration detector was utilized to examine the oxygen volume ratio. There were two temperature sensors in the shaft that could detect the real-time temperature of the loaded materials. Bonding temperature and rotating speed can be monitored and adjusted via the control panel. It is worth to know that the cylinder is made from PTFE that has extremely low microwave-absorption, so the microwave could heat the loaded particles efficiently. In particular, this machine is able to bond about 10kg powder at a time.

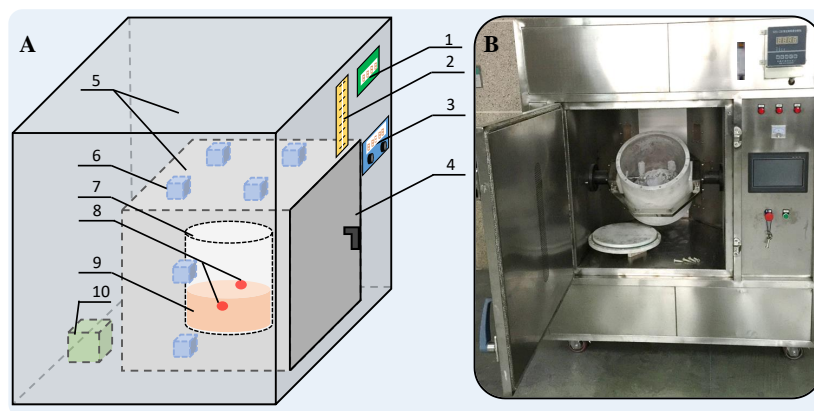


Figure 6.2: The schematic diagram (A) and picture (B) of the microwave bonding machine. 1. Digital display of nitrogen content; 2. Flowmeter of nitrogen; 3. Control panel; 4. Door; 5. Shell; 6. Microwave transmitters; 7. PTFE cylinder; 8. Temperature sensor; 9. Loaded materials; 10. Power system.

6.3.3 Preparation of samples

The non-bonded powders with low and high additions of Al flakes were prepared by mixing 200kg base powder coatings with 4kg and 10kg Al flakes, respectively. The thermal-bonded samples (commercial products) were prepared by Huajiang Powder Coating Co. using the above non-bonded powders and processed by the Sun-hitech (SHTBD10) bonding machine.

The microwave-bonded samples were made from the same non-bonded powders by the

following steps: a) loading the non-bonded powder into the cylinder; b) heating the loaded powder with 8 microwave transmitters at various rotating speeds (30 to 50rpm) till the temperature reaches the set value; c) stopping heating and keeping rotating for cooling the mixture to room temperature; d) the discharged mixture was sieved by a 120 mesh screen.

The samples of deposited powders were collected by two steps: a) separately spraying a powder onto six panels under a spray condition. Here four spray conditions of voltage and air supply, 30/6.5, 60/6.5, 60/5.5, and 90/6.5 (kV)/(m³h⁻¹), were adopted to spray powders (in industry, the spray voltage and air supply are generally in the ranges of 30-90kV and 5.5-6.5(m³h⁻¹), respectively.); b) carefully scraping off the deposited powders from the surfaces of three panels, the other three coated panels were cured into coating films. All powdered samples were treated by gold-sputtering before SEM canning. All the coating films were prepared by heating the deposited powders at 190°C for 10 minutes. All of the specimens for optical observation were cut from the films that sprayed at 60kV/6.5m³h⁻¹. Deposited powders were utilized for bonding quality analysis and the films were performed for color stability characterizations.

6.3.4 Characterizations of powders and films

The morphology and size distribution of coating powders were characterized by SEM and particle size analyzer, respectively. As stated before, the non-compatibility of the two components will cause color change and an effective solution is bonding the two ingredients together. Hence, the bonding quality of powders and color stability of films were studied in this work. The bonding quality is able to be evaluated by the Al contents of virgin and deposited powders. However, a quantitative analytical method has not been established so far to analyze the content of the metallic pigment in powder paint. In this work, aluminum flakes worked as metallic pigments, so the gas-volumetric method was carried out to have an accurate analysis of the content of the metallic pigment[28]. The involved chemical reaction in this analysis is given as:



Taking advantage of Eq. 6.1, the Al content of powdered samples could be deduced as:

$$\omega = \frac{2 V_{H_2} M_{Al}}{3 V_m M_{sample}} \times 100\% \quad (6.2)$$

where ω is the content of aluminum; V_{H_2} is the volume of hydrogen; M_{Al} is the relative atomic mass of aluminum; V_m is the molar volume of hydrogen at 25°C and 1 atm; M_{sample} is the total mass of a powdered sample.

The original Al content of non-bonded powder was labeled as ω_{ori} and the Al content of deposited coating powder was written as ω_{dep} (abbreviated as deposited Al content). Of course, the best bonding quality is when the two contents are equal. For a better understanding, the bonding rate (γ) was defined by the following equation:

$$\gamma = \left| \frac{\omega_{dep\ bond} - \omega_{dep\ non}}{\omega_{ori} - \omega_{dep\ non}} \right| \times 100\% \quad (6.3)$$

where, $\omega_{dep\ bond}$ and $\omega_{dep\ non}$ are the deposited Al contents when spraying bonded and non-bonded powders at the same condition, respectively. Since Al flakes are able to deposit onto the substrate even without bonding, the difference between ω_{ori} and $\omega_{dep\ non}$ stands for the total amount of Al flakes that need to be bonded, and the gap between $\omega_{dep\ bond}$ and $\omega_{dep\ non}$ represents the amount of Al flakes that have been bonded, so the ratio of the two differences could reveal the bonding quality. Based on the definition, it is clear that the higher the bonding rate, the better the binding quality.

The films were observed by an optical microscope to disclose the distribution of Al flakes in the film. Specifically, the final films were also tested by a colorimeter, which was on the basis of CIE-Lab color system [29], to discover the color stability of the paint. Total color difference (ΔE) with respect to the reference was calculated by the equation as follows:

$$\Delta E = \sqrt{(\Delta L^*{}^2 + \Delta a^*{}^2 + \Delta b^*{}^2)} \quad (6.4)$$

where, L^* represents brightness varying from 0.0 for black to 100.0 for a diffuse white; a^* describes the color change from red ($+a^*$) to green ($-a^*$); and b^* implies the color change from yellow ($+b^*$) to blue ($-b^*$). Accordingly, $\Delta L^* = L^*_{reference} - L^*_{sample}$, $\Delta a^* = a^*_{reference} - a^*_{sample}$, $\Delta b^* = b^*_{reference} - b^*_{sample}$. The film with the highest deposited Al content was selected as the reference. In the paint industry, keeping a stable appearance of the film is critical in the sense that any change of pigment or additive to the paint matrix should change the color of the film only in the pre-established scope. As a result, for any produced powder coating to be in an ac-

ceptable stable scale, the ΔE value was set to be between 0 and 1[30]. As is known, a smaller color difference represents a better color stability.

6.4 Results and discussion

6.4.1 Microwave-bonded samples with low Al addition

At first, the accurate original Al content was turned out to be $1.81 \pm 0.01 \text{ wt}\%$ after three parallel tests through the gas-volumetric method. After bonding the non-bonded sample by the thermal process, the size of the non-bonded sample increase from $11.85\mu\text{m}$ (D_{10}), $32.85\mu\text{m}$ (D_{50}), and $63.86\mu\text{m}$ (D_{90}) to $16.72\mu\text{m}$ (D_{10}), $41.47\mu\text{m}$ (D_{50}), and $74.11\mu\text{m}$ (D_{90}). The size increase of bonded sample is predictable and reasonable because the goal of the bonding process is uniting two or more particles together. So these diameter increments prove that some bondings are formed after the thermal treatment process, although mis-bondings are also taken into consideration.

As the temperature is the most important influencing factor on the bonding quality, five temperatures were set to bond the non-bonded powder with the microwave, while the rotating speed maintained at 40rpm . To examine the bonding quality of the microwave-bonded powders, the deposited Al contents of these samples were measured and summarized in Table 6.1. The deposited Al contents of the non-bonded sample are $\sim 1\%$ which are far below the original one (1.81%). This reduction of Al content suggests that the film has a much less metal shine and shininess than what it should be. After the thermal bonding treatment at the temperature of 64°C , the deposited Al contents increase by $\sim 0.35\%$, demonstrating that the thermal bonding process indeed acquires some bondings. When bonding by the microwave, the deposited Al content barely increases by around 0.1% after bonding at 54°C , however, the samples made at the other four temperatures have much higher increments, about 0.40% , which is a bit higher than the increase of the thermal-bonded one. Another finding is that all the Al contents at $60/6.5$ are slightly lower than that at $60/6.5$. The main reason for this phenomenon is that high-speed air is easy to blow Al flakes away on account of their light mass and high aspect ratio. It is remarkable that all the deposited Al contents are lower than the original Al addition (1.81%).

Also, there is a slight increase of the deposited Al content when the spray voltage goes up at the same air supply.

Table 6.1: Deposited Al contents (/wt%) of microwave-bonded powders with low Al addition.

	30/6.5*	60/6.5*	60/6.5*	90/6.5*
Non-bonded	0.92±0.00	1.04±0.01	1.03±0.02	1.01±0.07
Thermal 64°C	1.23±0.01	1.38±0.02	1.36±0.02	1.42±0.01
54°C	1.00±0.02	1.10±0.05	1.12±0.02	1.14±0.04
58°C	1.25±0.02	1.41±0.04	1.46±0.07	1.47±0.03
59.5°C	1.25±0.00	1.43±0.02	1.51±0.04	1.48±0.03
60.5°C	1.25±0.01	1.43±0.02	1.46±0.04	1.49±0.04
61.5°C	1.23±0.01	1.41±0.01	1.50±0.03	1.43±0.01

* The spray conditions are voltage (30-90kV) and air supply (5.5 and $6.5m^3 h^{-1}$).

A predominant explanation for these results is that the charge capacity of the coating particle and Al flake are different. The maximum charge (Q_{max}) accumulated by a particle passing through an electric field could be estimated by the following equation[31]:

$$Q_{max} = 4 \pi r_e^2 \epsilon_0 E \frac{3\epsilon_r}{\epsilon_r + 2} \quad (6.5)$$

where r_e is the equivalent spherical radius; ϵ_0 is the permittivity of vacuum; E is the electric field strength; ϵ_r is the relative dielectric constant. The average equivalent spherical radius of the involved Al flake and coating particle are $\sim 7.1\mu m$ and $\sim 32.9\mu m$, respectively. Calculating with reported data[32, 33, 34, 35], it is discovered that the maximum charge of the coating particle is ten times more than that of Al flake. So it is believed that coating particles are easier to capture electrons/anions in the process of electrostatic spraying, which results in a higher content of coating particles in the deposited powder. Another reason is that the high aspect ratio of Al flakes make themselves easy to be blown away. In other words, the Al content in the deposited powder will be less than the original Al addition.

For a more direct understanding of bonding quality, the bonding rates of thermal-bonded and microwave-bonded samples were calculated by Eq. 6.3 and plotted in Fig. 6.3. The sample prepared at 54°C has a much lower bonding rate than the others which means an inferior bonding quality. This is mostly because the surface of the coating particle is not adhesive enough to attach Al flake at this low temperature. With the exception of the sample prepared at 54°C, all

the bonding rates at evaluated temperatures are around 37% in the condition of 30/6.5. However, at the other three spray conditions, the samples prepared at 58 to 61.5°C have greater bonding rates than the thermal-bonded sample. In particular, the sample bonded at 59.5°C and sprayed at 60/6.5 reaches the highest value (60.68%) among these bonding rates which is 19% more than the thermal-bonded sample. Therefore, 59.5°C was considered as the optimal bonding temperature for this metallic powder paint among these five trials. In addition, there is an obvious trend that the bonding rate gradually increases with the increase of spray voltage. This is partly because the charges of the coating particle and Al flake become closer when the voltage increases due to the fact that the lower electric resistance of the Al flake enables a faster charge capture rate than the coating particle[36]. Also, the bonding rate is higher when the air supply is lower, which is in line with the previous result of deposited Al content. Through comparing the bonding rates of microwave- and thermal-bonded samples, it can be seen that the microwave bonding method acquires a better bonding quality.

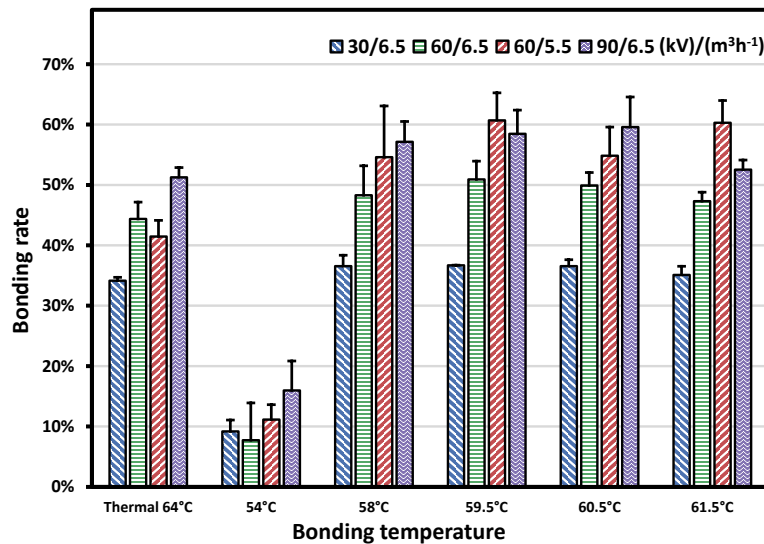


Figure 6.3: The bonding rates of samples bonded at different temperatures.

Notably, the temperature of microwave bonding (59.5°C) is much less than that of the thermal bonding (64°C). As described in Introduction, this finding is trusted to be the result of the heating-selectivity of the microwave. Microwave power absorbed by materials per unit volume is given as below[37]:

$$P = 2\pi f \epsilon_0 E^2 \epsilon''_{eff} \quad (6.6)$$

where, P is the microwave absorbing power per unit volume (W/m^3); f is the frequency of microwave (Hz); E is the electric field intensity (V/m); ϵ_0 is the permittivity of vacuum; ϵ''_{eff} is the effective dissipation factor of material.

In this work, all the to-be-heated samples were the mixtures of non-conductive particles (base coating particles) and conductive plates (Al flakes). According to Wagner's work[38], the main microwave absorption is due to two distinct mechanisms: a) dipolar polarization of base particles; b) interface polarization (Maxwell-Wagner polarization) of coating particles and Al flakes. In order to figure out which one is the dominate mechanism, the same mass (10kg) of base coating particles and non-bonded powders were separately heated by the microwave in the same condition.

Firstly, the base coating particles without Al flakes were singly heated by the microwave bonding machine. The major microwave absorption is believed to be dipolar polarization in this process. And the effective dissipation factor of dipolar polarization ($\epsilon''_{dipolar}$) can be estimated by the equation as below:

$$\epsilon''_{dipolar} = \epsilon' \tan\delta \quad (6.7)$$

where, ϵ' is the real part of dielectric constant of material; $\tan\delta$ is the loss tangent of material. The calculated $\epsilon''_{dipolar}$ is about 0.017 in the use of the data from some published studies[39, 40]. The experimental results show that the heating rate of base coating particles is $\sim 2^\circ C/min$.

Secondly, the non-bonded powder, a mixture of base coating particles and Al flakes, was heated by the microwave bonding machine. Wagner has indicated that for the simplest model featuring this type of polarization, consisting of conducting spheres distributed throughout a non-conducting medium, the effective dissipation factor is given by Eq. 6.8[27, 26, 38], and Sillars has implied that the τ in Eq. 6.8 can be estimated by Eq. 6.9 according to a double layer arrangement model[41]:

$$\epsilon''_{MW} = \frac{9 \nu \epsilon'_1 f_{max}}{1.8 \times 10^{10} \delta_2} \frac{2\pi f \tau}{1 + (2\pi f \tau)^2} \quad (6.8)$$

$$\tau = \epsilon_0 \frac{\epsilon'_1 + \epsilon'_2}{\delta_1 + \delta_2} \quad (6.9)$$

Where, ν is the volume fraction of conductive material; f_{max} in Hz is the frequency of maximum losses; δ is the conductivity in $S m^{-1}$ of the conductive phase; τ is the relaxation time

constant; the subscripts 1 and 2 refer to non-conductive and conductive phase, respectively. After collecting parameters from published articles[16, 40, 42], ϵ''_{MW} is turned out to be around 0.06 which is rather higher than that of the dipolar polarization. In Experiment, in contrast to the heating rate of base coating powders ($\sim 2^\circ\text{C}/\text{min}$), a much faster heating rate ($\sim 10^\circ\text{C}/\text{min}$) was found when heating the non-bonded powder. Therefore, the theoretic and experimental results both illustrate that the interface polarization is the main absorption mechanism. Consequently, the interface is able to have a higher temperature in contrast with non-touched and mis-touched surfaces when heating by the microwave. In general, the heating rate of a thermal bonding machine ranges from 3 to $6^\circ\text{C}/\text{min}$. Apparently, the high heating rate of microwave bonding is greatly beneficial for the improvement of bonding efficiency and reduction of power cost. Above all, microwave bonding is a considerably time-saving and effective method for producing metallic effect powder coating.

The color differences (ΔE) of final films prepared from various samples (non-, thermal- and microwave-bonded samples) and at different spray conditions, were measured and analyzed as seen in Fig. 6.4. There is no doubt that a smaller color difference in films signifies a higher color stability of a coating. As stated before, the reference film was the one with the highest deposited Al content, so one of the films cured from the sample bonded at 59.5°C and sprayed at 90kV was chosen as reference. As seen in Fig. 6.4, the films made by the non-bonded sample have the biggest color difference in the tested range, which indicates it has the worst color stability. Bonding at 54°C has the second highest color difference, representing that there are few bondings formed, which is consistent with the previous result of the bonding rate. The color difference at 61.5°C was apparently higher than that at 59.5 and 60.5°C , revealing the worsening of color stability and bonding quality, which does not agree with the bonding rate analysis. A generally accepted reason probably is that the high temperature leads to over-bonding and then causes uneven films. It is also noticed that all the color differences at 64°C (Thermal bonding), 59.5°C and 60.5°C are below 1, which are all within the range of color change acceptable by the paint industry. Moreover, all of the color differences at 59.5°C are lower than 0.5, indicating that the color of this bonded powder is highly stable. So the best bonding temperature is held as 59.5°C in these performed tests, which is in line with the conclusion of the bonding rate.

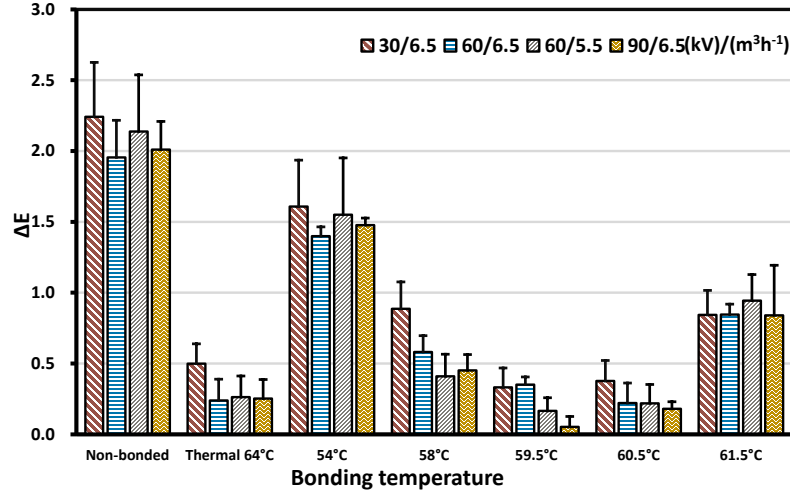


Figure 6.4: Color differences of final films prepared from the samples bonded at different temperatures.

The influence of rotating speed on the bonding quality and color stability was investigated because the motion of particles is largely impacted by the speed in the bonding process. Huang and coauthors recognized that the motion of powder in a drum went through five regimes with the increase of rotating speed: slipping regime, avalanching-sliding regime, aerated regime, fluidization regime, and re-compacted regime[43]. The maximum rotating speed, n_{max} , that allows powders to stay in the fluidization regime can be estimated by the following equation:

$$n_{max} = \frac{30}{\pi} \sqrt{\frac{g}{r}} \quad (6.10)$$

Where, r is the radius of drum (m); g is the acceleration of gravity (m/s^2). For obtaining a high bonding quality, the loaded powder has to remain in the fluidization regime to secure uniform heating. Thus, the theoretic highest rotating speed calculated by Eq. 6.10 is $68.6rpm$ at the drum radius of $19cm$. On the basis of the previous study, microwave-bonded samples were prepared at 30 , 40 , and $50rpm$ while the temperature remained as $59.5^\circ C$. It is seen that the loaded powder always stays in the fluidization regime at the three rotating speeds. Table 6.2 gives the deposited Al contents of microwave-bonded samples prepared at various rotating speeds. Bonding at 30 and $40rpm$ has close values, but slightly lower ones are found at the high speed of $50rpm$. A possible reason for this finding is that some weak bondings are ruined by the greater shear created at a higher rotating speed.

Based on these Al contents, bonding rates were further computed as shown in Fig. 6.5A.

Table 6.2: Deposited Al contents (/wt%) of bonded powders prepared at various rotating speeds.

	30/6.5*	60/6.5*	60/6.5*	90/6.5*
30rpm	1.20±0.05	1.44±0.01	1.48±0.00	1.42±0.04
40rpm	1.25±0.00	1.43±0.02	1.51±0.04	1.48±0.03
50rpm	1.25±0.02	1.34±0.05	1.43±0.06	1.43±0.01

* The spray conditions are voltage (30-90kV) and air supply (5.5 and $6.5\text{m}^3\text{h}^{-1}$).

The bonding rates of 40rpm are not lower than that of 30 and 50rpm at 30/6.5 and 60/6.5. Furthermore, the sample bonded at 40rpm has the highest bonding rates at 60/6.5 and 90/6.5 among the three samples. On the other hand, the color analysis in Fig. 6.5B tells that all the color differences at 40rpm are below 0.5 while those at the other two speeds are above 0.5 (below 1). Altogether, it is deemed that 40rpm is the best rotating speed among the three tested speeds. A greater bonding quality and color stability acquired at 40rpm is probably because the loaded powder has a more favorable fluidized state making bonding easier to form.

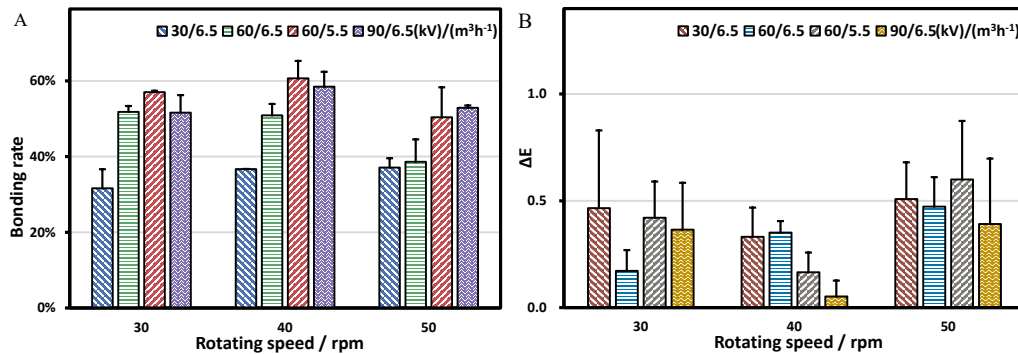


Figure 6.5: Bonding rates and color differences of bonded samples at various rotating speeds.

The morphology of non-bonded, thermal-bonded, and microwave-bonded powders was observed by SEM as presented in Fig. 6.6. The surfaces of Al flakes in non-bonded powders are clean and smooth (Fig. 6.6A and B), revealing that there is no bonding between coating particles and Al flakes. After thermal bonding, even though many Al flakes remain separated from coating particles as presented in the circle areas with dash lines in Fig. 6.6C, some effective bondings are formed between Al flakes and coating particles (areas with yellow lines). A small Al flake sticks to the surface of a large coating particle is seen in the zoomed-in image (Fig. 6.6D). Additionally, some mis-bondings (coating particles bond with each other) are found in these circle areas with solid dark lines. These mis-bondings could partly explain the

size increase of thermal-bonded samples as discussed before. The SEM image (Fig. 6.6E) of the microwave-bonded sample made at 59.5°C and 40rpm shows a greater number of flakes stick to the surfaces of coating particles. Unquestionably, there is still a small amount of clean flakes found as exhibited in the dashed circle areas, hinting that the bonding rate is not 100%. The square area in Fig. 6.6E is zoomed in and scanned by EDS as given in Fig. 6.6F and G, respectively. Two flakes in diameter of around $30\mu\text{m}$ separately adhere to the front and back sides of a big particle. The EDS scanning shows the flakes are mostly composed of the aluminum (green spots). The blue spots (titanium) coming from the titania that works as the white inorganic pigment are used to represent the positions of coating particles. And the EDS spectroscopy (Fig. 6.6H) of the white point in 6.6F also testifies that the flake is almost made by aluminum. Combining these analysis, the bondings in 6.6F are confirmed to happen between two Al flakes and a coating particle. Fig. 6.6I presents the medium diameter of the bonded sample is $39.96\mu\text{m}$ which is also higher than that of the non-bonded sample ($32.85\mu\text{m}$). Similar to the thermal bonding process, microwave bonding also results in size increase.

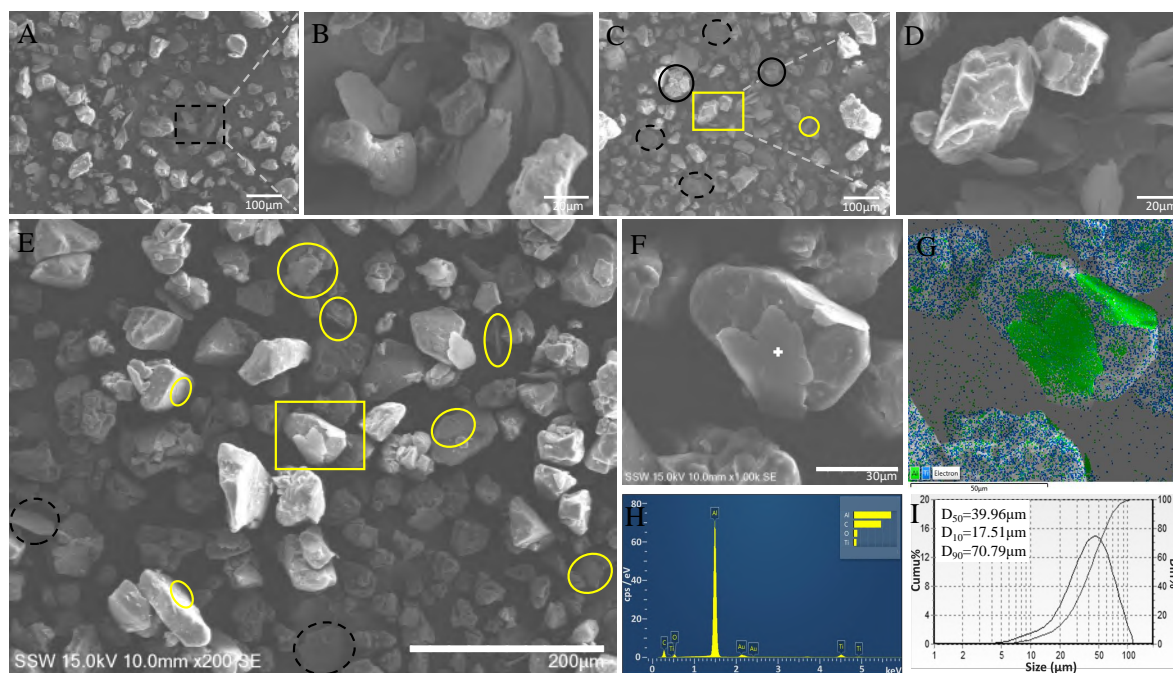


Figure 6.6: SEM, EDS and size distribution of the non-bonded, thermal-bonded and microwave-bonded powders. A,B) non-bonded; C,D) thermal-bonded; E,F) microwave-bonded; G) EDS scanning of F; H) EDS spectroscopy of the white point in F; I) Size distribution of the sample prepared at 59.5°C and 40rpm .

The situation and shape of coating particles and Al flakes were tested by SEM and EDS as discussed before. However, the distribution and state of Al flakes in the final films were still not clear, so the surfaces and cross-sections of these films were characterized by an optical microscope as illustrated in Fig. 6.7. The white areas in 6.7A, B and C are the results of the light reflections of Al flakes when observing the surfaces by an optical microscope. The total area of Al flakes in the film cured from the non-bonded powder (termed as non-bonded film), as viewed in Fig. 6.7A, apparently is much less than that of the other two. A higher Al area means that the film has a stronger metal shine and the powdered sample has a better bonding quality and color stability. Here, for a more clear comparison, an image software (Image J) was employed to have a statistical analysis on the total area of Al flakes as a percentage of the observed area. The Al area fraction of non-, thermal-, and microwave-bonded films are 7.9, 12.1, and 12.7%, correspondingly. A near 5% increase of Al area is found after microwave bonding treatments compared to the non-bonded one. The Al area analysis also illustrates that the microwave bonding obtains a litter better bonding quality than the thermal bonding. At the same time, the distributions of Al flakes inside these films are displayed in the images of these cross-sections. The approximate numbers, per millimeter, of Al flakes of the three films separately are 262, 519 and 579 as given in Fig. 6.7D, E and F. There is a good match between the cross-sectional and top surface images. In addition, all of the thickness of the three films were around 80 μ m. Moreover, these tendencies obtained from optical images coincide well with the previous results of bonding rate and color difference. For instance, a film with a higher deposited Al content generally has a higher Al area ratio of the surface as well as a larger number of Al flakes in the film.

6.4.2 Microwave-bonded samples with high Al addition

The bonding quality and color stability of metallic powder paint with low Al addition have been studied carefully and microwave bonding method has shown its advantages. For a stronger metal shine and higher protection, a metallic effect powder coating with high original Al addition (4.66 \pm 0.04%) was studied and discussed as well. At first, the deposited Al contents were obtained via the gas-volumetric method after spraying these powders at different voltages (30, 60 and 90kV) and air supplies (5.5 and 6.5 m^3h^{-1}). The deposited Al contents of the non-bonded

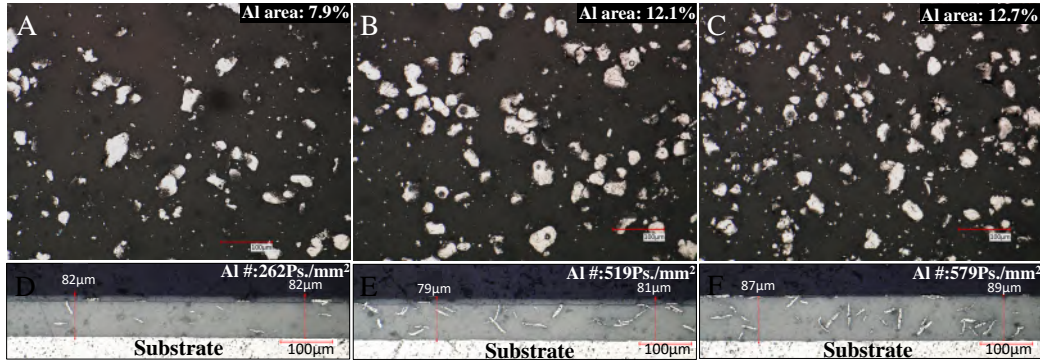


Figure 6.7: Optical images of top surface and cross-section of the final films obtained from non-bonded and bonded samples. A,D) Non-bonded powder; B,E) Thermal-bonded powder; C,F) Microwave-bonded powder prepared at 59.5°C and 40rpm.

sample are $\sim 1.24\%$ which are significantly lower than the original Al content, 4.66%. Comparing with the sample with low Al addition (1.88%), the reduction of the deposited Al contents is even greater. After the thermal bonding treatment, the deposited Al contents of thermal-bonded samples increase to $\sim 2.36\%$. As stated before, it is always difficult to bond a metallic effect powder coating with a high content of metallic pigment by the thermal bonding method. Since the best rotating speed had been to be 40rpm among the tested points, the microwave-bonded powders were also bonded under this speed, but the bonding temperatures were different (59 to 61°C). Table 6.3 describes that the deposited Al content is increased with the increase of bonding temperature at the same spray condition. An increment of deposited Al content is found again when the spray voltage increases from 30 to 90kV. The highest deposited Al content in the tested samples is around 3.07% when bonded at 61°C and sprayed at 90/6.5, while that of non-bonded and thermal-bonded samples are only about 1.28% and 2.43%, respectively.

Table 6.3: Deposited Al contents (/wt%) of bonded powders prepared at different temperatures.

	30/6.5*	60/6.5*	60/6.5*	90/6.5*
Non-bonded	1.15±0.05	1.25±0.02	1.27±0.09	1.28±0.04
Thermal 65°C	2.04±0.00	2.41±0.04	2.54±0.05	2.43±0.04
59°C	1.99±0.14	2.61±0.06	2.53±0.13	2.87±0.04
60°C	2.22±0.03	2.61±0.06	2.53±0.13	2.87±0.04
61°C	2.79±0.02	2.84±0.03	3.03±0.00	3.07±0.07

* The spray conditions are voltage (30-90kV) and air supply (5.5 and $6.5m^3 h^{-1}$).

In Fig. 6.8A, the bonding rates evaluated by Eq. 6.3 show that the sample bonded at a low

temperature of 59°C has close bonding rates with the thermal-bonded sample. It is clear that the bonding rate raises from ~35 to ~50% when the temperature increases from 59 to 61°C. The highest rate is found to be 53.2% at 61°C under the spray condition of 60/6.5. As discussed before, the highest bonding rate is 60.68% at 59.5°C when the Al addition is 1.81%. By comparing these numbers, it is discovered that a higher temperature leads to a lower bonding rate when the original Al addition increases from 1.81 to 4.66%, which demonstrates that bonding the metallic powder paint with a high Al addition is rather a much more difficult task. Unfortunately, a higher bonding quality is not found when the temperature reached 62°C due to the pre-curing and over-bonding of metallic effect powder coating. So it is believed that the best bonding temperature is 61°C among these trials. Meanwhile, the color differences of the films made from these bonded powders are displayed in Fig. 6.8B. It seems that the thermal-bonded sample has the highest color difference when compared in the same spray condition. All the color differences of microwave-bonded samples are smaller than 0.5, suggesting that these samples have a strong color stability. Comparing the color differences of 60°C and 61°C, it is suggested that the sample bonded at 61°C obtains a better bonding quality when considering the fact that the most frequently used range of spray voltage is 55 to 90kV. A similar finding is that the bonding temperature of microwave bonding is also lower than that of the thermal bonding.

Importantly, the heating rate increased from ~10 to ~15°C/min when the Al addition increased from 1.81 to 4.66%. This rather high heating rate could be explained by Eq. 6.6 and 6.8. A higher volume fraction of Al flake (v) results in a bigger ϵ''_{MW} , about 0.17, as well as a larger microwave absorption (P). Thus, the loaded materials absorb more energy per unit of time and have a higher heating rate. From the foregoing discussion, it can be deduced that a higher metal addition is conducive to cutting down the bonding time. Conversely, the processing time of thermal bonding might be a bit extended to try to secure a high bonding quality when the Al addition is high.

The non-bonded, thermal-bonded, and optimal microwave-bonded samples were further investigated by SEM, EDS, and particle size analyzer as viewed in Fig. 6.9. The surfaces of Al flakes in non-bonded powders (Fig. 6.9A and B) are smooth and clean. Some bonded particles (areas with yellow line) are found in the Fig 6.9C and D after thermal bonding, but many flakes

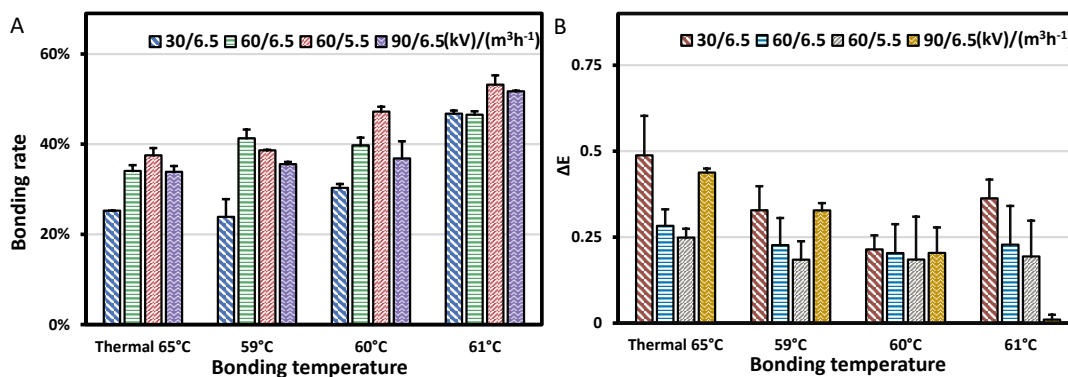


Figure 6.8: Bonding rates and color differences of the bonded samples prepared at various temperatures.

stay apart from coating particles (areas with dash lines) and some mis-bonded particles (solid circle areas) are also observed. After microwave bonding, many flakes adhere to the surfaces of the coating particles as shown in these solid circle areas in Fig. 6.9E. Specifically, many of the particles bond with more than one flake, which is mainly caused by the high weight percentage of the Al flake. Fig. 6.9F magnified from the rectangle area in Fig. 6.9E clearly exhibits that some flakes stick on the surfaces of particles. Besides, the EDS mapping (Fig. 6.9G) and spectroscopy (Fig. 6.9H) testify that these flakes are made up of aluminum, which provides the evidence for the existence of effective bonding between coating particles and Al flakes. The D_{10} , D_{50} , and D_{90} of the non-bonded and thermal-bonded samples are 11.72, 32.36, 62.66 μm and 15.27, 39.28, 72.77 μm , respectively. The size distribution of this sample (6.9I) suggests that it has similar diameters with the one produced by the thermal bonding process. Above all, microwave bonding method seems to obtain more effective bondings and fewer mis-bondings than with thermal bonding.

By analyzing the optical images, the Al area ratio of the non-bonded film is found to be about 10.3% which is higher than that of the former non-bonded one (6.6%). This illustrates that the shininess of film can be improved to a certain degree by only adding more Al flake. The Al area of thermal-bonded film is about 20.1%. However, the Al area dramatically increases to around 22.5% after the microwave bonding. Additionally, the numbers of Al flake per millimeter estimated from the sectional images approximately are 562, 1013 and 1242. Based on these analyses, a similar conclusion with the former optical observation could be drawn: microwave bonding has a better color stability quality compared to the thermal bonding when

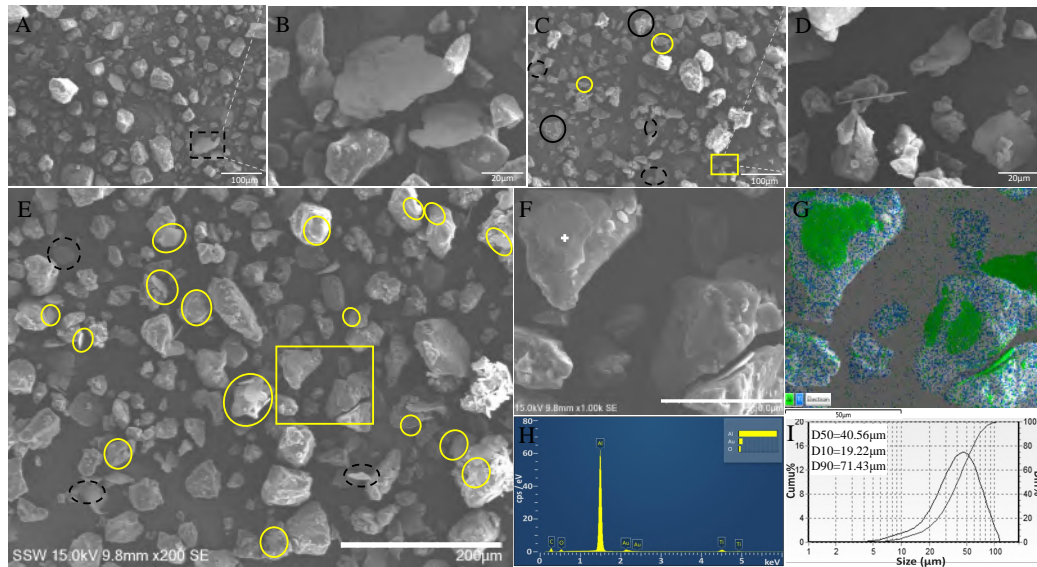


Figure 6.9: SEM, EDS and size distribution of the non-bonded, thermal-bonded and microwave-bonded powders. A,B) non-bonded; C,D) thermal-bonded; E,F) microwave-bonded; G) EDS scanning; H) EDS spectroscopy of the white point in F; I) Size distribution.

the Al addition is 4.66%.

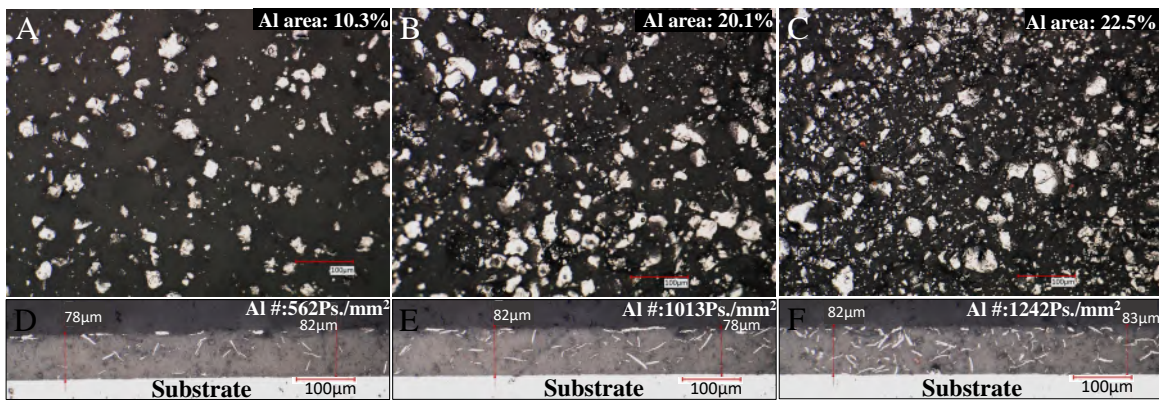


Figure 6.10: Optical images of top surface and cross-section of the final films obtained from non-bonded and bonded samples. A,D) Non-bonded sample; B,E) Thermal-bonded sample; C,F) Microwave-bonded sample prepared at 61°C and 40rpm.

6.5 Conclusions

An innovative microwave bonding method for metallic powder paint was developed and tested in a self-designed bonding machine. Compared to the conventional thermal bonding, the microwave bonding has higher bonding rate, less color difference, and more Al flakes shown on the surfaces and in the coating film itself, rendering microwave bonding a more effective method for the production of metallic effect powder coatings.

The heating-selectivity of the microwave resulting from interface polarization plays an essential role in the microwave bonding process, hence much faster heating could be obtained during the metallic effect powder coating bonding process: $\sim 10^{\circ}\text{C}/\text{min}$ (low Al addition) and $\sim 15^{\circ}\text{C}/\text{min}$ (high Al addition). As a result, the processing time of the microwave bonding is also largely reduced comparing to that of the thermal bonding. On the whole, microwave bonding method has a great potential to provide high bonding quality and stable metal shine for the efficient production of metallic effect powder coatings.

Bibliography

- [1] Zhongyan Du, Shaoguo Wen, Jihu Wang, Changle Yin, Dayang Yu, and Jian Luo. The review of powder coatings. *Journal of Materials Science and Chemical Engineering*, 4(3):54–59, 2016.
- [2] TA vd Misev and R Van der Linde. Powder coatings technology: new developments at the turn of the century. *Progress in Organic Coatings*, 34(1-4):160–168, 1998.
- [3] Wei Liu, Jing Fu, Haiping Zhang, Yuanyuan Shao, Hui Zhang, and Jesse Zhu. Cold bonding method for metallic powder coatings. *Materials*, 11(11):2086, 2018.
- [4] SM Mahajan, A Varade Mayur, N Mahajan Pratiksha, and V Patil Sneha. Review on automotive body coating process. *Int. J. Eng. Manage. Res.*, 9(2):103–106, 2019.
- [5] Abdel Salam Hamdy Makhlouf and Yashwanth Gajarla. Advances in smart coatings for magnesium alloys and their applications in industry. In *Advances in Smart Coatings and Thin Films for Future Industrial and Biomedical Engineering Applications*, pages 245–261. Elsevier, 2020.
- [6] Leena Kumari Prasad, James W McGinity, and Robert O Williams III. Electrostatic powder coating: Principles and pharmaceutical applications. *Int. J Pharm.*, 505(1-2):289–302, 2016.
- [7] Vijay Goud, Alagirusamy Ramasamy, Apurba Das, and Dinesh Kalyanasundaram. Box-behnken technique based multi-parametric optimization of electrostatic spray coating in the manufacturing of thermoplastic composites. *Mater. Manuf. Process.*, 34(14):1638–1645, 2019.
- [8] Douglas S Richart and Andrew T Daly. Thermosetting resin-based coating powders containing metal flakes, February 16 1993. US Patent 5,187,220.
- [9] P Haring Bolivar, Martin Brucherseifer, J Gómez Rivas, Ramón Gonzalo, Iñigo Ederra, Andrew L Reynolds, M Holker, and Peter de Maagt. Measurement of the dielectric constant and loss tangent of high dielectric-constant materials at terahertz frequencies. *IEEE T Microw. Theory.*, 51(4):1062–1066, 2003.
- [10] Hadi Rastin, Mohammad Reza Saeb, Milad Nonahal, Meisam Shabanian, Henri Vahabi, Krzysztof Formela, Xavier Gabrion, Farzad Seidi, Payam Zarrintaj, Morteza Ganjaee Sari, et al. Transparent nanocomposite coatings based on epoxy and layered double hydroxide: nonisothermal cure kinetics and viscoelastic behavior assessments. *Progress in Organic Coatings*, 113:126–135, 2017.
- [11] Hirotaka Ejima, Joseph J Richardson, Kang Liang, James P Best, Martin P van Koeveden, Georgina K Such, Jiwei Cui, and Frank Caruso. One-step assembly of coordination complexes for versatile film and particle engineering. *Science*, 341(6142):154–157, 2013.

- [12] Kyoko Miyauchi, Yuka Takita, Hidetoshi Yamabe, and Makoto Yuasa. A study of adhesion on stainless steel in an epoxy/dicyandiamide coating system: Influence of glass transition temperature on wet adhesion. *Progress in Organic Coatings*, 99:302–307, 2016.
- [13] Yusuke Yasuda, Toshiaki Morita, Eiichi Ide, Hiroshi Hozoji, and Toshiaki Ishii. Low temperature bonding material comprising metal particles and bonding method, June 7 2011. US Patent 7,955,411.
- [14] Mark A Smith. Fusion bonded epoxy coating compositions that include magnesium oxide, March 25 2014. US Patent 8,679,632.
- [15] TH Van Steenkiste, JR Smith, and RE Teets. Aluminum coatings via kinetic spray with relatively large powder particles. *Surface and Coatings Technology*, 154(2-3):237–252, 2002.
- [16] Jigar K Mistry, Jan Peter Frick, and James Petersen. Microwave bonding for coating compositions, July 6 2017. US Patent 15/463,131.
- [17] Chang-Yeol Yoo and Kong Byung-Seok. Surface treatment method of aluminum for bonding different materials, May 2 2019. US Patent App. 16/156,699.
- [18] Liam O’neill, Frederic Gubbels, Stuart Leadley, and Nick Shephard. Bonding an adherent to a substrate via a primer, October 14 2014. US Patent 8,859,056.
- [19] Keiichi Endoh, Aiko Nagahara, Yutaka Hisaeda, and Toshihiko Ueyama. Bonding material using metal nanoparticles coated with c6-c8 fatty acids, and bonding method, October 14 2014. US Patent 8,858,700.
- [20] Percy L Spencer. Prepared food article and method of preparing, August 30 1949. US Patent 2,480,679.
- [21] Emily T Kostas, Daniel Beneroso, and John P Robinson. The application of microwave heating in bioenergy: A review on the microwave pre-treatment and upgrading technologies for biomass. *Renew. Sust. Energ. Rev.*, 77:12–27, 2017.
- [22] Anne Kokel, Christian Schäfer, and Béla Török. Application of microwave-assisted heterogeneous catalysis in sustainable synthesis design. *Green Chem.*, 19(16):3729–3751, 2017.
- [23] Stefan Putz, Andreas Angerer, Dmitry O Krimer, Ralph Glattauer, William J Munro, Stefan Rotter, Jörg Schmiedmayer, and Johannes Majer. Spectral hole burning and its application in microwave photonics. *Nat. Photonics*, 11(1):36, 2017.
- [24] I Das and A Arora. Alternate microwave and convective hot air application for rapid mushroom drying. *J. Food Eng.*, 223:208–219, 2018.
- [25] Hossam Mahmoud Ahmad Fahmy. Wireless sensor networks essentials. In *Wireless Sensor Networks*, pages 3–39. Springer, 2020.

- [26] AC Metaxas and Roger J Meredith. *Industrial microwave heating*. Number 4. IET, 1983.
- [27] T Prodromakis and C Papavassiliou. Engineering the maxwell–wagner polarization effect. *Applied Surface Science*, 255(15):6989–6994, 2009.
- [28] Songsong Liu, Mingquan Ye, Aijun Han, and Xin Chen. Preparation and characterization of energetic materials coated superfine aluminum particles. *Applied Surface Science*, 288:349–355, 2014.
- [29] Alan R Robertson. The CIE 1976 color-difference formulae. *Color Res. Appl.*, 2(1):7–11, 1977.
- [30] Melda Isler Binay, Salih Kaan Kirdeciler, and Burcu Akata. Development of antibacterial powder coatings using single and binary ion-exchanged zeolite a prepared from local kaolin. *Appl. Clay Sci.*, 182:105251, 2019.
- [31] Daniel Goldwater, Benjamin Stickler, Lukas Martinetz, Tracy E Northup, Klaus Hornberger, and James Millen. Levitated electromechanics: all-electrical cooling of charged nano-and micro-particles. *Quantum Sci. Technol.*, 4, 2019.
- [32] Zhi-Min Dang, Tao Zhou, Sheng-Hong Yao, Jin-Kai Yuan, Jun-Wei Zha, Hong-Tao Song, Jian-Ying Li, Qiang Chen, Wan-Tai Yang, and Jinbo Bai. Advanced calcium copper titanate/polyimide functional hybrid films with high dielectric permittivity. *Adv. Mater.*, 21(20):2077–2082, 2009.
- [33] EMS Sanchez, CAC Zavaglia, and MI Felisberti. Unsaturated polyester resins: influence of the styrene concentration on the miscibility and mechanical properties. *Polymer*, 41(2):765–769, 2000.
- [34] DJ Suh, Ook Park, and KH Yoon. The properties of unsaturated polyester based on the glycolyzed poly (ethylene terephthalate) with various glycol compositions. *Polymer*, 41(2):461–466, 2000.
- [35] James D Christie and William C Howard. Bonded metal hydroxide-organic composite polymer films on particulate substrates, June 12 2001. US Patent 6,245,323.
- [36] Qiaoyan Ye and Joachim Domnick. On the simulation of space charge in electrostatic powder coating with a corona spray gun. *Powder Technology*, 135:250–260, 2003.
- [37] Tetsuya Hanai. Dielectric theory on the interfacial polarization for two-phase mixtures. *Bull. Inst. Chem. Res., Kyoto University*, 39(6):341–367, 1962.
- [38] K Wagner. Explanation of dielectric polarization processes on the basis of maxwellian concepts. *Arch Electrotech.*, 2:371–87, 1914.
- [39] Kwong Siong Kiew, Sinin Hamdan, and Md Rezaur Rahman. Comparative study of dielectric properties of chicken feather/kenaf fiber reinforced unsaturated polyester composites. *BioResources*, 8(2):1591–1603, 2013.

- [40] Hyoung Geun Kim et al. Dielectric cure monitoring for glass/polyester prepreg composites. *Composite Structures*, 57(1-4):91–99, 2002.
- [41] RW Sillars. The properties of a dielectric containing semiconducting particles of various shapes. *J. Inst. Electr. Eng.*, 80(484):378–394, 1937.
- [42] Motohiko Yoshizumi. Electroconductive powder and process for production thereof, June 5 1984. US Patent 4,452,830.
- [43] Qing Huang, Hui Zhang, and Jesse Zhu. Experimental study on fluidization of fine powders in rotating drums with various wall friction and baffled rotating drums. *Chem. Eng. Sci.*, 64(9):2234–2244, 2009.

7 Pilot-scale microwave bonding machine based on stirring

7.1 Abstract

Metallic effect powder coating studied in the present work is powder coating incorporated with metallic pigment and provides a finish with metal shine and sparkle. Although metallic effect powder coating confers environmental advantages over the liquid one by eliminating the use of solvents, it presents the challenge of ensuring that the metal shine only changes in an acceptable range during the electrostatic spraying process. Bonding the two components together is a practical approach to stabilize the metal shine by reducing the incompatibility between them. In the present work, to improve the bonding quality and avoid the inherent drawbacks of the present industrial bonding method (thermal bonding), a unique microwave-bonding machine was constructed and tested. The microwave bonding method was found to have a lower bonding temperature and a much faster heating rate than thermal bonding. Moreover, the analyses of bonding rates and color difference proved that the bonding quality and color stability of microwave-bonded samples were far better than those of the thermal-bonded ones. The optical images indicated that the microwave-bonded films had stronger metal shine than the thermal-bonded ones. This study demonstrates that the microwave bonding method has great potential to address the drawbacks of thermal bonding, such as mis-bonding and high-temperature bonding, and providing higher bonding quality and better color stability at the same time.⁶

Keywords: Microwave bonding; Powder coating; Metallic pigments; Metal shine.

⁶With minor editorial changes to fulfill formatting requirements, this chapter was submitted to *Progress in Organic Coatings* with the title of “Prepare Powder Coated Surfaces with Stable and High Metal Shine via microwave bonding”, Wei Liu, Haiping Zhang, Yuanyuan Shao, Yufu Wei, Hui Zhang, and Jesse Zhu.

7.2 Introduction

Metallic effect powder coating is a broad term and refers to, in this work, powder coating with metallic pigments addition. The key advantage of this type of coating is that the ability to provide a final finish that looks obviously glittery, shimmery, and subtly sparkly while emitting almost zero VOCs during the film formation [1]. Nowadays, many end-use products have a powder-coating metallic appearance, including guardrails, fences, windows, gates, appliances, office furniture and more [2, 3]. Metallic pigments are usually flaky and special-effect pigments made up of aluminum, copper, zinc, or metal-like materials [4, 5]. They have some essential advantages over organic pigments, such as odorless, safe, stable, eco-friendly, and sustainable, which enable them to gain popularity on the overall market. Metallic pigments have been widely applied in some expanding end-use industries such as packaging, cosmetics and printing inks, paint, particularly in powder coatings [6, 7]. These small metal flakes included in powder coatings increase the attractiveness and exclusivity of products by creating a sparkling effect and adding high protection.

In the beginning, the production method of the metallic effect powder coating is that merely blending the two components. However, a problem arises in the spray process as shown in the method A of Fig. 7.1: distinct metallic color change is found in the final finishes once the over-sprayed powder reclaimed because the virgin, deposited, and over-sprayed powders have considerably different contents of metallic pigments [8]. This color change mainly caused by the poor compatibility of metallic pigment and coating particles from their too different physical properties, such as conductivity, density, aspect ratio, and dielectric constant [9, 10]. In this case, the over-sprayed powder can not be reclaimed, resulting in high cost and material waste. Bonding the two materials together is an effective method to address the problem of compatibility, and then the color change will be much eliminated if the two ingredients are well bonded, as shown in the method B of Fig. 7.1. The present industrial bonding method is thermal bonding technology invented in 1993 by Richart et al [11]. This approach starts with heating the two components in a tank by high-speed stirring (friction heat) with or without the help of a water (or oil) jacket. Till the temperature reaches or slightly exceeds the glass transition temperature (T_g) of the coating particle (the resinous part of the coating particle begins to

become soft and adhesive at this particular temperature), maintaining the temperature at this point for 2-3 minutes to allow the metallic pigments adhere to the sticky surfaces of coating particles. Followed by rapid cooling, the bonded product can be collected from the tank.

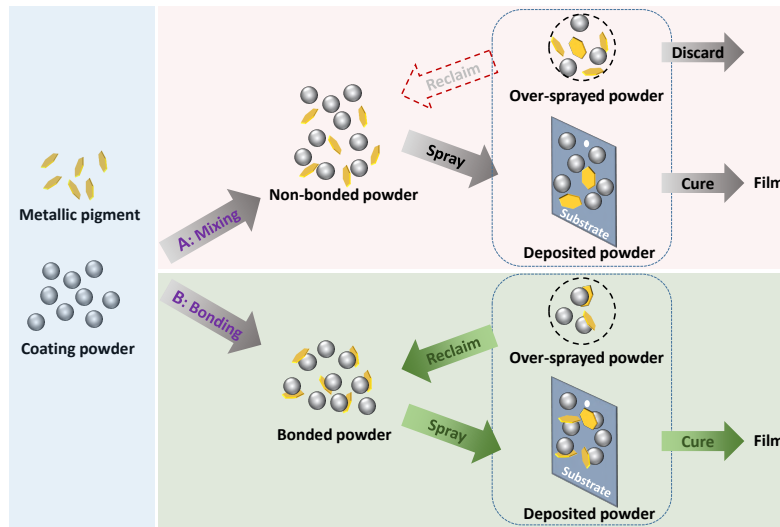


Figure 7.1: The diagram of the difference between non-bonded and bonded metallic effect powder coatings when sprayed by an electrostatic system. The grey spheres and gold plates represent coating particles and flaky metallic pigments, respectively.

As mentioned, metallic effect powder coating is used in numerous end-use products but seldom on high-end ones, such as trains, automobile bodies, cellphones, and laptops. These products have extremely high appearance requirements on the metallic coatings, for example, high color stability and extensive metal shine [12, 13]. At present, metallic effect powder coating is not a product that entirely meets these requirements due to several inherent issues of the thermal bonding process [14, 15, 16]. First, mis-bonding (sticky coating particle bonds other coating particles) easily occurs in this process. Second, high-speed stirring tends to bend or grind metallic pigment quickly and reduce the metal shine. Third, high-temperature bonding, such as 120°C, is a very difficult task for the thermal bonding approach because of the used heating modes—friction and jacket heating; Lastly, precise and fast temperature control is also challenging for the thermal bonding technology due to these heating models. The coexistence of these issues in the thermal bonding process restricts the applications of metallic effect powder coatings. A vast paint market of high-end products awaits an improved bonding process for metallic effect powder coatings.

Some efforts have been made to enhance the bonding quality of metallic effect powder coating in recent years. Gunde and coauthors reported that tuning the bonding time and the temperature can improve the bonding quality based on the thermal bonding process[17]. Some researchers suggested that modifying the surface of the metallic pigment with adhesive materials is an effective method, such as acrylic acid [18], polyethylene wax [19], C6-C8 fatty acids [20] and polyacrylic acid [9]. However, these methods have restrictions in various aspects, for example, cost, pollution, and industrialization. Microwave is a well-known heat source and has been successfully applied in a broad range of industrial applications, including cooking, sterilization, drying materials, medical treatments and more[21, 22, 23, 24]. Microwave heating has a series of advantages over the friction and jacket heating used by the present bonding technology, for instance, easy to control, safe, clean, efficient, and pollution-free. Recently, Mistry and coauthors employed a variable frequency microwave oven, which applied radio radiation in C-bands (5.8 to 7GHz) and X-bands (7.3 to 8.7GHz), to bind metallic pigments and coating particles [16]. However, these frequencies inevitably cause radio frequency interference (RFI) because they are not in the Industrial Scientific Medical (ISM) bands defined by the International Telecommunications Union-Radio communications (ITU-R) in 5.138, 5.150, and 5.280 of the Radio Regulation [25]. Therefore, this technique has not ever been developed and commercialized due to the high cost of the oven and the RFI of the involved bands. Metaxas and Meredith also pointed out that the interface of nonmetal and metal particles, in some cases, can have a higher microwave absorption than the other areas because of the heating-selectivity of the microwave [26]. According to this theory, a higher temperature is expected at the contact area of the coating particle (nonmetal) and metallic pigment (metal), which is deeply desired in the bonding process of metallic effect powder coatings.

This study aims to solve the above drawbacks of the current technology and enhance the bonding quality, so a self-designed microwave bonding machine, whose center frequency was fixed at 2.45GHz, was constructed to bind the metal effect powder coatings. The use of the fixed frequency of 2.45GHz that belongs to ISM bands avoids the RFI and reduces the cost largely. To secure uniform heating, the loaded materials were under continuous stirring during the microwave heating. Additionally, lower agitating speeds were used compared to the thermal bonding because the microwave served as the heat source rather than friction heat, which is a

substantial benefit in reducing the damage of the flaky metallic pigment. The bonding quality of the microwave bonding method and the color stability of final finishes were detailedly analyzed and discussed in the present work for further investigation and commercialization.

7.3 Materials and methods

7.3.1 Materials and equipment

High gloss polyester powder paint (bright white, HS144814) from Huajiang Powder Coating Co. (Guangdong, China) worked as base powder coating. Aluminum flakes (ZPC 330, with a stearic acid treated surface) from Zuxing New Material Co., Ltd. (Changsha, China) were used as laminar metallic pigments. Al panels (15cm in length, 7.6cm in width) from Q-Lab Co. (OH, USA) were utilized as substrates. Sodium hydroxide from Xilong Chemical Co., Ltd. (Guangdong, China) served as a reacting agent for gas-volumetric analysis.

7.3.2 Microwave bonding machine

A self-made microwave bonding machine, 130cm in length, 100cm in width, and 170cm in height, was built and tested. As seen in Fig. 7.2A, twelve microwave transmitters worked as the heat sources, and the frequency and power rating of each one is $2.45\text{GHz}\pm 50\text{Hz}$ and 1kW, respectively. A cylinder of 38cm in diameter, 40cm in height, and 2cm wall worked as a container for the metallic pigments and coating particles. Since the cylinder is made of polytetrafluoroethylene (PTFE) with minimal microwave absorption, the microwave could effectively heat the loaded powders. A three-layer impeller driven by a motor outside the shell was employed to mixing the two components. Two thermocouples were installed in the cylinder wall to measure the real-time temperature of the loaded powder. A flowmeter was applied to control the flowrate of nitrogen and a gas sensor was utilized to examine the oxygen volume fraction. The goal of nitrogen flow is to secure the safety of the bonding process by providing a low oxygen concentration in the cylinder. The control panel was used to monitor and adjust the bonding temperature and stirring speed. Fig. 7.2B is the front view of the machine and the top view of the three-layer impeller. To sum up, the microwave bonding machine used in this work is a testing prototype with a processing capacity of about 10kg at a time.

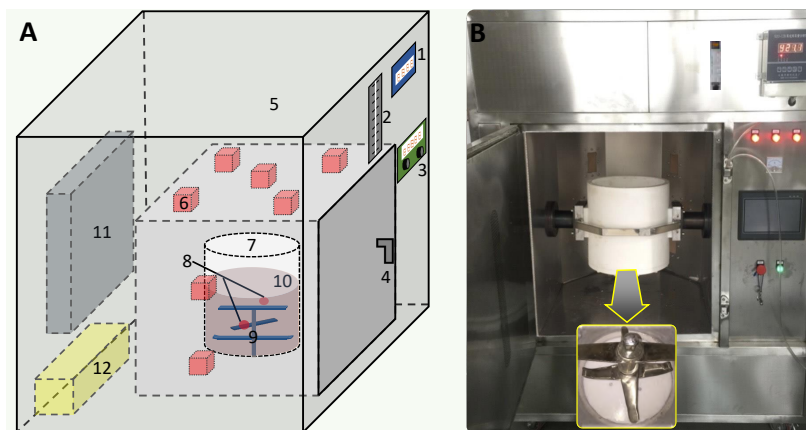


Figure 7.2: The schematic diagram (A) and picture (B) of the microwave bonding machine. 1. Digital display board of nitrogen content; 2. The flowmeter of nitrogen; 3. Control panel; 4. Door; 5. Shells; 6. Microwave transmitters; 7. PTFE cylinder; 8. Temperature sensors; 9. Three-layer impeller; 10. Coating particles and Al flakes; 11. Protective system of cold air of microwave transmitters; 12. Power system.

7.3.3 Preparation of samples

The non-bonded powders with low and high Al flake contents were prepared by dry blending 100kg base powder coatings with 2.5 and 5.5kg Al flakes, respectively. The thermal-bonded samples (commercial products) were manufactured by Huajiang Powder Coating Co. with the above non-bonded powders and via a thermal bonding machine (SHTBD10, Sun-hitech Technology Ltd., Xiamen, China).

The the microwave-bonded powder samples were prepared according to the following steps sequentially: a) loading the non-bonded powder into the cylinder; b) heating the loaded powder with nine microwave transmitters at the stirring speed of 500rpm to a set temperature (55-60°C); c) maintaining this temperature at a stirring speed (500-800rpm) for 120 seconds; d) discharging the loaded powder to a container for cooling down; e) sieving the discharged powder by a 120 mesh screen.

The deposited powders and final films were prepared as following: a) separately spraying a powder onto six substrates at a specific spray condition of voltage (30, 60, or 90kV) and air supply (5.5 or $6.5m^3h^{-1}$) via an electrostatic automatic spraying system and a corona gun (Gema Switzerland GmbH, St.Gallen, Switzerland), and four conditions were tested: 30/6.5, 60/6.5, 60/5.5, and 90/6.5; b) scraping off three of these deposited powders for bonding quality

analysis and curing (190°C, 10min) the other three into final films for surface comparison.

7.3.4 Characterization of powders

In this work, since Al flake served as metallic pigments, the bonding quality of powders was studied by analyzing the Al flake content of powders. For simplicity, the Al content of deposited powder was named as “deposited Al content”. As introduced, the smaller the difference between the deposited Al content and Al addition, the better the bonding quality. The Al contents were precisely analyzed by a gas-volumetric test based on the reaction between Al and NaOH [27, 28], and could be deduced as follows:

$$\omega = \frac{2 V_{H_2} M_{Al}}{3 V_m m_{sa}} \times 100\% \quad (7.1)$$

where ω is the Al content; V_{H_2} (mL) is the volume of hydrogen; M_{Al} (g/mol) is the relative atomic mass of aluminum; V_m (mL/mol) is the molar volume of hydrogen at 25°C and 1atm; m_{sa} (g) is the total mass of the powder sample.

The Al addition and deposited Al content were separately labeled as ω_{add} and ω_{dep} . To reveal the bonding quality quantitatively and directly, bonding rate (η_b) was defined by the following equation:

$$\eta_b = \left| \frac{\omega_{dep}^B - \omega_{dep}^N}{\omega_{add} - \omega_{dep}^N} \right| \times 100\% \quad (7.2)$$

where ω_{dep}^B and ω_{dep}^N are the deposited Al contents when spraying bonded and non-bonded powders at the same condition, respectively. Here, the difference between ω_{add} and ω_{dep}^N means the total amount of Al flakes that is necessary to be bonded, and the difference between ω_{dep}^B and ω_{dep}^N represents the content of Al flakes that has already been bonded. Consequently, the ratio of the two differences could discover the bonding quality. From the definition, the bonding rate of a non-bonded sample is 0%. When the deposited Al content of bonded-samples (ω_{dep}^B) equals the Al addition (ω_{add}), all Al flakes stick on the coating particles, and the bonding rate is 100%. It is very obvious that the higher the bonding rate, the better the bonding quality.

To observe the bonding situation between coating particles and Al flakes, the non-bonded, thermal-bonded and microwave-bonded powder samples were determined by a scanning electronic microscopy (SEM), equipped with energy dispersive spectrometer (EDS), (SU3500,

Hitachi Ltd., Tokyo, Japan) after gold-sputtering for 1.5min. The size distributions of non-bonded, thermal-bonded and microwave-bonded powder samples were characterized by a size analyzer (LS-POP6, Omec Instruments Ltd., Zhuhai, China).

7.3.5 Characterization of films

At first, the final films were examined by a colorimeter (CI62, X-rite Inc., Michigan, USA), on the basis of CIE-Lab color system [29], to reveal the color stability of a metallic effect powder coating. The following equation evaluated total color difference (ΔE) detected by the colorimeter concerning the reference:

$$\Delta E = \sqrt{(\Delta L^*{}^2 + \Delta a^*{}^2 + \Delta b^*{}^2)} \quad (7.3)$$

where L^* describes brightness varying from 0.0 for black to 100.0 for a diffuse white; a^* is the color change from red ($+a^*$) to green ($-a^*$); and b^* represents the color change from yellow ($+b^*$) to blue ($-b^*$). Accordingly, $\Delta X^* = X^*_{reference} - X^*_{sample}$ ($X^* = L^*, a^*, b^*$). The film with the highest deposited Al content was selected as the reference. A coating with stable color is critical in the paint industry, so any change of pigment to the paint matrix should change the color of the film only in the pre-established range. For any qualified powder-coating product, the ΔE value was set to be between 0 and 1[30].

In order to analyze the metal shine, the top and cross-sectional surfaces of the films that prepared from non-bonded, thermal-bonded and microwave-bonded powders and sprayed at 60/6.5 were observed by a Keyence VHX-6000 optical microscope (Keyence Corporation, Itasca, USA). These films were also characterized by a Zeiss Xradia 410 Versa Micro-CT (Jena, Germany). The hardness, adhesion and impact resistance of these films were determined based on ASTM D3363, D3359 and D2794 via an Elcometer 501 pencil hardness tester, an Elcometer 107 cross hatch cutter and an Elcometer 1615 variable impact tester (Elcometer Inc., MI, USA), respectively.

7.4 Results and discussion

7.4.1 Low addition of Al flakes

The addition of Al flakes in the powder paint is usually below 2.5wt%, so a non-bonded powder with ~2.4wt% Al flakes was first prepared. The accurate Al addition was confirmed to be $2.33\pm 0.03\%$ after three paralleled gas-volumetric tests. Moreover, the size analysis shows the D_{10} , D_{50} , and D_{90} of this non-bonded sample are 14.26 μm , 36.38 μm , and 67.04 μm . These diameters increase to 18.36 μm , 45.04 μm , and 81.17 μm after the thermal bonding at 62°C. The size increment is expectable because the thermal bonding process aims to cohere Al flakes with coating particles while accompanied by mis-bondings.

Optimization of stirring

To compare the thermal and microwave bonding methods, thermal-bonded and microwave-bonded samples were prepared from the same non-bonded powder. Since stirring plays an essential role in the microwave bonding process, four speeds were set to prepare microwave-bonded samples at the same temperature of 57°C. If the stirring speed is not high enough, sticky particles tend to form chunks and agglomerations in the cylinder. As seen in Fig. 7.3, the loaded powders became a giant solid bulk when the speed is 500rpm, resulting in a 100% sieve residue rate (120 mesh). Around 40wt% stripe-shape chunks were found when the stirring speed increased to 600rpm. This sieve residue rate is still too high for industrial production. After the stirring speed rising to 700 and 800rpm, the sieve residue rates are merely 8% and 0.5%, respectively. A further increase speed is not tested because it tends to bend Al flakes and break down bonded particles. Above all, considering to avoid material waste and reduce cost, 800rpm was adopted in the following microwave bonding processes.

Analysis of bonding quality

The influence of bonding temperature on the bonding and surface quality was studied after optimizing the stirring speed. At first, the deposited Al contents of these samples prepared at different conditions were determined as presented in Table 7.1. The deposited Al contents of the non-bonded sample range from 0.57 to 1.04% that reduces by about 63% compared to the original Al addition (2.33%), which reduces the metal shine obviously and causes a distinct

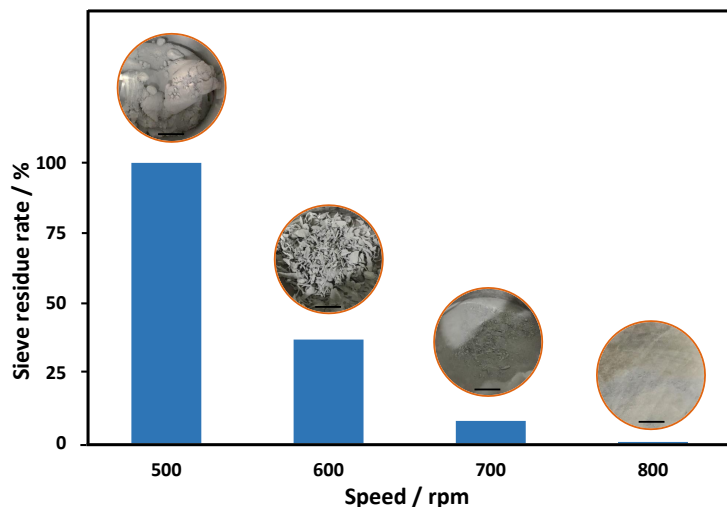


Figure 7.3: The sieve residue rates and pictures of microwave-bonded samples prepared at different temperatures. The scale bars are 10cm.

color change. After thermal bonding, the deposited Al contents increase by around 0.4% and get a bit closer to the Al addition, meaning higher metal shine and smaller color changes. However, after microwave bonding, the deposited Al contents raise by about 0.6% (55 and 57°C) and 0.9% (59°C). It is also found that the higher the microwave bonding temperature, the greater the deposited Al contents in the tested range. The deposited Al content is as high as 1.90% (59°C) that is much closer to 2.33%. A further higher temperature, 60°C, was tested, but it led to over-bonding and caking. Remarkably, it is clear that all the deposited Al contents are less than the original Al addition.

Table 7.1: Deposited Al contents (wt%) of non-, thermal- (TM), and microwave-bonded samples with low Al addition.

	Non	TM 62°C	55°C	57°C	59°C
30/6.5^a	0.57±0.06	1.20±0.01	1.57±0.02	1.58±0.02	1.86±0.01
60/6.5^a	0.90±0.07	1.31±0.05	1.63±0.06	1.65±0.01	1.86±0.02
60/5.5^a	1.04±0.00	1.46±0.03	1.75±0.07	1.65±0.02	1.90±0.05
90/6.5^a	0.91±0.07	1.35±0.04	1.64±0.05	1.66±0.04	1.90±0.02

^a The units for the voltage (30, 60, 90) and air supply (6.5, 5.5) are *kV* and *m³ h⁻¹*, separately.

A generally acceptable reason for this reduction of Al content after spraying is the difference of charge capacity between coating particle and Al flake. The maximum charge (Q_{max})

accumulated by a particle passing through an electric field could be estimated by the following equation [31]:

$$Q_{max} = 4 \pi r_e^2 \epsilon_0 E \frac{3\epsilon_r}{\epsilon_r + 2} \quad (7.4)$$

where r_e is the equivalent spherical radius; ϵ_0 is the permittivity of vacuum; E is the electric field strength; ϵ_r is the relative dielectric constant. The average equivalent spherical radius of adopted Al flake and coating particle approximately are $7\mu\text{m}$ and $33\mu\text{m}$, respectively. Calculating with published data [32, 33, 34, 35], it is found that the maximum charge of coating particle is about ten times more than that of Al flake. Thus, the coating particles capture more electrons or anions in the electrostatic spraying process, resulting in a high mass percentage of coating particles in the deposited powder. Meanwhile, the high aspect ratio of Al flake makes itself easy to be blown away during spraying. In brief, these reasons cause a lower deposited Al content than the original Al addition.

Bonding rates calculated with Eq. 7.2 are shown in Fig. 7.4. All the three microwave-bonded samples have higher bonding rates at the four spray conditions than the thermal-bonded sample ($\sim 32\%$). This means that microwave bonding is so efficient that it has relatively higher bonding quality, even at a much lower temperature. The samples bonded at 55°C and 57°C seem to have similar bonding rates of around 54% , but the one prepared at a higher temperature of 59°C obtains the highest bonding rates, $\sim 71\%$. As mentioned that 60°C led to powder caking and a high sieve residual rate, so 59°C was considered the optimal bonding temperature in the tested range. Overall, microwave bonding reaches an exceedingly high bonding rate of 71% which increases by 39% in contrast to that of thermal bonding ($\sim 32\%$). These results prove that microwave bonding obtains much better bonding quality over the present thermal bonding technology.

The bonding quality of powder samples have been investigated, so their SEM images were observed to analyze the microstructures and morphology of bondings, as illustrated in Fig. 7.5. The images of the non-bonded sample (Fig. 7.5A) describe the surfaces of the Al flakes are clean and smooth, meaning no bonding. As shown in Fig. 7.5B1, though several effective bondings are viewed in these yellow-circle areas, some separated Al flakes (dash-circle areas) and mis-bondings (black-circle areas) are also found. Fig. 7.5B2 exhibits the bondings of two

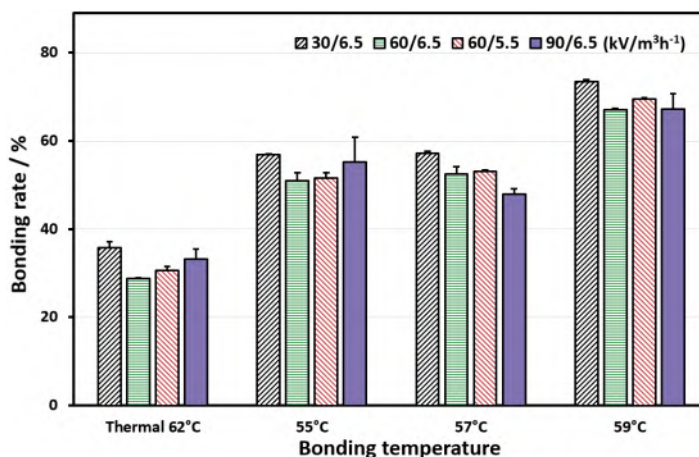


Figure 7.4: The bonding rates of microwave-bonded samples made at various temperatures.

Al flakes and a coating particle, but some small coating particles also stick on the surface of the big particle, indicating the existence of mis-bondings. The SEM images of the microwave-bonded sample (prepared at 59°C) shown in Fig. 7.5C1 presents a large number of effective bondings in these solid-circle areas and few separated flakes are found in these dash-circle areas. The zoomed-in image from the square area in Fig. 7.5C1 displays that three flakes adhere to the top, front, and back sides of a big particle, separately. To confirm the composition in Fig. 7.5C2, map and site EDS scanning have been conducted, and the results are displayed in Fig. 7.5D and E, respectively. The green and blue points separately stand for Aluminum and Titanium. The Titanium comes from the Titania that works as the inorganic pigment in the coating particle. EDS results prove that these bondings indeed form between Al flakes and coating particles. The D_{50} of the microwave-bonded powder (Fig. 7.5F) is found to be 46.14 μm which is close to that of thermal-bonded samples (45.04 μm).

Discussion of bonding temperature and composition

It is noted that the temperature of the microwave bonding (59°C) is relatively lower than that of the thermal bonding (62°C, close to T_g). As described in Introduction, this is believed to be the result of the heating-selectivity of the microwave. The ability of a material to absorb microwave can be described by the following equation [36]:

$$P = 2\pi f \epsilon_0 E^2 \epsilon''_{eff} \quad (7.5)$$

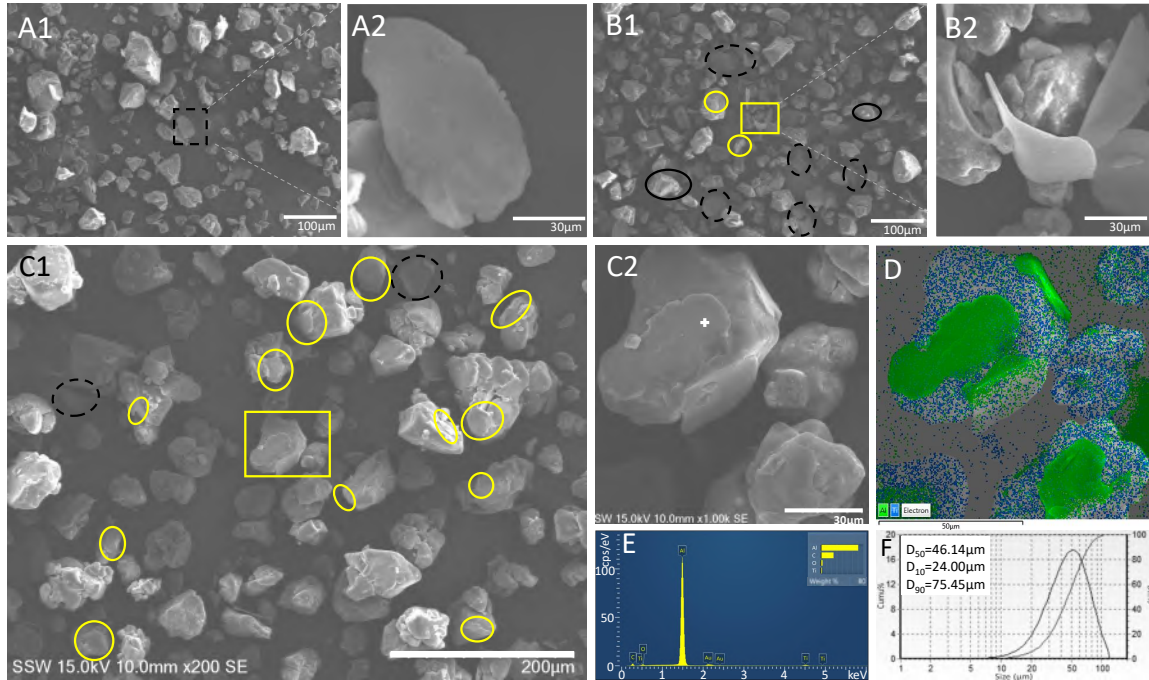


Figure 7.5: SEM, EDS and size distribution of the powder samples with low Al addition. A,B,C) SEM images of the non-bonded, thermal-bonded, and microwave-bonded powders, respectively; D) EDS mapping; E) EDS spectrum of the white point in C2 ; F) Size distribution.

where P is the microwave absorbing power per unit volume (W/m^3); f is the frequency of microwave (Hz); E is the electric field intensity (V/m); ϵ_0 is the permittivity of vacuum; ϵ''_{eff} is the effective dissipation factor of material. E and f can be regarded as constant when the microwave heating condition is the same, so a bigger value of ϵ''_{eff} will lead to a greater microwave absorption as well as a higher temperature.

When heating the mixture of nonmetal and metal particles, two main effects, interface and dipolar polarizations, contribute to the effective dissipation factor. The interface polarization occurs at the contacted surfaces of nonmetal and metal, while the dipolar polarization entirely comes from the nonmetal because metal reflects microwave (almost no absorption) [26]. Computations and experiments were both conducted to compare the two effects in the microwave bonding process.

According to Wagner's work, the effective dissipation factor of interface polarization between metal and nonmetal particles can be evaluated by Eq. 7.6 [37]. Sillars reported that the

relaxation time constant is able to estimated by Eq. 7.7 [38].

$$\epsilon''_{interface} = \frac{9 \nu \epsilon'_1 f_{max}}{1.8 \times 10^{10} \delta_2} \frac{2\pi f \tau}{1 + (2\pi f \tau)^2} \quad (7.6)$$

$$\tau = \epsilon_0 \frac{\epsilon'_1 + \epsilon'_2}{\delta_1 + \delta_2} \quad (7.7)$$

where ν is the volume fraction of conductive material; f_{max} in Hz is the frequency of maximum losses; δ is the conductivity in $S m^{-1}$ of the conductive phase; τ is the relaxation time constant; the subscripts 1 and 2 refer to non-conductive and conductive phase, respectively. After collecting parameter from published articles[39, 16, 40], $\epsilon''_{interface}$ is turned out to be around 0.08.

The effective dissipation factor for the dipolar polarization ($\epsilon''_{dipolar}$) of coating particle can be estimated by the equation as follows [41]:

$$\epsilon''_{dipolar} = \epsilon' \tan\delta \quad (7.8)$$

where ϵ' is the real part of dielectric constant of material; $\tan\delta$ is the loss tangent of material. By using the data from some reported researches [40, 42], the calculated $\epsilon'_{dipolar}$ is about 0.017 which is much smaller than the value of $\epsilon''_{interface}$ (0.08). Based on the Eq. 7.5, one can conclude that the interfaces will have a far faster microwave absorption and also a much higher heating rate.

Two comparative experiments were proceeded to study the effects of dipolar and interface polarizations on the heating rate. The same mass (10kg) of non-bonded powders and base coating particles were separately heated by microwave in the same condition. First, the non-bonded powder (a mixture of base coating particles and Al flakes) was heated by the microwave bonding machine. A fairly fast heating rate, around $11^\circ C/min$, was found. The microwave absorption mainly results from both interface and dipolar polarization in this trial. Second, the base coating particles (without Al flakes) were heated by the microwave bonding machine. The major microwave absorption is believed to be from dipolar polarization in this process, and the heating rate was only about $2^\circ C/min$. From the results of the above two experiments, the approximate heating rate only contributed by the interface polarization should be around

9°C/min, calculated by subtracting 2°C/min from 11°C/min. The heating rate from interface polarization is four times higher than that from the dipolar polarization, indicating that the dominant microwave absorption is from the interface polarization.

In summary, theoretic and experimental results manifest that the interfaces have a much higher heating rate over the other areas, such as non-touched and mis-touched areas (contacted surfaces between coating particles). Hence, It can be concluded that the interfaces already reach and exceed the T_g , but the other areas just achieve a much lower temperature ($<T_g$) in the microwave bonding process. The average temperature measured by the thermocouple is lower than the T_g consequently. This is the most crucial reason why microwave bonding has a lower bonding temperature than thermal bonding. Meanwhile, higher temperatures at the interfaces ($\geq T_g$) make the surfaces of coating particles sticky enough to firmly adhere to Al flakes and lead to better bonding quality. It is also worth to know that the heating rate of the thermal bonding machine ranges from 3 to 6°C/min. Compared to the thermal bonding method, the high heating rate of microwave bonding (11°C/min) has several key advances to the bonding process, such as improve bonding efficiency, reducing power cost, and achieving the high-temperature bonding easily. In a word, microwave bonding is a time-saving and effective method for producing metallic effect powder coating.

In order to study the effect of bonding processes on the compositions of powder coatings, the non-bonded (control), thermal-bonded and microwave-bonded (59°C) samples were characterized by FTIR, as seen in Fig. 7.6. The three spectra profiles are almost identical, proving that the two bonding processes cause little composition changes. Meanwhile, several characteristic transmittance peaks of polyester are observed, such as the stretching and bending frequencies of -OH at 3430 and 1171 cm^{-1} separately, the stretching frequency of C=O at 1718 cm^{-1} , the rocking frequency of -CH₂- at 1263 cm^{-1} , and the stretching frequencies of C-C and sutured C-H at 1101 cm^{-1} and 2955 cm^{-1} , respectively.

Analysis of stability of metal shine

After comparing the bonding quality of powders, the stability of metal shine of the films prepared from the non-bonded, thermal-bonded, and microwave-bonded powders was analyzed via color difference, as exhibited in Fig. 7.7. For simplicity, these films were separately called

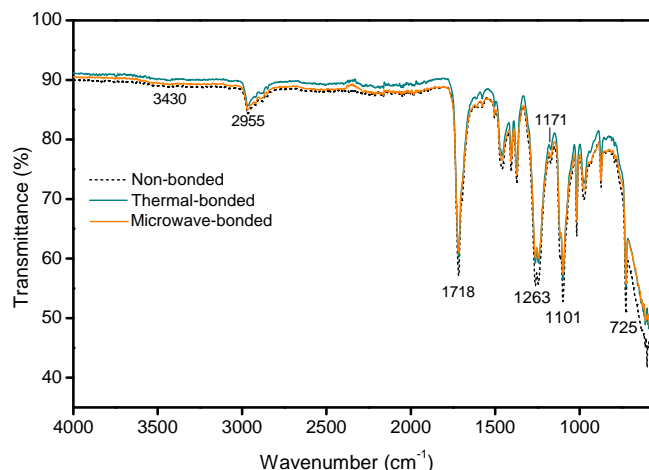


Figure 7.6: TIR spectra of non-bonded and microwave-bonded hybrid powder samples.

“non-bonded film”, “thermal-bonded film”, and “microwave-bonded film”. Table 7.1 shows the films with the highest deposited Al contents are the ones prepared at 59°C and sprayed at 90/6.5, so one of these films was chosen as the reference, and the color differences were then estimated, as seen in Fig. 7.7A. The non-bonded films have the highest color differences in the range of 5-6 and show inferior color stability. The color differences of thermal-bonded films reduce to 3-4 and exhibit a bit better color stability over the non-bonded film. The color differences of the microwave-bonded films at 55 and 57°C are both between 1.5-3. Moreover, the lowest color differences, 0-0.5, are viewed at the microwave-bonded sample prepared at 59°C. To summarize, the microwave-bonded films, especially bonded at 59°, have better color stability than the thermal-bonded ones. Also, the trend of color stability of films is in line with that of the bonding quality of powders, and a better bonding quality brings about a higher color stability.

To directly disclose the metal shine on the surfaces, the top and cross-sectional surfaces of the films were observed by an optical microscope as viewed in Fig. 7.8. These bright areas are the results of the light reflection by Al flakes under the observation of the optical microscope. It is evident that the Al flakes on the surface of the non-bonded film (7.8A1) are less than that of the thermal-bonded (7.8B1) and microwave-bonded (7.8C1) films. For a more accurate analysis, an image software (Image J) was adopted to evaluate the “Al area” defined as the percentage of Al flake area to the observed area. The result shows that the Al area of the non-

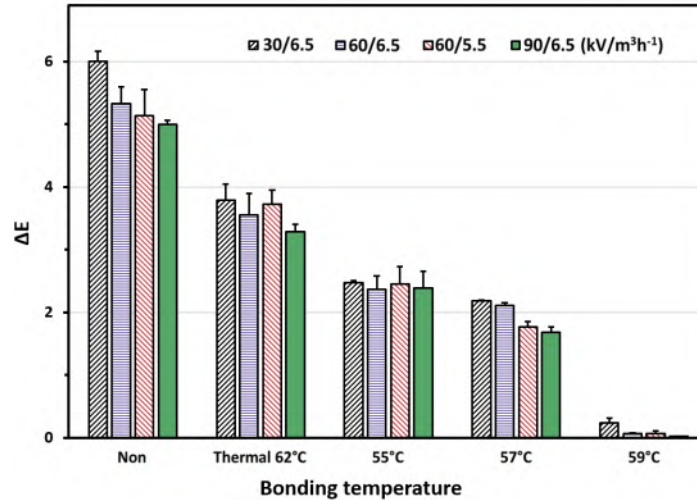


Figure 7.7: The color difference of the final films cured from different samples.

bonded film is as low as 6.6%, but it greatly increases to 12.5% after the thermal bonding. This increment implies that thermal bonding does obtain some effective binds. However, the Al area of the microwave-bonded film dramatically rises to 14.7% that is even 2.2% more than that of the thermal-bonded one. Meanwhile, the approximate numbers, per square millimeter, of Al flakes of the three films separately are 238, 468, and 664 as given in Fig. 7.8A2, B2 and C2. These results show a good match between the cross-sectional and top surface images. The images of the top and cross-sectional surfaces both indicate that microwave bonding has a higher metal shine over the thermal bonding.

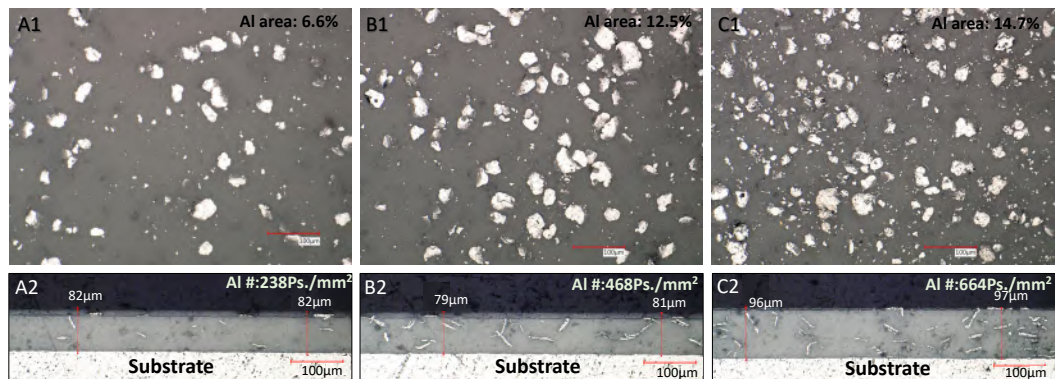


Figure 7.8: Optical images of the top surface (1) and cross-section (2) of the final films heat-cured from different powders. A) Non-bonded powder; B) Thermal-bonded powder; C) Microwave-bonded powder prepared at 59.5°C and 800rpm.

7.4.2 High addition of Al flakes

The bonding quality, color stability, and metal shine of the samples with low Al addition have been carefully analyzed, thus metallic effect powder coatings with relatively high addition of Al flake, aiming to produce an intense metal shine and high sparkling coating, were studied and discussed in this section. The precise Al addition is confirmed to be $4.94 \pm 0.07\%$ after three-parallel tests. The D_{10} , D_{50} , and D_{90} of this non-bonded sample is $13.86\mu\text{m}$, $34.88\mu\text{m}$, and $63.86\mu\text{m}$, respectively. Similar to the one with low Al addition, the thermal-bonded sample has a larger size, $D_{10}=15.38\mu\text{m}$, $D_{50}=39.47\mu\text{m}$, and $D_{90}=73.03\mu\text{m}$.

Analysis of bonding quality

The deposited Al contents of non-bonded, thermal-bonded, and microwave-bonded samples are compared in Table 7.2. The Al addition is 4.94% , but the deposited Al content merely are $0.82\text{-}1.51\%$ after spraying. The Al content decreases by around 75% that is even 12% more than the reduction with low Al addition (63%), indicating that more Al flakes needed to be bonded when the Al addition is high. This large reduction means that the metal shine is much less than it should be. The deposited Al contents of the thermal-bonded sample are around 3.0% that arises by around 1.6% with comparison to the non-bonded one. Similarly, the deposited Al contents of the three microwave-bonded samples increase when the bonding temperature is elevated. The highest deposited Al content is 3.51% when the bonding temperature and spray conditions are 60°C and $60/5.5$.

Table 7.2: Deposited Al contents (wt%) of non-, thermal- (TM), and microwave-bonded powders with high Al addition.

	Non	TM 62°C	55°C	58°C	60°C
30/6.5^a	0.82 ± 0.07	2.89 ± 0.34	2.11 ± 0.13	2.99 ± 0.04	3.36 ± 0.10
60/6.5^a	1.20 ± 0.21	2.85 ± 0.23	2.64 ± 0.03	3.16 ± 0.01	3.36 ± 0.03
60/5.5^a	1.51 ± 0.20	3.03 ± 0.10	2.70 ± 0.04	3.29 ± 0.12	3.51 ± 0.00
90/6.5^a	1.45 ± 0.14	3.14 ± 0.06	2.57 ± 0.06	3.23 ± 0.02	3.40 ± 0.05

^a The units for the voltage (30, 60, 90) and air supply (6.5, 5.5) are kV and $m^3 h^{-1}$, separately.

On the basis of these deposited and original Al content, bonding rates were evaluated and exhibited in Fig. 7.9. The bonding rates of the thermal-bonded sample are around 46% . When

bonding at 55°C by the microwave, the bonding rates are about 34% that is lower than the thermal bonding rates. The main reason is that this temperature is too low to attain enough adhesiveness and form effective bondings. However, two higher temperatures, 58 and 60°C, both have higher bonding rates over the thermal bonding. Furthermore, the highest bonding rate of these microwave-bonded samples is 62% (at 60°C) which is 16% higher than that of the thermal-bonded sample (46%). This implies that microwave bonding obtains a higher bonding quality over thermal bonding even when the Al addition is high. As discussed, the bonding rate increases by 39% after using microwave bonding when the Al addition is 2.33%, but there is just 16% increase when the Al addition is high. These numbers also suggest that bonding metallic effect powder coating with high Al addition is a much more difficult task than that with low Al dosage. Although it is a challenging work, microwave bonding still achieves better bonding quality over the thermal bonding. To sum up, the bonding temperature at 60°C is held as the best bonding condition in the tested range when the Al addition is high.

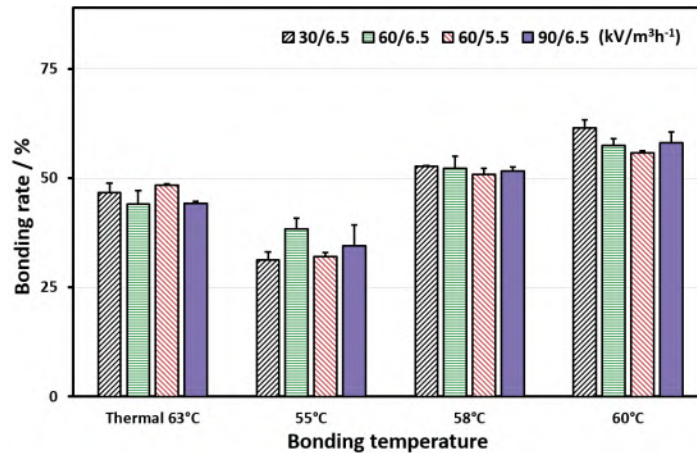


Figure 7.9: The bonding rates of microwave-bonded samples prepared at various temperatures.

Significantly, the heating rate approximately increased from 11 to 16°C/min as the Al addition increased from 2.33 to 4.94%. This dramatic high heating rate is mainly caused by the increased volume fraction of Al flakes. According to Eq. 7.5 and 7.6, a greater volume fraction (v) leads to bigger $\epsilon''_{interface}$ (~ 0.17) and P (microwave absorption). Therefore, the powders with high Al addition absorb more energy per unit of time and have a faster heating rate. This finding hints that the higher the Al addition, the faster the heating rate, and the less the processing time. On the contrary, when the Al addition is high, the processing time of the thermal bonding

might be a bit prolonged to try to ensure a high bonding quality.

SEM characterized the non-bonded, thermal-bonded, and microwave-bonded (at 60°C) powders, as shown in Fig. 7.10. More separated Al flakes are found in the images of the non-bonded sample compared to Fig. 7.5A. After thermal bonding treatment, some separated Al flakes (dash-circle areas) and effective bondings (solid-circle areas) are both found in Fig. 7.10B1. The magnified image shows that four small coating particles adhere to the front side of an Al flake. However, after microwave bonding, much more effective bondings are observable in these solid-circle areas in Fig. 7.10C1. The zoomed-in image (Fig. 7.10C2) from the squared area of 7.10C1 displays that several flakes stick on the surface of a big particle. And EDS results (Fig. 7.10 D and E) verify that these bondings indeed form between coating particles and Al flakes. In addition, the medium diameter of the microwave-bonded powder, 43.25 μm given in Fig. 7.10F, is slightly larger than that of the thermal-bonded one (39.47 μm).

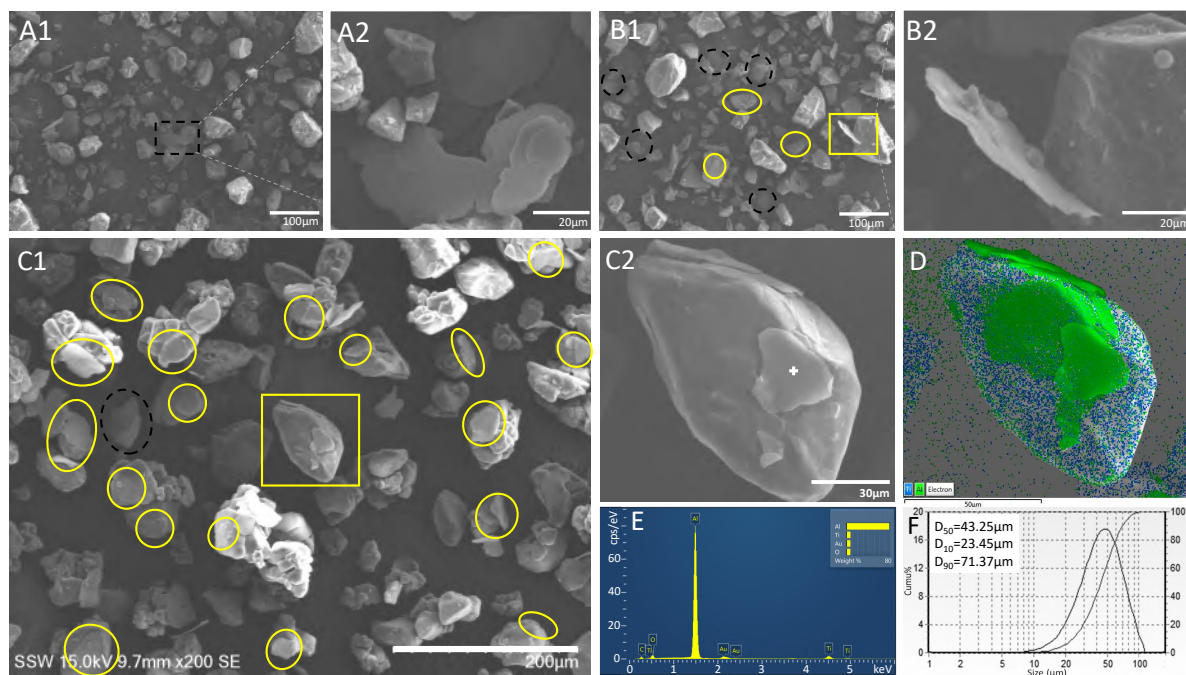


Figure 7.10: SEM, EDS and size distribution of the powder samples with high Al addition. A,B,C) SEM images of the non-bonded, thermal-bonded, and microwave-bonded powders, respectively; D) EDS mapping; E) EDS spectrum of the white point in C2 ; F) Size distribution.

Analysis of stability of metal shine

The color stability of the final films prepared from the non-bonded and bonded powders was estimated and analyzed as seen in Fig. 7.11. The reference for the color difference analysis is one of the microwave-bonded films prepared at 60°C and sprayed at $60\text{kV}/5.5\text{ m}^3\text{ h}^{-1}$. The non-bonded film has the biggest color difference because there are no binds. The color differences of the thermal-bonded films are around 2.5. However, the color differences of the three microwave-bonded films decrease from about 2.9 to 0.3 when the bonding temperature increases from 55 to 60°C. As it is known, a smaller color difference represents better color stability. Hence, it is believed that the microwave-bonded powder (made at 60°C) has the best color stability among these tested powders.

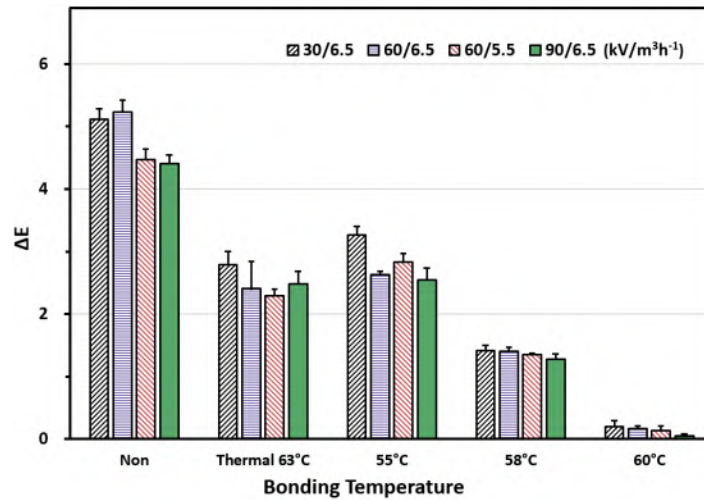


Figure 7.11: The color difference of the films prepared from various samples.

Fig. 7.12 presents the optical images of the top and cross-sectional surfaces of non-bonded, thermal-bonded, and microwave-bonded (60°C) films. The Al areas of the three films separately are 11.2%, 19.0%, and 22.8%, which increase by 5.6%, 6.5%, and 8.1% compared to those with low Al additions, respectively. The microwave-bonded sample owns a higher Al area over the thermal-bonded one, meaning microwave bonding obtains more intensive metal shine than thermal bonding. Moreover, the numbers of Al flakes, per square millimeter, in the cross-sections separately are 443, 825, and 1142. To summarize, these optical images testify that the microwave bonding method acquires higher metal shine over the thermal bonding.

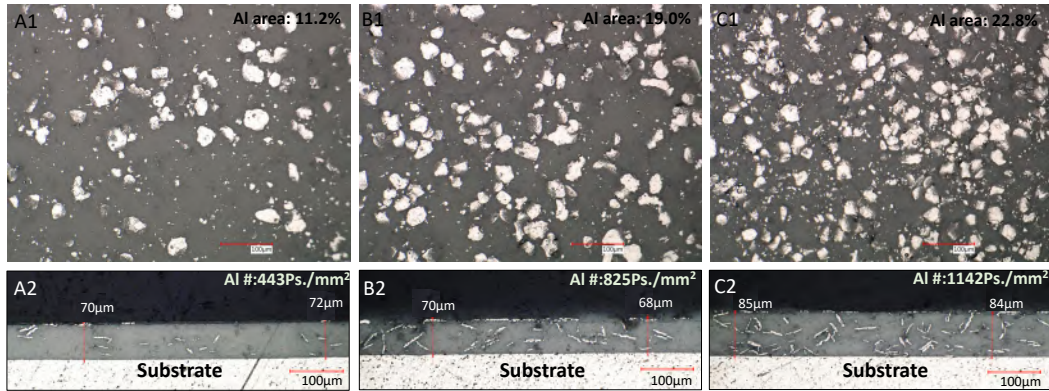


Figure 7.12: Optical images of top surfaces (1) and cross-sections (2) of the final films cured from different powders. A) Non-bonded powder; B) Thermal-bonded powder; C) Microwave-bonded powder prepared at 60°C and 800rpm.

7.4.3 Performances of films

The hardness, adhesion and impact resistance of non-bonded, thermal-bonded and microwave-bonded films were determined and compared in Table 5.6. No difference was found in the hardness and adhesion of these films except for the one prepared by microwave bonding with high Al addition (4.94wt%). Its hardness is one grade higher than the others, but its adhesion is one grade lower. The primary reason behind these changes is that this film contains a relatively higher content of Al flakes than the other one. The high content of Al flake enhances the film hardness by providing metal properties, but it correspondingly reduces the flexibility of the films because Al flakes block the interpenetrating resinous network. Besides, a declining trend was observed in the impact resistance after bonding treatments, which agrees with the changes of the Al content in these films. Accordingly, It is deduced that a film contains a higher Al content leads to lower impact resistance.

Table 7.3: The performances of non-bonded and bonded films with low and high Al additions.

		Hardness	Adhesion	Direct Impact
2.23wt% Al	Non-bonded	HB	5B	392 N·cm
	Thermal-bonded ^a	HB	5B	343 N·cm
	Microwave-bonded ^b	HB	5B	323 N·cm
4.94wt% Al	Non-bonded	HB	5B	352 N·cm
	Thermal-bonded ^c	HB	5B	157 N·cm
	Microwave-bonded ^d	F	4B	128 N·cm

Bonding temperatures separately are: a) 62°C, b) 59°C, c) 63°C, d) 60°C.

7.5 Conclusions

A novel preparation method, microwave bonding, for metallic effect powder coatings was investigated and discussed via a self-designed machine. The microwave bonding method shows great superiority over the present thermal bonding one. At both the low and high Al additions, microwave-bonded powder samples have better bonding quality over the thermal-bonded ones, and microwave-bonded films have higher color stability and metal shine than the thermal-bonded samples.

Taking advantage of the heating-selectivity of the microwave, the bond temperature of microwave bonding is 2-3°C lower than that of thermal bonding, and the heating rate of microwave bonding raises with the increase of the addition of Al flake. The heating rate of the metallic pigmented powder with low (2.33%) and high (4.96%) Al addition separately are about 11 and 16°C/min which are much higher than that of the thermal bonding. In conclusion, the microwave bonding method shows great potential to efficiently prepare metallic effect powder coatings with high and stable metal shine.

Bibliography

- [1] Jostein Mrdalen, John Erik Lein, Helene Bolm, Merete Hallenstvet, and Volker Rekowski. Time and cost effective methods for testing chemical resistance of aluminium metallic pigmented powder coatings. *Progress in Organic Coatings*, 63(1):49–54, 2008.
- [2] Zhongyan Du, Shaoguo Wen, Jihu Wang, Changle Yin, Dayang Yu, and Jian Luo. The review of powder coatings. *Journal of Materials Science and Chemical Engineering*, 4(3):54–59, 2016.
- [3] TA vd Misev and R Van der Linde. Powder coatings technology: new developments at the turn of the century. *Progress in Organic Coatings*, 34(1-4):160–168, 1998.
- [4] Eric Kirchner and Jacqueline Houweling. Measuring flake orientation for metallic coatings. *Progress in Organic Coatings*, 64(2-3):287–293, 2009.
- [5] Tengchao Guo, Guoyue Xu, Yanpeng Chen, Yong Jiang, and Shujuan Tan. Effect of Ni₂₀Cr alloy on infrared emissivity of inorganic silicate heat-resistant composite coatings. *Surface and Coatings Technology*, 288:46–51, 2016.
- [6] Chen Deng, Kuang-Hsu Wu, Jason Scott, Shenmin Zhu, Rose Amal, and Da-Wei Wang. Ternary mno/conn alloy@ n-doped graphitic composites derived from a bi-metallic pigment as bi-functional electrocatalysts. *J. Mater. Chem. A*, 7(36):20649–20657, 2019.
- [7] Kezhong Wang, Chaoxia Wang, Yunjie Yin, and Kunlin Chen. Modification of Al pigment with graphene for infrared/visual stealth compatible fabric coating. *J. Alloy. Compound.*, 690:741–748, 2017.
- [8] Yingchao Zhang, Hongqi Ye, Hui Liu, and Kai Han. Preparation and characterisation of aluminium pigments coated with silica for corrosion protection. *Corrosion Science*, 53(5):1694–1699, 2011.
- [9] Wei Liu, Jing Fu, Haiping Zhang, Yuanyuan Shao, Hui Zhang, and Jesse Zhu. Cold bonding method for metallic powder coatings. *Materials*, 11(11):2086, 2018.
- [10] TH Van Steenkiste, JR Smith, and RE Teets. Aluminum coatings via kinetic spray with relatively large powder particles. *Surface and Coatings Technology*, 154(2-3):237–252, 2002.
- [11] Douglas S Richart and Andrew T Daly. Thermosetting resin-based coating powders containing metal flakes, February 16 1993. US Patent 5,187,220.
- [12] SM Mahajan, A Varade Mayur, N Mahajan Pratiksha, and V Patil Sneha. Review on automotive body coating process. *Int. J. Eng. Manage. Res.*, 9(2):103–106, 2019.
- [13] Abdel Salam Hamdy Makhlouf and Yashwanth Gajarla. Advances in smart coatings for magnesium alloys and their applications in industry. In *Advances in Smart Coatings and Thin Films for Future Industrial and Biomedical Engineering Applications*, pages 245–261. Elsevier, 2020.

- [14] Yusuke Yasuda, Toshiaki Morita, Eiichi Ide, Hiroshi Hozoji, and Toshiaki Ishii. Low temperature bonding material comprising metal particles and bonding method, June 7 2011. US Patent 7,955,411.
- [15] Mark A Smith. Fusion bonded epoxy coating compositions that include magnesium oxide, March 25 2014. US Patent 8,679,632.
- [16] Jigar K Mistry, Jan Peter Frick, and James Petersen. Microwave bonding for coating compositions, July 6 2017. US Patent 15/463,131.
- [17] Marta Klanjšek Gunde, Matjaž Kunaver, Anton Hrovat, and Uroš Cvelbar. Bonding process efficiency and Al-flake orientation during the curing of powder coatings. *Progress in Organic Coatings*, 54(2):113–119, 2005.
- [18] Yasushi Takano. Metallic pigment and coating material containing the same, April 3 2008. US Patent App. 11/792,861.
- [19] Guangwen Wu and Demei Yu. Preparation and characterization of a new low infrared-emissivity coating based on modified aluminum. *Progress in Organic Coatings*, 76(1):107–112, 2013.
- [20] Keiichi Endoh, Aiko Nagahara, Yutaka Hisaeda, and Toshihiko Ueyama. Bonding material using metal nanoparticles coated with c6-c8 fatty acids, and bonding method, October 14 2014. US Patent 8,858,700.
- [21] Anne Kokel, Christian Schäfer, and Béla Török. Application of microwave-assisted heterogeneous catalysis in sustainable synthesis design. *Green Chem.*, 19(16):3729–3751, 2017.
- [22] Stefan Putz, Andreas Angerer, Dmitry O Krimer, Ralph Glattauer, William J Munro, Stefan Rotter, Jörg Schmiedmayer, and Johannes Majer. Spectral hole burning and its application in microwave photonics. *Nat. Photonics*, 11(1):36, 2017.
- [23] I Das and A Arora. Alternate microwave and convective hot air application for rapid mushroom drying. *J. Food Eng.*, 223:208–219, 2018.
- [24] Athira Raveendran, Mailadil Thomas Sebastian, and Sujith Raman. Applications of microwave materials: A review. *J. Electron. Mater.*, 48(5):2601–2634, 2019.
- [25] Hossam Mahmoud Ahmad Fahmy. Wireless sensor networks essentials. In *Wireless Sensor Networks*, pages 3–39. Springer, 2020.
- [26] AC Metaxas and Roger J Meredith. *Industrial microwave heating*. Number 4. IET, 1983.
- [27] Bing Lei, Man Li, Zhongxing Zhao, Lu Wang, Ying Li, and Fuhui Wang. Corrosion mechanism of an Al–BN abradable seal coating system in chloride solution. *Corrosion Science*, 79:198–205, 2014.

- [28] Wei Liu, Haiping Zhang, Yuanyuan Shao, Xinping Zhu, Yufu Wei, Hui Zhang, and Jesse Zhu. Applying microwave energy to fabricate powder coatings with strong and stable metal shine. *Progress in Organic Coatings*, 149:105929, 2020.
- [29] Alan R Robertson. The CIE 1976 color-difference formulae. *Color Res. Appl.*, 2(1):7–11, 1977.
- [30] Melda Isler Binay, Salih Kaan Kirdeciler, and Burcu Akata. Development of antibacterial powder coatings using single and binary ion-exchanged zeolite a prepared from local kaolin. *Appl. Clay Sci.*, 182:105251, 2019.
- [31] Daniel Goldwater, Benjamin Stickler, Lukas Martinetz, Tracy E Northup, Klaus Hornberger, and James Millen. Levitated electromechanics: all-electrical cooling of charged nano-and micro-particles. *Quantum Sci. Technol.*, 4, 2019.
- [32] Zhi-Min Dang, Tao Zhou, Sheng-Hong Yao, Jin-Kai Yuan, Jun-Wei Zha, Hong-Tao Song, Jian-Ying Li, Qiang Chen, Wan-Tai Yang, and Jinbo Bai. Advanced calcium copper titanate/polyimide functional hybrid films with high dielectric permittivity. *Adv. Mater.*, 21(20):2077–2082, 2009.
- [33] James D Christie and William C Howard. Bonded metal hydroxide-organic composite polymer films on particulate substrates, June 12 2001. US Patent 6,245,323.
- [34] DJ Suh, Ook Park, and KH Yoon. The properties of unsaturated polyester based on the glycolized poly (ethylene terephthalate) with various glycol compositions. *Polymer*, 41(2):461–466, 2000.
- [35] EMS Sanchez, CAC Zavaglia, and MI Felisberti. Unsaturated polyester resins: influence of the styrene concentration on the miscibility and mechanical properties. *Polymer*, 41(2):765–769, 2000.
- [36] Tetsuya Hanai. Dielectric theory on the interfacial polarization for two-phase mixtures. *Bull. Inst. Chem. Res., Kyoto University*, 39(6):341–367, 1962.
- [37] K Wagner. Explanation of dielectric polarization processes on the basis of maxwellian concepts. *Arch Electrotech.*, 2:371–87, 1914.
- [38] RW Sillars. The properties of a dielectric containing semiconducting particles of various shapes. *J. Inst. Electr. Eng.*, 80(484):378–394, 1937.
- [39] Motohiko Yoshizumi. Electroconductive powder and process for production thereof, June 5 1984. US Patent 4,452,830.
- [40] Hyoung Geun Kim et al. Dielectric cure monitoring for glass/polyester prepreg composites. *Composite Structures*, 57(1-4):91–99, 2002.
- [41] Lin-Feng Chen, CK Ong, CP Neo, Vasundara V Varadan, and Vijay K Varadan. *Microwave electronics: measurement and materials characterization*. John Wiley & Sons, 2004.

- [42] Kwong Siong Kiew, Sinin Hamdan, and Md Rezaur Rahman. Comparative study of dielectric properties of chicken feather/kenaf fiber reinforced unsaturated polyester composites. *BioResources*, 8(2):1591–1603, 2013.

8 The industrial-scale microwave bonding machine for metallic effect powder coating

8.1 Abstract

The lab-scale and pilot-scale data have proved that microwave bonding is feasible and effective. It can not only solve the inherent problems of the current commercial bonding technology but also provide better bonding quality and higher stability of metal color. Based on the previous work, an industrial microwave bonding machine, which is able to bond 100 kg metal effect powder coating in a single batch, was designed and manufactured with the help of Donghui powder equipment Co., Ltd. (Shandong, China). Some basic experiments have been done to optimize some parameters of the microwave bonding method in industrial production. The experimental results show that the heating rate of the powder is stable and can reach about 18 °C/min, and the metal color stability is better than that of the current commercial bonding machine.⁷

Keywords: Industrial-scale machine; Microwave bonding; Powder coating; Metal effect

⁷With minor editorial changes to fulfill formatting requirements, this chapter is to be submitted to *Coatings* with the title of “Industrial investigation on microwave bonding for metallic effect powder coatings”, Wei Liu, Yufu Wei, Hui Zhang, and Jesse Zhu.

8.2 Introduction

At present, the commercial bonding machine mainly relies on high-speed stirring to heat and bond metallic effect powder coatings, supplemented with water or oil jacket. When the temperature of powder loaded in the bonding tank reaches or close to the glass transition temperature (T_g) of coating particles, the temperature is maintained for 1-3 minutes. Bonded products will be obtained after the rapid cooling by transferring the heated powder to the cooling tank. Due to the design, the current commercial bonding machine mainly has the following problems [1, 2]: first, sticky coating particles are easy to bond with each other, forming mis-bonded particles; second, the high-speed stirring tends to bend and grind metallic pigments, which reduces metal shine; third, since the heating rate is relatively slow, it is difficult to realize high-temperature bonding, such as 120°C ; fourth, it is hard to achieve high bonding quality when the content of the metallic pigment is high (5-10 wt%); fifth, the temperature control system of high-speed stirring and jacket heating is too complex.

In view of the above problems, an industrial microwave-bonding machine was developed to solve the above problems. Compared to the current commercial bonding machines, it uses microwave as a heating source instead of friction heating. First, it will reduce mis-bonding by taking the advantage of selective heating of the microwave [3]. Our previous data have confirmed that there is a stronger microwave absorption at the interface between metallic pigment and coating particles than other areas, which means that the interface between them has a relatively higher temperature [4, 5]. As shown in Fig. 8.1, the contact areas of coating particles or metal pigments have less microwave absorption, but the interfaces between metallic pigments and coating particles have more absorption. Meanwhile, A higher temperature between coating particles and the metal pigment is exactly what the bonding process needs, so the mis-bonding can be greatly reduced.

When using the microwave to heat, the bending and breakage of metallic pigment can be reduced by decreasing the speed of stirring. However, the current commercial bonding machine requires high-speed stirring to heat. The reduction of the stirring speed of this machine protects metallic pigment from bending and damage but lowers down the heating rate at the same time. Especially when bonding coating particles with high T_g [6, 7], it needs an even higher heating

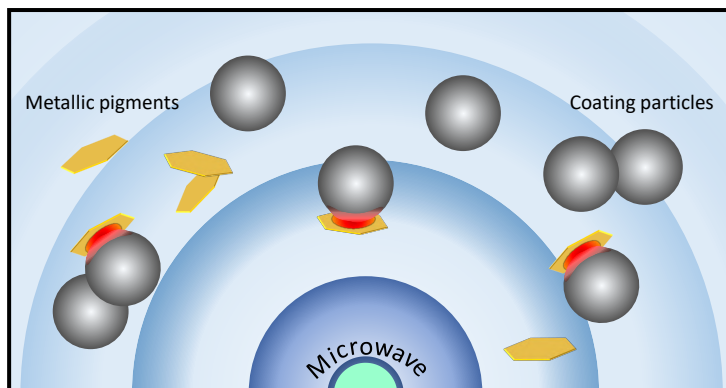


Figure 8.1: The selective heating of microwave bonding method.

rate to save production time. This of course leads to more bending and breakage of metallic pigment. Lots of present commercial machines equipped with water or oil jackets to help to heat, however, which increases the machine cost and complicates the temperature control system.

Microwave bonding machine is easy to reach high temperature by using the property of selective heating, such as 120°C . Moreover, the heating rate is quite even, fast and controllable. On the contrary, the current bonding technology must heat with the help of an oil jacket to reach such a high temperature. The heating rate is not only unstable but hard to control, and the oil jacket needs pre-heating. Microwave bonding machines avoid the above problems intrinsically by design.

Nowadays, the metallic effect powder coating usually contains less than 2 wt% metallic pigments to ensure bonding quality when produced by the current bonding machine. Once the content of the metallic pigment is too high, such as 5-10 wt%, it will largely increase the difficulty of bonding. The color difference will more likely happen when it comes to the high addition of metallic pigment. For instance, when the metallic pigment is only 1 wt%, the color difference is inapparent even if the bonding quality is not high. Conversely, when the metallic pigment increases to 5 wt%, the color difference will be very clear if the bonding quality is not high enough. Our previous results prove that microwave bonding can obtain higher bonding quality at both low and high content of metallic pigment.

The temperature control system of the commercial bonding machine is complex due to the mixed heating mode (high-stirring and jacket heating). The partial reason behind the high cost

of bonding machines is the software and hardware for the temperature control. Oppositely, one of the biggest advantages of the microwave bonding machine is the easy control of the temperature via tuning the power of the microwave. In addition, microwave heating can be stopped and started at any time.

In this work, the primary study of an industrial microwave bonding machine was conducted, such as the heating test, bonding quality, and color difference. The goal of this work is to optimize the bonding parameters of the industrial microwave bonding machine for metallic effect powder coatings.

8.3 Materials and methods

8.3.1 Materials and equipment

Aluminum flakes (PCU 3500 and PCU 1000) from Eckart ECKART GmbH (Germany) was used as the metallic pigment; Polyester and PVDF powder paint and from Huajiang Powder Coating Co. (Guangdong, China) served as base powder coating; Nano alumina oxide (AluC) from Evonik Resource Efficiency GmbH (Germany) worked as flow promoter; An electrostatic automatic spraying system with a corona spray gun from Gema Switzerland GmbH (St.Gallen, Switzerland) was applied to spray powders. Al panels (15cm in length, 7.6cm in width) from Huajiang Powder Coating Co. (Guangdong, China) were utilized as substrates.

An electrostatic automatic spraying system with a corona spray gun from Gema Switzerland GmbH (St.Gallen, Switzerland) was applied to spray powders. A commercial bonding machine (SHT-500/1000) from Sun-hitech Technology Co., Ltd. (Xiamen, China) was used to produce thermal-bonded samples. A laser particle size analyzer (LS-POP6) from Omec Instruments Ltd. (Zhuhai, China) was utilized to analyze the size distributions of powdered samples. A Scanning Electron Microscope (SEM) (SU3500) with energy dispersive spectrometer (EDS) from Hitachi Limited (Tokyo, Japan) was employed to observe the bonding situation between Al flake and coating particle. A colorimeter (CI62) from X-rite Inc. (Michigan, USA) was used to evaluate the color difference of final films.

The precise color difference between the films prepared at spraying gas pressures of 1 and 3 bar was analyzed by the following steps: (a) take the color at central area of film prepared at 1 bar as the reference; (b) determine the color difference of the film prepared at 3 bar by testing

four areas as shown in 8.2. The color difference can be calculated by 6.4:

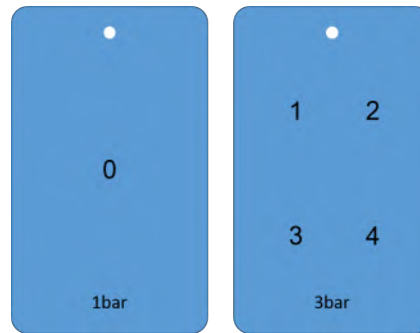


Figure 8.2: The tested area of the films prepared at 1 and 3 bar.

8.3.2 Industrial microwave bonding machine

The self-designed industrial microwave bonding machine is shown in Fig. 8.3, which is capable of bonding 100 kg metallic effect powder coating per batch. The machine is mainly composed of a feeding port (1), 30 microwave transmitters (2, under the shell), a heating tank (3), a cooling tank (4), and a discharging port (5). In addition, it also includes a heating tank motor, cooling system for microwave transmitters, pneumatic valve, mixing blade, automatic temperature control system, control box, water cooling jacket, nitrogen protection, oxygen content detector, cold air system, etc. The power of each microwave transmitter is adjustable in the range of 10-1000 W. The operation mode is divided into automatic and manual modes. In the automatic mode, the machine automatically performs heating, heat preservation, discharging, and cooling operations according to the set temperature and preservation time. The machine is equipped with a temperature control system, which will automatically reduce the power of the microwave generator when it is close to the set bonding temperature.

A four-layer agitator was installed inside the bonding tank to mixing powder as presented in Fig. 8.4. There is a nitrogen inlet at the bottom of the agitator. The nitrogen goes through the whole bonding chamber and exits from the top outlet, and then the oxygen content of the exhaust gas is measured. Microwaves can only be turned on when the oxygen content is less than 5 vol%. In order to prevent the blade from overheating during bonding, there is a cooling system inside the agitator. To clean the bonding tank easily, the agitator blades are detachable. Two temperature probes are applied to (red circle) monitor the real-time temperature of

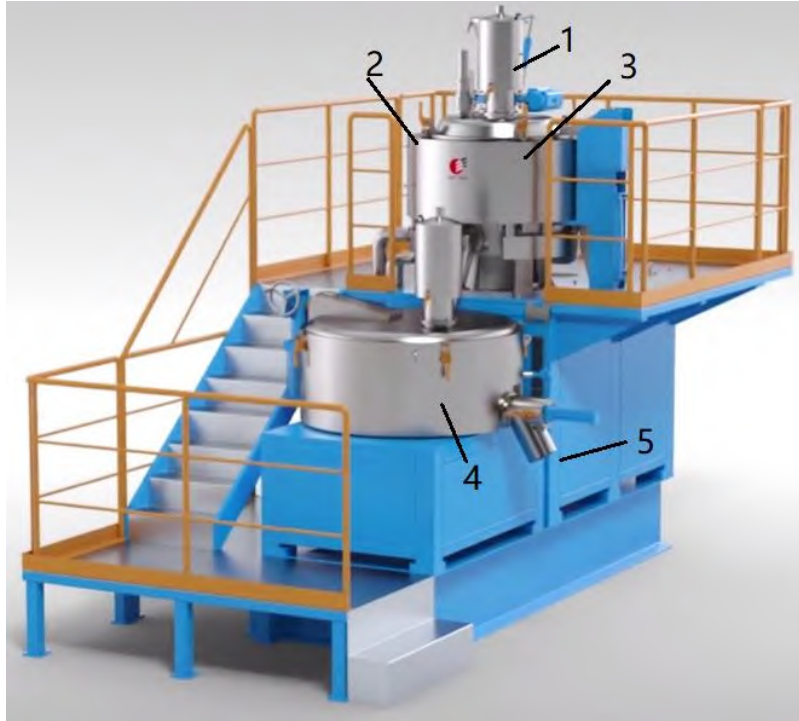


Figure 8.3: The picture of the industrial microwave bonding machine.

the powder inside the chamber with an accuracy of 0.1 °C. Microwave generators are evenly distributed on the outer wall of the mixing tank, and then a cylindrical metal shell is put on the outer layer of the microwave transmitters to prevent microwave leakage.



Figure 8.4: The four-layer agitator inside the bonding tank.

The control panel, shown in Fig. 8.5, monitors and adjusts the whole bonding process. A touch-sensitive screen makes the bonding operation easy. The upper side of the panel is the

display of current, voltage, and temperature inside the chamber; the right side of the control panel is the controller of stirring speed; the bottom ones are a series of instrument switches and an emergency stop button.



Figure 8.5: The control panel of the industrial microwave bonding machine.

8.4 Results and discussion

8.4.1 Heating test

Heating of PVDF metallic effect powder coating

At first, some basic functions of the industrial-scale microwave bonding machine were tested, such as heating property, stirring speed, nitrogen protection system, temperature measurement, etc. Here, a type of powder coating with high T_g of around 115°C , PVDF, was heated by the machine. Due to the consumption of powder is as high as about 100 kg for one test, only limited tests have proceeded. The non-bonded PVDF metallic effect powder coating (90kg PVDF and 2kg PCU3500 Al flakes) was heated by the machine through the manual model. The effect of stirring speed and microwave power on the heating rate were analyzed and discussed.

The heating process:

1. Add the non-bonded PVDF metallic effect powder coating into the bonding tank until the powder just covers the top blade and close the lid;
2. Introduce nitrogen into the bonding tank from the bottom and adjust the stirring speed to 200 *rpm*;
3. Switch on microwave transmitters when the oxygen content is reduced to below 5 vol%, and then raise the stirring speed to 502 or 837 *rpm*
4. Record the temperature and current during the heating process and the total time needed to reach targeted temperature;
5. Turn off microwave when reaching the targeted temperature and discharge the powder to the cooling tank.

As shown in Table 8.1, the heating rate is 1.2 °C/min without microwave radiation. This temperature rise is mainly caused by the friction heat from the stirring. The heating rate increases along with the increase of microwave power. When the power is kept at 0.8 kW, the heating rate of the two tests (40-65 and 40-90°C) are both around 6.2 °C/min, indicating that the heating rate of the machine is relatively stable at different temperatures. In addition, the heating rate can be as high as 8.3 °C/min, which is much higher than that of pure stirring.

Table 8.1: The heating data of PVDF metallic effect powder coating.

Stirring speed/ <i>rpm</i>	502					837
	0	0.3	0.5	0.8	0.8	1.0
Power/kW						
Current/A	~34	~34	~35	~35	≤40	≤60
Initial temperature/°C	33	39	40	40	40	34
Final temperature/°C	41	64.5	65	65	90	100
Heating duration/min	5	12.5	5	4	8.5	8
heating rate/(°C/min)	1.2	2.0	5.0	6.3	6.1	8.3

To further analyze the accurate relationship between microwave power and heating rate, the curves of them at the same stirring speed (502 *rpm*) were drawn in Fig. 8.6. The test at 0.3 kW was excluded due to some technical problems. The total heating rate, coming from microwave and friction heat, is proportional to the microwave power (blue patterns). Excluding the friction heat, the heating rate of the microwave is about 6.72 times the power of the microwave (red

line). To further enhance the heating rate, increase the microwave power and the number of microwave transmitters are both effective options.

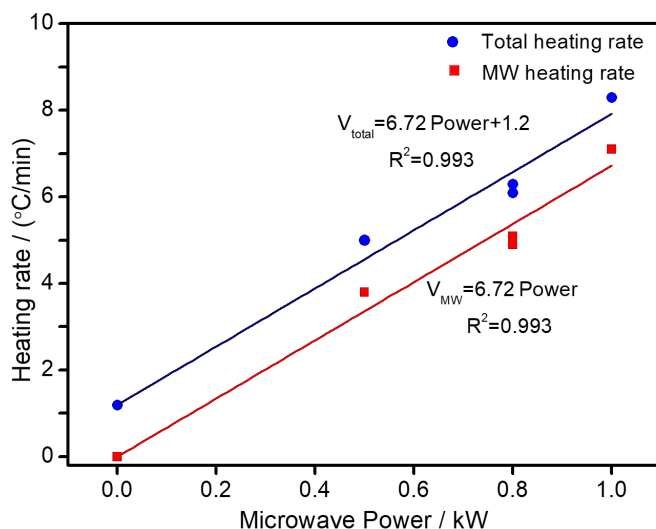


Figure 8.6: The relationship between power and heating rate of the machine.

After the test, there was almost no residual powder on the inner wall of the bonding cylinder, and no agglomerated powder was found, but some small agglomerates are found at the end of the mixing blade and temperature probes. This means that the powder is stirred evenly and uniformly. These slight agglomerations may be caused by the heat accumulation due to the restricted local heat transfer of the powder. In the low-temperature stage (25-60°C), the temperature difference between the two probes is small, about 1-3°C. When the temperature rises to 100°C, the temperature difference has reached 10°C, which is mainly due to the fewer up-down and internal-external circulations of the loaded powder. Above all, these results show that the main performances of the machine, such as heating and stirring, meet our expectations, and the heating rate is significantly higher than that of the current bonding machine. At the same time, the machine also has some minor problems, which need to be further improved.

Heating of polyester metallic effect powder coating

Based on the above results, the cooling water system and stirring blades of the machine were improved. Specifically, the stirring blades were modified according to CFD simulation results in Chapter 9. Two-thirds of the blades were reversely folded. After the modification, the temperature difference of the two probes reduced to <5°C, which is much lower than the

original gap (10°C), implying the blade modification improves the stirring uniformity effectively. Then, the second heating test was carried out by using about 100 kg polyester powder coating (T_g is 66°C), 0.4 kg PCU1000 and 0.6 kg PCU3500 Al flakes. According to the heating results, the power of a single microwave transmitter was set to 0.8 kW, and the heating data of the machine are given in Table 8.2.

Table 8.2: The heating data of polyester powder coating.

Stirring speed/ <i>rpm</i>	285	71	126	258	335
Power/kW	0	0.8	0.8	0.8	0.8
Current/A	~41	~25.1	~21.9	~36.4	~37.1
Initial temperature/°C	30.3	28	29.8	41.1	38.8
Final temperature/°C	45	53.7	45.1	50.4	55.8
Heating duration/min	9	1.5	1	1	0.5
Heating rate/(°C/min)	1.6	17.1	15.3	18.6	17.0

When there is no microwave, the heating rate is only 1.6 °C/min, which is slightly lower than that of the first test at 502 *rpm* due to the lower stirring speed (285 *rpm*). The heating power was fixed at 0.8 kW, and the effect of different stirring speeds on the heating rate was investigated. The results show that the heating rate of microwave is much higher than that of pure stirring. Moreover, stirring speed has a small impact on microwave heating. The average heating rate of the powder coating is 16.1 °C/min, and the maximum heating rate from the microwave is about 17 °C/min. Compared to the first heating data of PVDF, the heating rate of polyester is much faster. This might be due to the improvement of the machine and different effective dissipation coefficients between the two powder coatings. Such a fast heating rate is very helpful to shorten the bonding process time and improve production efficiency.

8.4.2 Bonding test

Because of the large consumption of powder, the experiment was carried out in the way of industrial production and experiment. The non-bonded powder contains 98 kg polyester powder coating and 2 kg PCU3500 Al flakes. Additionally, 0.15 wt% (5013) of bonding agent was added before bonding, and 0.2 wt% (AluC) was introduced after bonding.

Comparison of bonding machine parameters

The non-bonded powder was simultaneously bonded by a commercial machine (SHT-500/1000) and a microwave bonding machine. The difference in bonding quality between the two

machines can be directly compared in this way. Table 8.3 shows the basic parameters of the two bonding machines. To cool down powder rapidly, the volume of the cooling tank is usually two times that of the bonding tank. The production capacity of the commercial machine is 200 kg that is two times that of the microwave bonding machine. The capacity and power can be used to calculate the energy consumption.

Table 8.3: Some basic parameter comparisons between the commercial and microwave bonding machines.

Parameters	Commercial	Microwave
Volume of bonding tank/L	500	260
Volume of cooling tank/L	1000	475
Capacity/(kg/batch)	200	100
Power of stirring (bonding)/kW	37	37
Power of stirring (cooling)/kW	11	5.5

Bonding conditions

The commercial and microwave bonding processes both start with heating powder to a certain temperature, then keep at this temperature for several minutes, and end with rapid cooling down. The operation conditions of the two bonding machines are listed in Table 8.4. The bonding temperature of the commercial machine is 66°C, but that of the microwave machine is only 59.5°C. The reason behind this is the selective heating of microwaves on the interface of coating particles and Al flakes. Since the bonding temperature of microwave machines is lower, the stirring speeds of microwave machines are slightly lower than that of the commercial machine.

Table 8.4: Comparisons of bonding parameters between commercial and microwave machines.

Conditions	Commercial	Microwave
Bonding temperature/°C	66	59.5
Stirring speed of heating/(rpm)	636	602
Stirring speed of holding/(rpm)	636	602
Stirring speed of cooling/(rpm)	70	70

Bonding temperature vs. process time

Bonding temperature is the most important factor during the bonding process. Fig. 8.7 presents the powder temperature change over time of the two machines. The blue curve (commercial) shows that the heating phase lasts about 11 minutes and the average heating rate is 3.7

°C/min, and the temperature of the holding phase slightly fluctuates around 66°C for 5 minutes, and the cooling phase is about 9 minutes. The red curve (microwave-0.5kW) indicates that the heating rate is about 8.8 °C/min, and the holding phase lasts 8 minutes and the cooling phase is just 3 minutes. Comparing the two curves, it is easy to find that the microwave machine has a much higher heating rate at the heating phase and a shorter process time than the commercial machine.

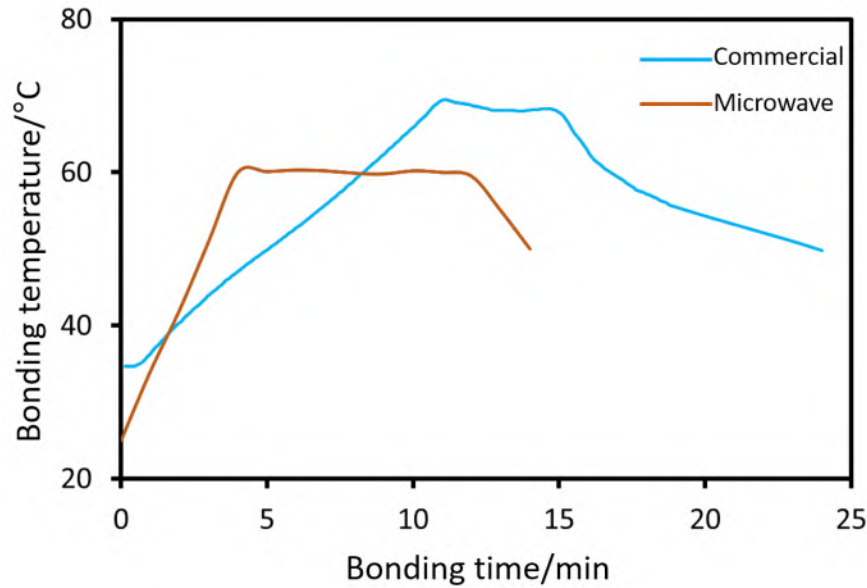


Figure 8.7: The real-time temperature in commercial and microwave bonding machines along with process time.

Productivity and energy consumption

At first, the productivity of the two bonding machines is calculated according to the above parameters. Although the capacity of the microwave machine is 100 kg that is less than the commercial one, the bonding time is only 11 minutes. The productivity of the microwave machine is 0.52 t/h. Meanwhile, the capacity of the commercial machine is 200 kg and the bonding duration is 24.5 minutes, and the productivity is about 0.49 t/h. The energy consumption is evaluated by the current and power presented in Table 8.5. The energy consumption of stirring (E_{stir} , kWh/t) can be calculated by the following equation:

$$E_{stir} = \frac{UIt}{1000m} \quad (8.1)$$

where, U is the voltage of motor (both are 380 V); I is current, unit is A; t is time, unit is h; m is powder mass, unit is ton.

The energy consumption of microwave (E_{MW} , kW) can be estimated by the following equation:

$$E_{MW} = \frac{nPt}{m} \quad (8.2)$$

where, n is the number of microwave transmitters; P is the power of each microwave transmitter, unit is kW. The total energy consumption ($E_{stir}+E_{MW}$) of commercial and microwave machines are 41 and 37 (kWh/t), respectively. The energy consumption of microwave bonding machine can be further reduced if the capacity increase to 200 kg.

Table 8.5: Parameters of heating, holding and cooling.

	Commercial bonding			Microwave bonding		
	Heating	Holding	Cooling	Heating	Holding	Cooling
Current/A	59	46	50	45	31	35
Stirring duration/min	11	4.5	9	4.5	5	1.5
Power/kW	0	0	0	2.6	5	0
MW heating duration/min	0	0	0	0.8	0.01	0
Energy consumption/(kWh/t)	41			37		

Comparison of particle size distributions of bonded samples

Fig. 8.8 shows the particle size distributions of non-bonded, commercial-bonded, and microwave-bonded samples. The medium diameter of the non-bonded powder is 28.35 μm . The medium size slightly increases to 29.51 and 30.03 μm after commercial and microwave bonding, respectively. The medium size of the two bonded powders is very close, but the D_{10} and D_{90} of the two bonded samples are quite different. The D_{10} of the non-bonded sample is 11.15 μm , which increases by 0.6 μm after commercial bonding. Remarkably, the D_{10} largely raises by 3.5 μm after microwave bonding. This big D_{10} means small particles are highly reduced after microwave bonding, which effectively improves the flowability and spraying of the powder coating. While the D_{90} of the microwave-bonded sample (52.71 μm) is less than that of commercial-bonded one (54.06 μm), illustrating that there are fewer mis-bonded particles in the microwave-bonded sample.

The span of particle size distribution can be calculated by Eq. 8.3. The smaller the span,

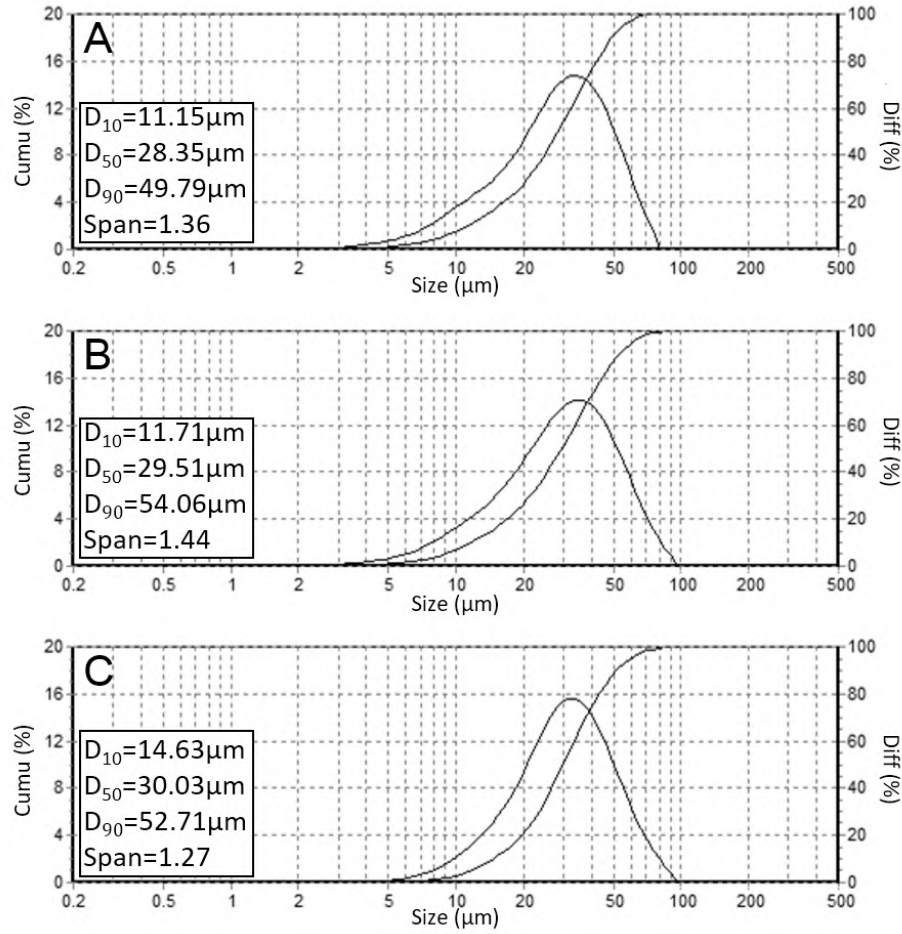


Figure 8.8: The particle size distribution of non-bonded and bonded samples. A) non-bonded; B) commercial-bonded; C) microwave-bonded.

the better the powder flowability, and the smoother the final film.

$$Span = \frac{D_{90} - D_{10}}{D_{50}} \quad (8.3)$$

The span of the non-bonded powder is 1.36, which increases to 1.44 after commercial bonding. This is mainly because commercial bonding leads to more mis-bonded particles. Reversely, the span of the microwave-bonded powder reduces to 1.27, meaning that the particle size distribution is more narrow than the other two samples. Overall, the span increases after commercial bonding but decreases after microwave bonding.

Bonding quality

After analyzing the particle size distributions of the three samples, the final films were prepared after spraying and curing as viewed in Fig. 8.9. Each sample was sprayed at 1 and 3 bar to judge the bonding quality. The final films show a sparkling effect after adding Al flakes. As the color of the base powder is gray, the more Al flake on the surface, the less gray the surface. The color of the films prepared from non-bonded powder (A1 and A2) is slightly darker, indicating that the Al contents in the films are less than those of the other four films.



Figure 8.9: The images of films prepared at 1 and 3 bar from different powders. A) non-bonded; B) commercial bonded; C) microwave bonded.

The color differences of the films prepared at 1 and 3 bar are summarized in Table 8.6. When spraying metallic effect powder coating, the color difference is required to be less than 1.5 (1.5 is usually the lowest level that can be distinguished by the naked eye). Furthermore, the color difference should be less than 1.0 when coming to more strict requirements. Without bonding, the color difference of the two films is 2.07. After commercial bonding, the color difference unexpectedly increases to 3.87. However, after microwave bonding, the color difference is only about 0.96, proving that the color stability is very high. This small color difference (<1) also provides side evidence for qualified bonding quality.

Table 8.6: The color difference between films prepared at 1 and 3 bar.

	1	2	3	4	Ave.
Non-bonded	1.44	2.20	2.90	1.77	2.07±0.63
Commercial	3.17	4.51	3.67	4.11	3.87±0.58
Microwave	1.14	0.77	1.10	0.85	0.96±0.18

8.5 Conclusions

The industrial microwave bonding machine meets the expected requirements. The heating rates of PVDF and polyester metallic effect powder coating are about 8.3 and 18 °C/min, respectively. The heating rate is proportional to the microwave power and is almost not affected by the stirring speed. The heating rate is stable in the whole temperature range and can be easily controlled within the allowable range. The energy consumption of microwave bonding machines is slightly lower than that of the commercial machine, and the productivity is slightly higher. After microwave bonding, the particle size distribution of powder becomes narrow. The color difference of the films obtained from the microwave-bonded sample meets the industrial requirements. In conclusion, microwave bonding machine obtains better bonding quality and consumes less energy as well as provides higher productivity.

Bibliography

- [1] Mark A Smith. Fusion bonded epoxy coating compositions that include magnesium oxide, March 25 2014. US Patent 8,679,632.
- [2] Jigar K Mistry, Jan Peter Frick, and James Petersen. Microwave bonding for coating compositions, July 6 2017. US Patent 15/463,131.
- [3] Jostein Mrdalen, John Erik Lein, Helene Bolm, Merete Hallenstvet, and Volker Rekowski. Time and cost effective methods for testing chemical resistance of aluminium metallic pigmented powder coatings. *Progress in Organic Coatings*, 63(1):49 – 54, 2008.
- [4] AC Metaxas and Roger J Meredith. *Industrial microwave heating*. Number 4. IET, 1983.
- [5] T Prodromakis and C Papavassiliou. Engineering the maxwell–wagner polarization effect. *Applied Surface Science*, 255(15):6989–6994, 2009.
- [6] Badr-Eddine El Mohajir and Nicole Heymans. Changes in structural and mechanical behaviour of pvdf with processing and thermomechanical treatments. 1. change in structure. *Polymer*, 42(13):5661–5667, 2001.
- [7] R Gregorio and EM Ueno. Effect of crystalline phase, orientation and temperature on the dielectric properties of poly (vinylidene fluoride)(pvdf). *Journal of materials science*, 34(18):4489–4500, 1999.

9 The optimization of impeller blade by CFD simulation

9.1 Abstract

In this work, CFD simulation is used to optimize the shape of the impeller blades in microwave bonding machines. The powder coating tends to agglomerate due to uneven and nonuniform stirring during the microwave bonding process, resulting in many wastes of raw materials. Therefore, modifications (parts of the blades were reversely angled in different sections on each blade arm) on these blades were made and CFD simulation was applied to find an impeller configuration that can provide better stirring uniformity. The results show that the blade with reversely angled sections obtains higher average, radial, and axial velocity than the unmodified one, which leads to better internal circulation of powders in the bonding tank. This new type of blade can provide better stirring efficiency and reduce powder agglomeration during bonding.⁸

Keywords: CFD simulation; Impeller modification; Powder coating; Stirring.

⁸With minor editorial changes to fulfill formatting requirements, this chapter is to be submitted to *Surface and Coatings Technology* with the title of “Optimization of impeller blades by CFD numerical simulation”, Wei Liu, Zhengyuan Deng, Hui Zhang, and Jesse Zhu.

9.2 Introduction

At the beginning of the pilot-scale bonding research, it was found that the powder tends to agglomerate possibly related to unsatisfactory impeller design. Many hard lumps of powder were found at the bottom of the bonding tank due to uneven stirring. As a result, significant amount of raw materials was wasted and much time was consumed to clean the machine. This problem becomes pronounced in the pilot-scale and industrial experiments. Considering the large consumption of powders, it is difficult to optimize the impeller blade by physical experiments for each test. Therefore, this work proposes to optimize the blade shape by CFD simulation to save materials and time. The calculated results were then testified by experiments.

The main purpose of the blade is to strengthen the internal circulation of the powder, which ensures the powder absorbs microwave uniformly [1]. Although the microwave has certain penetrability to heat the inside powder, the outside powder still has a higher microwave absorption, causing temperature differences between the outside and inside powders [2, 3]. Therefore, the powder needs to circulate rapidly in the bonding tank during microwave bonding.

An proper impeller blade configuration is very important to the motion of powders in industry, but most of the simulation is focused on the optimization of a liquid stirrer [4, 5]. Some works for simulating the stirring of coarse particles ($>1000\ \mu\text{m}$) were reported, while very few work on the optimization of blades for small particles ($<50\ \mu\text{m}$) were reported [6, 7]. Micale and coauthors designed a small and one-stage impeller to mix particles ($100\text{-}1000\ \mu\text{m}$) with a turbine impeller. The comparison between the experimental data and the fluent simulation results shows that the modeling technology can precisely predict the formation of the transparent layer on the upper layer of the vessel, and the simulation results almost quantitatively reproduced the expansion process of the layer [8].

In this study, some modifications, such as reverse angling and different inclination angles of the blade, were made on the conventional blade to improve the stirring ability. Six impellers with different blade configurations were simulated and calculated. The blade stirred the air and powder in a sealed tank at a certain speed. The movement of powders was analyzed by the particle concentration and velocity distribution in the tank. The numerical results illustrate that the internal circulation is relatively better after the modification. Also, the physical experiments

found that the modified impeller led to a more uniform temperature distribution during the microwave bonding.

9.3 Numerical simulation

9.3.1 Geometry and mesh

The DesignModeler was used to build the three-dimensional configurations of the impellers. The diameters of the bottom, middle, and top blades are 300, 312, and 312 mm, and their distances to the tank bottom are 6, 100, and 190 mm, respectively. The thickness and width of these blades are 5 and 20 mm. Every blade is detachable and the height of these shaft sleeves is 5 mm. The height and radius of the tank are 300 and 172 mm. The diameter of the shaft is 40 mm. The impeller and tank are combined by Boolean operations, and the tank is formed by Sweep. The top blades are not inclined, and the inclination angle of the middle blades is always 10 degrees, while the bottom blade has two inclination angles of 10 and 20°. In addition, a part of the bottom and mid blades were reversely angled. The unmodified (10d-0 and 20d-0) and the modified impellers are shown in Fig. 9.1.

Three rotational regions were defined as given in Fig. 9.2. The rotation type of the three regions is meshed motion during the solving. The height of each area is 20 mm and the diameters (from top to bottom) are 164, 164, and 160 mm, respectively. These regions just cover the three blades as exhibited in Fig. 9.2. Five lines are marked, as viewed in Fig. 9.2b, near the blades for analyzing the particle velocity and volume fraction.

The finite element of the above models was built in Mesh via the automatic tetrahedron method. The main grid size is 0.010 m, and the grid size of the interface of the rotational and static regions is set to 0.0073 m. The total number of the grid is about 500,000. The mesh of the tank and rotational regions are presented in Fig. 9.3.

9.3.2 CFD model

RNG k - ε model

In this study, CFD software Fluent is used for performing 3D two-fluid model (TFM) simulations closed by the kinetic theory of granular flow (KTGF). The governing equations listed in

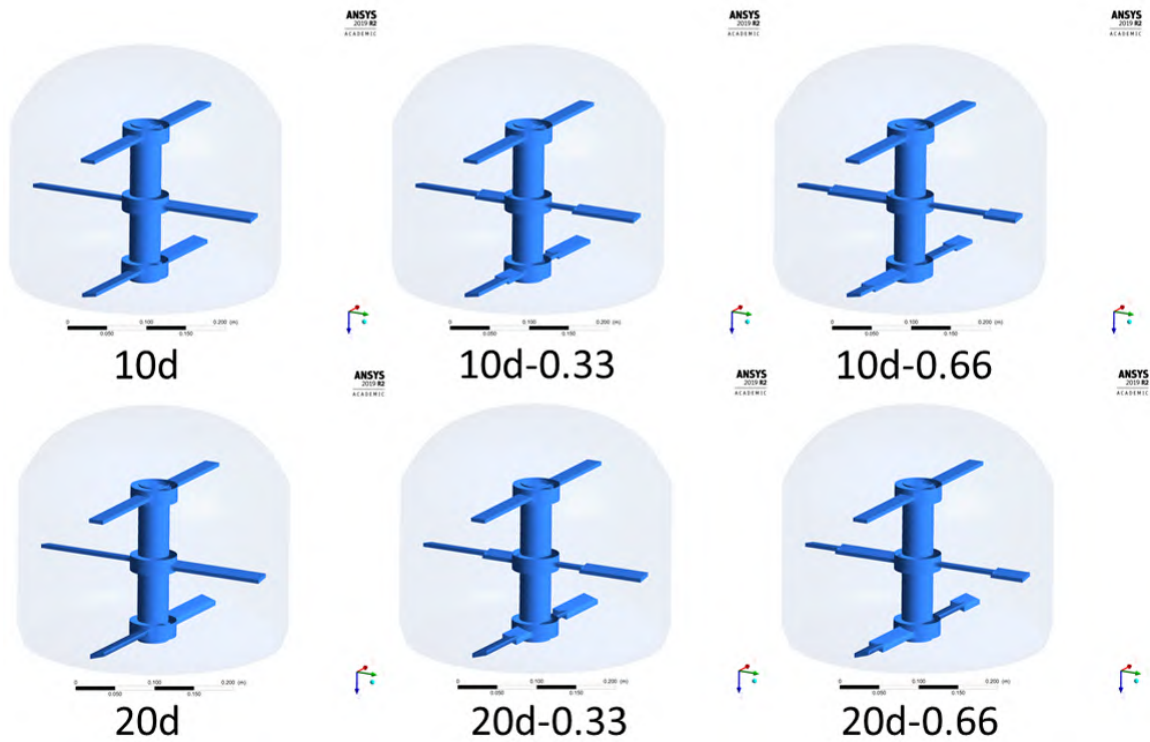


Figure 9.1: Six impellers: **10d-0)** inclination angle is 10° ; **10d-33)** inclination angle is 10° , reverse-angling ratio is $1/3$; **10d-66)** inclination angle is 10° , reverse-angling ratio is $2/3$; **20d-0)** inclination angle is 20° ; **20d-33)** inclination angle is 20° , reverse-angling ratio is $1/3$; **20d-66)** inclination angle is 20° , reverse-angling ratio is $2/3$.

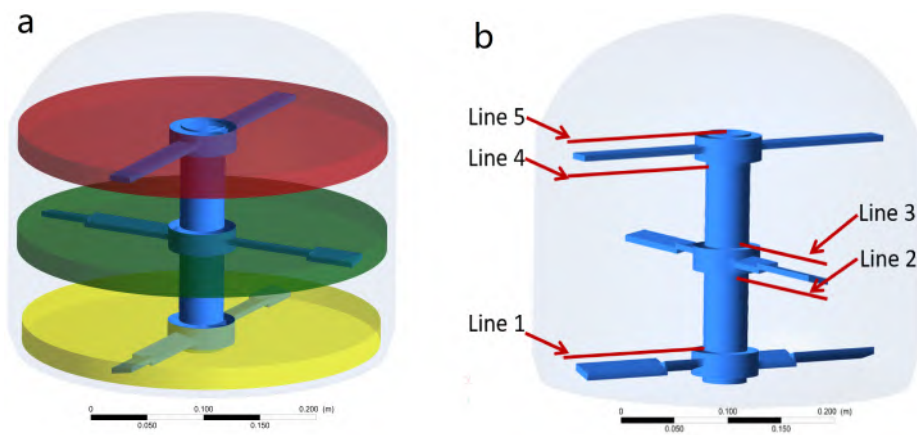


Figure 9.2: Three rotational regions (a) and five marked lines (b).

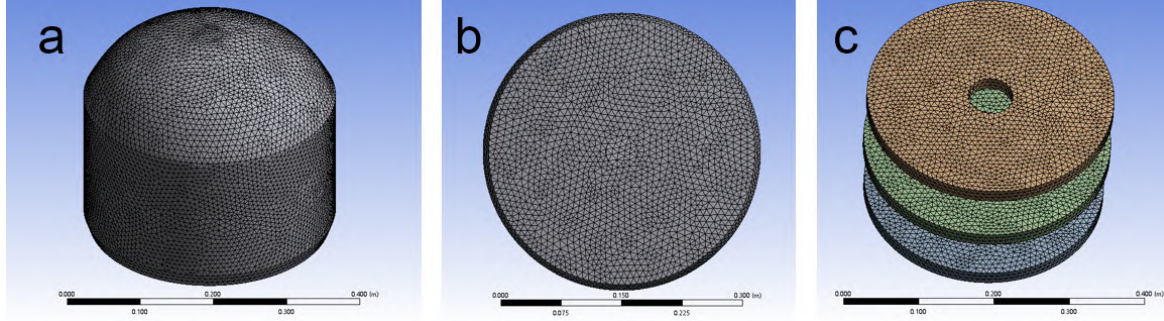


Figure 9.3: The images of the meshes of tank (a,b) and rotational regions (c)

Gidaspow's book are well developed and known, so no further modification is made on these equations [9].

The RNG k - ε turbulent model is developed using Re-Normalisation Group (RNG) by Yakhot et al to account for the effects of smaller scales of motion [10]. When neglecting bouyancy, Eq. 9.1 and 9.2 are the k equation and the ε equation , respectively.

$$\frac{\partial}{\partial t}(\rho_g k_g) + \frac{\partial}{\partial x_i}(\rho_g k_g u_{g,i}) = \frac{\partial}{\partial x_j} \left[\left(\mu_g + \frac{\mu_{g,t}}{\sigma_{k_g}} \right) \frac{\partial k_g}{\partial x_j} \right] + P_{k_g} - \rho_g \varepsilon_g \quad (9.1)$$

$$\frac{\partial}{\partial t}(\rho_g \varepsilon_g) + \frac{\partial}{\partial x_i}(\rho_g \varepsilon_g u_{g,i}) = \frac{\partial}{\partial x_j} \left[\left(\mu_g + \frac{\mu_{g,t}}{\sigma_\varepsilon} \right) \frac{\partial \varepsilon_g}{\partial x_j} \right] + C_{1\varepsilon_g} \frac{\varepsilon_g}{k_g} P_{k_g} - C_{2\varepsilon_g}^* \rho_g \frac{\varepsilon_g^2}{k_g} \quad (9.2)$$

where the turbulent viscosity, $\mu_{g,t} = \rho_g C_{\mu_g} k_g^2 / \varepsilon_g$, $C_{2\varepsilon_g}^* = C_{2\varepsilon_g} + [C_{\mu_g} \eta^3 (1 - \eta / \eta_0)] / (1 + \beta \eta^3)$, and $\eta = k_g / \varepsilon_g (2 S_{ij} S_{ij})^{0.5}$. The constants are listed as follow: $C_{\mu_g} = 0.0845$, $C_{1\varepsilon_g} = 1.42$, $C_{2\varepsilon_g} = 1.68$, $\eta_0 = 4.38$, and $\beta = 0.012$.

Gidaspow drag model

The Gidaspow model is a combination of the Wen and Yu model and the Ergun equation [11]. In this model, the drag coefficient can be calculated by the following equations.

$$K_{sg} = \frac{3 \alpha_s \alpha_g \rho_g |\vec{v}_s - \vec{v}_g|}{4 d_s} C_D \alpha_g^{-2.65} \quad \text{For } \alpha_g > 0.8 \quad (9.3)$$

$$K_{sg} = \frac{150 \alpha_s (1 - \alpha_g) \mu_g}{\alpha_g d_s^2} + \frac{1.75 \alpha_s \rho_g |\vec{v}_s - \vec{v}_g|}{d_s} \quad \text{For } \alpha_g \leq 0.8 \quad (9.4)$$

$$C_D = \frac{24 [1 + 0.15(\alpha_g Re_s)^{0.687}]}{\alpha_g Re_s}, \quad (9.5)$$

$$Re_s = \frac{\rho_g d_s |\vec{v}_s - \vec{v}_g|}{\mu_g}. \quad (9.6)$$

9.3.3 Boundary conditions and solver

The setting of boundary conditions are: 1) The rotation mode of the rotational region is set as mesh motion, and the rotation speed at 500 *rpm*, and the rotation direction as $x = 0$, $y = 0$, $z = 1$ (clockwise rotation at the top view); 2) The interface near the rotational region is set as relative to advanced cell zone with the velocity of 0 and the direction is the same as the rotational regions; 4) The tank and the shell are set as the static region; 5) The interface near the static region is set as absolute motion, and the rotation speed is 500 *rpm*, and the direction is the same as that of the rotational region; 6) The shaft is set as absolute motion with the speed at 500 *rpm*, and the direction is the same as the rotational region.

Table 9.1 summarizes some numerical values and settings of the computational model. All of the cases are solved by pressure-based and transit equations. Mesh motion rather than frame motion was used to obtain higher precision. Because there are a tremendous amount of swirls during the stirring, RNG with the swirl-dominated flow was applied. The second-order equations were utilized to ensure computational accuracy. The converged residuals of continuity, volume faction, energy, etc during the calculation were 10^{-4} . The stirring speed of the impeller maintains at a constant of 500 *rpm*.

9.4 Results and discussion

9.4.1 Volume fraction of particle

At first, the volume fraction distribution of the case 10d-0 changes over time was analyzed as seen in Fig. 9.4. The volume fraction of the bottom and top sections are 0.3 and 0.1 at the beginning, respectively. With the increase of stirring time, the top boundary of the powder fluctuates (0.5-1.0 second) and finally turns into a cone shape (2.0-3.9 seconds). The powder volume fraction at the bottom section is about 0.17 except for the rotational regions. The volume fractions at these rotational regions will be discussed later. In view of volume fraction, the movement of the powder stabilizes after 2.0 seconds.

Here, the volume fraction distributions of the six cases at 3.9 seconds are compared in

Table 9.1: Computational model parameters

Parameter/Model	Numerical value/Case setting
Solver type	Pressure-based
Solver time	Transit
Cell zone condition	Mesh motion
Turbulence multiphase model	RNG with swirl dominated flow
Turbulence model	Standard wall functions
Operating pressure	101325 Pa
Pressure-velocity coupling	SIMPLE algorithm
Spatial discretisation - gradient	Green-Gauss cell based
Spatial discretisation - pressure	Presto!
Spatial discretisation - volume fraction	QUICK
Spatial discretization - momentum	Second order upwind
Spatial discretization - turbulent kinetic energy	Second order upwind
Spatial discretisation - turbulent dissipation rate	Second order upwind
Transit formulation	Second-order implicit
All of residuals	10^{-4}
Timestep	2.5×10^{-5}
Solids packing limit	0.2
Particle diameter	40 μ m
Frictional pressure (pascal)	based-ktgf
Frictional viscosity	schaeffer
Granular viscosity	Gidaspow
Granular temperature	Algebraic
Radial distribution	Lun et al.
Solids pressure	Lun et al.
Granular bulk viscosity	Lun et al.
Angle of internal friction	30.00007°
Drag model	Gidaspow
Specularity coefficient	0.1
Coefficient of restitution	0.5
Gravitational acceleration	9.81m/s ²
Rotational speed	500 rpm

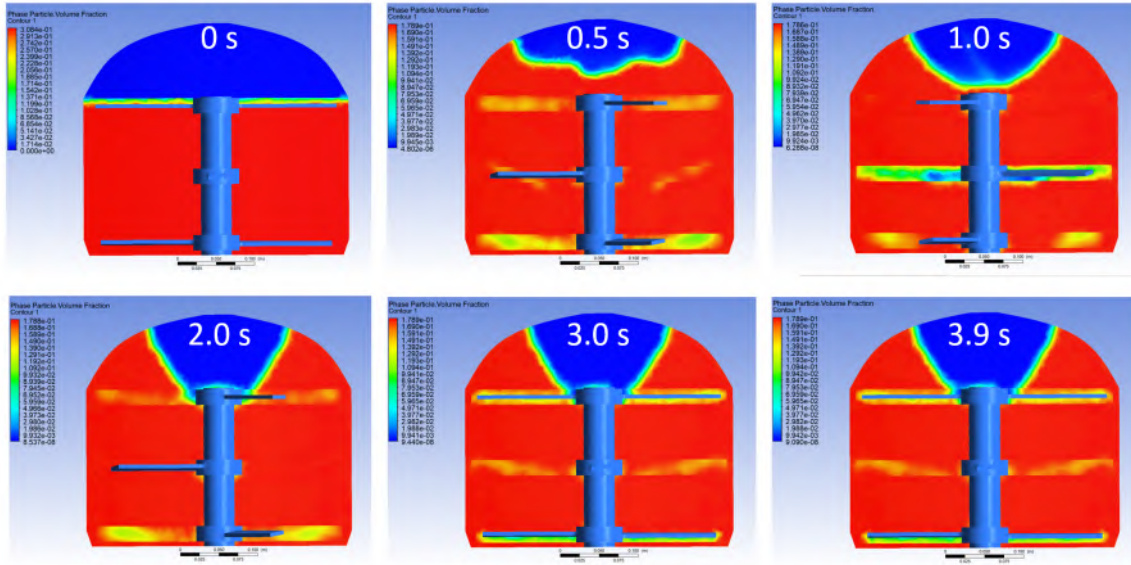


Figure 9.4: The volume fraction change along with time in the case of 10d-0.

Fig. 9.5. It is found that the volume fraction distributions of 10d-0, 10d-66, 20-0, and 20d-66 are quite close. However, 10d-33 and 20d-33 have slightly larger cone-shaped top boundaries than the others. This is mainly because one-third of the reverse-angled blades enhance the downward movement of the powder near the shaft. When increasing the reverse-angling ratio to two-thirds, the top boundary of volume fractions becomes almost the same as the unmodified blades. The reason behind this is that more reverse angling enhances the downward velocity of a much larger region of the powder, weakening the central swirl near the shaft.

The volume fraction distributions of the six cases at the five lines (shown in Fig. 9.2b) are compared in Fig. 9.6. The six cases have similar volume fractions in lines 2, 3, and 5. When the inclination angle is 20° , fluctuations at $X=0.13\text{m}$ are observed probably because of the turbulence of powder. As mentioned, the inclination angle of the mid-blade is 10° which does not match the bottom blade, bringing out significant turbulence. Near the shaft ($X=0.02\text{--}0.04\text{m}$), 10d-33 and 20d-33 have much lower volume fractions than the other four. This is in line with the volume fraction distributions in Fig. 9.5. In all, the six cases obtain considerably similar volume fractions with few differences.

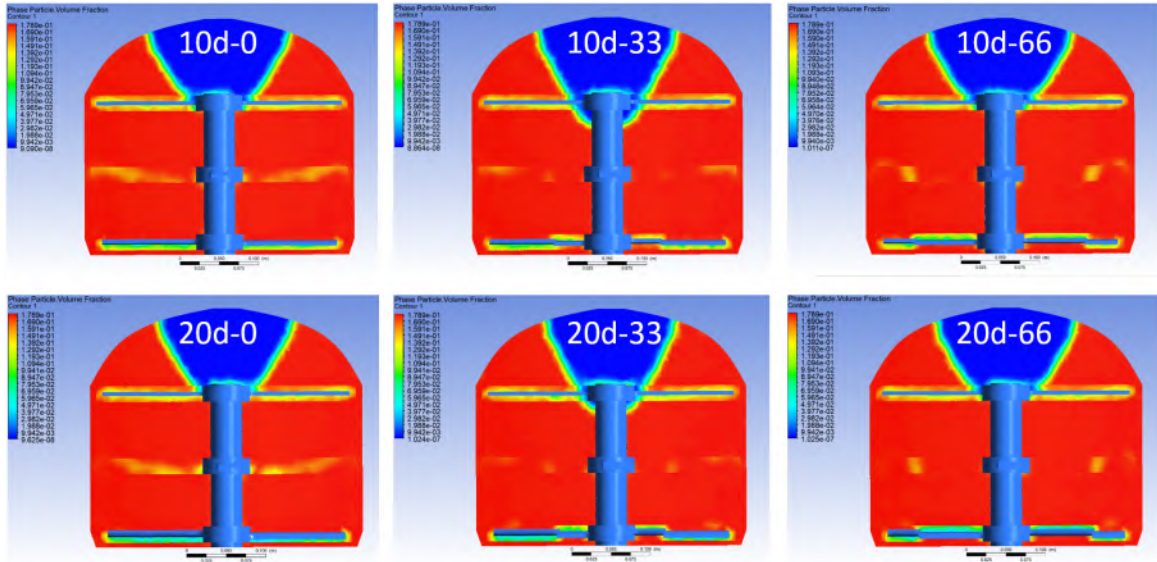


Figure 9.5: The volume fractions of different cases at 3.9 seconds.

9.4.2 Average velocity

The average velocities in the static regions of the six cases with respect to time were presented in Fig. 9.7. The six cases have almost the same trend: fast increase at the start and then a slight decrease, followed by a gradual rise to a stable state. From the magnified area, it is found that the blades with 20° inclination gain higher average velocities than those with 10°. It is clear that a higher inclination provides a stronger thrust to powder and leads to a higher velocity. In addition, a bigger reverse-angling ratio seems to achieve a higher average velocity in the tested range recently viewed because the reverse-angled blades increase the powder circulation. On the whole, a higher inclination angle and reverse-angling ratio both help to improve the average velocity of the powder.

To further compare the velocity of the six cases, the velocity distributions at the XY planes are given in Fig. 9.8. The area closer to the shaft appears to have a smaller velocity. The maximum values of the blades with 20° inclination are bigger than those with 10°. Also, the greater reverse-angling ratio leads to more yellow and red areas (near the wall). These findings are consistent with the result in Fig. 9.7.

To compare the average velocity near the blades, the relationship between v and X at the five lines is plotted in Fig. 9.9. It is obvious that the curves of average velocities along with X (0.02-

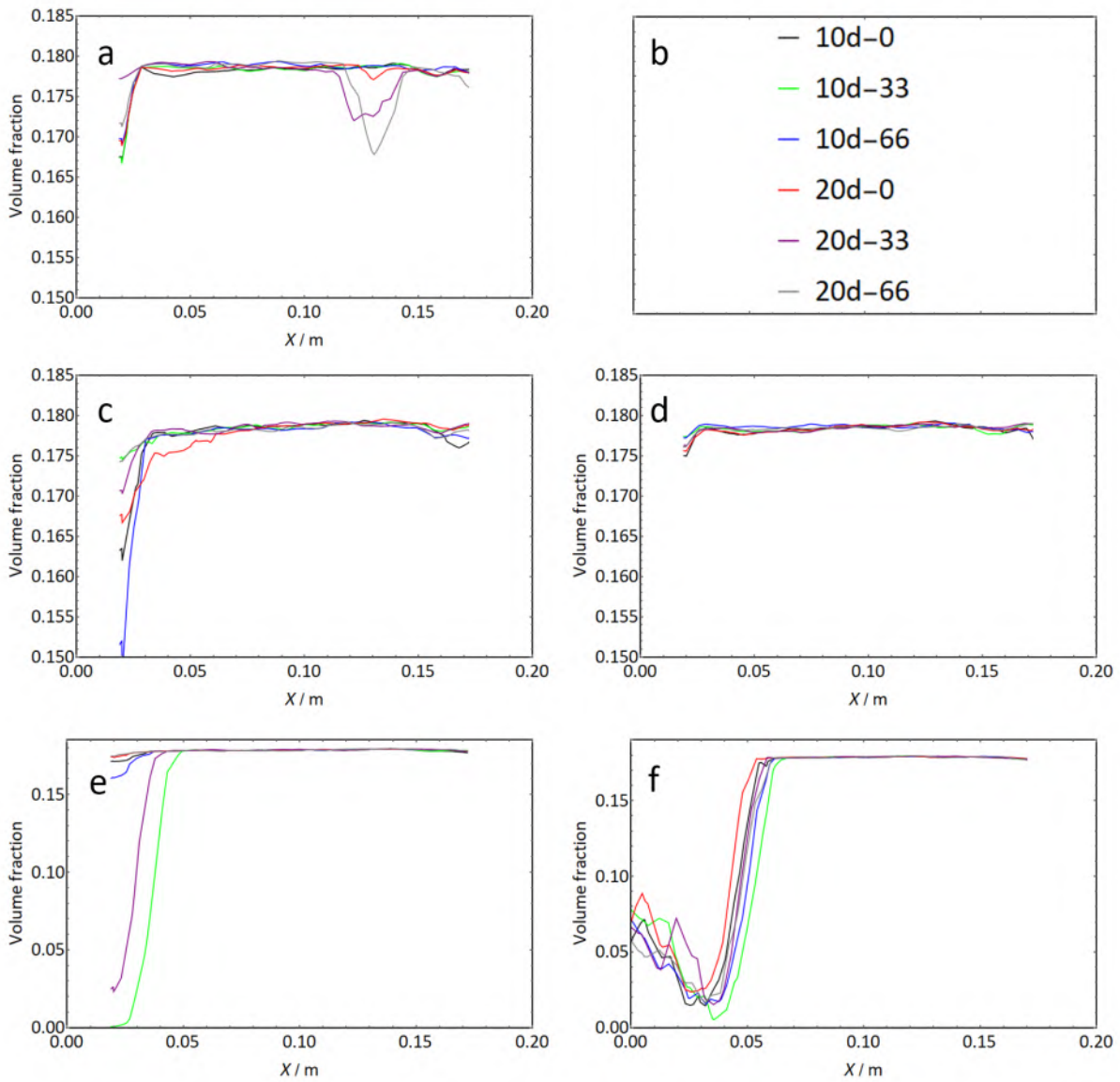


Figure 9.6: The volume fractions at the five lines in different cases. a) line 1; c) line 2; d) line 3; e) line 4; f) line 5.

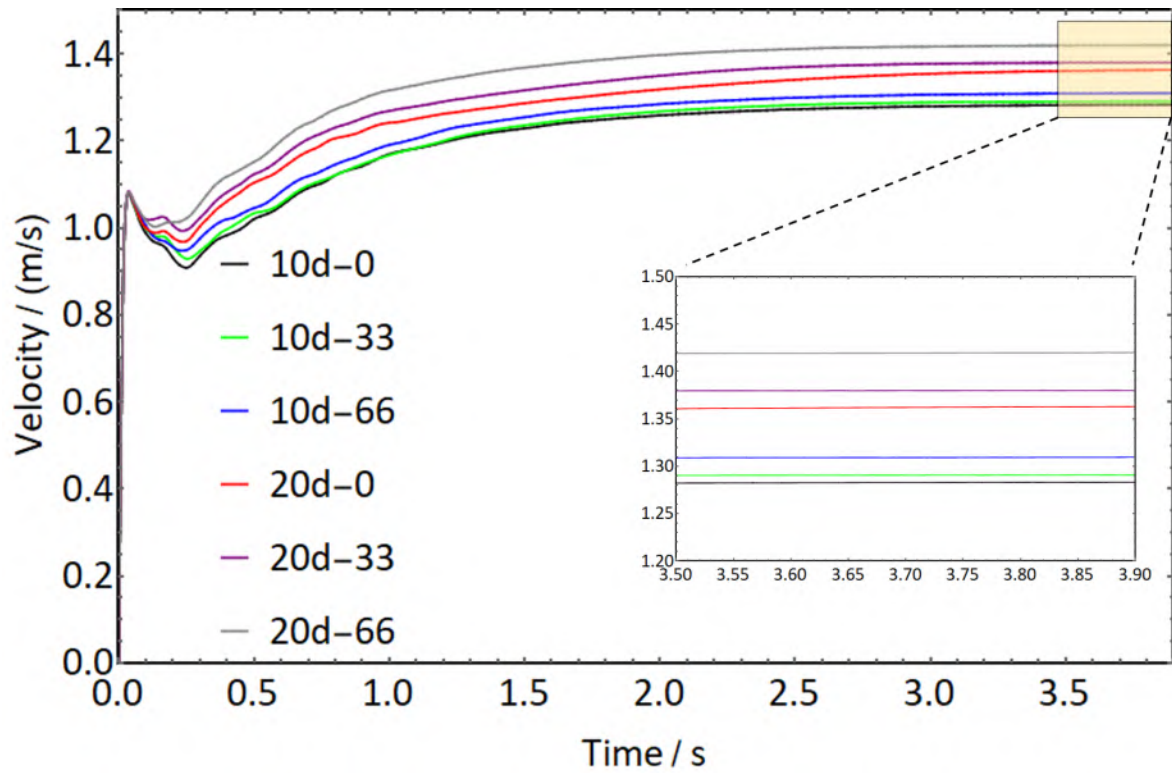


Figure 9.7: The average velocities of the six cases with respect to time.

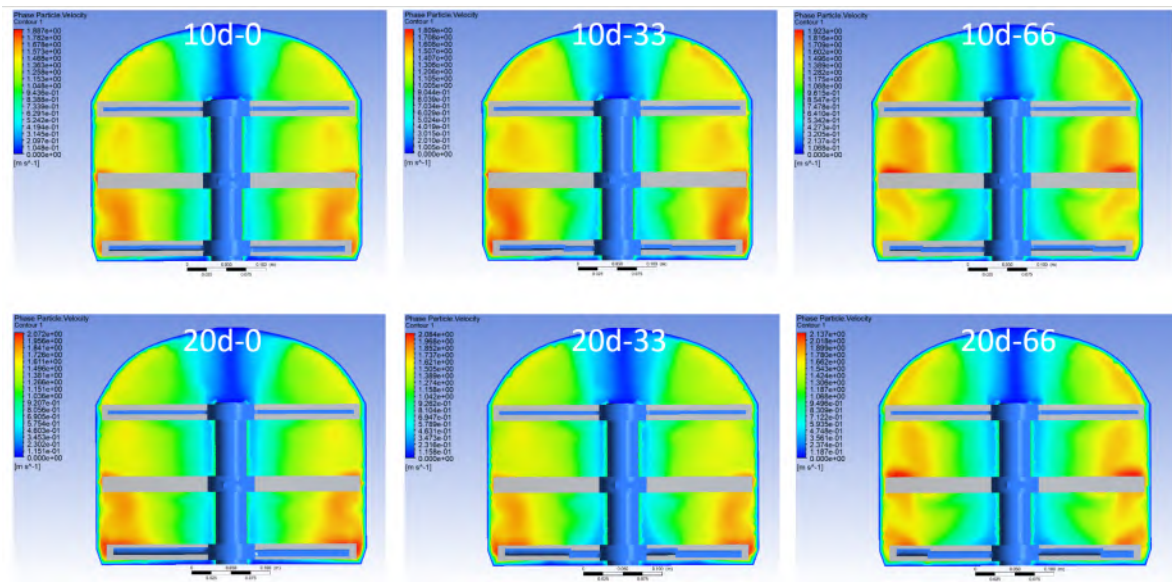


Figure 9.8: The average velocity distributions of the six cases at 3.9 seconds.

0.172m) have a similar trend that decreases at the beginning, and then gradually increases, and finally declines to zero at the wall. In line 2, one-third and two-thirds reverse angling show some reductions at the $X=0.7\text{m}$ and $X=0.11\text{m}$, respectively. This is caused by the junctions of angled and reverse-angled sections of the blades. In summary, the average velocity above and below the blade gradually increases from the inside to the outside.

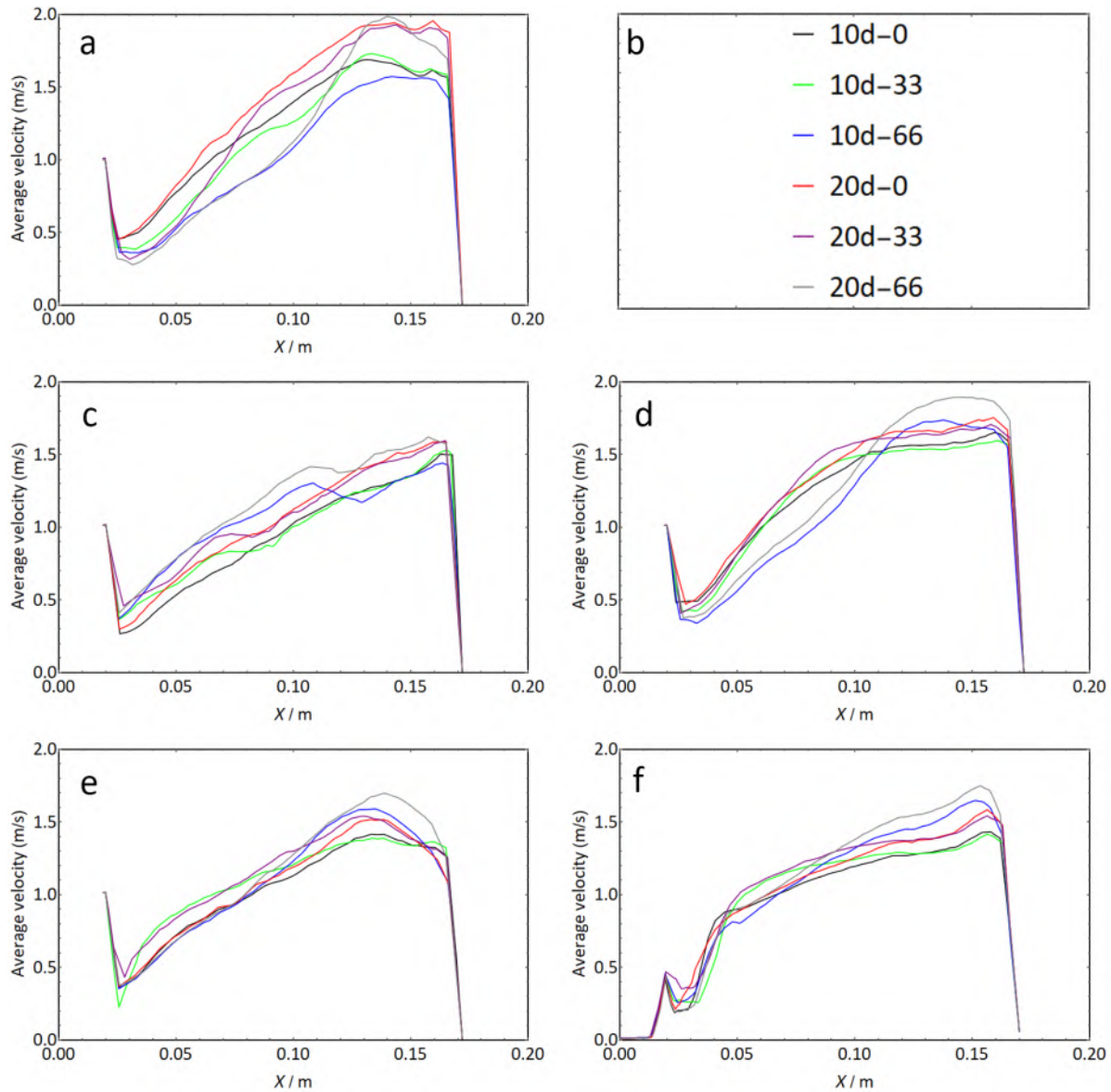


Figure 9.9: The average velocities at the five lines of the six cases (3.9 seconds). a) line 1; c) line 2; d) line 3; e) line 4; f) line 5.

9.4.3 Radial velocity

The radial velocity indicates the state of the inward and outward motions of the powder. Positive and negative values stand for outward and inward movements, respectively. Fig. 9.10 shows that the curves of radial velocity (in the static region) vs. time soar to about 0.02 m/s and then fluctuate to stable values. 10d-0 and 10-33 gain similar radial velocities, about -0.006 m/s, indicating particles move inward overall. After increasing the reverse-angling ratio to 2/3, the velocity is a positive value, 0.01 m/s, meaning that the two-thirds reverse angling changes the motion direction of the powder and also improve the radial velocity. When the inclination angle is 20°, the radial velocities are all above zero. Also, the velocity decreases slightly to 0.006 m/s with one-third reverse angling but greatly increases to 0.022 m/s after two-thirds reverse angling. The above results imply that two-thirds reverse angling can largely improve the radial velocity.

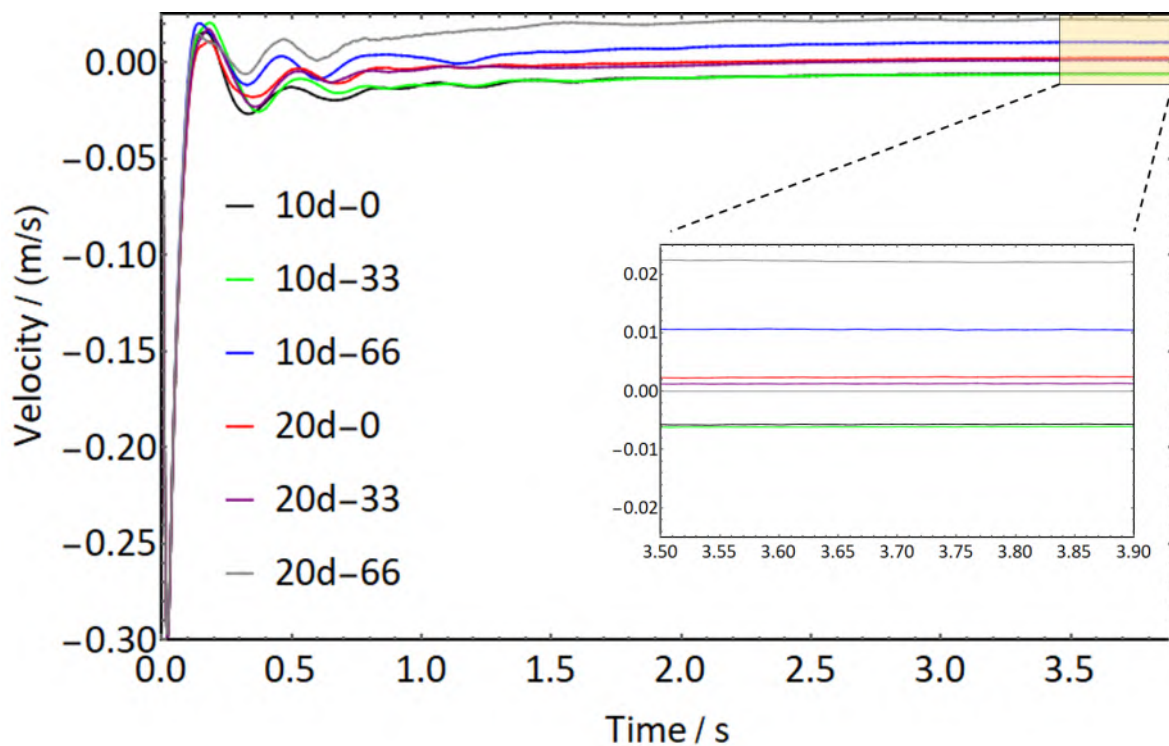


Figure 9.10: The radial velocities of the six cases along with time.

To have an overall sense of the inward and outward movements of the powder, the radial velocity distributions of the six cases at 3.9 seconds were given in Fig. 9.11. Compared to

the conventional impellers (10d-0 and 20d-0), there are small yellow areas (outward motion) underneath the junctions of angled and reverse-angled blades. Also, the maximum values of 10d-66 and 20d-66 are much larger than those of conventional ones, which agrees with the previous results.

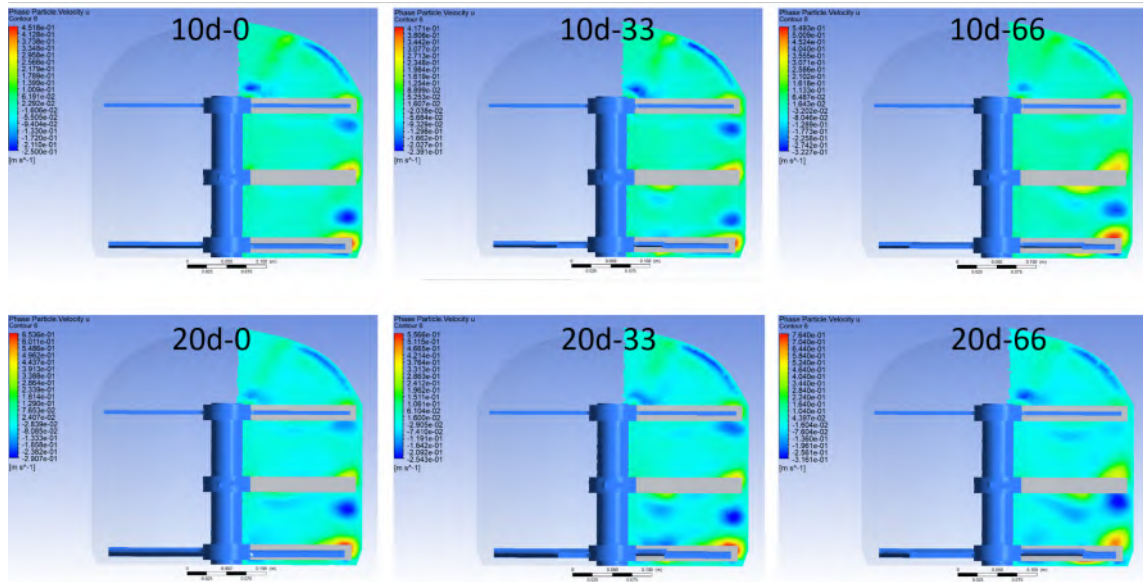


Figure 9.11: The radial velocity distributions of the six cases at 3.9 seconds.

Quantitative analysis on the radial velocity at the five lines is shown in Fig. 9.12. In line 1 (Fig. 9.12a), some fluctuations are found at the junctions of one-third (green and purple, $X=0.07$) and two-thirds (blue and gray, $X=0.11$ m) reverse angling. Also, larger outward velocities are observed at $X=0.15$ m (the front part of the blades) with two-thirds reverse angling. In line 2, greater outward velocities are seen at the junction (blue and gray, $X=0.11$ m) which is in line with the result in Fig. 9.11. Only 20d-66 has an inward velocity at $X=0.13$ - 0.17 m due to the enforcement of internal circulation. The trend in line 3 (Fig. 9.12d) is the same as that in line 1 because their positions are both just above the blades. In addition, there is no big difference in lines 4 and 5 because the top blades are not inclined. In a word, reverse angling exerts a positive influence on the enhancement of radial velocity.

9.4.4 Axial velocity

The axial velocity, standing for the upward (positive value) and downward (negative value) motions, is used to analyze the upward-downward circulation of powder. The axial velocities

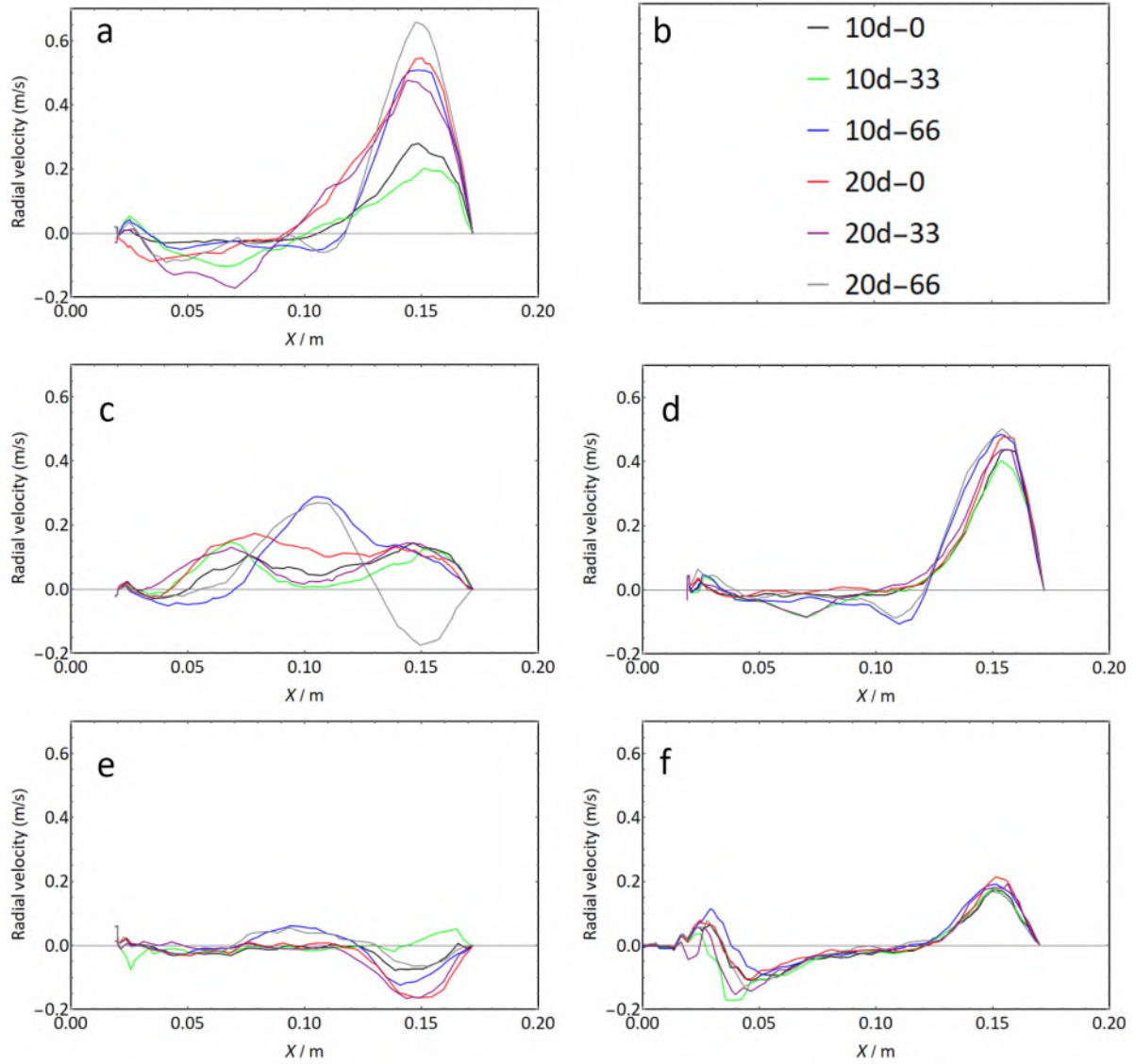


Figure 9.12: The radial velocities at the five lines of the six cases (3.9 seconds). a) line 1; c) line 2; d) line 3; e) line 4; f) line 5.

in the static regions of the six cases with respect to time were drawn in Fig. 9.13. All of the axial velocities at 3.9 seconds are negative, suggesting that particles in the static region move downward during the stirring. The axial velocities of 10d-0, 10d-33, 20d-0 and 20d-33 are all close to -0.03 m/s. However, the axial velocities substantially increase to -0.033 m/s after two-thirds reverse angling.

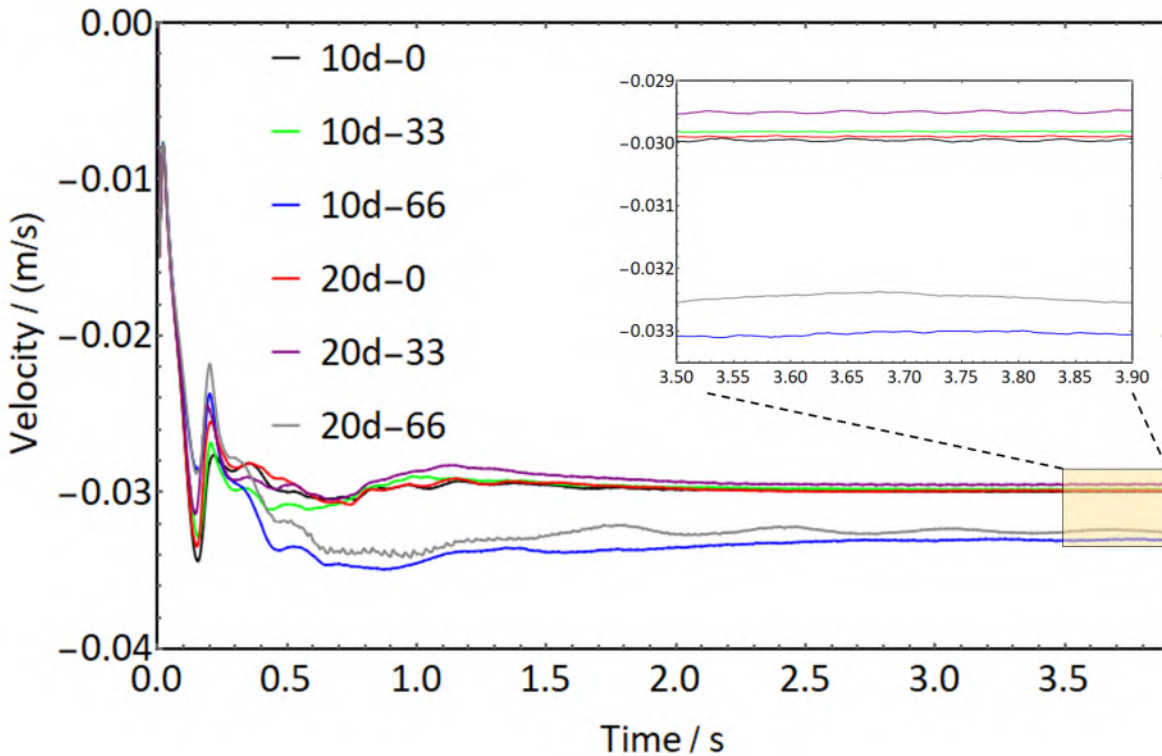


Figure 9.13: The axial velocities of the six cases along with time.

The axial velocity distributions at the XY plane of the six cases are shown in Fig. 9.14. Here, the yellow and red areas represent downward velocity, and the green and blue areas stand for upward velocity. With reverse angling, it is found that the downward movement of the area near the shaft is enhanced, while the upward motion is inhibited especially at the area above the bottom blade. The changing trend of the minimum values is consistent with the average axial velocity described in Fig. 9.13.

The numerical analysis on the axial velocity of the six cases at the five lines is shown in Fig. 9.15. In lines 1 and 3, 10d-0 and 20d-0 gain upward velocity at all spots. The velocity direction change from upward to downward at the reverse-angled section after one-third reverse

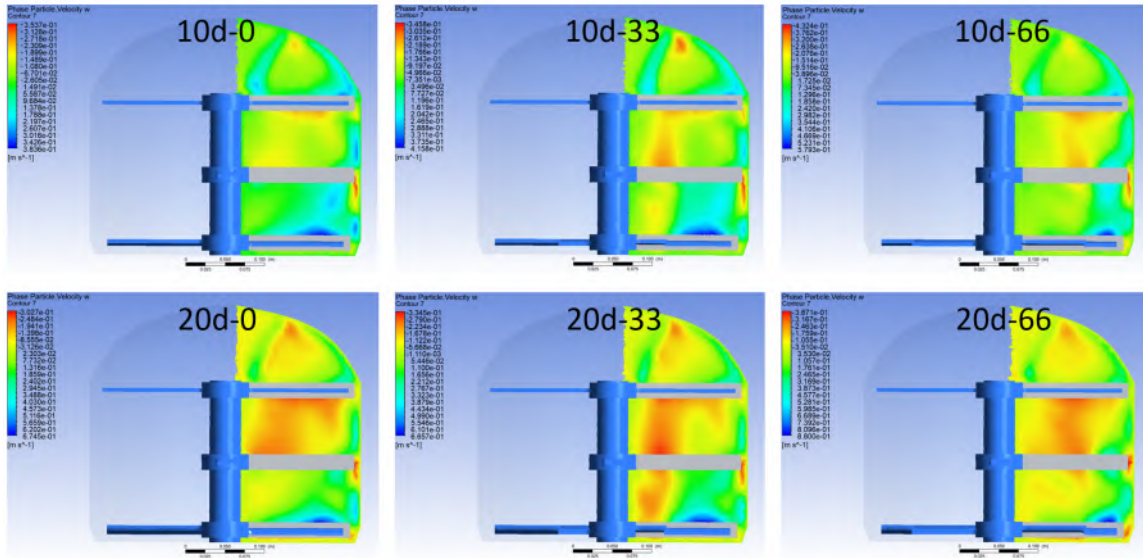


Figure 9.14: The axial velocity distributions of the six cases at 3.9 seconds.

angling (green and purple curves). With two-thirds reverse angling, the velocity at the reverse-angled section decreases a little bit but increases to a larger value at the angled section. In line 2, the one-third reverse angling exerts less impact on the axial velocity, but the two-thirds reverse angling enhances the downward motion at the junction. There is no such distinction of the axial velocity among the six cases in lines 4 and 5 due to no modification on the top blade. On the whole, the modification of reverse angling shows a clear effect on the axial velocity distribution.

To have a comprehensive understanding of the effect of reverse angling on the internal circulation of powder, the average, radial, and axial velocities of the six cases are summarized in Table 9.2. The average velocity rise with the increase of inclination angle and reverse-angling ratio. The one-third reverse angling obtains similar average radial and axial velocities with the unmodified case. However, the two-thirds reverse angling leads to much higher radial and axial velocities compared to the unmodified blades.

Table 9.2: The summary of average, radial and axial velocity

	10d-0	10d-33	10d-66	20d-0	20d-33	20d-66
Average velocity (m/s)	1.28213	1.29031	1.30918	1.36191	1.37983	1.41957
Radial velocity (m/s)	-0.00578	-0.00618	0.01052	0.00237	0.00127	0.02224
Axial velocity (m/s)	-0.02995	-0.02981	-0.03305	-0.02989	-0.02950	-0.03251

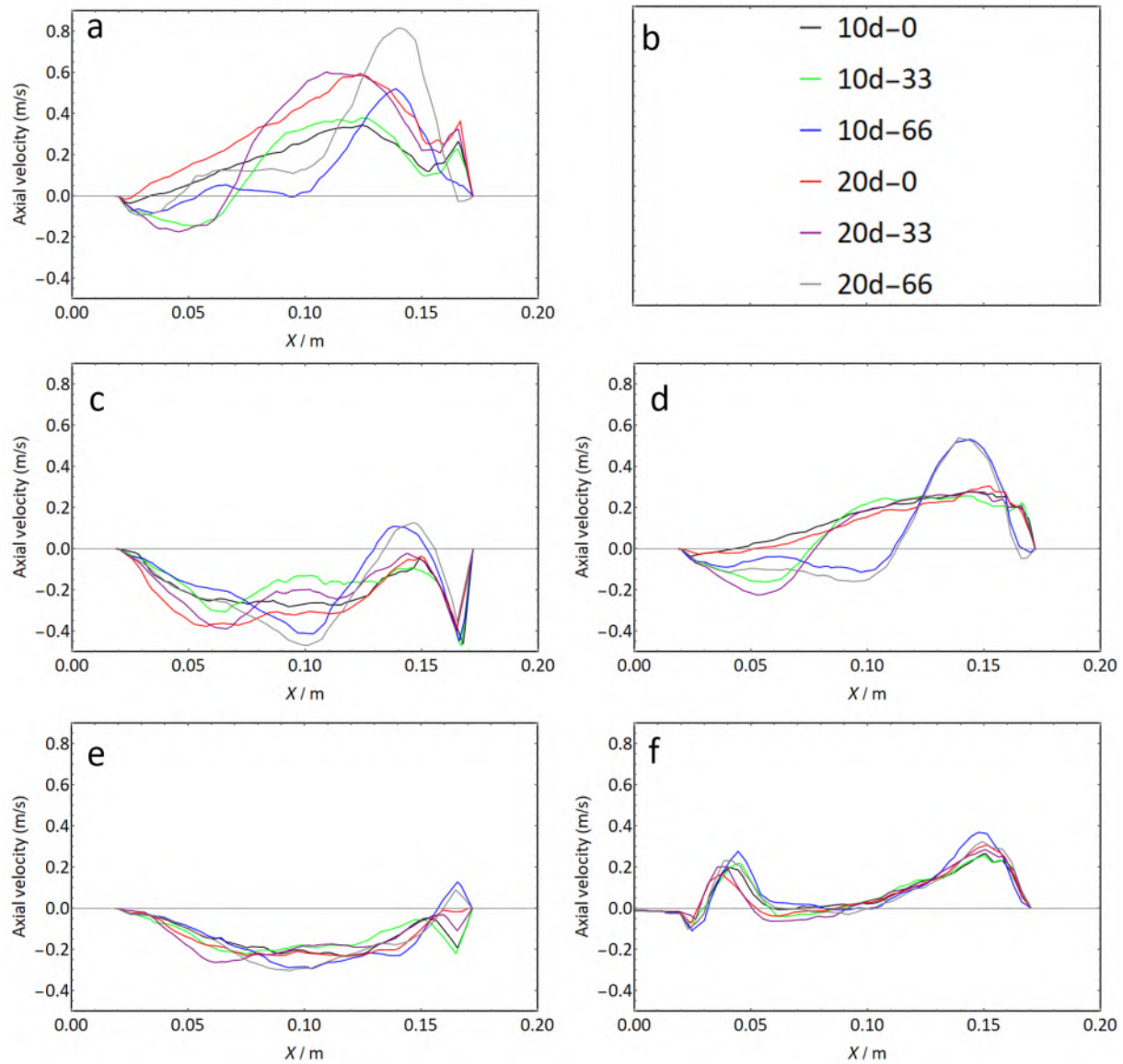


Figure 9.15: The axial velocities at the five lines of the six cases (3.9 seconds). a) line 1; c) line 2; d) line 3; e) line 4; f) line 5.

9.5 Conclusions

The modifications of reverse angling and inclination angle of blades achieve better internal powder circulation in the stirring tank. In the calculated range, a greater reverse-angling ratios and a larger inclination angle both result in a higher average particle velocity. The two-thirds reverse angling gains better internal circulation than the one-third. In contrast to the unmodified case, the two-thirds reverse angling increases the average velocity by 1 cm/s (inclination angle is 10°) and 6 cm/s% (inclination angle is 20°). Specifically, the axial velocity increases by about 10%, and the axial velocity by 50-90%. All in all, 20d-66 is considered as the case that can provide the best internal powder circulation in the tested range.

Bibliography

- [1] L Tang, Y Ji, XY Zhang, J Liu, and L Ren. Stirring tank design for powder-mixed edm SiC/Al and solid-liquid suspension uniformity research. *The International Journal of Advanced Manufacturing Technology*, pages 1–15, 2020.
- [2] Zhiwei Peng, Jiann-Yang Hwang, Joe Mouris, Ron Hutcheon, and Xiaodi Huang. Microwave penetration depth in materials with non-zero magnetic susceptibility. *ISIJ international*, 50(11):1590–1596, 2010.
- [3] RJ Arthern, DJ Wingham, and AL Ridout. Controls on ice albedo measurements over ice sheets: Footprint-scale topography, backscatter fluctuations, and the dependence of microwave penetration depth on satellite orientation. *Journal of Geophysical Research: Atmospheres*, 106(D24):33471–33484, 2001.
- [4] DA Deglon and CJ Meyer. Cfd modelling of stirred tanks: Numerical considerations. *Minerals Engineering*, 19(10):1059–1068, 2006.
- [5] AK Sahu, P Kumar, AW Patwardhan, and JB Joshi. Cfd modelling and mixing in stirred tanks. *Chemical Engineering Science*, 54(13-14):2285–2293, 1999.
- [6] JJ Derksen. Numerical simulation of solids suspension in a stirred tank. *AIChE Journal*, 49(11):2700–2714, 2003.
- [7] Sumsun Naher, Dermot Brabazon, and Lisa Looney. Simulation of the stir casting process. *Journal of Materials Processing Technology*, 143:567–571, 2003.
- [8] G Micale, G Montante, F Grisafi, A Brucato, and J Godfrey. CFD simulation of particle distribution in stirred vessels. *Chemical Engineering Research and Design*, 78(3):435–444, 2000.
- [9] Dimitri Gidaspow. *Multiphase flow and fluidization: continuum and kinetic theory descriptions*. Academic press, 1994.
- [10] VSASTBCG Yakhot, SA Orszag, Siva Thangam, TB Gatski, and CG Speziale. Development of turbulence models for shear flows by a double expansion technique. *Physics of Fluids A: Fluid Dynamics*, 4(7):1510–1520, 1992.
- [11] Dimitri Gidaspow, Rukmini Bezburuah, and J Ding. Hydrodynamics of circulating fluidized beds: kinetic theory approach. Technical report, Illinois Inst. of Tech., Chicago, IL (United States). Dept. of Chemical . . . , 1991.

10 Applying fine powder coatings to plastic substrates via a bifunctional additive

10.1 Abstract

A fine-powder-coating process is a promising approach for tackling the drawbacks of present powder-coating technology, such as the inability to achieve thin coatings. In recent years, the progress in fine powder coatings mainly focus on painting metal articles. As plastic materials gradually increase in high-end products, such as automotive parts and laptops, a big market is awaiting a fine-powder-coating process to replace present solvent-paint technology. Hence, it is necessary to find a viable fine-powder-coating process for providing thin and aesthetic films on these plastic components. In the present work, a bifunctional additive was prepared and employed to simultaneously improve the flowability and lower the curing temperature of fine powder coatings, enabling the fine powder coatings to succeed in painting plastic substrates. The lowest additive content and curing temperature for the epoxy fine powder coating were 0.5 wt% and 140°C and for the fine hybrid one were 0.3 wt% and 130°C, respectively. By using the fine powder coatings, the film thickness was declined by around 50%, the defects of pinhole and blister were apparently reduced, the surface roughness was primarily decreased, and the thin films had comparable or even better water resistance than the thick ones. The utilization of the bifunctional additive was demonstrated to be a feasible and practical approach for providing thin and smooth powder-coating surfaces on plastic substrates.⁹

Keywords: Fine powder coatings; Plastic; Bifunctional additive; Roughness; Thin film.

⁹With minor editorial changes to fulfill formatting requirements, this chapter was submitted to *Progress in Organic Coatings* with the title of “Application of fine powder coatings to plastic substrates via a bifunctional additive”, Wei Liu, Yufu Wei, Hui Zhang, and Jesse Zhu.

10.2 Introduction

Powder coating, usually composed of resin, pigment, filler and additives, is a type of paint applied as a free-flowing and 100%-solid powder [1]. Its high performance and low environmental impact make itself attractive for a wide range of markets, such as automotive clear top coatings [2], appliance coatings [3], bike coatings [4], coatings for construction materials [5], coatings for woods and plastics [6], etc. Powder coating technology takes advantage of fluidization by using air to encourage powders to behave in a liquid-like way instead of using a solvent like traditional solvent-borne paint. As a result, powder coatings confer environmental advantages by preventing VOC emissions associated with solvent use from the film formation process [7, 8].

However, since the inability of present powder coatings to provide very thin and smooth finish surfaces like traditional solvent paints, powder coatings have so far been just applied to low and middle-end products. One main reason behind this is that the present powder coatings are using 35-45 μm ("coarse") particles that belong to Geldart Group A powders [9]. This type of particles have been proved to have excellent flowability but brings about some unavoidable drawbacks, such as thick films and orange peels [10]. These inherent drawbacks impede the use of present powder coatings to some high-end products, such as automotive (topcoat), laptops, cellphones, etc. Fabricating the Geldart Group A powders Group C powders [11, 12], whose medium diameter is 10-20 μm ("fine"), is a promising method to address these issues of present powder coatings [13].

The challenge of using fine powder coating is securing the powder flows smoothly during the spraying process since the attractive forces between particles increase significantly with decreasing particle size. Some attempts have been made to improve the flowability of fine powders. For instance, some solvents, such as water [14] and supercritical fluid [15], were used to help the fine powders flow smoothly and attain thin films. To eliminate solvents, Jesse et al. employed SiO_2 , Al_2O_3 , TiO_2 , etc., nanoparticles that work as fluidization additives to separate the fine powder particles and reduce interparticle forces allowing the flowability of the fine powder to be increased [16]. Some experimental and simulation works also suggested that composite nanoparticles are capable of enhancing the flowability of fine particles [17, 18].

Jesse et al. also presented that the above approach enables fine and ultrafine powder coatings to paint metal workpieces [19].

In recent years, more and more metal parts have been replaced by plastic parts in some high-end products to reduce weights and costs, for example, plastic covers for laptops and cellphones [20, 21], fibre-reinforced plastic (FRP) automotive hood [22]. A vast market of plastic parts awaits a feasible fine-powder-coating approach. As mentioned, the use of fine powder coating to metal substrates has been realized with nanoscale fluidization additives. However, the utilizations of fine powder coatings on the above plastic parts have been seldom reported so far. Hence, this work aims to establish a method to achieve thin and smooth powder-coating finish surfaces on these plastic parts.

Generally, due to the poor high-temperature resistance of plastic substrates, low-temperature curatives, such as imidazole and its derivatives [23, 24], choline chloride [25], benzyltrimethylammonium halides [26], bisphenol A-amine adduct [24], etc., have to be melted or blended into powder coatings to reduce the curing temperature. Also, as stated before, fluidization additives have to be added to enhance the flowability of fine powders. Based on these concepts, a bifunctional additive in nanoscale was prepared in the present work that aims to improve the flowability and lower the curing temperature at the same time. This study tested the self-made additive in an epoxy-polyester (hybrid) and an epoxy fine powder coatings. It is found that the addition of a small amount of this additive enables the fine powder coating to coat plastic substrates with glossy and thin films at low curing temperatures, 130°C and 140°C for fine hybrid and epoxy powder coatings, respectively.

10.3 Materials and methods

Epoxy-polyester (TCI6920-9000) and epoxy (TCI7380-9000) powder coatings from TCI Powder Coatings Inc. (GA, USA) served as coarse powder paints. Glass long fibre-reinforced polyamide panels (7 cm×5 cm×0.5 cm) from the Fraunhofer Project Centre (ON, Canada) worked as substrates. Aluminum oxide nanoparticles ($D_{50}=13$ nm) from Evonik Industries (Essen, Germany) and 2-methylimidazole from Sigma-Aldrich (MI, USA) were utilized to prepare the composite additive. Methyl ethyl ketone (MEK) from Fisher Scientific (MA, USA) was used to test the degrees of cure of coatings.

10.3.1 Preparation of bifunctional additive and powder-coating surfaces

The following steps obtained the bifunctional additive: (a) disperse 2 g 2-methylimidazole and 8 g aluminum oxide nanoparticles into 1L DI water; (b) dry the slurry by the spray dryer (B-290, Buchi Labortechnik AG, Switzerland) at temperature of 130°C and pump speed of 2.5mL/min; (c) collect the dried nanoparticles after cooling down to room temperature. The following steps gained the powder-coating surfaces on plastic panels: (a) Add a certain amount of the prepared bifunctional additive (0.1, 0.3, or 0.5 wt%) into the 100 g fine powder coating; (b) mixing the two materials well by a mixer; (c) preheat the plastic panels at 140°C for 30min; (d) electrostatically spray the prepared fine powder coatings of step b onto the surface of the heated substrates via an electrostatic spraying system with a corona spray gun (Gema Switzerland GmbH); (e) heat both the deposited powders and plastic panels at a certain temperature (120 to 160°C) for 15min; (f) cooldown the coated plastic panels in the air.

10.3.2 Characterizations of powder samples

At first, the chemical composition of the bifunctional additive was characterized by X-ray diffraction (Rigaku MiniFlex, Tokyo, Japan) and fourier transform infrared (Perkin-Elmer TGA-FTIR coupled system, MA, USA). X-ray diffraction (XRD) measurements were operated in the reflection mode with Cu-K α radiation (35 kV, 15 mA) and diffracted beam monochromator, using a step scan mode with the step of 0.02°(2 θ). In the KBr-FTIR analysis process, each sample was analyzed directly with a universal ATR accessory in the range of 3500-1000 cm⁻¹ with attenuated total reflectance.

The size distributions of powders were also analyzed via a laser particle size analyzer (BT-2000B, Bettersize Instruments Ltd., Liaoning, China). The flowability of powders was represented by the angle of repose (AOR) which were determined by a powder tester (Hosokawa Micron Corporation, Tokyo, Japan) in terms of ASTM C1444-00. A smaller AOR indicates a better flowability. AOR less than 40° is the minimum requirement of the flowability for a powder to have good pneumatic transportation [27]. Coarse and fine epoxy powders were treated by gold-sputtering, followed by SEM and EDS analysis (SU3500, Hitachi Limited, Tokyo, Japan). At last, thermal properties and degrees of cure of epoxy and hybrid powders were measured by differential scanning calorimeter (DSC, Mettler Toledo, Chicago, USA).

The samples (5-10mg) were placed in a 40 μ L aluminum crucible with a pierced lid and then heated at 180°C for 16min (isothermal scanning), and from 25 to 275°C at a heating rate of 10°C/min (dynamic scanning) under nitrogen purge at a flow rate of 40mL/min. According the DSC results of heating at 180°C, the following equation calculate the degree of cure of a film at time t :

$$\text{Degree of cure}(t) = \frac{\Delta H_t}{\Delta H_0} \times 100\% \quad (10.1)$$

where ΔH_0 is the total heat of reaction for full cure, ΔH_t is the amount of heat released up to time t .

10.3.3 Characterizations of films.

The degrees of cure of powder-coating films were determined through MEK-rubbing test according to ASTM D5402. Rubbing the film with a swab dipped with MEK till the coating starts to dissolve. One forward and back motion is one double rub. Typically, the minimum number of double rubs for a coating is usually fifty in industry [28].

The top and cross-sectional surfaces of qualified films were observed by an optical microscope (Keyence VHX-6000, IT, USA). Three surface characters, Gloss 60°, Distinctness of Image (DOI), and Haze, of films were measured via a 408 triple glossmeter (Elcometer Inc., MI, USA) at six uniformly distributed sites. Higher Gloss 60° and DOI, and a lower Haze mean better surface-coating quality for the involved powder coatings. The surface roughness of a film at three different areas (each area is 1.2×1.2 mm) were assessed by a confocal laser scanning microscope (Zeiss LSM800, Jena, Germany). Three height parameters, S_a , S_z and R_a , were used to evaluate surface roughness in this work according to ISO 25178.

The water resistance of films was measured by testing the increased weight percentage after 24-hour water immersion in the light of ASTM D570-98(2018). Each film was tested three times. A higher water absorption indicates inferior water resistance. The hardness of the films was measured by a 501 pencil hardness tester (Elcometer Inc., MI, USA) based on ASTM D3363. The lowest hardness value of the pencil, which marks the coating, determines the hardness grade. The hardness is estimated on a 6B to 6H scale. The adhesion of the films was evaluated by an Elcometer 107 cross hatch cutter (Elcometer Inc., MI, USA) on the basis of ASTM D3359. According to the percent of removed area after cross cutting, adhesion is

assessed by the following five grades: 0B (>65%), 1B (35-65%), 2B (35-65%), 3B (35-65%), 4B (<5%), and 5B (0%).

10.4 Results and discussion

10.4.1 Characterizations of the bifunctional additive

X-ray diffraction and FTIR study were conducted on the bifunctional additive and its diffractograms and infrared spectroscopy are shown in Fig. 10.1. As both 2-methylimidazole (2-MI) and Al_2O_3 were crystalline in nature so they exhibited very sharp peaks in their respective X-ray diffractograms. Fig. 10.1a shows peaks at 2θ equals to 17.86° , 21.78° , and 26.08° , resulting from 2-MI according to Mahendra and coauthor's work [29], whereas peaks at 2θ equals to 19.90° , 32.12° , 37.66° , 39.50° , 45.50° are the result of $\gamma\text{-Al}_2\text{O}_3$ based on JCPDS 50-741 (Fig. 10.1). Beside, some tiny peaks caused by trace amount of $\alpha\text{-Al}_2\text{O}_3$ were also found by comparing with JCPDS 71-1123 (Fig. 10.1c). FTIR spectrum of the additive is presented in Fig. 10.1d. The broad absorption peaks were seen in the range of $3300\text{-}2500\text{ cm}^{-1}$ assigned to bonding vibration of water molecules due to moisture absorption [30]. Secondary amine N-H stretching and bending frequency was present at 3018 cm^{-1} . Whereas C-H stretching and deformation bends frequency were respectively found at 2653 cm^{-1} and 1303 cm^{-1} . The vibrations of C-N bonds were observed at 1365 cm^{-1} , 1217 cm^{-1} , 1154 cm^{-1} and 1114 cm^{-1} . Also, C=N and C=C stretching were seen at 1742 cm^{-1} , 1593 cm^{-1} and 1441 cm^{-1} . Meantime, these absorption are consistent with the reported IR spectra of 2-MI [29]. The characterizations of XRD and FTIR verify that the bifunctional additive consists of 2-methylimidazole, $\gamma\text{-Al}_2\text{O}_3$ and a small amount of $\alpha\text{-Al}_2\text{O}_3$.

The morphology of the additive and its distribution in the powder coating system were observed by SEM, and the compositions of marked sites were analyzed by EDS, as shown in Fig 10.2. A great number of agglomerations in the diameter of about $4\text{ }\mu\text{m}$ were found in the additive (Fig. 10.2). And the EDS results show that the additive consists of three main elements, Al, C and O, which agrees with its ingredients, Al_2O_3 and 2-dimethylimidazole. The traces of Na and Cl might come from the extensive usage of DI water (1L). The particle surface is clean when excluding the bifunctional additive (Fig. 10.2c). However, after mixing the additive and epoxy powder coating, plenty of nanoparticles are found on the surface of the coating particle

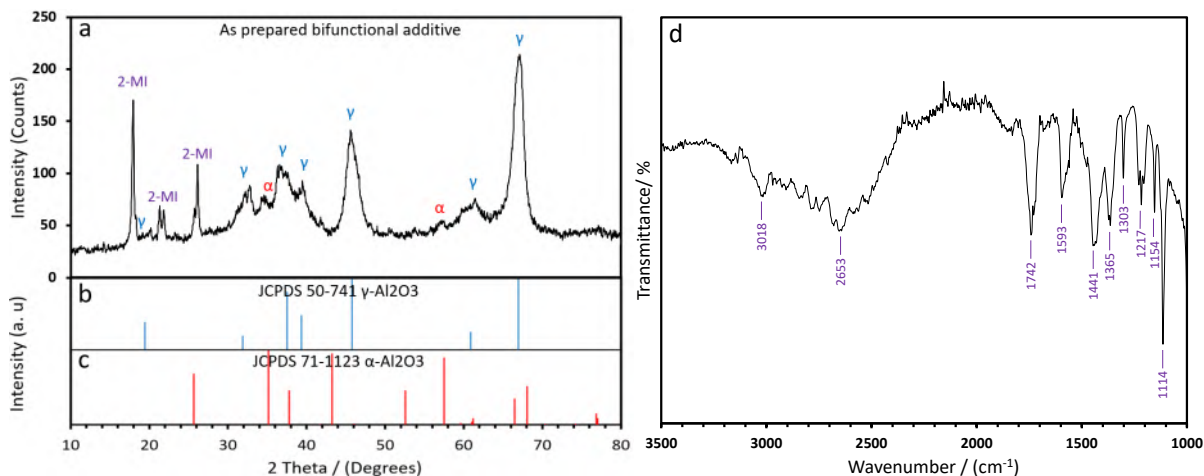


Figure 10.1: XRD patterns of as prepared bifunctional additive (a) along with the stick patterns for the JCPDS files No. 50-741 (b) and 71-1123 (c). d) FTIR spectrum of the bifunctional additive.

(Fig. 10.2e). By comparing Fig. 10.2d and f, a much higher peak at the aluminum element (red arrows) was seen at the powder sample that contains the bifunctional additive. This proves that these nanoparticles are the bifunctional additive because the additive owns a very high peak at aluminum (Fig. 10.2a). On the whole, the mixing process breaks down the agglomerations of the bifunctional additive and enables the additive to reach uniform distributions on the surfaces of coating particles.

10.4.2 Epoxy powder coating

The coarse and fine epoxy powder coatings were prepared and studied. First of all, the morphology and size distributions of the two types of epoxy powders were determined as given in Fig. 10.3. It is easy to find that most particles in Fig. 10.3a are much larger than those in Fig. 10.3b. Also, Fig. 10.3c and d show the medium sizes of the coarse and fine powder coatings are 42.34 and 19.98 μm , respectively. These values are quite in line with the SEM observation.

On the one hand, the dosage of the bifunctional additive needs to be as low as possible because it leads to the reduction of surface-coating quality [24, 31], but on the other hand, sufficient addition is needed to ensure good flowability and low curing temperature. Consequently, the balance of the above concerns requires an appropriate content of the bifunctional additive.

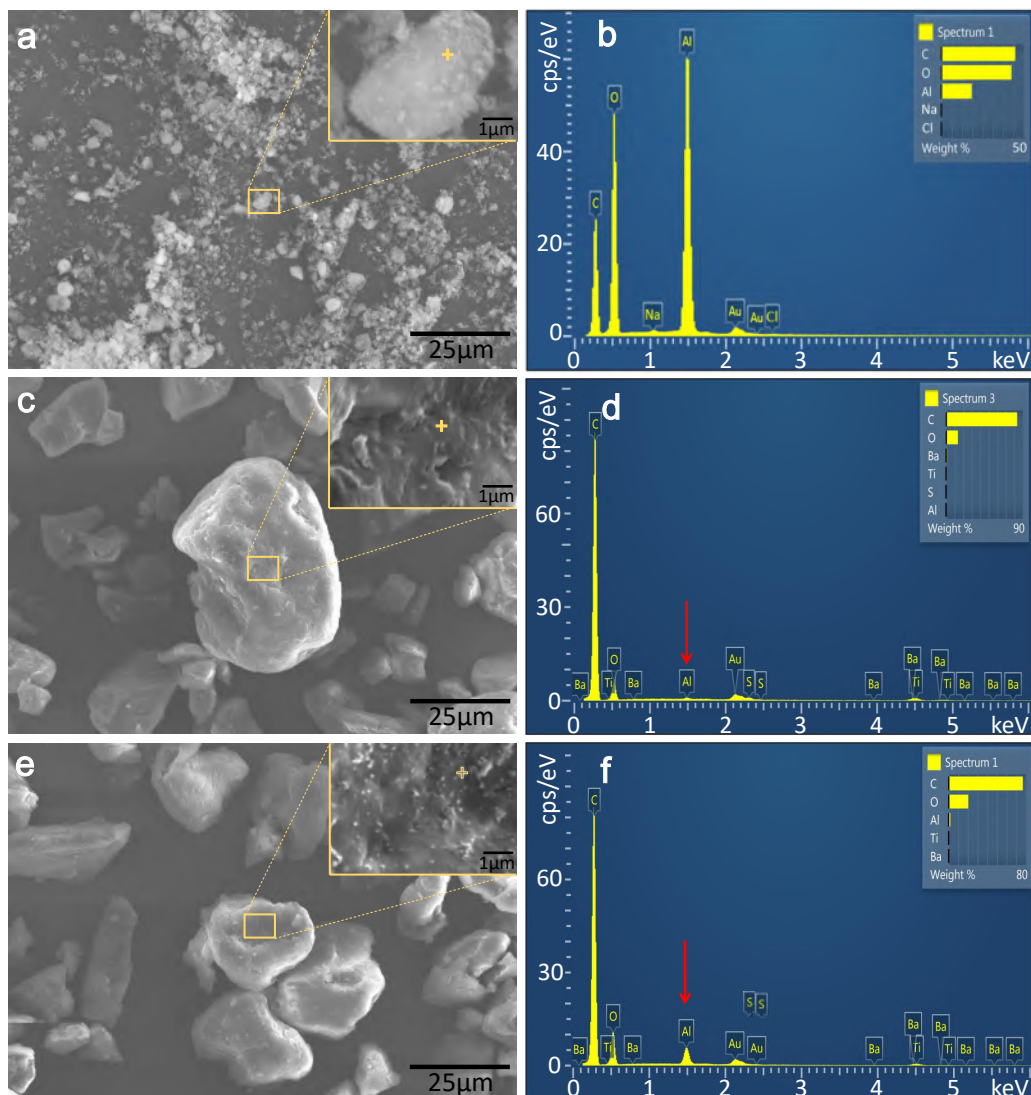


Figure 10.2: SEM and EDS characterizations of different powders, (a, b) the bifunctional additive; (c, d) the epoxy coating powder; (e, f) the epoxy coating powder added the additive.

At first, the effect of the additive dosages on the flowability of fine epoxy powder coating was studied as shown in Fig. 10.4. The coarse epoxy powder coating ($D_{50}=42.34 \mu\text{m}$) with a small AOR of around 36.8° owns a good flowability. Oppositely, the AOR of the fine powder coating ($D_{50}=19.98 \mu\text{m}$) dramatically increase to $44.8^\circ (>40^\circ)$, indicating the fine powder coating has a poor flowability. The flowability of fine powders improves obviously when the additive content increase from 0.1 to 0.5 wt%. The main reason behind this is that the nanoscale bifunctional additive increases the distances between fine particles and leads to the decline of the interparticle forces, such as van der Waals force and electrostatic attraction [32]. The AOR at 0.3 and 0.5

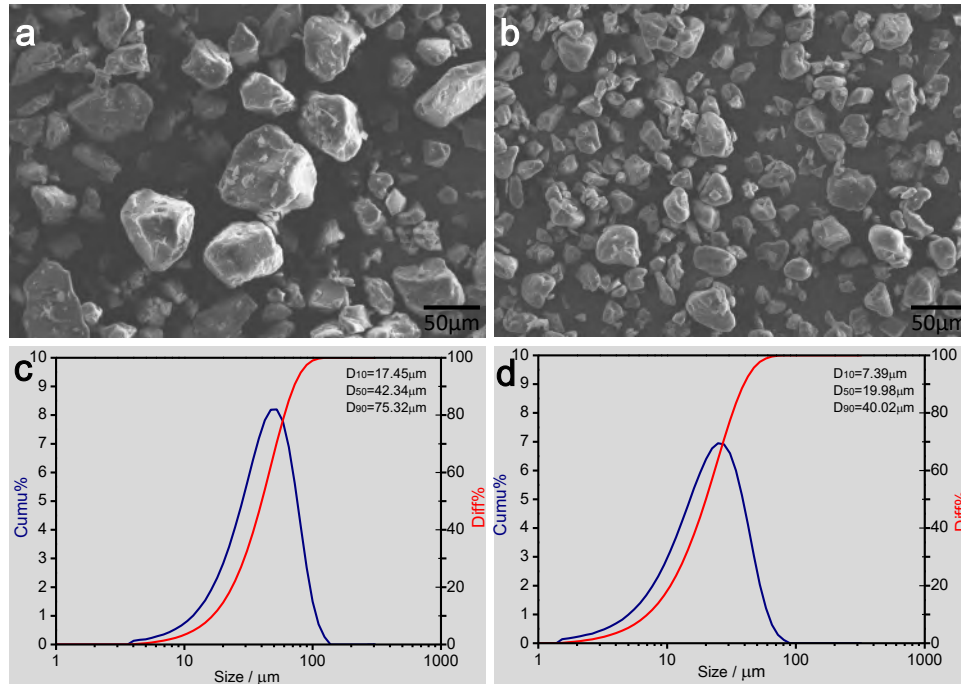


Figure 10.3: SEM images and size distributions of the coarse (a,c) and fine (b,d) epoxy powder coatings.

wt%, in particular, are both less than 40°, implying that these fine powders meet the minimum requirement of flowability for the powder-coating spray process.

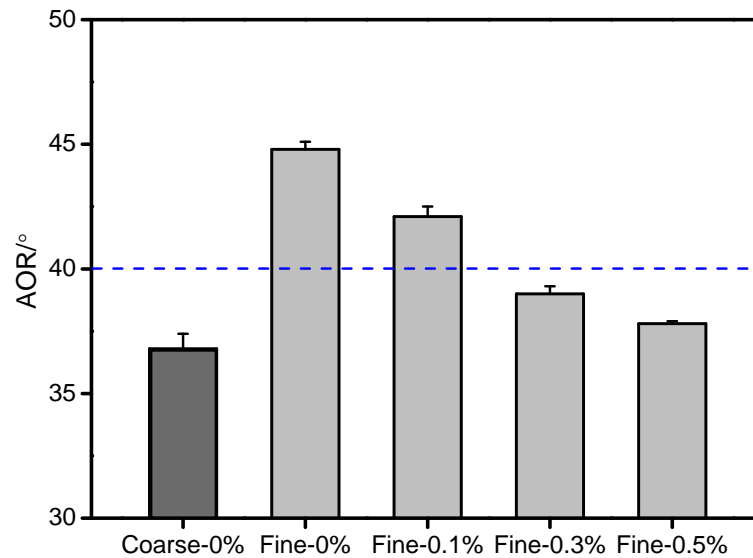


Figure 10.4: The flowability of the fine epoxy powder coatings with various contents of the bifunctional additive (wt%).

The influence of the additive content on the degree of cure was estimated in Table 10.1.

The degree of cure for a coating system, which highly depends on the curing temperature, is often measured by MEK-rubbing tests. Larger double rubs indeed suggest higher degrees of cure. In the present work, fifty-time double rubs were used as the minimum requirement for a qualified film. Epoxy powders with various content of additives were cured at different temperatures. It is found that the cure degree increases with the increases in curing temperature and additive content. This majorly because higher temperatures and additive contents result in faster crosslinking-reaction rates [33, 34]. In detail, the lowest curing temperature to have a qualified degree of cure is 160°C for the coarse epoxy powder coating. The curing temperature still has to be as high as 160°C when merely adding 0.1 wt% additive. The respective lowest curing temperatures are 150°C and 140°C when the additive content rises to 0.3 wt% and 0.5 wt%. To sum up, the lowest curing temperature for the fine epoxy powder coating is 140°C, and the proper content of the bifunctional additive is 0.5 wt%.

Table 10.1: The double rubs of epoxy films prepared at different curing temperatures and additive contents.

	120°C	130°C	140°C	150°C	160°C
Coarse-0 wt%	1	1	6	43	>50
Fine-0.1 wt%	1	1	1	41	>50
Fine-0.3 wt%	2	5	7	>50	>50
Fine-0.5 wt%	20	29	>50	>50	>50

More than 50 double rubs means the film has a qualified degree of cure.

The effect of the bifunctional additive on the degree of cure of epoxy film was further analyzed by the dynamic and isothermal DSC quantitatively as given in Fig. 10.5. As heat is applied, the epoxy resin gradually melts following by the onset of crosslinking (oligomers interconnections) and then reaches the peak reaction rate before full cure (a tridimensional and interpenetrating polymeric network). The coarse (0wt% additive) and fine (0.5wt% additive) epoxy powders were dynamically heated from 25 to 275°C at the heating rate of 10°C/min, and the heat flows were exhibited in Fig. 10.5a. The grinding process rarely impacts the cure of a powder coating [13], so the coarse and fine epoxy powder have the same cure properties theoretically when excluding the bifunctional additive. After adding 0.5wt% bifunctional additive, it is found that the melting point decreases from 74.3 to 72.7°C, and the curing onset and peak exothermic temperatures reduce from 98.3 to 90.3 and 192.0 to 182.7°C, respectively. From the

isothermal DSC analysis at 180°C (Fig. 10.5b), the fine epoxy powder with 0.5wt% additive reaches 100% of degree of cure at 8.8min, while the coarse one needs 15.2min to complete the cure. The above DSC comparisons provide evidence for the ability of the bifunctional additive to accelerate the curing reaction and lower the curing temperature of the epoxy sample.

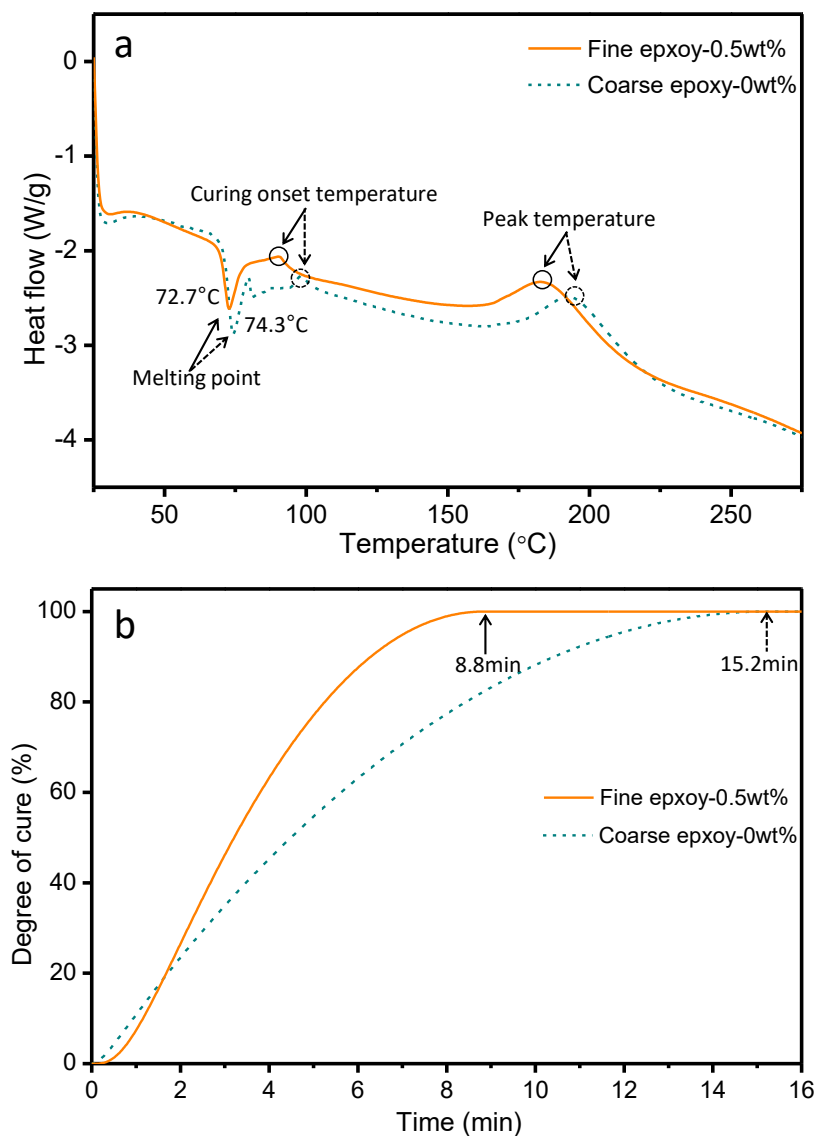


Figure 10.5: The DSC analyses of coarse and fine epoxy powders. a) Dynamic scanning of heat flow; b) Isothermal scanning for determining the degree of cure.

From the above results, the conditions (curing temperature / additive content) for coarse and fine powder coatings to achieve qualified powder-coating films are 160°C / 0wt% and 140°C / 0.5wt%, respectively. The macroscopic surface-coating quality and microstructure of these films were further analyzed, as shown in Fig. 10.6. The left (Fig. 10.6a) and right films

(Fig. 10.6b) are separately named as “coarse film” and “fine film” for simplicity. The reflections of a beam of light on the coarse and fine films are given in Fig. 10.6a and b, and the light spot on the fine film seems to have a more uniform and smooth boundary. The marks at the bottom-right corners of the two surfaces result from the MEK-rubbing test. In addition, the macroscopic surface-coating quality of fine and coarse films was represented by three surface characters (Gloss 60°, DOI and Haze) as shown in the top-right tables of Fig. 10.6a and b, respectively. The fine film possesses similar gloss, DOI and haziness compared to the coarse film. The above analyses prove that the coarse and fine films have comparable visual appearances. Fig. 10.6c and d present the magnified images of the central areas of the coarse and fine films, respectively. A large number of pinholes with diameters of 5-10 μm are seen on the top surface of the coarse film (Fig. 10.6c). Notwithstanding, the pinhole sizes of the fine film decrease to 1-5 μm as presented in Fig. 10.6d. An acceptable reason for the occurrence of pinholes is the degassing of plastic substrates at high temperatures. Also, the size reduction of the pinholes is mainly the result of the lower curing temperature of the fine powder coating, which allows the substrate to release a smaller amount of gases. The cross-sectional images clearly show that the thicknesses of coarse and fine films are 89 ± 4 μm and 41 ± 5 μm , respectively. In summary, the fine film has smaller pinholes, comparable surface-coating quality, and a much thinner thickness with comparison to the coarse film.

The surface roughness of the above films (Fig. 10.6) was further assessed on surfaces (areas) and profiles (lines) to compare their smoothness, as shown in Fig. 10.7. The two areas have the same legend in Fig 10.7a and b, and the color varies from blue to pink, representing the height increasing from 0 to 3.8 μm . More elevated areas (red and pink areas) are observed in the coarse film, and almost no pink or red areas are found in the fine film. In detail, the two height parameters (S_a and S_z) of the fine film separately are 0.45 ± 0.03 and 3.60 ± 0.20 μm , which are both smaller than those of the coarse film. The profiles of the diagonal lines (AC and BD) of the presented areas were further analyzed, and the results of the AC lines in Fig. 10.7a and b are described in Fig. 10.7c and d, respectively. The fine film profile appears to be closer to zero over the coarse film, and the R_a of the fine film is confirmed to be smaller. Conclusively, both area and profile height parameters testify that the fine epoxy film has a smoother surface than the coarse film.

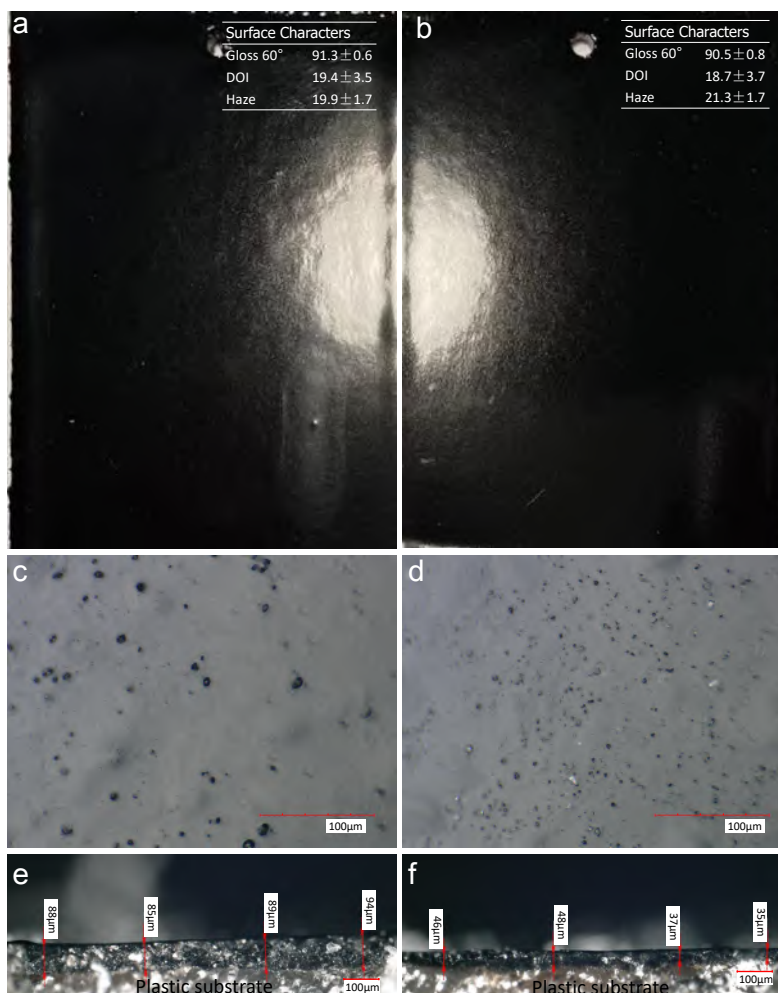


Figure 10.6: The top and cross-sectional surfaces of qualified epoxy films. a, c, e) Coarse powder coating (160°C / 0wt%); b, d, f) fine powder coating (140°C / 0.5wt%).

10.4.3 Epoxy-polyester powder coating

Since the feasibility of applying the fine epoxy powder coating to plastic substrates via the functional additive has been detailedly analyzed and discussed, the additive was extendedly tested in a fine epoxy-polyester (hybrid) powder coating system. First of all, the flowability of coarse and fine hybrid powders was determined as seen in Fig. 10.8. The medium size of the coarse and fine powder coatings separately are 43.54 µm and 21.06 µm. The coarse powder exhibits a good flowability due to the small AOR of 35.9°. The increasing dosage of the additive apparently improve the flowability of fine powders. After adding just 0.1wt% additive, the AOR of the fine hybrid powder is about 39.6°, which already meets the minimum

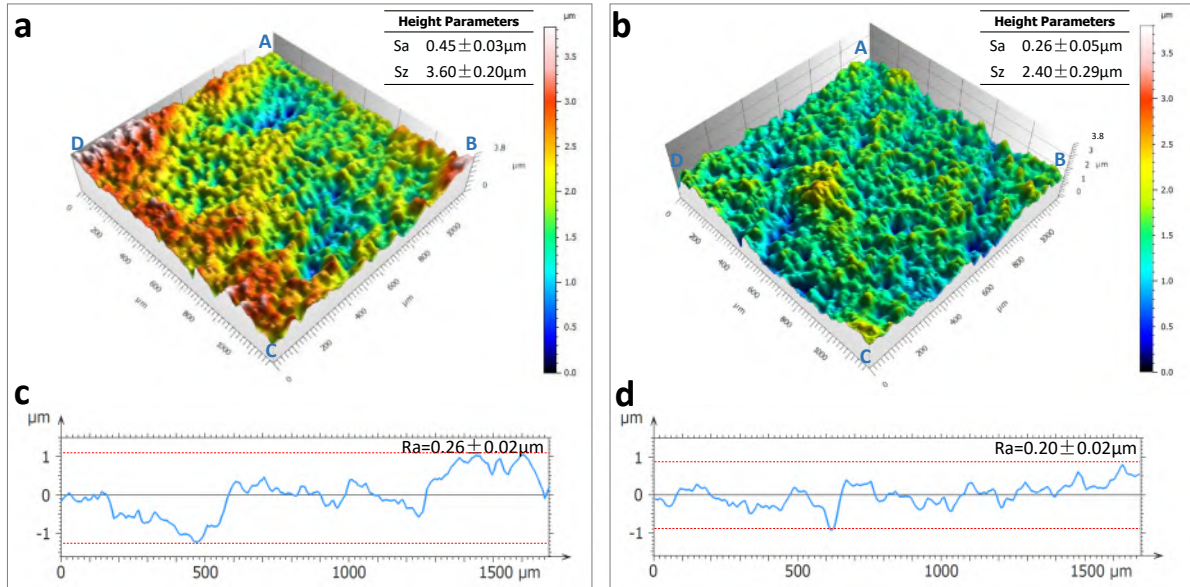


Figure 10.7: The surface roughness of the coarse and fine epoxy powder-coating films, a) coarse film; b) fine film; c) the profile of AC line in a; d) the profile of AC line in b.

requirement of flowability ($<40^\circ$). Above all, the minimum additive content is figured out to be 0.1 wt% for the fine hybrid powder coating.

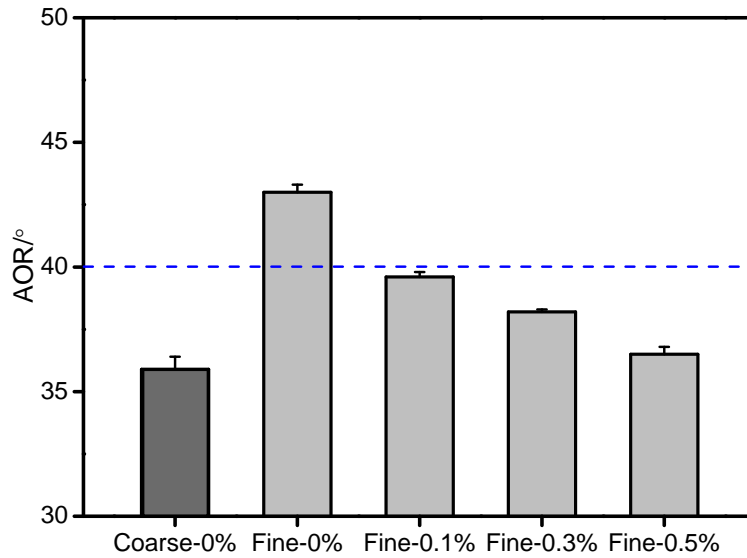


Figure 10.8: The flowability of the fine hybrid powder coatings with various contents of the bifunctional additive.

To find the lowest curing temperature for the coarse and fine hybrid powder coatings, the degrees of cure of films prepared at different temperatures and additive contents were examined by the MEK-rubbing test and illustrated in Table 10.2. The films prepared from the coarse

powder coating attains a qualified cure when the curing temperature is 150°C. The lowest curing temperature for the fine powder coatings is turned out to be 130°C after testing different conditions. Compared to the epoxy powder coatings, both the coarse and fine hybrid powder coatings have smaller lowest curing temperatures. A probable reason behind this is that the crosslinking reaction rate of the hybrid powder coating is moderately faster than that of the epoxy one at the same condition. By combining the results of flowability and degree of cure, the appropriate content of the bifunctional additive is found to be 0.3 wt%. In summary, the lowest curing temperature and additive content for the fine hybrid powder coating to obtain a qualified film are 130°C and 0.3 wt%, respectively.

Table 10.2: The double rubs of hybrid films prepared at different curing temperatures and additive contents.

	120°C	130°C	140°C	150°C	160°C
Coarse-0 wt%	1	3	30	>50	>50
Fine-0.1 wt%	3	10	38	>50	>50
Fine-0.3 wt%	35	>50	>50	>50	>50
Fine-0.5 wt%	45	>50	>50	>50	>50

More than 50 double rubs means the film has a qualified degree of cure.

The dynamic and isothermal DSC analyses of hybrid powders were illustrated in Fig. 10.9. By dosing 0.3wt% bifunctional additive, the melting point slightly declines from 70.0 to 68.9°C, and the curing onset and peak temperatures separately decrease from 103.1 to 101.8°C and from 174.8 to 169.0°C. Also, the isothermal results in Fig. 10.9b show that the heating time for the full cure at 180°C reduces from 14.1 to 7.8 after using 0.3wt% additive. These comparisons prove that the bifunctional additive accelerates the crosslinking reaction of the hybrid powder. In other words, the bifunctional additive has the ability to lower the curing temperature of the hybrid powder coating.

The surface-coating quality of the above qualified films prepared from the coarse and fine powder coatings have been compared in Fig. 10.10. From the visual observations of coarse (Fig. 10.10a) and fine (Fig. 10.10b) films, some small bulges are seen at the edge of the coarse film, and uneven boundaries are found at the light spots on both the coarse and fine films. The surface-coating quality of the films was also quantitatively presented by Gloss 60°, DOI and Haze as displayed in the top-right tables of Fig 10.10a and b. The fine film shows a

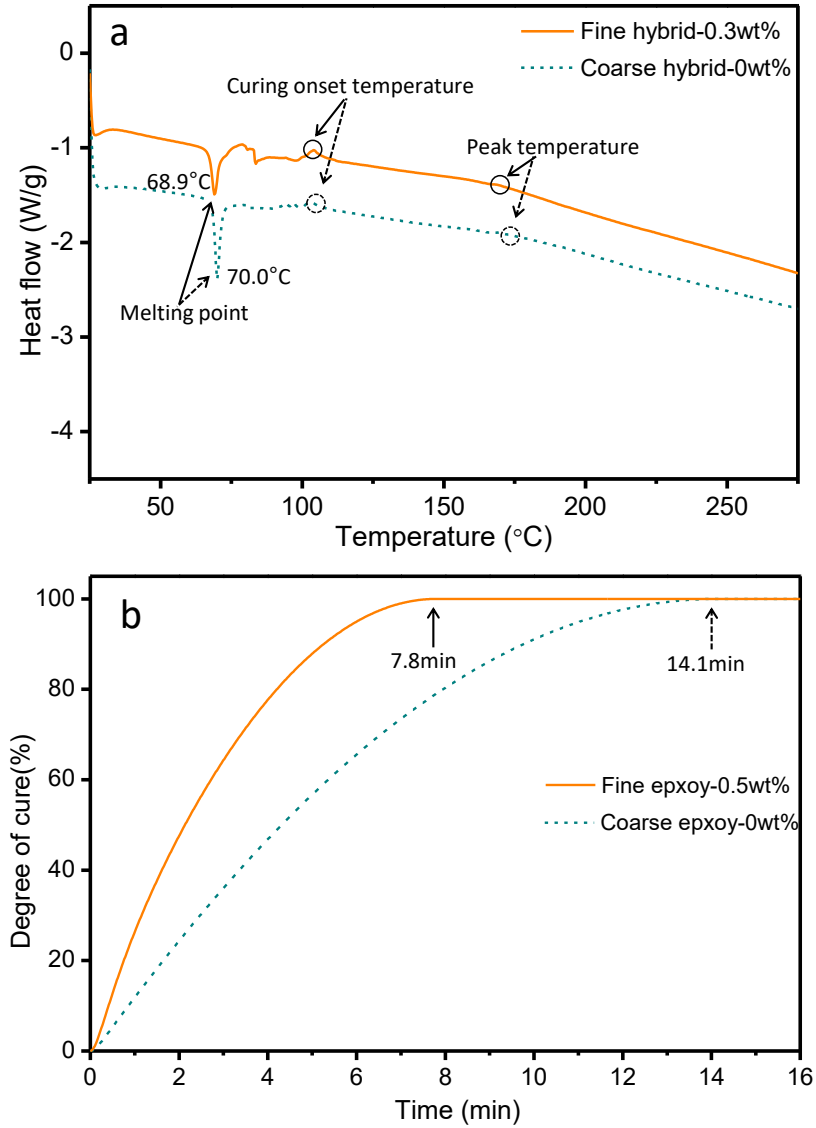


Figure 10.9: The DSC analyses of coarse and fine hybrid powders. a) Dynamic scanning of heat flow; b) Isothermal scanning for determining the degree of cure.

slightly higher gloss but a lower DOI and a higher haziness. The magnified image of the coarse (Fig. 10.10c) and fine (Fig. 10.10d) films were employed to reveal the difference in microstructure. Plenty of tiny blisters in the diameters of 0.5-2 μm are observed on the surface of the coarse film because of the degassing of the plastic substrate during curing. On the contrary, no apparent blisters are found on the surface of the fine film. A possible reason behind this that the plastic panel releases a minimal amount of gases at this relatively low curing temperature of 130°C. Fig. 10.10e and f respectively present the cross-sectional surface of the coarse and fine films. In industry, to guarantee the surface-coating quality, the thickness

of powder-coating film is generally 1.5 to 2 times of the medium size of powder. Hence, by using the fine hybrid powder coating, the film thickness reduces from $78 \pm 6 \mu\text{m}$ to $39 \pm 6 \mu\text{m}$.

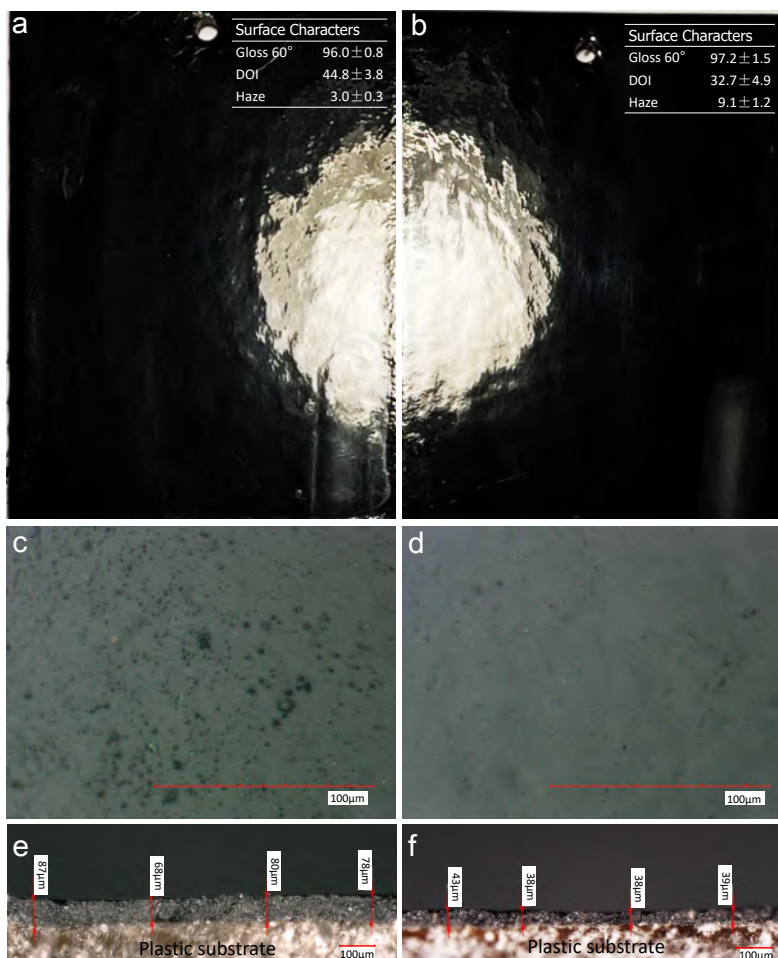


Figure 10.10: The top and cross-sectional surfaces of qualified hybrid films. a, c, e) Coarse powder coating (150°C / 0wt%); b, d, f) fine powder coating (130°C / 0.3wt%).

To compare the smoothness of the above hybrid films, the surface roughness was analyzed in Fig. 10.11. The surface of the coarse film (Fig. 10.11a) has much more yellow and red areas than that of the fine film, meaning that the coarse film possesses more elevated structures than the fine film. The surface and profile roughness parameters of S_a , S_z and R_a of the fine film (0.21, 1.93 and $0.16 \mu\text{m}$) are considerably lower than those of the coarse film (0.35, 3.00 and $0.10 \mu\text{m}$). With comparison to the previous epoxy films (Fig. 10.7), the fine hybrid film attains the smallest values of the three parameters, hinting that it has the lowest roughness. The main reason probably is that the fine hybrid film almost does not have blisters or pinholes

(Fig. 10.10d). In a word, the fine hybrid film obtains a much better smoothness than the coarse film.

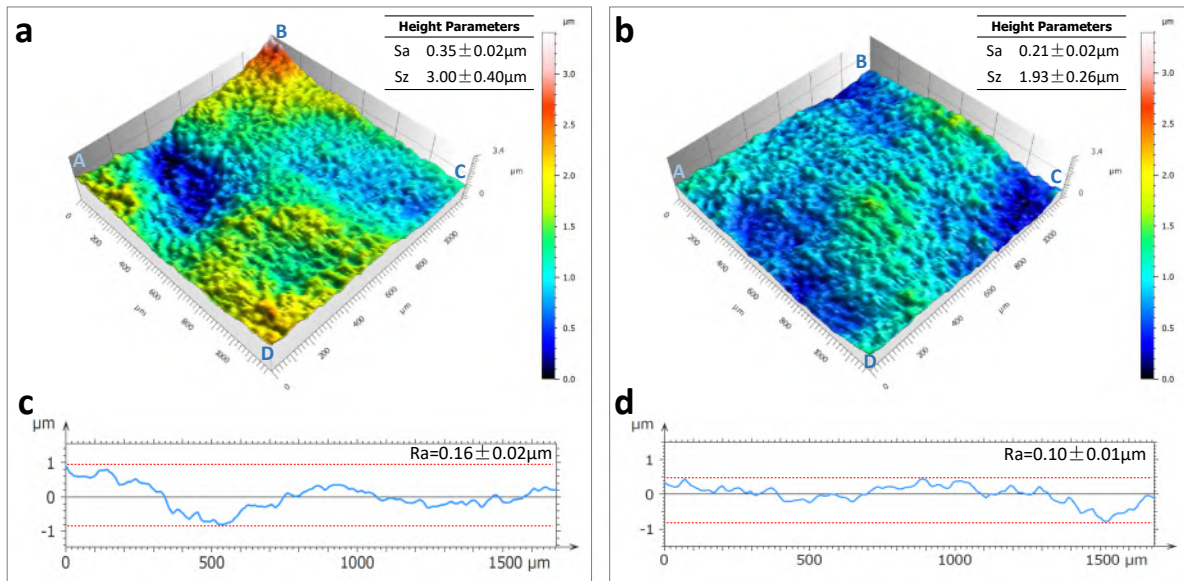


Figure 10.11: The surface roughness of the coarse and fine hybrid powder-coating films, a) coarse film; b) fine film; c) the profile of AC line in a; d) the profile of AC line in b.

10.4.4 Properties and performances of films

The hardness and adhesion, as two essential properties of coatings, of the above epoxy and hybrid films were measured as summarized in Table 10.3. The hardness of the fine/thin epoxy film (H) is one grade higher than that of the coarse/thick film (F), while their adhesion is at the same level of 2B. The fine/thin and coarse/thick hybrid films present the same hardness, but the fine/thin film has one grade lower adhesion than the coarse/thick hybrid one. By comparing the epoxy and hybrid coatings, it can be concluded that the epoxy coatings have higher hardness, but the hybrid films own better adhesion.

In addition, the mechanical performance of some fibre-reinforced plastics, for example polyamides, will vastly reduce after absorbing water [35], so the water resistance of these coatings was assessed by the water absorption. The involved plastic panels without coatings absorbed about 1.0 wt% water after 24-hour water immersions. However, the water absorption markedly decreases to a deficient level of 0.12-0.14 wt% after covered by coating, illustrating that these coatings have considerably high water resistance. The coarse (thick) and fine (thin)

epoxy films appear to own similar water resistance, indicating that the thin film (~41 μm) is capable of providing similar protection as the thick film (~89 μm). Remarkably, the thin hybrid film prepared from fine powders shows even better water resistance. A mostly possible explanation is that they contain no obvious blister or pinhole (Fig. 10.10d), which efficiently block the permeation of water molecules. In conclusion, the fine/thin coatings can provide comparable or even better protection to the plastic substrate from water.

Table 10.3: The comparisons of hardness, adhesion and water absorption of films.

Coating type	Conditions^a	Hardness	Adhesion	Water Ab./wt%
No coating	N/A	N/A	N/A	1.027±0.005
Coarse/thick epoxy	160 / 0	F	2B	0.138± 0.005
Fine/thin epoxy	140 / 0.5	H	2B	0.141± 0.007
Coarse/thick hybrid	150 / 0	HB	4B	0.137± 0.004
Fine/thin hybrid	130 / 0.3	HB	3B	0.120± 0.005

^a The units of conditions for curing temperature and additive content are °C and wt%, respectively.

10.5 Conclusions

With the assistance of the bifunctional additive, the fibre-reinforced plastic substrates were successfully coated by the fine epoxy and hybrid powder coatings. The thicknesses of the films prepared from fine powders were only about half of those made from coarse powders. The thin films made from fine powders had similar macroscopic surface-coating quality with thick films prepared from coarse powders. Meanwhile, the utilization of the bifunctional additive to fine powder coatings significantly attenuated the impacts of blister and pinhole in the films. The surface roughness of the thin films was smaller than those of the thick films. The thin films provided similar or even better protection to the plastic substrates from water penetration. The application of the bifunctional additive is a feasible method to expand fine epoxy and hybrid powder coatings to plastic substrates.

Bibliography

- [1] Tosko Aleksandar Misev. *Powder coatings: chemistry and technology*. John Wiley & Sons Inc, 1991.
- [2] Hans-Joachim Streitberger and Karl-Friedrich Dossel. *Automotive paints and coatings*. John Wiley & Sons, 2008.
- [3] Wei Liu, Haiping Zhang, Yuanyuan Shao, Hui Zhang, and Jesse Zhu. Preparation of aluminium metallic pigmented powder coatings with high color stability using a novel method: Microwave bonding. *Progress in Organic Coatings*, 147:105787, 2020.
- [4] Springer Fachmedien Wiesbaden. High-quality finish with ultra-thin coatings. *IST International Surface Technology*, 6(2):18–19, 2013.
- [5] Anna Rudawska and Magd Abdel Wahab. The effect of cataphoretic and powder coatings on the strength and failure modes of en aw-5754 aluminium alloy adhesive joints. *International Journal of Adhesion and Adhesives*, 89:40–50, 2019.
- [6] Adrian G Bailey. The science and technology of electrostatic powder spraying, transport and coating. *J. Electrostat.*, 45(2):85–120, 1998.
- [7] John Farrell Hughes. Electrostatic powder coating. Technical report, Southampton Univ (UK) Dept of Electrical Engineering, 1984.
- [8] Wei Liu, Haiping Zhang, Yuanyuan Shao, Xinping Zhu, Yufu Wei, Hui Zhang, and Jesse Zhu. Applying microwave energy to fabricate powder coatings with strong and stable metal shine. *Progress in Organic Coatings*, 149:105929, 2020.
- [9] D Geldart. The effect of particle size and size distribution on the behaviour of gas-fluidised beds. *Powder Technology*, 6(4):201–215, 1972.
- [10] AS Biris, MK Mazumder, CU Yurteri, RA Sims, J Snodgrass, and S De. Gloss and texture control of powder coated films. *Particulate science and technology*, 19(3):199–217, 2001.
- [11] RR Cranfield and D Geldart. Large particle fluidisation. *Chemical Engineering Science*, 29(4):935–947, 1974.
- [12] D Geldart. Estimation of basic particle properties for use in fluid—particle process calculations. *Powder Technology*, 60(1):1–13, 1990.
- [13] S Gao, XP Zhu, H Zhang, and J Zhu. *Powder coating of plastic components, in Novi, MI: SPE Automotive Composites Conference & Exhibition*. 2016.
- [14] Andrew T Daly, Navin B Shah, Glenn D Correll, and Karl R Wursthorn. Smooth thin film powder coatings, January 13 1998. US Patent 5,708,039.
- [15] Richard D Smith. Supercritical fluid molecular spray thin films and fine powders. Technical report, BATTELLE MEMORIAL INSTITUTE, 1988.

- [16] Jesse Zhu and Hui Zhang. Fluidization additives to fine powders, December 21 2004. US Patent 6,833,185.
- [17] U Shah, C Zhang, and J Zhu. Comparison of electrostatic fine powder coating and coarse powder coating by numerical simulations. *Journal of electrostatics*, 64(6):345–354, 2006.
- [18] Qing Huang, Hui Zhang, and Jesse Zhu. Flow properties of fine powders in powder coating. *Particuology*, 8(1):19–27, 2010.
- [19] Jing-Xu Zhu and Hui Zhang. Ultrafine powder coatings: an innovation. *Powder Coat*, 16:39–47, 2005.
- [20] Arnaud L Amadjikpè, Debabani Choudhury, George E Ponchak, Bo Pan, Yuan Li, and John Papapolymerou. Proximity effects of plastic laptop covers on radiation characteristics of 60-ghz antennas. *IEEE Antennas and Wireless Propagation Letters*, 8:763–766, 2009.
- [21] Wang Qiang. Mould design of front cover of double-cover cellphone. *Forging & Stamping Technology*, 2, 2006.
- [22] Akshat Patil, Arun Patel, and Rajesh Purohit. An overview of polymeric materials for automotive applications. *Materials Today: Proceedings*, 4(2):3807–3815, 2017.
- [23] Moonhyun Choi, Maeng Gi Kim, Kevin Injoe Jung, Tae Hee Lee, Miran Ha, Woochan Hyung, Hyun Wook Jung, and Seung Man Noh. Reactivity and curing efficiency of isocyanate cross-linkers with imidazole-based blocking agents for low-temperature curing of automotive clearcoats. *Coatings*, 10(10):974, 2020.
- [24] Sang Sun Lee, Jung Hee Koo, Sung Soo Lee, Soo Gyum Chai, and Jong Chan Lim. Gloss reduction in low temperature curable hybrid powder coatings. *Progress in organic coatings*, 46(4):266–272, 2003.
- [25] Glen Merfeld, Steve Mordhorst, Rainer Koeniger, A Ersin Acar, Chris Molaison, Joe Suriano, Pat Irwin, Ron Singh Warner, Ken Gray, Mark Smith, et al. Development of low temperature curing, 120 c, durable, corrosion protection powder coatings for temperature sensitive substrates. *Journal of Coatings Technology and Research*, 2(8):661–668, 2005.
- [26] Glen Merfeld, Chris Molaison, Rainer Koeniger, A Ersin Acar, Steve Mordhorst, Joe Suriano, Pat Irwin, Ron Singh Warner, Ken Gray, Mark Smith, et al. Acid/epoxy reaction catalyst screening for low temperature (120 c) powder coatings. *Progress in organic coatings*, 52(2):98–109, 2005.
- [27] United states pharmacopeia, powder flow, 2002. page 618 of PF 28(2).
- [28] National coil coating association, using solvent resistance to measure the cure of a coating system, 2012. page 1-2.
- [29] MK Trivedi, A Branton, D Trivedi, G Nayak, G Saikia, et al. Physical and structural characterization of biofield treated imidazole derivatives. *Nat Prod Chem Res*, 3(187):2, 2015.

- [30] Mahendra Trivedi, Gopal Nayak, Shrikant Patil, Rama Mohan Tallapragada, Omprakash Latiyal, and Snehasis Jana. The potential impact of biofield treatment on physical, structural and mechanical properties of stainless steel powder. *Journal of Applied Mechanical Engineering*, 4(4), 2015.
- [31] Mohammadreza Kalaei, Shahin Akhlaghi, Ali Nouri, Saeedeh Mazinani, Mehrzad Mortezaei, Mehdi Afshari, Dariush Mostafanezhad, Ahmad Allahbakhsh, Hamidreza Aliasgari Dehaghi, Ali Amirsadri, et al. Effect of nano-sized calcium carbonate on cure kinetics and properties of polyester/epoxy blend powder coatings. *Progress in Organic Coatings*, 71(2):173–180, 2011.
- [32] Matthew Krantz, Hui Zhang, and Jesse Zhu. Characterization of powder flow: Static and dynamic testing. *Powder Technology*, 194(3):239–245, 2009.
- [33] Can Li, Shuxuan Li, Li Lv, Baowei Su, and Michael Z Hu. High solvent-resistant and integrally crosslinked polyimide-based composite membranes for organic solvent nanofiltration. *Journal of Membrane Science*, 564:10–21, 2018.
- [34] Scott D Kelman, Scott Matteucci, Christopher W Bielawski, and BD Freeman. Crosslinking poly (1-trimethylsilyl-1-propyne) and its effect on solvent resistance and transport properties. *Polymer*, 48(23):6881–6892, 2007.
- [35] MA Shazed, AR Suraya, S Rahmanian, and MA Mohd Salleh. Effect of fibre coating and geometry on the tensile properties of hybrid carbon nanotube coated carbon fibre reinforced composite. *Materials & Design (1980-2015)*, 54:660–669, 2014.

11 Conclusions

11.1 Conclusions

Metallic effect powder coatings (MEPC), made by bonding metallic pigments onto regular powder coating materials, have become increasingly popular around the world due to their sparkling metallic effects and protection enhancements. Mainstream industrial production of MEPC applies a thermal bonding technology to bind the two components. However, some intrinsic drawbacks of the current commercial thermal bonding technology hinder the development and promotion of MEPC. In this thesis work, three new bonding methods for MEPC have been established and assessed.

The first investigated one was the cold bonding method. Low relative differences of the aluminum content ($\Delta\omega$) were achieved which implies that cold bonding can readily realize stable and high bonding quality at room temperature. The bonding quality of this method is found to be highly related to the dosages of binders (PA and PVA) and D.I. water. The second one studied was the SCHB method. Unlike commercial bonding, SCHB does not damage the metallic pigment and keeps the Al flakes intact, which greatly improves retainment of the metallic effect. High bonding quality can be acquired when the bonding temperature is in a wide range, 75-150 °C.

As the third but most investigated method in this study, microwave bonding was considered to give the perceived advantage of fast, controllable and selective heating of microwave. At first, the feasibility and possibility of the microwave bonding method for MEPC were tested and analyzed via a series of lab experiments. The microwave bonding (with a center frequency of 2.45GHz) of the clear polyester powder coating shows that microwave bonding is an unexpectedly effective method to bond Al flakes to coating particles. It was also found that the selective heating of the microwave plays a vital role in the bonding process, which makes heating rates (around 16 to 23°C/min) dramatically higher than that of the thermal bonding (3 to 5°C/min) and the bonding temperature lower than the T_g of powder coating. Secondly, the applicability and generality of microwave bonding for MEPC were examined by applying it to more types of MEPCs, such as epoxy-polyester and PVDF. The lab experiment results prove

that microwave bonding is also able to achieve high bonding quality for these MEPCs, proving that it is an adaptable and applicable method for the production of MEPC.

Upon successfully demonstrating its feasibility and applicability by lab experiments, the microwave bonding method was thoroughly investigated and compared to current commercial thermal bonding technology via pilot-scale tests (10 kg/batch). The results show that microwave bonding achieves a higher bonding rate (58%) and smaller color differences (0.1-0.5) compared to commercial thermal bonding (0.3-0.6), confirming that microwave bonding is a more effective and better method for the production of MEPCs. The selective heating of the microwave leads to much faster heating rates, about 10 to 15°C/min, which significantly reduces the processing time and improves bonding efficiency. By changing the powder motion from rotation to agitation, an even higher bonding rate was gained (72%). Above all, the pilot-scale results demonstrate that the microwave bonding method is superior to commercial thermal bonding.

Since the pilot-scale data proved that microwave bonding provided higher bonding quality and better color stability than commercial thermal bonding, the color stability, productivity and energy consumption of the two methods were further tested and compared by industrial-scale tests (100 kg/batch). The results re-confirmed that microwave bonding is capable of providing better quality products with lower costs and larger productivity compared to current thermal bonding. The color difference of the microwave-bonded films (0.96) is much lower than those of non-bonded (2.07) and thermal-bonded (3.87) samples. Overall, microwave bonding can produce more and better MEPCs at a lower cost in contrast to current commercial bonding.

In conclusion, the microwave bonding method, given its incomparable advantages, has achieved superior bonding quality and higher color stability than the thermal bonding method currently used commercially. Moreover, based on the solid experiments and reliable results, the microwave bonding apparatus has been scaled up from a lab-scale device (0.05 kg/batch) to a pilot-scale (10 kg/batch) and finally to an industrial-scale (100 kg/batch) machine that is expected to create enormous commercial value in the foreseeable future.

11.2 Contributions

Several contributions of this work were brought to the scientific community.

Firstly, developing several new bonding methods for metallic powder coatings, such as cold bonding, SCHB bonding, and microwave bonding.

Secondly, a quantitative and direct analysis method for bonding quality was firstly established, which uses Al contents that determined by the gas-volumetric method.

Thirdly, scaling up the microwave bonding machine from lab-scale to pilot-scale and finally to industrial-scale.

Fourthly, the reverse-folded blade of the agitator was firstly proved to be able to improve the internal circulation of powders.

Lastly, preparing a new bi-functional additive for fine powder coatings that not only lowers the curing temperature but also improves the powder flowability.

11.3 Future Work

The scale-up theory of microwave bonding device should be further explored and discussed, which was not discussed in this thesis to avoid releasing business information. In addition, the durability of the prepared metallic powder coatings should be determined. There are still lots of work about the industrial microwave bonding machine in the future. First, the current cooling system is using air to cool down the powder, which is too slow to reach room temperature. This prolongs the processing time and also makes the color adjusting hard. Second, The optimization of the heating rate still needs to be further investigated. As mentioned, the heating rate of the machine is controllable and can be as high as 18 °C/min. For obtaining a high bonding quality, there is a heating rate being optimized for each type of powder coating. Third, the number of microwave transmitters should be further adjusted. At present, the power of each transmitter is 1 kW, and the total number of transmitters is 30. However, it seems the power of microwave radiation (30 kW) is too high for the current capacity (100 kg). To reduce the cost of the machine, the number of transmitters should be further optimized.

Appendix A Original data for the figures in each chapter

A.1 Chapter 2

Table A.1: The original data for Fig. 2.5

	0.01g	0.03g	0.06g
0.1	247.03	35.16	0.9
0.2	242.86	48.17	2.94
0.3	249.75	93.94	17.12
0.5	292.72	180.37	57.94

Table A.2: The original data for Fig. 2.8

	0.01g	0.03g	0.06g
0.1	247.03	35.16	0.9
0.2	242.86	48.17	2.94
0.3	249.75	93.94	17.12
0.5	292.72	180.37	57.94

A.2 Chapter 3

Table A.3: The original data for Fig. 3.3

	before srpaying		after spraying	
	AI%	std	AI%	std
non-bonded	2.23	0	1.085	0.06
50	2.15	0	1.12	0.05
75	2.25	0.01	2.26	0.08
100	2.3	0	2.17	0.06
125	1.86	0	2.02	0.1
150	2.25	0	2.37	0.08

A.3 Chapter 4

Table A.4: The original data for Fig. 4.4A

	30		60		90	
	Ave.	std	Ave.	std	Ave.	std
0.3g	5.36	0.11	3.14	0.08	1.28	0.02
0.4g	5.18	0.09	1.49	0.01	1.16	0.05
0.5g	5.17	0.15	1.47	0.02	1.28	0.04

Table A.5: The original data for Fig. 4.4B

	30		60		90	
	Ave.	std	Ave.	std	Ave.	std
0.3g	149.30	5.33	140.93	3.12	140.47	6.67
0.4g	46.05	2.55	41.86	1.71	-31.63	2.10
0.5g	-40.47	2.07	-46.05	3.93	-40.47	3.10

Table A.6: The original data for Fig. 4.6

	Non		30rpm		45rpm		60rpm	
	Ave.	std	Ave.	std	Ave.	std	Ave.	std
30kV	140.93	3.12	47.52	5.19	39.17	2.22	40.69	3.37
60kV	41.86	1.71	27.67	2.09	24.42	2.89	22.89	1.23
90kV	-46.05	3.93	-22.51	2.09	-20.28	2.12	-33.06	1.92

Table A.7: The original data for Fig. 4.7

	Non		45		47		48		49		50	
	Ave.	std	Ave.	std	Ave.	std	Ave.	std	Ave.	std	Ave.	std
30kV	142.06	3.62	46.33	8.75	39.17	3.41	27.83	3.04	48.88	4.71	69.57	4.18
60kV	41.86	2.29	10.55	4.49	24.42	2.87	2.83	2.33	-6.28	5.41	-6.28	5.41
90kV	-45.79	4.38	-38.07	1.72	-20.28	3.58	-24.06	2.11	-21.53	1.89	-30.44	7.22

A.4 Chapter 5

Table A.8: The original data for Fig. 5.7

	30		60		90	
	Ave.	std	Ave.	std	Ave.	std
non	0.31209	0.01316	0.07265	0.01392	-0.24866	-0.00878
48°C-50%	0.32414	0.0124	0.23853	0.00149	-0.17558	-0.01263
48°C-70%	0.2994	0.00859	0.13572	0.00125	-0.16995	-0.03957
48°C-100%	0.27992	0.00812	0.08641	0.01584	-0.15684	-0.00822
50°C-50%	0.11754	0.01013	0.08647	0.00537	-0.1599	-0.0135
50°C-70%	0.11564	0.00431	0.01899	0.00385	-0.15723	-0.01621
50°C-100%	0.21316	0.01257	0.04673	0.00164	-0.11382	-0.00819

Table A.9: The original data for Fig. 5.3

	30		60		90	
	Ave.	std	Ave.	std	Ave.	std
non	0.57401	0.05686	0.55693	0.05947	-0.23644	0.03892
62°C	0.62991	0.07963	0.51773	0.06455	-0.14056	0.01931
65°C	0.57488	0.0377	0.46929	0.01759	-0.07801	0.04043
68°C	0.37208	0.03087	0.31071	0.01586	-0.05734	0.00212

Table A.10: The original data for Fig. 5.11

	30		60		90	
	Ave.	std	Ave.	std	Ave.	std
non	1.03804	0.14	0.13225	0.03	-0.15217	0.06
62°C	1.0163	0.1	0.22666	0.05	-0.0846	0.02
65°C	0.68478	0.099	0.03231	0.02	-0.05827	0.005
68°C	0.44022	0.081	0.12568	0.05	-0.03268	0.015

A.5 Chapter 6

Table A.11: The original data for Fig. 6.3

	Thermal	MW 54°C	MW 58°C	MW 59.5°C	MW 60.5°C	MW 61.5°C
30/6.5	34.14%	9.20%	36.55%	36.69%	36.55%	35.10%
60/6.5	44.38%	7.74%	48.30%	50.91%	49.92%	47.33%
60/5.5	41.46%	11.15%	54.60%	60.68%	54.84%	60.30%
90/6.5	51.25%	15.96%	57.13%	58.48%	59.58%	52.53%
std	0.56%	1.87%	1.80%	0.03%	1.07%	1.43%
	2.78%	6.16%	4.87%	3.01%	2.14%	1.48%
	2.67%	2.46%	8.47%	4.58%	4.74%	3.69%
	1.64%	4.90%	3.37%	3.91%	4.99%	1.59%

Table A.12: The original data for Fig. 6.4

	Non-bonded	Thermal	MW 54°C	MW 58°C	MW 59.5°C	MW 60.5°C	MW 61.5°C
30/6.5	2.242266	0.499244	1.60815	0.88606	0.331424	0.376467	0.842985
60/6.5	1.954738	0.238834	1.39893	0.581179	0.3511	0.220567	0.845746
60/5.5	2.137965	0.262711	1.549994	0.409127	0.165512	0.218456	0.943638
90/6.5	2.00979	0.25314	1.477	0.451334	0.05244	0.180736	0.839661
std	0.383604	0.139164	0.327143	0.18994	0.136639	0.144662	0.173064
	0.262447	0.150831	0.065225	0.11566	0.053984	0.141351	0.073595
	0.39921	0.14953	0.401775	0.156774	0.092342	0.133912	0.183839
	0.199471	0.133941	0.04943	0.111784	0.074162	0.049687	0.354033

Table A.13: The original data for Fig. 6.5A

	30r/min	40r/min	50r/min
30/6.5	31.61%	36.69%	37.08%
60/6.5	51.81%	50.91%	38.62%
60/5.5	57.02%	60.68%	50.39%
90/6.5	51.60%	58.48%	52.89%
std	5.06%	0.03%	2.50%
	1.55%	3.01%	5.94%
	0.37%	4.58%	7.92%
	4.63%	3.91%	0.63%

Table A.14: The original data for Fig. 6.5B

	30r/min	40r/min	50r/min
30kV	0.465569	0.331424	0.508006
60kV	0.171939	0.3511	0.472677
60kV/5.5	0.420919	0.165512	0.599802
90kV	0.365	0.05244	0.39152
std	0.363585	0.136639	0.172441
	0.097079	0.053984	0.138101
	0.169389	0.092342	0.273614
	0.219203	0.074162	0.306307

Table A.15: The original data for Fig. 6.8A

	Thermal 65°C	MW 59°C	MW 60°C	MW 61°C
30/6.5	25.25%	23.90%	30.33%	46.77%
60/6.5	34.08%	41.31%	39.77%	46.54%
60/5.5	37.52%	38.64%	47.22%	53.21%
90/6.5	33.88%	35.57%	36.86%	51.72%
std	0.02%	3.90%	0.86%	0.69%
	1.28%	1.94%	1.67%	0.77%
	1.61%	0.10%	1.08%	2.05%
	1.26%	0.51%	3.78%	0.15%

Table A.16: The original data for Fig. 6.8B

	Thermal 65°C	MW 59°C	MW 60°C	MW 61°C
30/6.5	0.487729	0.328359	0.214539	0.36273
60/6.5	0.283062	0.226654	0.203466	0.228079
60/5.5	0.248632	0.184544	0.184786	0.193738
90/6.5	0.438049	0.327843	0.203989	0.01
std	0.114999	0.069689	0.04059	0.054705
	0.047869	0.07908	0.084034	0.112676
	0.025657	0.053405	0.124679	0.103917
	0.011219	0.020921	0.074008	0.014142

A.6 Chapter 7

Table A.17: The original data for Fig. 7.3

speed	500	600	700	800
sieve residue	100	37	8	0.5

Table A.18: The original data for Fig. 7.4

	Thermal 65°C	MW 59°C	MW 60°C	MW 61°C
30/6.5	0.35758778	0.56913738	0.57184601	0.73469817
60/6.5	0.28764236	0.50936866	0.52410708	0.67093391
60/5.5	0.30648623	0.51550222	0.5312696	0.69464366
90/6.5	0.33144542	0.55218956	0.47882732	0.6719378
std	0.01442536	0.00179711	0.00404053	0.00471048
	0.00116708	0.01909174	0.01779596	0.00248797
	0.00938296	0.0118224	0.00282131	0.00350575
	0.02290542	0.05607399	0.01256795	0.03524434

Table A.19: The original data for Fig. 7.7

	30/6.5	60/6.5	60/5.5	90/6.5
Non	6.00	5.33	5.14	5.00
Thermal 62°C	3.79	3.55	3.72	3.29
55°C	2.47	2.37	2.45	2.39
57°C	2.18	2.11	1.77	1.68
59°C	0.24	0.07	0.07	0.02
std	0.16	0.27	0.41	0.06
	0.25	0.35	0.23	0.11
	0.03	0.21	0.28	0.27
	0.02	0.04	0.08	0.09
	0.07	0.01	0.04	0.00

Table A.20: The original data for Fig. 7.9

	Non	Thermal 62°C	55°C	57°C	59°C
30/6.5	78.95	69.1625	64.675	61.525	57.625
60/6.5	77.325	68.5625	67.025	62.0875	59.2
60/5.5	76.7625	69.2625	64	62.5	58.975
90/6.5	76.6625	67.1875	64.925	62.4125	59.55
std	0.994269	1.048724	0.712641	1.005343	1.785457
	0.808438	1.3564	1.482999	0.75297	1.128843
	0.48679	2.423656	1.091526	0.498569	1.081996
	0.61861	1.503745	1.841389	0.923406	1.228239

Table A.21: The original data for Fig. 7.11

	30/6.5	60/6.5	60/5.5	90/6.5
Non	5.12	5.2275	4.4725	4.41
Thermal 63°C	2.785	2.4025	2.2925	2.48
MW 55°C	3.2675	2.6325	2.83	2.5475
MW 57°C	1.4175	1.4025	1.345	1.28
MW 59°C	0.195	0.165	0.1375	0.05
std	0.17	0.19	0.17	0.13
	0.22	0.44	0.1	0.2
	0.13	0.05	0.14	0.19
	0.08	0.06	0.03	0.08
	0.1	0.04	0.07	0.03

A.7 Chapter 8

Table A.22: The original data for Fig. 8.6

kW	heat speed	heat speed
0	1.2	0
0.5	5	3.8
0.8	6.3	5.1
0.8	6.1	4.9
1	8.3	7.1

Table A.23: The original data for the red curve in Fig. 8.7

time	0.00	1.00	1.17	1.67	2.17	2.67	3.17	3.67	4.17	4.33	4.50	5.00
temp.	30.00	57.00	60.00	51.00	40.00	52.00	60.00	50.00	60.00	58.00	60.00	60.50
time	5.83	6.67	7.50	8.33	9.50	9.75	9.92	10.42	10.92	10.42	10.92	
temp.	60.10	59.50	59.80	60.20	60.00	52.00	44.00	39.00	36.00	39.00	36.00	

Table A.24: The original data for the blue curve in Fig. 8.7

time	0.14	0.22	0.30	0.39	0.47	0.55	0.64	0.72	0.81	0.89	0.97	1.06	1.14
temp.	34.70	34.70	34.70	34.70	34.70	34.90	35.00	35.20	35.50	35.90	36.20	36.60	37.00
time	1.22	1.31	1.39	1.47	1.56	1.64	1.73	1.81	1.88	1.97	2.05	2.14	2.21
temp.	37.30	37.60	38.00	38.30	38.70	39.00	39.40	39.70	40.00	40.30	40.50	40.90	41.20
time	2.30	2.39	2.47	2.56	2.63	2.72	2.79	2.89	2.97	3.05	3.14	3.21	3.30
temp.	41.50	41.80	42.10	42.40	42.60	42.90	43.20	43.50	43.90	44.10	44.40	44.60	44.90
time	3.39	3.47	3.56	3.63	3.72	3.79	3.88	3.97	4.05	4.14	4.21	4.30	4.39
temp.	45.20	45.40	45.80	46.00	46.20	46.50	46.70	47.00	47.20	47.50	47.70	48.00	48.20
time	4.46	4.55	4.63	4.72	4.81	4.88	4.97	5.05	5.14	5.21	5.30	5.39	5.46
temp.	48.40	48.70	48.90	49.10	49.40	49.60	49.80	50.00	50.30	50.50	50.70	51.00	51.20
time	5.55	5.64	5.72	5.81	5.88	5.97	6.04	6.13	6.22	6.30	6.39	6.46	6.55
temp.	51.50	51.70	52.00	52.20	52.40	52.70	52.90	53.10	53.40	53.60	53.90	54.10	54.40
time	6.64	6.72	6.81	6.88	6.97	7.05	7.14	7.22	7.30	7.39	7.46	7.55	7.64
temp.	54.70	54.90	55.20	55.40	55.70	55.90	56.20	56.50	56.70	57.00	57.30	57.50	57.80
time	7.72	7.81	7.88	7.97	8.04	8.14	8.22	8.30	8.39	8.46	8.55	8.64	8.72
temp.	58.10	58.40	58.60	58.90	59.20	59.50	59.80	60.00	60.30	60.60	60.90	61.20	61.40
time	8.81	8.88	8.97	9.05	9.13	9.22	9.30	9.39	9.47	9.55	9.64	9.72	9.81
temp.	61.70	62.00	62.30	62.50	62.90	63.20	63.40	63.80	64.00	64.30	64.70	64.90	65.20
time	9.88	9.97	10.05	10.14	10.21	10.30	10.39	10.47	10.55	10.64	10.72	10.80	10.88
temp.	65.50	65.80	66.00	66.40	66.70	67.00	67.30	67.60	68.00	68.40	68.70	68.90	69.20
time	10.98	11.05	11.14	11.22	11.31	11.38	11.47	11.54	11.63	11.72	11.80	11.89	11.96
temp.	69.40	69.50	69.50	69.40	69.30	69.20	69.10	69.10	69.00	69.00	68.90	68.90	68.80
time	12.05	12.14	12.22	12.31	12.38	12.47	12.55	12.64	12.71	12.80	12.89	12.97	13.06
temp.	68.70	68.60	68.60	68.50	68.40	68.40	68.30	68.20	68.10	68.10	68.10	68.10	68.10
time	13.13	13.22	13.30	13.38	13.47	13.55	13.64	13.71	13.80	13.89	13.97	14.06	14.13
temp.	68.10	68.10	68.10	68.10	68.10	68.00	68.00	68.00	68.00	68.10	68.10	68.20	68.20
time	14.22	14.30	14.38	14.47	14.55	14.64	14.71	14.80	14.89	14.97	15.06	15.14	15.22
temp.	68.20	68.20	68.30	68.30	68.30	68.30	68.30	68.20	68.10	67.90	67.70	67.40	67.00
time	15.31	15.38	15.47	15.55	15.63	15.72	15.80	15.89	15.96	16.05	16.14	16.22	16.30
temp.	66.50	66.00	65.40	65.00	64.60	64.20	63.80	63.30	62.90	62.30	61.90	61.60	61.30
time	16.38	16.47	16.56	16.63	16.72	16.80	16.89	16.96	17.05	17.14	17.22	17.30	17.39
temp.	61.10	60.80	60.50	60.30	60.10	59.90	59.70	59.50	59.30	59.10	58.90	58.60	58.40
time	17.47	17.56	17.63	17.72	17.79	17.88	17.97	18.05	18.14	18.21	18.30	18.39	18.47
temp.	58.20	58.00	57.70	57.60	57.50	57.40	57.20	57.10	57.00	56.80	56.70	56.50	56.30
time	18.56	18.63	18.72	18.79	18.88	20.22	21.56	22.35	23.65	24.33			
temp.	56.20	56.10	55.90	55.70	55.60	54.30	53.20	52.10	51.00	49.80			

A.8 Chapter 10

Table A.25: The original data for Fig. 10.4

Additive content/%	0	0.1	0.3	0.5
AOR/°	44.8	42.1	39	37.8
std	0.3	0.4	0.3	0.1

Table A.26: The original data for Fig. 10.8

Additive content/%	0	0.1	0.3	0.5
AOR/°	43	39.6	38.2	36.5
std	0.3	0.2	0.1	0.3

Appendix B The settings of CFD simulation

The image shows the 'Turbulence Model' settings panel. It is divided into several sections:

- Model:** Radio buttons for Laminar, k-epsilon (2 eqn) (selected), k-omega (2 eqn), and Reynolds Stress (7 eqn).
- k-epsilon Model:** Radio buttons for Standard, RNG (selected), and Realizable.
- RNG Options:** Checkboxes for Differential Viscosity Model (unchecked) and Swirl Dominated Flow (checked).
- Near-Wall Treatment:** Radio buttons for Standard Wall Functions (selected), Scalable Wall Functions, Non-Equilibrium Wall Functions, Enhanced Wall Treatment, Menter-Lechner, and User-Defined Wall Functions.
- Options:** Checkboxes for Curvature Correction, Production Kato-Lauder, and Production Limiter (all unchecked).
- Turbulence Multiphase Model:** Radio buttons for Mixture, Dispersed (selected), and Per Phase.
- Model Constants:** A list of input fields: Cmu (0.0845), C1-Epsilon (1.42), C2-Epsilon (1.68), C3-Epsilon (1.3), Swirl Factor (0.07), and Dispersion Prandtl Number (0.75).
- User-Defined Functions:** Two dropdown menus for Turbulent Viscosity, set to 'none' for 'phase-air' and 'phase-particle'.

Figure B.1: The turbulence model

The image shows the 'Cell Zone Conditions' panel for a rotor area. It includes the following settings:

- Zone Name:** inner_domainb
- Phase:** mixture
- Options:**
 - Frame Motion, 3D Fan Zone, Source Terms (unchecked)
 - Mesh Motion (checked), Laminar Zone, Fixed Values (unchecked)
 - Porous Zone (unchecked)
- Reference Frame:** Mesh Motion (selected)
- Relative Specification:** Relative To Cell Zone: absolute; UDF: Zone Motion Function: none
- Rotation-Axis Origin:** X (mm): 0, Y (mm): 0, Z (mm): 0
- Rotation-Axis Direction:** X: 0, Y: 0, Z: 1
- Rotational Velocity:** Speed (rpm): 500
- Translational Velocity:** X (m/s): 0, Y (m/s): 0, Z (m/s): 0
- Copy To Frame Motion:** (button)

Figure B.2: Cell zone conditions of rotor areas.

Zone Name: out_domain Phase: mixture

Frame Motion 3D Fan Zone Source Terms

Mesh Motion Laminar Zone Fixed Values

Porous Zone

Reference Frame | Mesh Motion | Porous Zone | 3D Fan Zone | Embedded LES | Reaction | Source Terms | Fixed Values | Multiphase

Rotation-Axis Origin: X (mm) 0, Y (mm) 0, Z (mm) 0

Rotation-Axis Direction: X 0, Y 0, Z 1

Figure B.3: Cell zone conditions of static area.

Zone Name: inpellerm Phase: mixture

Adjacent Cell Zone: inner_domain

Momentum | Thermal | Radiation | Species | DPM | Multiphase | UDS | Wall Film | Potential | Structure

Wall Motion: Stationary Wall, Moving Wall

Motion: Relative to Adjacent Cell Zone, Absolute

Speed (rpm): 0

Rotation-Axis Origin: X (mm) 0, Y (mm) 0, Z (mm) 0

Rotation-Axis Direction: X 0, Y 0, Z 1

Wall Roughness: Standard, High Roughness (Icing)

Sand-Grain Roughness: Roughness Height (mm) 0, Roughness Constant 0.5

Figure B.4: Boundary conditions of rotor areas.

Zone Name: wall-26 Phase: mixture

Adjacent Cell Zone: inner_domain

Interface Zone: contact_region_2-src

Momentum | Thermal | Radiation | Species | DPM | Multiphase | UDS | Wall Film | Potential | Structure

Wall Motion: Stationary Wall, Moving Wall

Motion: Relative to Adjacent Cell Zone, Absolute

Speed (rpm): 0

Rotation-Axis Origin: X (mm) 0, Y (mm) 0, Z (mm) 0

Rotation-Axis Direction: X 0, Y 0, Z 1

Wall Roughness: Standard, High Roughness (Icing)

Sand-Grain Roughness: Roughness Height (mm) 0, Roughness Constant 0.5

Figure B.5: Boundary conditions of the surface close to the rotor area.

Zone Name	wall-27		Phase	mixture											
Adjacent Cell Zone	out_domain														
Interface Zone	contact_region_2-trg														
<table border="1"> <tr> <td>Momentum</td> <td>Thermal</td> <td>Radiation</td> <td>Species</td> <td>DPM</td> <td>Multiphase</td> <td>UDS</td> <td>Wall Film</td> <td>Potential</td> <td>Structure</td> </tr> </table>						Momentum	Thermal	Radiation	Species	DPM	Multiphase	UDS	Wall Film	Potential	Structure
Momentum	Thermal	Radiation	Species	DPM	Multiphase	UDS	Wall Film	Potential	Structure						
Wall Motion															
<input type="radio"/> Stationary Wall <input checked="" type="radio"/> Moving Wall		<input type="radio"/> Relative to Adjacent Cell Zone <input checked="" type="radio"/> Absolute		Speed (rpm) 500											
		<input type="radio"/> Translational <input checked="" type="radio"/> Rotational <input type="radio"/> Components		Rotation-Axis Origin											
		<input type="text"/> X (mm) 0		<input type="text"/> X ₀											
		<input type="text"/> Y (mm) 0		<input type="text"/> Y ₀											
		<input type="text"/> Z (mm) 0		<input type="text"/> Z ₁											
Wall Roughness															
<input checked="" type="radio"/> Standard <input type="radio"/> High Roughness (Icing)		Sand-Grain Roughness													
		<input type="text"/> Roughness Height (mm) 0													
		<input type="text"/> Roughness Constant 0,5													

Figure B.6: Boundary conditions of the surface close to the static area.

Zone Name	wall		Phase	mixture											
Adjacent Cell Zone	out_domain														
<table border="1"> <tr> <td>Momentum</td> <td>Thermal</td> <td>Radiation</td> <td>Species</td> <td>DPM</td> <td>Multiphase</td> <td>UDS</td> <td>Wall Film</td> <td>Potential</td> <td>Structure</td> </tr> </table>						Momentum	Thermal	Radiation	Species	DPM	Multiphase	UDS	Wall Film	Potential	Structure
Momentum	Thermal	Radiation	Species	DPM	Multiphase	UDS	Wall Film	Potential	Structure						
Wall Motion															
<input checked="" type="radio"/> Stationary Wall <input type="radio"/> Moving Wall		<input checked="" type="checkbox"/> Relative to Adjacent Cell Zone													
Wall Roughness															
<input checked="" type="radio"/> Standard <input type="radio"/> High Roughness (Icing)		Sand-Grain Roughness													
		<input type="text"/> Roughness Height (mm) 0													
		<input type="text"/> Roughness Constant 0,5													

Figure B.7: Boundary conditions of the tank wall.

Name
phase-particle

Phase Material

Granular
 Packed Bed

Granular Temperature Model

Phase Property
 Partial Differential Equation

Properties

Diameter (mm)	constant	<input type="button" value="Edit..."/>
	<input type="text" value="0.04"/>	
Granular Viscosity (kg/m-s)	gidaspow	<input type="button" value="Edit..."/>
	<input type="text"/>	
Granular Bulk Viscosity (kg/m-s)	lun-et-al	<input type="button" value="Edit..."/>
	<input type="text"/>	
Frictional Viscosity (kg/m-s)	schaeffe	<input type="button" value="Edit..."/>
	<input type="text"/>	
Angle Of Internal Friction (deg)	constant	<input type="button" value="Edit..."/>
	<input type="text" value="30.00007"/>	
Frictional Pressure (pascal)	based-ktgf	<input type="button" value="Edit..."/>
	<input type="text"/>	
Frictional Modulus (pascal)	derived	<input type="button" value="Edit..."/>
	<input type="text"/>	
Friction Packing Limit	constant	<input type="button" value="Edit..."/>
	<input type="text" value="0.2"/>	
Granular Temperature (m2/s2)	algebraic	<input type="button" value="Edit..."/>
	<input type="text"/>	
Solids Pressure (pascal)	lun-et-al	<input type="button" value="Edit..."/>
	<input type="text"/>	
Radial Distribution	lun-et-al	<input type="button" value="Edit..."/>
	<input type="text"/>	
Elasticity Modulus (pascal)	derived	<input type="button" value="Edit..."/>
	<input type="text"/>	

Figure B.8: Properties of the particle phase.


```

iter continuity u-phase-ai u-phase-pa v-phase-ai v-phase-pa w-phase-ai w-phase-pa k-phase-ai eps-phase-ai vf-phase-p time/iter
i2305073 solution is converged
2305073 9.5034e-05 5.5455e-07 1.1958e-08 5.5540e-07 7.0326e-07 5.0002e-07 4.9137e-07 1.1641e-07 1.0015e-06 5.1528e-05 0:00:00 100
2305074 1.2893e-02 3.9872e-05 1.4535e-05 4.0072e-05 2.0421e-05 1.8742e-04 4.7822e-05 1.4341e-04 4.0768e-04 6.0503e-05 0:01:58 99
2305075 5.7264e-03 2.7418e-05 3.5065e-05 2.7206e-05 3.5249e-04 1.2897e-04 3.6540e-04 8.6545e-05 2.5269e-04 5.5411e-05 0:01:48 98
2305076 3.6445e-03 1.6978e-05 6.4702e-05 1.6765e-05 4.5398e-04 8.8415e-05 3.8624e-04 5.2997e-05 1.5722e-04 5.3233e-05 0:01:39 97
2305077 2.7065e-03 1.1578e-05 6.5199e-05 1.1508e-05 4.4172e-04 6.1819e-05 3.2070e-04 3.2539e-05 9.8282e-05 5.2294e-05 0:01:32 96
2305078 2.1291e-03 8.5398e-06 5.3628e-05 8.5791e-06 3.8794e-04 4.3801e-05 2.3366e-04 2.0052e-05 6.1752e-05 5.1869e-05 0:01:25 95
2305079 1.7067e-03 6.6304e-06 3.7472e-05 6.7001e-06 3.2340e-04 3.1197e-05 1.5732e-04 1.2420e-05 3.9052e-05 5.1678e-05 0:01:21 94
2305080 1.3799e-03 5.4838e-06 2.2179e-05 5.5465e-06 2.6169e-04 2.2302e-05 9.1445e-05 7.7492e-06 2.4989e-05 5.1585e-05 0:01:13 93
2305081 1.1221e-03 4.7484e-06 9.7691e-06 4.7940e-06 2.0791e-04 1.6012e-05 5.9797e-05 4.8905e-06 1.6269e-05 5.1545e-05 0:01:07 92
2305082 9.1813e-04 4.1575e-06 1.4079e-06 4.1882e-06 1.6355e-04 1.1581e-05 3.3811e-05 3.1331e-06 1.0827e-05 5.1525e-05 0:01:07 91
2305083 7.5721e-04 3.6592e-06 3.5088e-06 3.6775e-06 1.2796e-04 8.4459e-06 1.7097e-05 2.0517e-06 7.4163e-06 5.1516e-05 0:01:08 90

iter continuity u-phase-ai u-phase-pa v-phase-ai v-phase-pa w-phase-ai w-phase-pa k-phase-ai eps-phase-ai vf-phase-p time/iter
2305084 6.3012e-04 3.2224e-06 5.9515e-06 3.2312e-06 9.9815e-05 6.2600e-06 6.6694e-06 1.3847e-06 5.2980e-06 5.1511e-05 0:01:07 89
2305085 5.2955e-04 2.8425e-06 6.8023e-06 2.8458e-06 7.7719e-05 4.7044e-06 4.2815e-07 9.7150e-07 3.9513e-06 5.1510e-05 0:01:06 88
2305086 4.5080e-04 2.5116e-06 6.7082e-06 2.5063e-06 6.0450e-05 3.6114e-06 3.0737e-06 7.0871e-07 3.0514e-06 5.1505e-05 0:01:06 87
2305087 3.8770e-04 2.2309e-06 6.1045e-06 2.2232e-06 4.6990e-05 2.8313e-06 4.8251e-06 5.4152e-07 2.4841e-06 5.1507e-05 0:01:04 86
2305088 3.3682e-04 1.9815e-06 5.2974e-06 1.9719e-06 3.6501e-05 2.2738e-06 5.4998e-06 4.3125e-07 2.1249e-06 5.1505e-05 0:01:02 85
2305089 2.9618e-04 1.7721e-06 4.4349e-06 1.7605e-06 2.8346e-05 1.8765e-06 5.5301e-06 3.5662e-07 1.8858e-06 5.1507e-05 0:01:02 84
2305090 2.6284e-04 1.5883e-06 3.6130e-06 1.5772e-06 2.2009e-05 1.5847e-06 5.2011e-06 3.0404e-07 1.7200e-06 5.1505e-05 0:01:01 83
2305091 2.3459e-04 1.4325e-06 2.8879e-06 1.4205e-06 1.7077e-05 1.3656e-06 4.6971e-06 2.6543e-07 1.5950e-06 5.1506e-05 0:01:01 82
2305092 2.1218e-04 1.2976e-06 2.2674e-06 1.2853e-06 1.3250e-05 1.2024e-06 4.1288e-06 2.3551e-07 1.4956e-06 5.1506e-05 0:01:00 81
2305093 1.9247e-04 1.1790e-06 1.7458e-06 1.1675e-06 1.0283e-05 1.0728e-06 3.5576e-06 2.1287e-07 1.4143e-06 5.1505e-05 0:00:59 80
2305094 1.7564e-04 1.0743e-06 1.3330e-06 1.0621e-06 7.9717e-06 9.6642e-07 3.0275e-06 1.9427e-07 1.3461e-06 5.1505e-05 0:01:01 79

iter continuity u-phase-ai u-phase-pa v-phase-ai v-phase-pa w-phase-ai w-phase-pa k-phase-ai eps-phase-ai vf-phase-p time/iter
2305095 1.6186e-04 9.8910e-07 9.9914e-07 9.7723e-07 6.1829e-06 8.8561e-07 2.5516e-06 1.7948e-07 1.2906e-06 5.1507e-05 0:00:59 78
2305096 1.4949e-04 9.0851e-07 7.3244e-07 8.9779e-07 4.7974e-06 8.1126e-07 2.1314e-06 1.6760e-07 1.2439e-06 5.1505e-05 0:00:57 77
2305097 1.3825e-04 8.3996e-07 5.3144e-07 8.2944e-07 3.7172e-06 7.4880e-07 1.7743e-06 1.5773e-07 1.2040e-06 5.1507e-05 0:00:52 76
2305098 1.2971e-04 7.8220e-07 3.7893e-07 7.7236e-07 2.8817e-06 6.9980e-07 1.4745e-06 1.4909e-07 1.1676e-06 5.1504e-05 0:00:48 75
2305099 1.2131e-04 7.2636e-07 2.5321e-07 7.1671e-07 2.3292e-06 6.5066e-07 1.2184e-06 1.4157e-07 1.1356e-06 5.1505e-05 0:00:44 74
2305100 1.1331e-04 6.7534e-07 1.6870e-07 6.6607e-07 1.7325e-06 6.0464e-07 1.0098e-06 1.3455e-07 1.1066e-06 5.1505e-05 0:00:41 73
2305101 1.0693e-04 6.3493e-07 1.0304e-07 6.2621e-07 1.3447e-06 5.7033e-07 8.3885e-07 1.2899e-07 1.0779e-06 5.1507e-05 0:00:38 72
2305102 1.0130e-04 5.9648e-07 5.2732e-08 5.8808e-07 1.0466e-06 5.3721e-07 6.9532e-07 1.2343e-07 1.0486e-06 5.1505e-05 0:00:36 71
i2305103 solution is converged
2305103 9.5337e-05 5.6047e-07 1.9736e-08 5.5273e-07 8.0944e-07 5.0518e-07 5.7938e-07 1.1826e-07 1.0184e-06 5.1506e-05 0:00:36 70
Flow time = 3.65005s, time step = 73001
9999999 more time steps

```

Figure B.9: Parts of the residuals.

```

12305103 solution is converged
iter continuity u-phase-ai u-phase-pa v-phase-ai v-phase-pa w-phase-ai w-phase-pa k-phase-ai eps-phase- vf-phase-p time/iter
2305103 9.5337e-05 6.6047e-07 1.9736e-08 5.5273e-07 8.0944e-07 5.0518e-07 5.7938e-07 1.1826e-07 1.0184e-06 5.1506e-05 0:00:52 100
2305104 1.3181e-02 3.9838e-05 2.9788e-05 3.9897e-05 8.2623e-05 1.8622e-04 3.6511e-06 1.4282e-04 4.0491e-04 6.0643e-05 0:01:02 99
2305105 5.7479e-03 2.7458e-05 7.6282e-05 2.7138e-05 4.1703e-04 1.2830e-04 3.0432e-04 8.6585e-05 2.5117e-04 5.5453e-05 0:01:03 98
2305106 3.6600e-03 1.7004e-05 9.6025e-05 1.6666e-05 5.0741e-04 8.7928e-05 3.0750e-04 5.3026e-05 1.5642e-04 5.3241e-05 0:01:04 97
2305107 2.7154e-03 1.1618e-05 8.8630e-05 1.1421e-05 4.7945e-04 6.1437e-05 2.4344e-04 3.2558e-05 9.7765e-05 5.2289e-05 0:01:04 96
2305108 2.1333e-03 8.5587e-06 1.1051e-04 8.5158e-06 4.0752e-04 4.3507e-05 1.9885e-04 2.0063e-05 6.1400e-05 5.1861e-05 0:01:04 95
2305109 1.7076e-03 6.6296e-06 1.0058e-04 6.6570e-06 3.3129e-04 3.0986e-05 1.4972e-04 1.2426e-05 3.8814e-05 5.1668e-05 0:01:03 94
2305110 1.3793e-03 5.4745e-06 7.7628e-05 5.5215e-06 2.6319e-04 2.2153e-05 1.0841e-04 7.7484e-06 2.4741e-05 5.1578e-05 0:01:03 93
2305111 1.1208e-03 4.7395e-06 5.6994e-05 4.7829e-06 2.0657e-04 1.5903e-05 7.6801e-05 4.8817e-06 1.6007e-05 5.1537e-05 0:01:03 92
2305112 9.1708e-04 4.1527e-06 4.1078e-05 4.1868e-06 1.6112e-04 1.1500e-05 5.3639e-05 3.1222e-06 1.0548e-05 5.1517e-05 0:01:03 91
2305113 7.5622e-04 3.6533e-06 2.9540e-05 3.6822e-06 1.2528e-04 8.3975e-06 3.7049e-05 2.0420e-06 7.1406e-06 5.1509e-05 0:01:02 90

iter continuity u-phase-ai u-phase-pa v-phase-ai v-phase-pa w-phase-ai w-phase-pa k-phase-ai eps-phase- vf-phase-p time/iter
2305114 6.2975e-04 3.2165e-06 2.1405e-05 3.2433e-06 9.7269e-05 6.2153e-06 2.5330e-05 1.3740e-06 5.0638e-06 5.1503e-05 0:01:01 89
2305115 5.2978e-04 2.8374e-06 1.5706e-05 2.8609e-06 7.5468e-05 4.6692e-06 1.7138e-05 9.5907e-07 3.7635e-06 5.1501e-05 0:01:00 88
2305116 4.5123e-04 2.5053e-06 1.1711e-05 2.5245e-06 5.8549e-05 3.5854e-06 1.1453e-05 7.0249e-07 2.9695e-06 5.1499e-05 0:00:59 87
2305117 3.8877e-04 2.2242e-06 8.8765e-06 2.2418e-06 4.5414e-05 2.8120e-06 7.5448e-06 5.3967e-07 2.4722e-06 5.1499e-05 0:00:59 86
2305118 3.3807e-04 1.9754e-06 6.8365e-06 1.9908e-06 3.5234e-05 2.2582e-06 4.8769e-06 4.3317e-07 2.1447e-06 5.1498e-05 0:01:01 85
2305119 2.9758e-04 1.7656e-06 5.3374e-06 1.7783e-06 2.7332e-05 1.8637e-06 3.0712e-06 3.6106e-07 1.9242e-06 5.1500e-05 0:00:59 84
2305120 2.6433e-04 1.5827e-06 4.2274e-06 1.5951e-06 2.1208e-05 1.5754e-06 1.8631e-06 3.1005e-07 1.7632e-06 5.1497e-05 0:00:58 83
2305121 2.3647e-04 1.4253e-06 3.3805e-06 1.4373e-06 1.6453e-05 1.3580e-06 1.0652e-06 2.7253e-07 1.6421e-06 5.1498e-05 0:00:57 82
2305122 2.1371e-04 1.2907e-06 2.7295e-06 1.3016e-06 1.2772e-05 1.1961e-06 5.4312e-07 2.4369e-07 1.5467e-06 5.1499e-05 0:00:56 81
2305123 1.9490e-04 1.1723e-06 2.2199e-06 1.1816e-06 9.9093e-06 1.0662e-06 2.1117e-07 2.1778e-07 1.4250e-06 5.1498e-05 0:00:55 80
2305124 1.7771e-04 1.0682e-06 1.8193e-06 1.0766e-06 7.6951e-06 9.6222e-07 5.2982e-09 2.0412e-07 1.4242e-06 5.1498e-05 0:00:54 79

iter continuity u-phase-ai u-phase-pa v-phase-ai v-phase-pa w-phase-ai w-phase-pa k-phase-ai eps-phase- vf-phase-p time/iter
2305125 1.6345e-04 9.8297e-07 1.4952e-06 9.9083e-07 5.9750e-06 8.8282e-07 1.1918e-07 1.3471e-06 1.3471e-06 5.1499e-05 0:00:53 78
2305126 1.5102e-04 9.0264e-07 1.2371e-06 9.1065e-07 4.6475e-06 8.0934e-07 1.8892e-07 1.7352e-07 1.2800e-06 5.1497e-05 0:00:51 77
2305127 1.3972e-04 8.3310e-07 1.0248e-06 8.4109e-07 3.6102e-06 7.4631e-07 2.2149e-07 1.6325e-07 1.2399e-06 5.1499e-05 0:00:51 76
2305128 1.3059e-04 7.7431e-07 8.5604e-07 7.8282e-07 2.8102e-06 6.9636e-07 2.3282e-07 1.5555e-07 1.2203e-06 5.1497e-05 0:00:50 75
2305129 1.2228e-04 7.1979e-07 7.1960e-07 7.2679e-07 2.1825e-06 6.4856e-07 2.2805e-07 1.4779e-07 1.1909e-06 5.1498e-05 0:00:50 74
2305130 1.1416e-04 6.6758e-07 6.0711e-07 6.7496e-07 1.7011e-06 6.0252e-07 2.1614e-07 1.3940e-07 1.1457e-06 5.1497e-05 0:00:49 73
2305131 1.0761e-04 6.2698e-07 5.1013e-07 6.3392e-07 1.3223e-06 5.6773e-07 2.0227e-07 1.3380e-07 1.1279e-06 5.1500e-05 0:00:49 72
2305132 1.0181e-04 5.8915e-07 4.3555e-07 5.9544e-07 1.0328e-06 5.3516e-07 1.8620e-07 1.2953e-07 1.1144e-06 5.1497e-05 0:00:48 71
12305133 solution is converged
2305133 9.6056e-05 5.5285e-07 3.7035e-07 5.5949e-07 8.0276e-07 5.0360e-07 1.6842e-07 1.2517e-07 1.0950e-06 5.1498e-05 0:00:48 70
Flow time = 3.6501s, time step = 73002
99999998 more time steps

```

Figure B.10: Parts of the residuals.

```

iter continuity u-phase-ai u-phase-pa v-phase-ai v-phase-pa w-phase-ai w-phase-pa k-phase-ai eps-phase-ai eps-phase-ai vf-phase-p time/iter
12305133 solution is converged
2305133 9.6056e-05 5.5285e-07 3.7035e-07 5.5949e-07 8.0276e-07 5.0360e-07 1.6842e-07 1.2517e-07 1.0950e-06 5.1498e-05 0:01:08 100
2305134 1.3300e-02 3.9623e-05 7.7372e-05 3.9816e-05 6.1033e-05 1.8590e-04 2.6057e-05 1.4236e-04 3.9933e-04 6.0817e-05 0:01:16 99
2305135 5.9324e-03 2.7491e-05 1.4371e-04 2.7224e-05 4.4825e-04 1.2812e-04 1.7940e-04 8.6285e-05 2.4757e-04 5.5493e-05 0:01:14 98
2305136 3.7566e-03 1.7143e-05 1.5887e-04 1.6890e-05 5.2129e-04 8.7988e-05 1.8117e-04 5.2835e-05 1.5405e-04 5.3235e-05 0:01:11 97
2305137 2.7857e-03 1.1760e-05 1.2357e-04 1.1636e-05 4.7938e-04 6.1588e-05 1.3878e-04 3.2444e-05 9.6305e-05 5.2270e-05 0:01:08 96
2305138 2.1857e-03 8.6951e-06 8.4215e-05 8.7034e-06 4.0267e-04 4.3672e-05 9.6982e-05 2.0000e-05 6.0597e-05 5.1839e-05 0:01:06 95
2305139 1.7472e-03 6.7573e-06 5.3730e-05 6.8157e-06 3.2420e-04 3.1133e-05 6.5210e-05 1.2403e-05 3.8431e-05 5.1648e-05 0:01:05 94
2305140 1.4101e-03 5.5941e-06 3.6873e-05 5.6549e-06 2.5468e-04 2.2288e-05 4.5432e-05 7.7487e-06 2.4693e-05 5.1559e-05 0:01:03 93
2305141 1.1462e-03 4.8467e-06 4.7976e-05 4.8961e-06 1.9261e-04 1.6026e-05 4.6306e-05 4.8964e-06 1.6215e-05 5.1518e-05 0:01:04 92
2305142 9.3834e-04 4.2566e-06 4.6018e-05 4.2667e-06 1.4588e-04 1.1613e-05 4.1725e-05 3.1463e-06 1.0931e-05 5.1498e-05 0:01:03 91
2305143 7.7452e-04 3.7517e-06 3.9939e-05 3.7697e-06 1.1073e-04 8.5012e-06 3.5511e-05 2.0692e-06 7.6446e-06 5.1488e-05 0:01:03 90

iter continuity u-phase-ai u-phase-pa v-phase-ai v-phase-pa w-phase-ai w-phase-pa k-phase-ai eps-phase-ai eps-phase-ai vf-phase-p time/iter
2305144 6.4624e-04 3.3102e-06 3.3190e-05 3.3219e-06 8.4319e-05 6.3099e-06 2.9287e-05 1.4049e-06 5.5917e-06 5.1484e-05 0:01:03 89
2305145 5.4428e-04 2.9215e-06 2.6999e-05 2.9324e-06 6.4370e-05 4.7584e-06 2.3687e-05 9.9128e-07 4.2891e-06 5.1481e-05 0:00:57 88
2305146 4.6452e-04 2.5833e-06 2.1173e-05 2.5916e-06 4.9269e-05 3.6693e-06 1.8912e-05 7.3309e-07 3.5015e-06 5.1478e-05 0:00:57 87
2305147 4.0082e-04 2.2959e-06 1.7355e-05 2.3029e-06 3.7802e-05 2.8882e-06 1.4961e-05 5.6968e-07 2.9851e-06 5.1480e-05 0:00:56 86
2305148 3.4908e-04 2.0419e-06 1.3812e-05 2.0482e-06 2.9063e-05 2.3298e-06 1.1750e-05 4.6215e-07 2.6328e-06 5.1477e-05 0:00:59 85
2305149 3.0764e-04 1.8267e-06 1.0965e-05 1.8314e-06 2.2387e-05 1.9287e-06 9.1786e-06 3.8857e-07 2.3727e-06 5.1479e-05 0:00:57 84
2305150 2.7439e-04 1.6400e-06 8.6906e-06 1.6434e-06 1.7272e-05 1.6365e-06 7.1378e-06 3.3164e-07 2.1407e-06 5.1477e-05 0:00:56 83
2305151 2.4533e-04 1.4801e-06 6.8819e-06 1.4822e-06 1.3348e-05 1.4133e-06 5.5283e-06 2.9765e-07 2.0488e-06 5.1478e-05 0:00:55 82
2305152 2.2160e-04 1.3422e-06 5.4436e-06 1.3440e-06 1.0328e-05 1.2497e-06 4.2673e-06 2.6452e-07 1.8967e-06 5.1479e-05 0:00:54 81
2305153 2.0130e-04 1.2197e-06 4.3080e-06 1.2210e-06 8.0032e-06 1.1145e-06 3.2828e-06 2.3813e-07 1.7664e-06 5.1477e-05 0:00:53 80
2305154 1.8982e-04 1.1120e-06 3.4067e-06 1.1143e-06 6.2092e-06 1.0063e-06 2.5171e-06 2.1802e-07 1.6689e-06 5.1477e-05 0:00:52 79

iter continuity u-phase-ai u-phase-pa v-phase-ai v-phase-pa w-phase-ai w-phase-pa k-phase-ai eps-phase-ai eps-phase-ai vf-phase-p time/iter
2305155 1.6934e-04 1.0230e-06 2.6987e-06 1.0241e-06 4.8226e-06 9.2064e-07 1.9239e-06 2.0198e-07 1.6021e-06 5.1478e-05 0:00:51 78
2305156 1.5653e-04 9.4025e-07 2.1398e-06 9.4214e-07 3.7517e-06 8.4539e-07 1.4667e-06 1.8715e-07 1.5249e-06 5.1478e-05 0:00:51 77
2305157 1.4473e-04 8.6823e-07 1.6916e-06 8.7020e-07 2.9231e-06 7.7876e-07 1.1114e-06 1.7394e-07 1.4596e-06 5.1479e-05 0:00:50 76
2305158 1.3527e-04 8.0721e-07 1.3482e-06 8.0921e-07 2.2800e-06 7.2726e-07 8.3876e-07 1.6504e-07 1.4235e-06 5.1476e-05 0:00:49 75
2305159 1.2657e-04 7.5038e-07 1.0789e-06 7.5094e-07 1.7829e-06 6.7585e-07 6.3204e-07 1.5690e-07 1.3836e-06 5.1478e-05 0:00:48 74
2305160 1.1820e-04 6.9639e-07 8.6027e-07 6.9813e-07 1.3949e-06 6.2827e-07 4.6987e-07 1.4928e-07 1.3425e-06 5.1477e-05 0:00:48 73
2305161 1.1204e-04 6.5310e-07 6.9026e-07 6.5435e-07 1.0947e-06 5.9038e-07 3.4685e-07 1.3922e-07 1.2556e-06 5.1479e-05 0:00:47 72
2305162 1.0575e-04 6.1380e-07 5.5554e-07 6.1514e-07 8.6173e-07 5.5685e-07 2.5383e-07 1.3741e-07 1.2784e-06 5.1478e-05 0:00:46 71
12305163 solution is converged
2305163 9.9394e-05 5.7718e-07 4.4967e-07 5.7800e-07 6.7998e-07 5.2346e-07 1.8334e-07 1.3333e-07 1.2682e-06 5.1477e-05 0:00:46 70
Flow time = 3.65015s, time step = 73003
9999997 more time steps

```

Figure B.11: Parts of the residuals.

Curriculum Vitae

Name:	Wei Liu
Post-Secondary Education and Degrees:	University of Science and Technology Beijing, Beijing, China 2013 - 2016 M.S. University of Western Ontario, London, ON, CA 2017 - 2021 Ph.D.
Honours	The National Scholarship for Master 2016
Related Work and Experience	Cooperative Research with Huajiang Powder Coating Co. 2017 Teaching Assistant, The University of Western Ontario 2017 - 2021

Publications:

1. **Liu, W.**, Zhang, H., Shao, Y., Zhang, H., & Zhu, J. (2021). Produce various powder coated surfaces with stable metal shine via microwave energy. *Progress in Organic Coatings*, 154 : 106199.
2. **Liu, W.**, Zhang, H., Shao, Y., Zhu, X., Wei, Y., Zhang, H., & Zhu, J. (2020). Applying microwave energy to fabricate powder coatings with strong and stable metal shine. *Progress in Organic Coatings*, 149, 105929.
3. **Liu, W.**, Zhang, H., Shao, Y., Zhang, H., & Zhu, J. (2020). Preparation of aluminium metallic effect powder coatings with high color stability using a novel method: Microwave bonding. *Progress in Organic Coatings*, 147, 105787.
4. **Liu, W.**, Wang, K., Zhou, Y., Guan, X., Che, P., & Han, Y. (2019). Rational synthesis of silver nanowires at an electrode interface by diffusion limitation. *CrystEngComm*, 21(9), 1466–1473.
5. Liu, T., **Liu, W.**, Chen, Y., Yang, T., & Han, Y. (2018). Silver morphology indicating the evolution of concentration heterogeneity. *Chemical Engineering and Processing-Process Intensification*, 134,38.
6. **Liu, W.**, Fu, J., Zhang, H., Shao, Y., Zhang, H., & Zhu, J. (2018). Cold bonding method for metallic powder coatings. *Materials*, 11(11), 2086.
7. Che, P., **Liu, W.**, Chang, X., Wang, A., & Han, Y. (2016). Multifunctional silver film with superhydrophobic and antibacterial properties. *Nano Research*, 9(2), 442–450.
8. **Liu, W.**, Yang, T., Liu, J., Che, P., & Han, Y. (2016). Controllable synthesis of silver dendrites via an interplay of chemical diffusion and reaction. *Ind. Engin. Chem. Res.*, 55(30), 8319–8326.
9. **Liu, W.**, Yang, T., Li, C., Che, P., & Han, Y. (2015). Regulating silver morphology via electrochemical reaction. *CrystEngComm*, 17(31), 6014–6022.